Eyelid pressure on the cornea

Alyra J. B. Shaw
BAppSc(Optom)Hons

A thesis in partial fulfilment of the requirements for the degree of Doctor of Philosophy

Professor Michael Collins (Principal Supervisor)
Mr Brett Davis (Associate Supervisor)
Professor Leo Carney (Associate Supervisor)

Institute of Health of Biomedical Innovation
School of Optometry
Queensland University of Technology
Brisbane, Australia
2009

Keywords

Eyelid pressure

Cornea

Eyelids

Corneal topography

Videokeratoscopy

Near tasks

Reading

Marx’s line

Eyelid morphology

Digital imaging

Piezoresistive sensors

Abstract

The eyelids play an important role in lubricating and protecting the surface of the eye. Each blink serves to spread fresh tears, remove debris and replenish the smooth optical surface of the eye. Yet little is known about how the eyelids contact the ocular surface and what pressure distribution exists between the eyelids and cornea. As the principal refractive component of the eye, the cornea is a major element of the eye's optics. The optical properties of the cornea are known to be susceptible to the pressure exerted by the eyelids. Abnormal eyelids, due to disease, have altered pressure on the ocular surface due to changes in the shape, thickness or position of the eyelids. Normal eyelids also cause corneal distortions that are most often noticed when they are resting closer to the corneal centre (for example during reading). There were many reports of monocular diplopia after reading due to corneal distortion, but prior to videokeratoscopes these localised changes could not be measured. This thesis has measured the influence of eyelid pressure on the cornea after short-term near tasks and techniques were developed to quantify eyelid pressure and its distribution.

The profile of the wave-like eyelid-induced corneal changes and the refractive effects of these distortions were investigated. Corneal topography changes due to both the upper and lower eyelids were measured for four tasks involving two angles of vertical downward gaze (20° and 40°) and two near work tasks (reading and steady fixation). After examining the depth and shape of the corneal changes, conclusions were reached regarding the magnitude and distribution of upper and lower eyelid pressure for these task conditions. The degree of downward gaze appears to alter the upper eyelid pressure on the cornea, with deeper changes occurring after greater angles of downward gaze. Although the lower eyelid was further from the corneal centre in large angles of downward gaze, its effect on the cornea was greater than that of the upper eyelid.

Eyelid tilt, curvature, and position were found to be influential in the magnitude of eyelid-induced corneal changes. Refractively these corneal changes are

clinically and optically significant with mean spherical and astigmatic changes of about 0.25 D after only 15 minutes of downward gaze (40° reading and steady fixation conditions). Due to the magnitude of these changes, eyelid pressure in downward gaze offers a possible explanation for some of the day-to-day variation observed in refraction. Considering the magnitude of these changes and previous work on their regression, it is recommended that sustained tasks performed in downward gaze should be avoided for at least 30 minutes before corneal and refractive assessment requiring high accuracy.

Novel procedures were developed to use a thin (0.17 mm) tactile piezoresistive pressure sensor mounted on a rigid contact lens to measure eyelid pressure. A hydrostatic calibration system was constructed to convert raw digital output of the sensors to actual pressure units. Conditioning the sensor prior to use regulated the measurement response and sensor output was found to stabilise about 10 seconds after loading. The influences of various external factors on sensor output were studied. While the sensor output drifted slightly over several hours, it was not significant over the measurement time of 30 seconds used for eyelid pressure, as long as the length of the calibration and measurement recordings were matched. The error associated with calibrating at room temperature but measuring at ocular surface temperature led to a very small overestimation of pressure. To optimally position the sensor-contact lens combination under the eyelid margin, an *in vivo* measurement apparatus was constructed. Using this system, eyelid pressure increases were observed when the upper eyelid was placed on the sensor and a significant increase was apparent when the eyelid pressure was increased by pulling the upper eyelid tighter against the eye.

For a group of young adult subjects, upper eyelid pressure was measured using this piezoresistive sensor system. Three models of contact between the eyelid and ocular surface were used to calibrate the pressure readings. The first model assumed contact between the eyelid and pressure sensor over more than the pressure cell width of 1.14 mm. Using thin pressure sensitive carbon paper placed under the eyelid, a contact imprint was measured and this width used for the second model of contact. Lastly as Marx's line has been implicated as the

region of contact with the ocular surface, its width was measured and used as the region of contact for the third model.

The mean eyelid pressures calculated using these three models for the group of young subjects were 3.8 ± 0.7 mmHg (whole cell), 8.0 ± 3.4 mmHg (imprint width) and 55 ± 26 mmHg (Marx's line). The carbon imprints using Pressurex-micro confirmed previous suggestions that a band of the eyelid margin has primary contact with the ocular surface and provided the best estimate of the contact region and hence eyelid pressure. Although it is difficult to directly compare the results with previous eyelid pressure measurement attempts, the eyelid pressure calculated using this model was slightly higher than previous manometer measurements but showed good agreement with the eyelid force estimated using an eyelid tensiometer.

The work described in this thesis has shown that the eyelids have a significant influence on corneal shape, even after short-term tasks (15 minutes). Instrumentation was developed using piezoresistive sensors to measure eyelid pressure. Measurements for the upper eyelid combined with estimates of the contact region between the cornea and the eyelid enabled quantification of the upper eyelid pressure for a group of young adult subjects. These techniques will allow further investigation of the interaction between the eyelids and the surface of the eye.

TABLE OF CONTENTS

Shaw, A. J., Collins, M.J., Davis, B.A., Carney, L.G. (2009). "Eyelid pressure: inferences from corneal topographic changes." Cornea 28(2): 181-188.

Shaw, A. J., Davis, B.A., Collins, M.J., Carney, L.G. (2009). “A technique to measure eyelid pressure using piezoresistive sensors.” IEEE Transactions on Biomedical Engineering 56(10): 2512-2517.

Shaw, A. J., Collins, M.J., Davis, B.A., Carney, L.G. (2009). “Eyelid pressure and contact with the ocular surface." Investigative Ophthalmology and Visual Science (in press).

Figures

Tables

Statement of original authorship

The work contained in this thesis has not been previously submitted for a degree or diploma at this or any other higher education institution. To the best of my knowledge and belief, the thesis contains no material previously published or written by another person except where due reference is made.

Signature: _____

Date: _____

Acknowledgments

Completing this PhD has been a most rewarding experience and I wouldn't have rather spent the past few years doing anything else. But work of this magnitude does not come together without the assistance of others and I would like to thank the following people.

To my principal supervisor Professor Michael Collins, I wish to express my sincere gratitude for the opportunity to complete this PhD. I have valued your wisdom, expertise and ability to interpret my thoughts and ideas into meaningful arguments. Under your guidance I believe I have developed research skills that I will be able to use as an independent researcher.

I wish to thank my associate supervisors for the role you have played in the achievement this milestone. Thanks to Brett Davis for his valuable advice and the many and often lengthy discussions, particularly in regards to the design of the eyelid pressure measurement system. Also I have appreciated the mentoring and encouragement of Professor Leo Carney.

Many thanks to all my colleagues in the Contact Lens and Visual Optics Laboratory for your friendship and support. Thanks to Dr Robert Iskander and Brett Davis for the custom analysis software used extensively throughout this PhD and to Dr Diana Battistutta for advice on the statistical analysis used in Chapter 2. Also thanks to Brett, Johanna and Kathrin for their patience as subjects in the countless pilot trials of the eyelid pressure measurement technique and to Shila, Emily, Shiow and Catherine who assisted with the digital image processing in Chapter 4.

On a personal note, I am thankful for the love of my family, particularly my parents for their continued support throughout my life. Thanks to my husband, Rodney, with whom life is never boring and who never fails to remind me of the lighter side of life. And above all else thanks to Yahweh: my rock and my redeemer.

Chapter 1: Literature Review

1.1 Introduction

The cornea accounts for more than two thirds of the total refractive power of the eye, the majority arising from refraction at the anterior corneal surface. Therefore any slight change in corneal contour may alter refractive error and cause visual distortion. Generally the cornea has a high level of stability however it is influenced by external forces such as digital pressure, tonometer probes and orthokeratology contact lenses. The anterior corneal surface is also altered by the eyelids. While abnormal eyelids that have altered shape, weight or position may be expected to influence the cornea, normal eyelids in downward gaze also cause corneal distortions. Videokeratoscopes have a high level of accuracy and repeatability and have allowed detection of eyelid-induced changes to the anterior corneal surface. Due to the significant influence of the eyelids, there have been attempts to quantify eyelid pressure. However these were limited by the available technology. Several decades later, technology advancements have allowed improved instrumentation to measure eyelid pressure.

1.2 Corneal topography measurement

The measurement of corneal topography is important in the assessment of corneal shape for contact lens fitting and in diagnosing and monitoring corneal abnormalities. It also provides useful information for several surgical procedures including penetrating keratoplasty, refractive surgery, phototherapeutic keratectomy, cataract surgery, trabeculectomy, strabismus surgery and pterygium surgery. In the past few decades the ability to accurately measure the corneal surface has greatly improved. Videokeratoscopes allow for easy capture and fast processing of several thousand data points describing corneal shape. Much research has been conducted on the accuracy and precision of these instruments and the interpretation of their output.

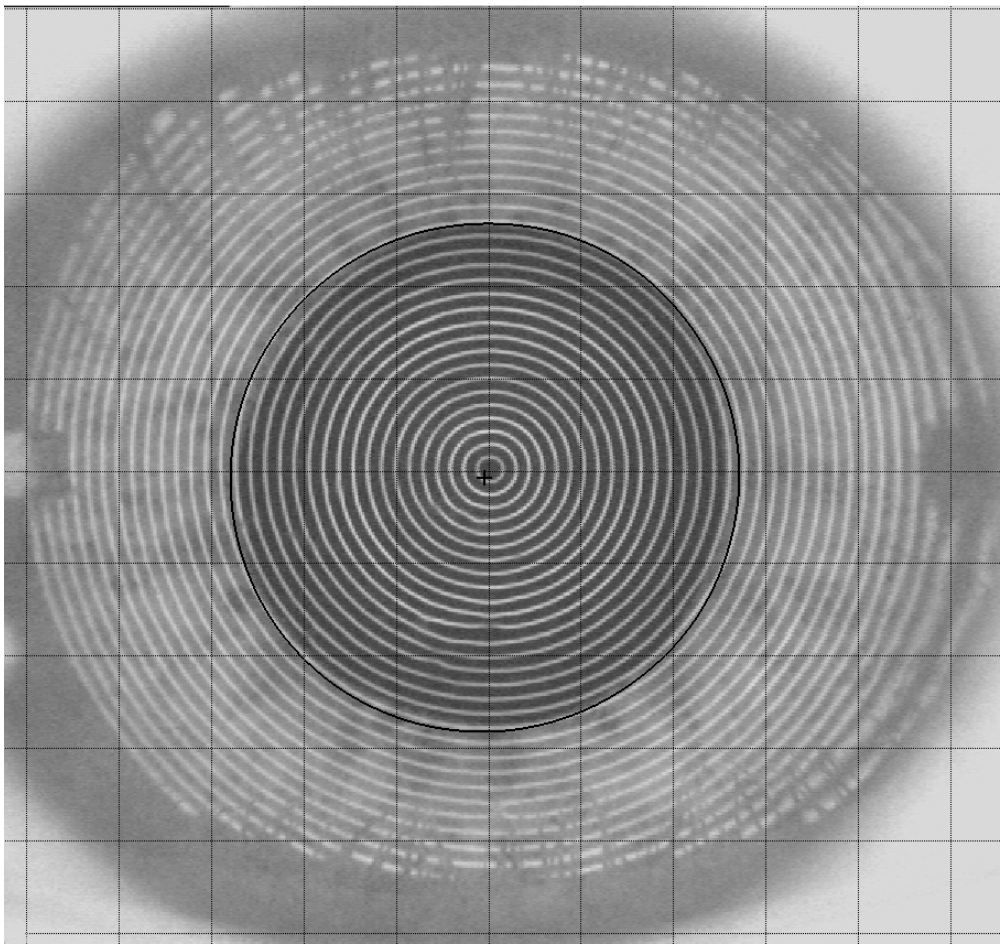

Figure 1-1: A typical Placido-ring image reflected from cornea as captured by the Medmont videokeratoscope.

1.2.1 Corneal topography instruments

One of the first instruments developed to measure corneal shape was the keratometer. This measures corneal curvature in two principal meridians approximately 3 mm from the corneal apex. The limitations are that corneal shape is only sampled over a small area and these instruments have limited value for irregular corneas as the reflection of the mires becomes distorted.

Photokeratoscopes were developed for qualitative and quantitative analysis of a larger area of the cornea. These instruments use the Placido concept with light and dark concentric rings projected onto the cornea and the reflected image is captured by a camera (Figure 1-1). The basic principle is that the mires become larger in diameter, broader, and more widely separated when the area is of lower power (Knoll 1961; Rabinowitz 1993). Technology advances have enabled the concept of the photokeratoscope to be combined with the processing power of video cameras and computers (videokeratoscopes). A large area of the cornea (about 9 mm horizontally and 7 mm vertically) can be easily captured and computer computation allows fast derivation of the anterior corneal surface. Corneal topography data is usually analysed in 256 meridians and mathematical algorithms reconstruct the corneal surface shape. A limitation of Placido instruments is that interpolation of the surface is required within the central ring.

There are many types of Placido ring videokeratoscopes available with a number of hardware and software options. They are designed with either large or small diameter targets. Larger targets allow for a large working distance which decreases the influence of alignment inaccuracies, while small diameter cones can be positioned close to the eye reducing the corneal area lost to shadows from the nose, brow or eyelashes (Courville *et al.* 2004). The Medmont E300 Corneal Topographer (Medmont Pty. Ltd., Victoria, Australia) is an example of a Placido ring system which utilises a highly curved cone to capture a relatively large diameter of the cornea (Cho *et al.* 2002) (Figure 1-2). An arc-step algorithm is used for image reconstruction which allows accurate corneal height interpretation.

Figure 1-2: Medmont Placido-disk videokeratoscope.

Other topography instruments have been developed that do not use the Placido design include raster photogrammetry, optical beam scanning, Scheimpflug imaging and laser holographic interferometry. Raster stereography photogrammetry produces a topographic map of the cornea using a grid pattern projected onto the cornea and viewed from a defined oblique angle. Stereo-image pairs are used to compute elevations at each grid section from known projection and camera angles. Compared to the Placido instruments this system avoids shape assumptions as the elevation of the cornea is directly measured. So it does not require a smooth reflective surface and precise spatial alignment for accurate imaging is less critical (Belin and Ratliff 1996). As this system is not dependent on reflection it is particularly useful in measuring the topography on corneas that do not reflect light due to scarring, epithelial defects, or irregular shapes. Other advantages are that a large area of the cornea can be analysed although these instruments are generally not as accurate as Placido-ring videokeratoscopes (Tang *et al.* 2000).

The Orbscan (Orbtek Inc, Salt Lake City, UT, USA) uses optical beam scanning slits projected onto the anterior corneal surface to reconstruct both the anterior and posterior corneal surfaces and corneal thickness (Liu *et al.* 1999). A study on test surfaces found that while the results from the Orbscan differed significantly from Form Talysurf Analysis, the elevation maps would be clinically acceptable and comparable to Placido ring systems (Cairns *et al.* 2002). However, the Orbscan has reverted to using a Placido disk system for the front surface due to better sensitivity. Recently the Pentacam (Oculus Inc, Dutenhofen, Germany) was released which uses rotating Scheimpflug imaging to measure the anterior and posterior corneal surfaces and corneal thickness.

Laser holographic interferometry (e.g. the CLAS 1000, Kerametrics Corp., Solana Beach, CA) uses a spherical wavefront projected onto the cornea and the interference of the illuminating and reflected beams is used to measure corneal elevation. However due to the wide variation in corneal shapes, it is difficult to represent every variation with a single interference reference (Courville *et al.* 2004).

Table 1-1: Types of corneal topography maps and their advantages, disadvantages and applications

Map Type	*Description*
Sagittal - Axial	Measures the distance along a normal from a point on the corneal surface to the optic axis of the videokeratograph Equivalent to keratometric radius Smooth surface representation Advantages: easily derived algorithm, measurements are repeatable Disadvantages: localised corneal changes may be masked
Tangential - Instantaneous	Independent of any axis and is based on the local curvature at each point More appropriate/sensitive for detecting localised changes in radius True apex of cornea can be located
Elevation – Height - Sag	Height of cornea measured relative to an established reference, either a fixed plane (absolute height) or a reference sphere (elevation)
Refractive – True Power	Based on optical ray tracing using Snell's law by modelling the cornea as a single refracting surface and analysing the path of incoming parallel rays

(Salmon and Horner 1995; Mandell 1996; Roberts 1998).

1.2.2 Interpretation of corneal topography maps

Due to the analytical power of computers, a number of measures and graphical representations of corneal shape have been developed. There are four different maps of corneal topography that can be derived: axial, tangential, elevation and refractive. Each of these maps provides different information and together they provide a comprehensive description of the anterior corneal surface (Salmon and Horner 1995; Roberts 1998). The required application of the topography data determines which map or combination of maps should be considered (Table 1-1, Figure 1-3).

Graphically portraying corneal topography as colour coded maps allows for easy comprehension. Normalised or absolute colour scales can be used. An absolute scale allows for easy comparison between maps and 1.5 dioptre intervals has been suggested to provide the best combination of sensitivity and range (Wilson *et al.* 1993). However in some instances, a finer scale (with smaller intervals) may be needed to reveal more subtle changes in the cornea.

Several indices have been developed to aid interpretation of corneal topography maps. Simulated keratometry (SimK) values simulate the curvature measurements given by a typical keratometry exam for each of the two principal meridians. The Average Corneal Power (ACP) index is an area-corrected average of corneal power in front of the entrance pupil. The Surface Regularity Index (SRI) describes fluctuations in power between the hemi-meridians and so represents the impact of corneal irregularities on optical quality. The Surface Asymmetry Index (SAI) assesses the differences in corneal power between corresponding points 180° apart. Both the SRI and SAI have been linked to visual acuity measures (Wilson and Klyce 1991). There are also indices to define and diagnose various conditions such as keratoconus (Schwiegerling and Greivenkamp 1996). Attempts to standardise the interpretation of corneal topography include the Holladay Diagnostic Summary which uses a collation of power and shape parameters and indices (Holladay 1997).

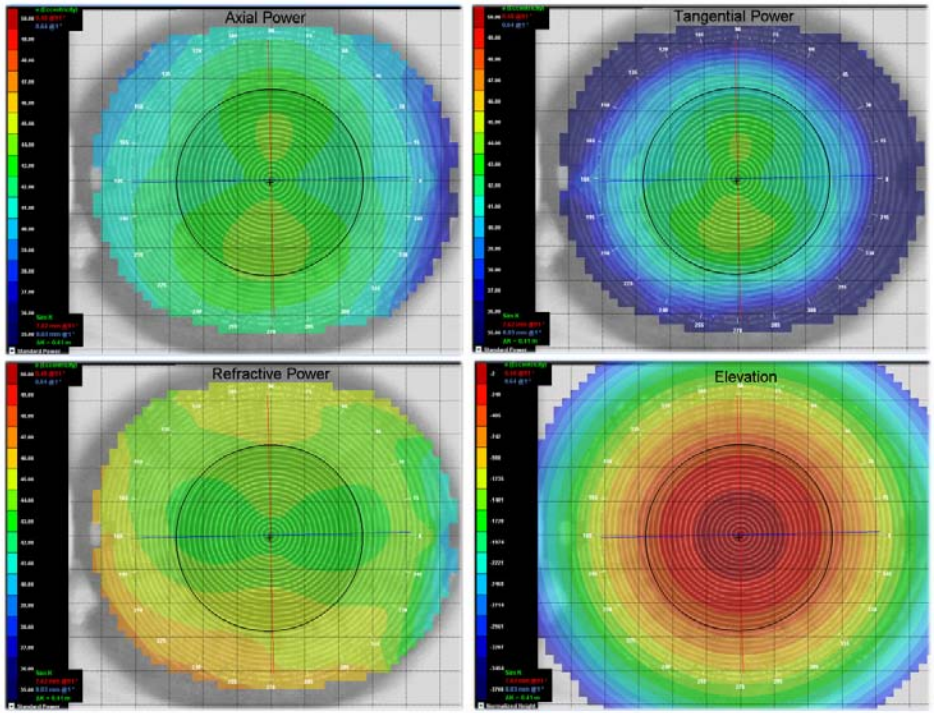

Figure 1-3: Types of topography maps as captured by the Medmont videokeratoscope. Axial power (top left), Tangential power (top right), Refractive power (lower left) and Elevation (lower right).

1.2.3 Corneal reference axes and points

The alignment of videokeratoscopes is crucial to the precision of corneal topography measurements. The most appropriate reference axis is the line of sight as it is closely related to the optical properties of the ocular system. This line connects a fixation point to the centre of the entrance pupil and the centre of the exit pupil to the fovea (Figure 1-4). However while it makes sense for a videokeratoscope to be aligned along this axis with the chief bundle of rays, the algorithms operate around the vertex normal as this is more easily located. So videokeratoscopes are aligned at a point perpendicular to the cornea along an axis known as the videokeratoscope axis (Figure 1-4).

The major corneal reference points are the geometric centre, sighting centre, and corneal apex (Mandell *et al.* 1995) (Figure 1-4). Where the line of sight passes through the cornea marks the sighting centre. This is used as a reference when describing the refractive power of the cornea. The perpendicular corneal intersection point (along the videokeratoscope axis) is the vertex normal which is the centre of a topography map. The corneal apex is the point of maximum curvature of the cornea and is a reference point used to describe corneal shape. The exact location of the apex of the cornea is difficult to determine (Dingeldein and Klyce 1989). The geometric centre is located at the intersection of the largest and smallest corneal diameters and is useful when describing contact lens positions on the eye.

1.2.4 Accuracy and precision of videokeratoscopes

A number of factors can affect the measurements of a Placido disk-based videokeratoscope including user errors (such as intra-observer variability, inter-observer variability, alignment, focusing, and centration) and system errors (calibration, hardware, and software).

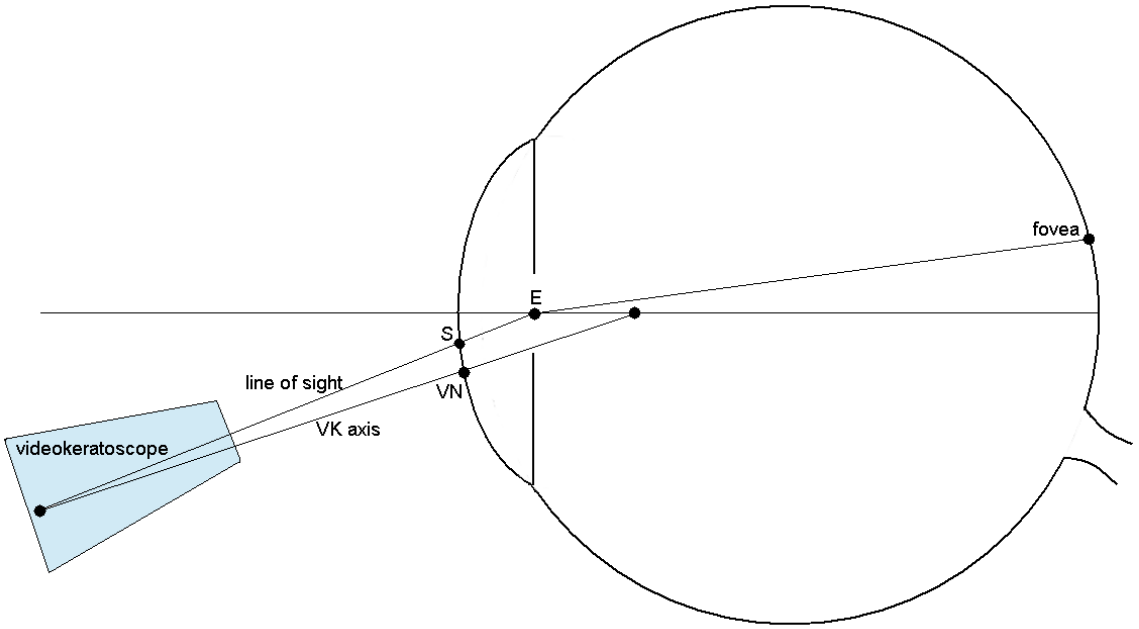

Figure 1-4: The major reference of the eye (the line of sight) through the corneal sighting centre (S) and the entrance pupil (E) to the fovea. The videokeratoscope is aligned along the videokeratoscope axis that is perpendicular to the cornea passing through the corneal vertex normal (VN). (Adapted from Atchison and Smith 2000).

Potential sources of inaccuracy in videokeratoscopy operation are mainly associated with misalignment due to the lack of appropriate corneal reference position, fixation and focussing error. Some instruments have employed automatic focusing systems so that an image will only be taken when the instrument is appropriately focused and aligned. This includes using a side camera which confirms the position of the corneal apex to determine the correct distance between the camera and the cornea. Alignment is controlled by the operator to align the image of the fixation point with respect to a reference pattern on the monitor, which is coaxial with the videokeratograph optical axis. Alignment for most instruments is normal to the cornea along the videokeratoscope axis which may not be ideal for certain applications, such as refractive surgery. Misalignment of the videokeratoscope can introduce asymmetry to the corneal topography maps (Douthwaite and Pardhan 1998).

Variation in the subject's fixation is a potential source of error, however it is not usually significant providing that the patient concentrates on the fixation target. Although it may be an issue in some instances when fixation on the luminous fixation target may be difficult due to nystagmus or low visual acuity from a large refractive error or pathology. Fixation deviations as small as 5° have been shown to produce significant changes to the inferior-superior (I-S) value resulting in a pattern similar to keratoconus and misdiagnosis (Hubbe and Foulks 1994).

The algorithms used for image reconstruction may add inaccuracy and bias. Some assume that the cornea is spherical, and reconstruction is based on axis-centred spheres with the corneal apex aligned with the videokeratoscope axis. A more accurate representation arises from arc-step algorithms that reconstruct corneal shape based on several multiple arcs, avoiding the problem of spherical bias and providing more accurate surface profiles (Tripoli *et al.* 1995). The accuracy of the arc-step algorithm used by the Keratron has been assessed and only small height errors were recorded for astigmatic test surfaces (Mattioli and Tripoli 1997). Improved analysis methods also result in more accurate corneal topography data. The standard deviation of measurements can be decreased by adjusting for the tilt, displacement, and cyclotorsion that occurs with fixation

errors and cyclorotations before averaging multiple maps of the same cornea. Although this is computationally intensive, it improves the precision performance of the videokeratoscope (Buehren *et al.* 2002).

Generally the precision of videokeratoscopes is good for the central cornea with instantaneous power showing about ± 0.5 D standard deviation and refractive power displaying ± 0.25 D standard deviation (Buehren *et al.* 2001). The precision is generally worse for peripheral topography and can be reduced to more than 1 D (Mandell 1996; Buehren *et al.* 2001).

A number of studies have compared the capabilities for several videokeratoscope systems for test surfaces. The accuracy of the Medmont is high when measuring spheres (2 µm RMSE), aspheres (2 µm RMSE) but was worse for the multicurve surfaces (up to 93 µm RMSE) (Tang *et al.* 2000). There is also lower accuracy in topography estimation when sudden changes in curvature are present due to the limitations of the Placido ring spacing (Tang *et al.* 2000). Overall in terms of accuracy and precision, the Medmont performed slightly better than the Keratron (Alliance Medical Marketing, Jacksonville, Fl) and significantly better than Topographic Modelling System (TMS version 1.61 Computed Anatomy Inc, New York, NY) and PAR Corneal Topography System (PAR-CTS Version2.0 PAR Vision Systems, New Hartfield, NY). The superior performance of the Medmont has been attributed to the automatic capture which ensures correct alignment and the image updating feature which continuously captures better images replacing the poorer images. The accuracy and repeatability of videokeratoscopes has also been assessed on human subjects. For different brands the repeatability and reproducibility varies (Cho *et al.* 2002), with the number of repeated measures to achieve a 2 µm precision ranging from 2 to 552.

1.2.4.1 Influence of ocular dynamics

Naturally occurring fluctuations of the eye also influence the measurement of corneal topography so the repeatability of test objects is higher than natural eyes. These fluctuations may occur due to the tear film, eyelid forces, intraocular pressure, normal ocular blood pulsation or micro-movements of the eye.

A regular tear layer is required to maintain an optically smooth surface. The tear film is measured to be 3.3 ± 1.5 µm thick using optical coherence tomography (Wang *et al.* 2003) which agrees with the results using interferometry (King-Smith *et al.* 2004). After a blink it takes several seconds for the tear film to stabilize. Using a high speed videokeratoscope (50 Hz) between 0.5 to 3 seconds (Zhu *et al.* 2007) and between 1.5 to 7 seconds (Iskander *et al.* 2005) has been reported for tear film build up. Comparably Owens and Phillips (2001) found a tear stabilization time of 1.05 ± 0.30 seconds by analysing the movement of particles in the tear film and Montés-Micó and Alió (2004) found there to be minimum aberrations of air-tear film interface after 6 seconds.

After stabilization and without a blink to renew the tear layer, the tear film begins to break up (Erdélyi *et al.* 2005). It has been suggested that the breakup of the tear film is due to lipid layer thinning and that tear hyperosmolarity may be related to tear instability (King-Smith 2008).

Due to changes in the tear film layer, it is important to standardise the post blink capture time for topography measurements (Koh *et al.* 2002). Based on the measured tear build up and break up times, the recommended topography capture time after a blink is between 2 to 7 seconds (Owens and Phillips 2001; Németh *et al.* 2002; Montés-Micó *et al.* 2004; Iskander *et al.* 2005). The decrease in precorneal tear film stability between the ages of 7 to 80 years may also need to be taken into account (Patel and Farrell 1989 Mohidin, 2002 #968), along with the influence of ethnicity (Albietz *et al.* 2005).

In summary, videokeratoscopes are accurate and precise corneal topography instruments, particularly when the influence of ocular dynamics such as the tear film are minimised and alignment control and arc-step algorithms are used. The computational power of computers allows a variety of corneal shape descriptions to be derived so that subtle changes in corneal shape can be detected. Thus videokeratoscopes remain the principal and most comprehensive method to study the topography of the anterior corneal surface.

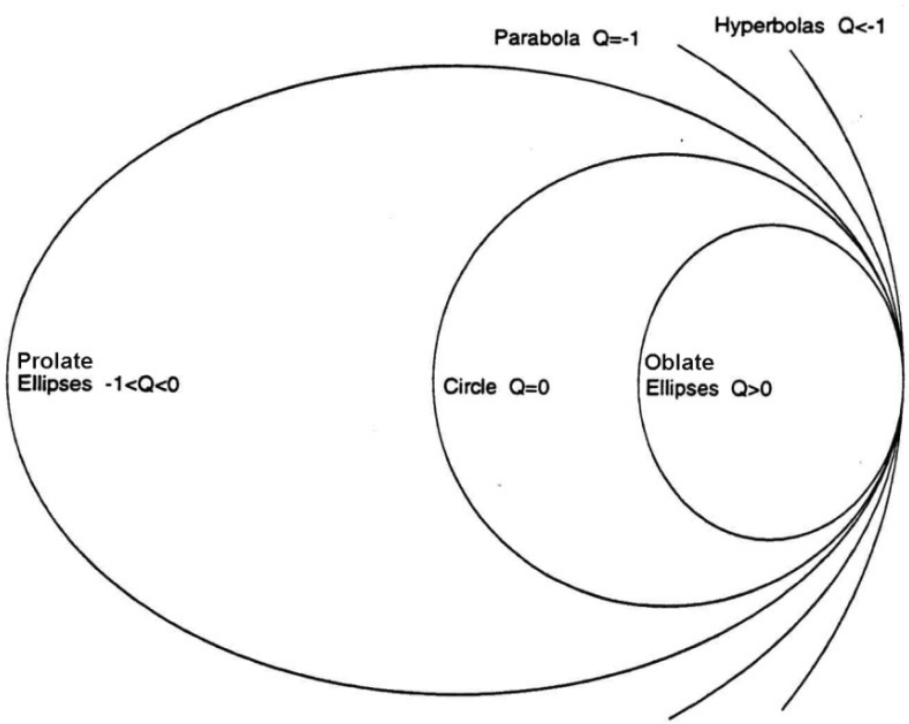

Figure 1-5: Conic sections and their respective Q values where Q=0 is a circle, Q>0 an oblate ellipse and -1<Q<0 a prolate ellipse.

1.3 Corneal Shape

Videokeratoscopes allow detailed examination of corneal shape. There are a number of surface descriptors such as radius of curvature, conic sections, peripheral asphericity and wavefront aberrations. Initially it was believed that the anterior cornea was a sphere, however with the use of early keratometers it was soon found to be ellipsoid (Dingeldein and Klyce 1989). With videokeratoscopes the anterior corneal surface can now be studied in detail allowing the population norms of corneal shape to be defined and abnormal shapes to be detected. Corneal surface shape is dynamic with short-term changes associated with diurnal variations (Kiely *et al.* 1982). The effect of other influences on corneal shape such as accommodation and extra-ocular muscles is inconclusive.

1.3.1 Mathematical descriptions

The contour of the human cornea can be closely modelled using a conic section specifying asphericity (Q), which is an index of the rate of flattening or steepening of the curve. Mathematically this is represented by the conic equation $X^2 + Y^2 + (1 + Q) Z^2 – 2ZR = 0$, where R is the vertex radius of curvature and Q is the surface asphericity (Atchison and Smith 2000). A circle is described by an asphericity of $Q = 0$ while $Q > 0$ is an oblate ellipse (steepening away from centre) and $-1 < Q < 0$ is a prolate ellipse (flattening away from centre) (Figure 1-5).

However while ellipses may be adequate approximations for the central cornea (Mandell and St Helen 1971), they are not always a good descriptor of corneal shape when considering larger corneal diameters or irregular corneas. Recently Franklin *et al.* (2006) produced topography maps of the entire cornea from limbus to limbus (by combining a central 6 mm diameter map with 6 peripheral maps) and found that conic fits are a poor representation of corneal shape in the periphery of the cornea.

Maloney *et al.* (1993) developed a method to describe the optical characteristics of the cornea by fitting a best fit sphero-cylinder to the corneal power data. The dioptric difference between the sphero-cylinder fit and the actual data for all data points can also be calculated, and the root mean square of the sum of the differences (RMS error) is a measure of the corneal irregularity or corneal higher-order aberrations.

To describe the more complex components of corneal shape, Zernike polynomials can be applied to elevation topography maps (Schwiegerling *et al.* 1995; Guirao and Artal 2000). The equation needed to describe the surface is the sum of linear combinations of several simple surfaces with each term describing a different aspect of the surface shape. The set of functions are orthogonal so the coefficients are independent of one another and of the number of terms used. Therefore terms may be added or subtracted without influencing the coefficient values of other terms. Several different numbering systems have been used to represent the Zernike polynomials, however the system suggested by Thibos *et al.* (2002) using double indexing so that the radial order (subscript) and frequency (superscript) are specified is most often used.

Fourier series analysis uses cosine and sine functions to decompose the complex corneal topography into optical components such as spherical power, regular astigmatism, and higher order (irregular) components (Hjortdal *et al.* 1995). Other analytical approximations for corneal contour include a hyperbolic cosine function with two parameters: the radius of curvature at the apex and a descriptor of stability in the central curvature (Kasprzak and Jankowska-Kuchta 1996). However a generalised conic function has been found to be superior to the hyperbolic cosine approximation, particularly for extended corneal topography from limbus to limbus (Kasprzak and Iskander 2006).

In summary, the cornea has an ellipsoid basic shape but can be described in greater detail mathematically using Zernike polynomials. The complex descriptors of corneal shape are particularly useful to highlight small changes that would otherwise be obscured in more general representations.

1.3.2 Normal corneal shape

1.3.2.1 Corneal radius and asphericity

Many investigations have assessed the central corneal radius with similar results: 7.72 mm (176 eyes) (Kiely *et al.* 1982); 7.775 mm (220 eyes) (Guillon *et al.* 1986), 7.83 mm with a range from 7.4 to 8.6 mm (Mandell 1996) and 7.79 ± 0.27 mm (Dubbelman *et al.* 2006). There are also meridional variations with the mean corneal radius of 98 subjects being 7.93 mm horizontally and 7.78 mm vertically, reflecting the tendency towards with-the-rule astigmatism in the population (Douthwaite *et al.* 1999).

With photokeratoscopes the peripheral cornea and rate of curvature change can be assessed along with the central cornea. Considering approximately the central 6 mm, the normal cornea is closely represented by a prolate ellipse with various rates of flattening (Knoll 1961; Kiely *et al.* 1982; Guillon *et al.* 1986). Kiely *et al.* (1982) also reported that the cornea is generally non-rotationally symmetric with an average asphericity of Q = -0.26. In a retrospective study of 41 subjects prior to radial keratotomy surgery, the mean asphericity was -0.18 with 80% being prolate (Eghbali *et al.* 1995). Similar to radius of curvature, there are meridional variations with the mean asphericity reported to be -0.17 in the flattest meridian and -0.19 in the steepest (Guillon *et al.* 1986) and -0.24 horizontally and -0.18 vertically (Douthwaite *et al.* 1999).

Kiely *et al.* (1982) found a slight correlation between the radius of curvature and the asphericity with a steeper cornea having greater peripheral flattening. Dingeldein and Klyce (1989) also reported an association between steeper central corneas and peripheral flattening, with most subjects having asymmetric flattening beginning on the nasal side of the cornea. However a correlation between central radius of curvature and asphericity was not found in the study by Douthwaite (2003). The rate of peripheral flattening is evident when comparing radii and asphericity averages over different corneal diameters. For 100 subjects the mean corneal radius was 7.77 ± 0.2 mm and asphericity, Q was -0.19 ± 0.1

over a 6 mm corneal diameter. While over a 10 mm diameter the average corneal radius was 7.72 ± 0.2 mm and the asphericity (Q) was -0.36 ± 0.1, suggesting a greater rate of flattening in the periphery (Read *et al.* 2006). Right and left eyes show a high degree of mirror symmetry (enantiomorphism) and so the principal meridians for curvature and asphericity are likely to be the same for an individual (Rabinowitz and Klyce 1993).

1.3.2.2 Astigmatism

The cornea contributes most of the astigmatism of the total eye as seen in Javal's rule: total astigmatism = 1 (corneal astigmatism) – 0.50 D x 90. Keller *et al.* (1996) confirmed this relationship (Grosvenor's modified Javal rule) using videokeratoscopes and it was found to apply across a range of pupil sizes. Regular astigmatism is typically observed as a figure of eight or bowtie corneal topographical pattern. As the toricity increases the bowtie becomes narrower and more obvious. Irregular astigmatism is usually due to ocular surface diseases such as epithelial corneal dystrophies or keratoconus, infections, surgery or trauma (Rabinowitz 1993).

The use of videokeratoscopes has allowed for more sophisticated qualitative descriptors of corneal shape. Bogan *et al.* (1990) described a system that divided corneas into five groups: round, oval, symmetric bowtie, asymmetric bowtie and irregular. An expanded version was produced by Rabinowitz *et al.* (1996) to classify more complex patterns seen in normal topography maps. It has been found to be quite robust even for less experienced observers (Rasheed *et al.* 1998). The distribution of these corneal patterns within the normal population has been investigated (Table 1-2).

Another classification of corneal shape involves both central and peripheral corneal shape (Read *et al.* 2006). These leads to five categories: spherical centre and periphery; spherical centre with toric periphery; toric centre with stable toric periphery; toric centre with increasing toric periphery and toric centre with decreasing toric periphery. Examples of these corneal shapes and their relative incidence from a sample of 78 subjects are presented in Figure 1-6.

Table 1-2: Percentage of Corneal Topography Patterns

	Bogan et al. (1990)	*Kanpolat et al. (1997)*	*Riley et al. (2001)*
Videokeratoscope	CMS	TMS -1	Orbscan II
Sample size	399	114	451
Round (%)	22.6	14	34
Oval (%)	20.8	11	10
Symmetric bowtie (%)	17.5	29	31
Asymmetric bowtie (%)	32.1	33	12
Irregular (%)	7.1	12	13

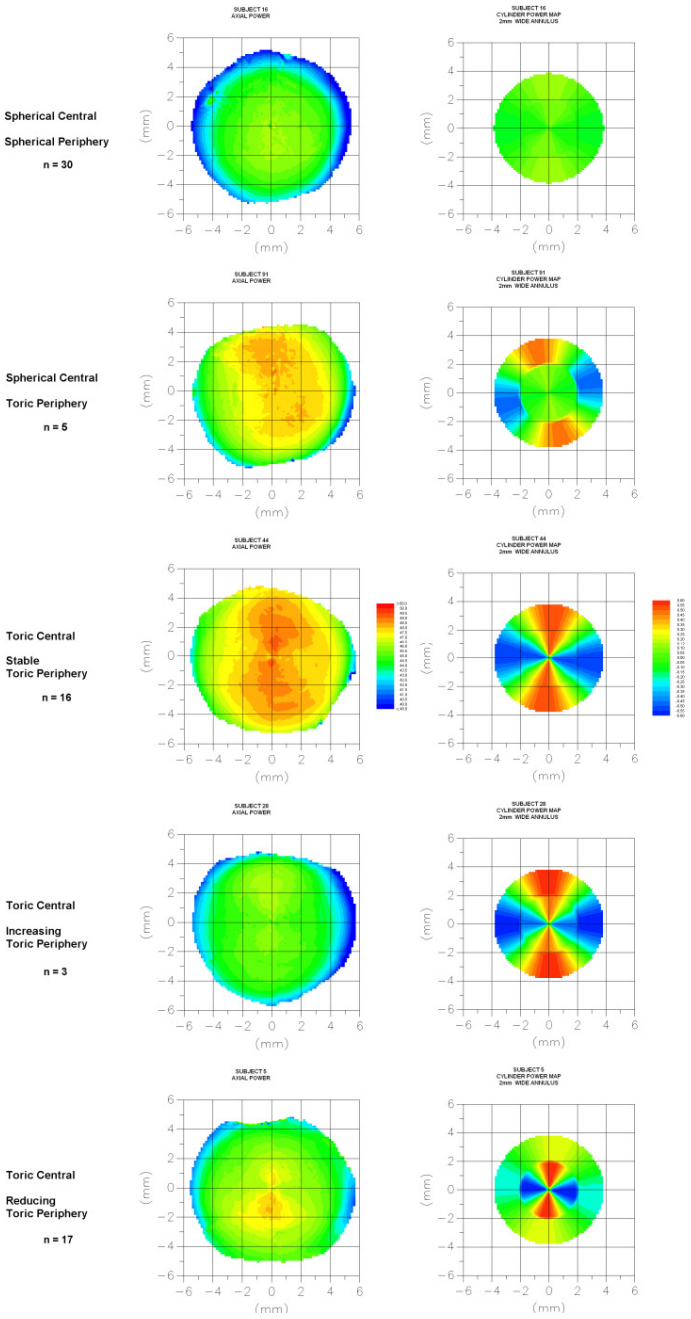

Figure 1-6: Corneal topography classification based on central and peripheral astigmatic toricity. Left hand images are axial power maps and on the right corresponding topography maps with the corresponding cylinder power (best power removed) (Courtesy of Scott Read).

1.3.2.3 Corneal aberrations

Zernike expansion is now widely used to describe the ocular characteristics of the corneal surface. The corneal elevation data (from videokeratography) is fit with a Zernike polynomial expansion to estimate the corneal wave aberration (Guirao and Artal 2000). These more complicated descriptions of the cornea enable the shape to be more thoroughly defined. Generally as the radial order of the Zernike aberrations increases, the magnitude and contribution to the total corneal aberrations decreases. Usually the largest contributions from higher-order aberrations are from the 3rd order (coma and trefoil) and 4th order (spherical aberration, which is usually positive).

Normal corneas have a wide variation in corneal aberrations (Wang *et al.* 2003) though 4th order polynomials have been found to be a good approximation (Guirao and Artal 2000; Iskander *et al.* 2001; Smolek and Klyce 2005). Generally any more than 11 terms does not add extra information for a normal surface shape. The aberrations of the cornea are larger than for the complete eye, indicating that the internal optics partially compensate for the corneal aberrations (Artal *et al.* 2001).

Corneal diseases often alter the higher-order aberrations, for example the total corneal aberrations and spherical aberration often increases after refractive surgery (Oshika *et al.* 1999) and coma is usually increased in keratoconus (Schwiegerling and Greivenkamp 1996). For irregular surfaces more terms are required to reach the same minimum fit error. Carvalho (2005) suggested that for irregular surfaces (for example due to radial keratotomy (RK) or keratoconus), 36 or more terms may be necessary and similarly Iskander *et al.* (2001) using a refined boot-strap method to improve accuracy, agreed that up to 7th radial orders may be required. The limitations involved in fitting Zernike polynomials to corneal elevation data are the accuracy of the videokeratoscope in measuring corneal elevation, the numerical accuracy of fitting Zernike polynomials, approximations in the wave aberration expansion and experimental error.

1.3.2.4 Association of corneal shape and refractive error

There seems to be an association between mean corneal power and refractive error (Sheridan and Douthwaite 1989). A study of 79 subjects (youth-onset myopes, early adult-onset myopes and emmetropes) found the mean corneal power to be steeper for both groups of myopes than for the emmetropes (Grosvenor and Scott 1993) and similarly Goss *et al.* (1997) reported steeper corneas for myopes compared with emmetropes. Furthermore, a study of myopes found that eyes with higher levels of myopia had steeper central corneas and less rapid peripheral flattening (Carney *et al.* 1997). This is supported by Budak *et al.* (1999) who found that as the degree of myopia and negative asphericity increased, the corneal radius of curvature decreased. However there is some disagreement as more myopic eyes have been reported to have flatter corneas (Chang *et al.* 2001) and others have not found an association between asphericity and corneal curvature (Sheridan and Douthwaite 1989; Dubbelman *et al.* 2006).

There seems to be an association between axial length and corneal radius. The ratio of axial length to corneal radius (AL/CR) varies with refractive error being approximately 3.00 for emmetropic eyes and ranging from 2.60 for the most highly hyperopic eye to 4.10 for the most highly myopic eye (Grosvenor and Scott 1994). The AL/CR ratio could be useful when examining the role of the cornea in the development and progression of myopia (Grosvenor and Goss 1998) with the horizontal corneal meridian showing a high sensitivity and specificity (Goss and Jackson 1995).

While an increase in axial length is the primary outcome from myopia progression (Hyman *et al.* 2005), there is disagreement on whether steepening of the cornea is also occurs. An association between corneal steepening and myopia progression has been reported in young adults (Goss and Erickson 1987; Goss and Jackson 1995). The myopic progression in the study by Adams (1987) was not accompanied by any significant changes in corneal astigmatism, horizontal and vertical corneal curvatures, or other shape factors. In another investigation, myopia increased by an average of 1.46 D and was strongly correlated with a

0.56 mm increase in axial length while no contribution to the myopia progression was due to the cornea (Horner *et al.* 2000). So axial elongation of the eyeball seems to be the primary anatomical change in myopia development with little corneal involvement (Adams 1987; Pärssinen 1993).

There has not been as much research into the relationship between hyperopia and corneal curvature and an association is less conclusive. A weak but statistically significant relationship was found between mean corneal radius measures and mean spherical refractive errors (R^2=0.128, p=0.009), with the mean corneal radius flattening with increasing hyperopia (Strang *et al.* 1998). Though there does not seem to be an association between corneal asphericity and hyperopic refractive error (Mainstone *et al.* 1998).

1.3.2.5 The influence of gender and ethnicity on corneal shape

Concerning the influence of gender on corneal shape, males are likely to have flatter corneas than females while the asphericity is generally the same between genders (Douthwaite *et al.* 1999). Cheung *et al.* (2000) examined 63 Hong-Kong Chinese and agreed that on average males have a longer corneal radius than females. The average radii of curvature for the flattest and steepest meridians were 7.72 mm and 7.88 mm for the males and 7.54 mm and 7.71 mm for the females. Similarly the male and female mean corneal curvature radii were 7.93 mm and 7.75 mm respectively for 454 subjects between 5 and 80 years (Fledelius and Stubgaard 1986). Corneal shape may also vary depending on ethnicity. A study of Hong-Kong Chinese subjects found that Asian eyes have on average steeper corneas than Caucasians, with no difference in corneal asphericity (Cheung *et al.* 2000).

1.3.2.6 The cornea and age-related changes

The normal cornea undergoes significant astigmatic changes throughout life. Newborns have steep corneas and high amounts of against-the-rule astigmatism (Friling *et al.* 2004). The against-the-rule astigmatism was found to be greatest for newborns with the lowest birth weight and for those who had the lowest post-

conception age. While against-the-rule astigmatism predominates in the very young, there is a shift towards mainly with-the-rule by 6 years of age (Gudmundsdottir *et al.* 2000; Montés-Micó 2000).

Generally for young adult subjects there is still a predominance of with-the-rule astigmatism with the cornea progressively flattening in the periphery (Goto *et al.* 2001). In later years (over 60 years) the cornea becomes steeper (Guirao *et al.* 2000) and spectacle and corneal astigmatism is principally in the against-the-rule or oblique astigmatism direction (Lam *et al.* 1999). There are alterations in the higher-order aberrations due to corneal changes with age (Oshika *et al.* 1999; Guirao *et al.* 2000). The amount of corneal aberration increases and there is a corresponding decrease in the retinal image quality (Guirao *et al.* 2000). Age-related changes in corneal aberrations are predominantly coma-like aberrations that correlate with age (Oshika *et al.* 1999).

Gender-specific corneal changes occur with increasing age. A significant decrease in corneal radius has been reported for older males but not older females (>50 years) (Fledelius and Stubgaard 1986). While in the younger age group (<50 years), there was no difference in corneal radius between the genders. Similarly Goto *et al.* (2001) found that the corneas of older men were flatter than those of older women. The older men had significantly higher levels of against-the-rule astigmatism which seemed to be primarily due to changes in the vertical corneal meridian. It has been suggested that these gender-specific changes relate to differences in sex hormones (Goto *et al.* 2001).

The age-related progression of change in corneal astigmatism, from against-the-rule at birth to with-the-rule during adulthood and back to against-the-rule in later years, has been measured using keratometers and videokeratoscopes and for several ethnicities (Fledelius and Stubgaard 1986; Lam *et al.* 1999).

1.3.3 Short-term stability of corneal shape

The cornea is resistant to large changes in corneal shape, however small short-term changes occur due to ocular and systemic influences.

1.3.3.1 Diurnal variations

There are many parameters of the eye that undergo changes throughout the day including intraocular pressure (Laiquzzaman *et al.* 2006), corneal thickness (Kiely *et al.* 1982; Harper *et al.* 1996; du Toit *et al.* 2003; Read *et al.* 2008), anterior chamber depth (Read *et al.* 2008), tonic accommodation, corneal sensitivity (du Toit *et al.* 2003), axial length (Stone *et al.* 2004; Read *et al.* 2008), tear film stability (Patel *et al.* 1988) and tear menisci height (Shen *et al.* 2008).

Similarly, it has been shown that corneal shape varies depending on the time of day (Reynolds and Poynter 1970; Cronje and Harris 1997; Read *et al.* 2005; Read *et al.* 2007). There is general agreement that the cornea is flattest on waking and undergoes steepening throughout the day (Reynolds and Poynter 1970; Kiely *et al.* 1982). Cronje and Harris (1997) recorded that keratometric measurements vary throughout the day and noted that the greatest change occurred near the vertical meridian.

It was recently confirmed with videokeratoscopy that for most people a slight steepening of the cornea occurs throughout the day (Read *et al.* 2005), with changes to wavefront aberration terms trefoil (30^{o}) and astigmatism (45^{o}). These corneal changes were considered to be due to a cumulative effect of eyelid pressure during the day. It has also been shown that for females, variation in hormones during the menstrual cycle can influence the diurnal variation of corneal topography (Kiely *et al.* 1983; Handa *et al.* 2002).

1.3.3.2 Accommodation and the cornea

The effect of accommodation on corneal topography has been the subject of interest for many years. It has been postulated the anterior insertions of the

ciliary muscle, which contracts with accommodation, may influence the corneal surface. Early investigations failed to show any corneal change with accommodation when convergence was controlled (Fairmaid 1959; Löpping and Weale 1965; Mandell and St Helen 1968; Clark 1973). However due to the available equipment of the time, only the central cornea was considered.

More recent studies have recorded corneal changes with accommodation. Up to 0.4 D of corneal steepening (Pierścionek *et al.* 2001), a very small flattening in corneal radius of 0.02 mm (He *et al.* 2003) and by pharmacologically stimulating ciliary muscle contraction a steepening of 0.13 ± 0.17 D over the first four Placido rings (Yasuda and Yamaguchi 2005) have all been reported. However, the measurement techniques need to be very well controlled in order to reliably detect any corneal changes. An example is the study that measured up to 0.72 D corneal change (Yasuda *et al.* 2003). Later when the videokeratoscope alignment function was improved the corneal change was revised to 0.13 D (Yasuda and Yamaguchi 2005).

A well-controlled investigation using a videokeratoscope analysed corneal changes with accommodation (Buehren *et al.* 2003). It was revealed that when excyclotorsion that accompanies accommodation is taken into account there are no significant corneal topography changes. This offers a possible explanation for previous contradictory evidence and demonstrates that excyclotorsion needs to be considered when examining the influence of accommodation on corneal topography. Also recently using the Pentacam's rotating Scheimpflug camera the shape of both the anterior and posterior corneal surfaces were considered (Read *et al.* 2007). There was no significant change in the best-fit sphero-cylinder for either surface over an 8 mm analysis diameter. So although there has been some disagreement, when accurate techniques are used and excyclotorsion is accounted for, it seems that the corneal surfaces do not alter with accommodation.

1.3.3.3 Extra-ocular muscles and the cornea

Along with accommodation, the influence of extra-ocular muscle tension on corneal shape has been considered. Much of this work was conducted several decades ago and has not been revised using new technology such videokeratoscopes and so the conclusions remain uncertain.

Many early studies recorded small corneal topography changes with convergence (Fairmaid 1959; Löpping and Weale 1965; Mandell and St Helen 1968). It has been suggested that the contraction of the medial rectus would pull on its insertion resulting in flattening of the horizontal meridian. Although considered not to be clinically significant, this was the direction of change recorded by Fairmaid (1959) and by Löpping and Weale (1965) for pre-presbyopic but not presbyopic subjects. In conflict, Mandell and St Helen (1968) used a photokeratoscope and did not find any corneal changes with convergence or in different angles of gaze.

Indirect evidence shows that extra-ocular muscle surgery alters the corneal surface (Kwitko *et al.* 1991; Nardi *et al.* 1997), which may be due to a change in muscle tension or tractional tension (Denis *et al.* 1995; Bagheri *et al.*). However there may also be other factors that are involved including post-surgical inflammation (Denis *et al.* 1995).

Many of these studies were limited by the technology of their time and used small samples with significant individual variations. While the change in extra-ocular muscle tension from surgery seems to result in corneal changes, further investigations are needed to determine the effect of everyday extra-ocular muscle tension (convergence and angle of gaze). These should be well-controlled investigations using current technology to be able to draw sound conclusions into the influence of the extra-ocular muscles on corneal topography.

1.4 Structure and function of the cornea

The cornea is a unique avascular structure, consisting of 5 major layers: epithelium, Bowman's layer, stroma, Descemet's membrane and endothelium. These anatomical layers determine its major optical properties including the contour, transparency, surface smoothness and refractive index. As the predominant layer of the cornea, the stroma determines many of the mechanical properties of the cornea.

1.4.1 Epithelium

As the most anterior portion of the cornea, the epithelium is responsible for its physical protection and provides an optically smooth surface in conjunction with the tear film. The epithelium is approximately 50 µm thick and consists of layers of non-keratinized, stratified squamous epithelial cells. These cells are in a process dynamic equilibrium with continual self-renewal and complete turnover is estimated to occur every 3.5 to 7 days (Lemp and Mathers 1991). An increased epithelial shedding rate has been found with increased shear forces for in vitro tests on rabbit corneas (Ren and Wilson 1997). Posteriorly, a monolayer of basal cells adheres to the underlying Bowman's layer. These cells are mitotically active and as the daughter cells move towards the apical surface they change to "wing" and then superficial cells. Eventually the cells disintegrate and shed into the tear film in the process known as desquamation. This state of dynamic equilibrium has been described as the X, Y, Z hypothesis as cell loss is balanced by cell replacement (Thoft and Friend 1983). The dynamic nature of the cornea is valuable in the event of trauma as adjacent cells can slide or migrate to the damaged area (Kuwabara *et al.* 1976). There is a diurnal variation in corneal epithelial permeability due to cell mitosis which predominantly occurs between 4 hours before waking and continuing for two hours after waking (Tierney *et al.* 2008). When nonviable cells are at the corneal surface they are sloughed off, compromising the tight intercellular junctions, so barrier function is worse on waking for approximately 1 to 3 hours.

1.4.2 Stroma

The stroma accounts for about 90% of the corneal thickness and so determines many of its structural properties. Cellular components are only 2-3% of this layer with the extracellular matrix being predominant. The extracellular material is responsible for the corneas strength as it consists of collagen fibres regularly arranged in bundles embedded in a matrix of proteoglycans and glycoproteins (Duan and Sheardown 2006). There are approximately 240 layers or lamellae of these bundles throughout the central corneal thickness with increased layers in the periphery (Bergmanson *et al.* 2005). The fibrils are strongest axially and run approximately parallel with each other, their structure dictating the mechanical properties of the cornea (Daxer *et al.* 1998). In the central region of the cornea about 66% of the lamellae are preferentially oriented in horizontal and vertical directions in approximately equal proportions, while the remaining 33% are randomly oriented (Daxer and Fratzl 1997).

1.4.3 Mechanical properties of cornea

The mechanical properties of a material determine how it behaves under applied forces and loads. Any force or load applied to a material will result in stress and strain in the material. Stress represents the intensity of the reaction to force at any point and is measured as the force acting per unit area. The alteration in the shape or dimensions of a body resulting from stress is the strain or deformation. Strain is expressed in dimensionless units such as millimetres per millimetre or as a percentage. Biological materials generally have a complex non-linear stress/strain relationships, with hysteresis between loading and unloading forces (Buzard 1992).

While the epithelium has tight junctions with desmosomes and hemidesmosomes maintaining the intercellular attachments, the stroma is principally responsible for the cornea's mechanical properties. This was confirmed by loading intact corneas and corneas without an epithelium (Elsheikh *et al.* 2008). There was

little difference in the response of the two samples with the intact specimens carrying only slightly more pressure at the same deformation.

A simplified model of the material properties of the cornea uses its principal component, collagen. It is elastic, has high adhesive and tensile strength, low extensibility and a resistance to shear forces. Regional variations in the mechanical properties of the cornea are due to anatomical characteristics such as lamellar composition or orientation of the fibrils. The cornea is anisotropic with the ratio of corneal stiffness between the horizontal and vertical directions being about 3:1 (Jayasuriya *et al.* 2003). There is increased adhesive strength in the stromal periphery due to the presence of circumferential orientated lamellae (Newton and Meek 1998; Newton and Meek 1998). Similarly the higher cohesive strength exhibited by the anterior stroma is likely to be due to the more frequent intertwining of lamellae. Anatomical changes occur to the cornea with age and so it is expected that the biomechanical properties will also alter. A number of collagen fibril dimensions are dependent on age including radius, axial period and the lateral intermolecular Bragg spacing (Daxer *et al.* 1998). It has been found that the cornea increases in stiffness with increasing age (Elsheikh *et al.* 2007), altering its biomechanical properties (Kotecha *et al.* 2006).

The newly developed Ocular Response Analyser (Reichart Inc, Depew, NY) enables clinical measures of corneal biomechanics. The instrument measures intraocular pressure using a bi-directional applanation process and takes into account biomechanical properties of the cornea. A biomechanical measure is corneal hysteresis which is the ability of the cornea to absorb and dissipate the applied force while the corneal resistance factor is thought to be a measure of the viscoelastic resistance of the cornea. A number of conditions have been reported to influence these biomechanical measures. These include keratoconus (Martinez-Afanador and Ortiz-Nieva 2008), long term contact lens wearers (Xu *et al.* 2008), post-lasik surgery (Pepose *et al.* 2007; Kirwan and O'Keefe 2008), high myopia > 9.00 D (Shen, 2008), corneal thickness (Kotecha *et al.* 2006; Shah *et al.* 2006) and age (Elsheikh *et al.* 2007). While this instrument provides a

measure of corneal biomechanical properties, it is not known exactly what they physically or structurally represent.

1.4.3.1 Young's Modulus of Elasticity

A material is described as elastic if it completely recovers after deformation. The cornea demonstrates viscoelastic properties (Moses and Grodzki 1971) and so not only has an elastic response to force but also exhibits viscosity with a high resistance to flow. This means that a force on the cornea will result in a biphasic response with an immediate deformation followed by a time-dependent and usually rather slow deformation. The cornea does not have a linear stress and strain relationship but its response is complex (Nyquist 1968).

The modulus of elasticity is termed Young's modulus (E) (slope of the stress/strain curve) and is an approximation of the cornea's mechanical properties, with a smaller value representing higher elasticity and more deformation with an increase in strain. The mechanical properties of the cornea are not well understood due to the challenges associated with their measurement with estimates spanning two orders of magnitude. The large range of estimates of Young's modulus is due partly to a variety of measurement techniques. Some investigations have performed stress-strain tests on strips of excised cornea (Nyquist 1968; Nash *et al.* 1982) with estimates ranging from 9.03 to 57 MPa (Andreassen *et al.* 1980; Edmund 1988). It is questionable whether this method truly represents the mechanical properties of an in vivo cornea, as cutting a strip interrupts the structure of the stroma. Others have used intact corneas in vitro by measuring the displacement of mercury drops on the corneal surface while inducing an intraocular pressure increase. These results are between 5 and 20 MPa (Hjortdal 1996). Other in vivo techniques have modelled the cornea's elasticity based on measures during applanation tonometry, taking account of the influence of corneal thickness and intraocular pressure (Sjontoft and Edmund 1987; Orssengo and Pye 1999).

A flaw in many early investigations was the assumption that the cornea is isotropic, as it was thought that the number and diameter of the collagen fibres

per square area remained constant across all parts of the cornea (Sjontoft and Edmund 1987). However, it is now well known that the cornea is not isotropic and there are large regional and directional variations due predominantly to the variation in fibril orientation (Hjortdal 1996; Shin *et al.* 1997; Boote *et al.* 2005; Li and Tighe 2007). Jayasuriya *et al.* (2003) recorded Young's modulus to be 3, 1 and 0.3 MPa for horizontal, vertical and obliquely cut samples respectively. Regional variations are also evident when using digital image processing to study the central, paracentral, peripheral and limbal regions of the cornea, with meridional strains being smallest for the paracentral and peripheral areas and largest at the limbus, while circumferentially strains are smallest at the limbus (Hjortdal 1996).

Other factors associated with measuring corneal elasticity that may influence the results include the type of storage media, storage temperature, measurement temperature and humidity (Ahearne *et al.* 2007). Some variation in the estimates of Young's modulus may be due to the dynamic nature of the cornea and its mechanical properties. Mathematical models have demonstrated that Young's modulus is sensitive to intraocular pressure, with a 1 mmHg difference in pressure altering the elastic modulus by 7.3% (Sjontoft and Edmund 1987). Also the hydration and redistribution of water may account for some variation, as this affects the mechanical properties of biological tissues (Hjortdal 1995; Jayasuriya *et al.* 2003). For bovine corneas, it has been recorded that Young's modulus increases with decreasing hydration (Jayasuriya *et al.* 2003).

1.5 External forces on the cornea

Deliberate application of pressure can alter the cornea, provided it has sufficient force. Corneal changes have been observed after digital pressure, applanation tonometry and from contact lens wear. As well as the resultant corneal distortions from applied forces, the recovery of the cornea has also been measured. Normal healthy corneas recover their shape quickly and completely after deformation.

1.5.1 Digital pressure

Using a photokeratoscope, significant corneal curvature changes were found from digital pressure and eye rubbing of 15 seconds duration. The refractive change was at least 0.5 D and lasted for several minutes (Mandell and St Helen 1968).

Changes in corneal topography from ocular rubbing have also been measured with videokeratoscopes (Mansour and Haddad 2002). Corneal topography was measured with the Topographic Modelling System TMS-1 (Computed Anatomy Inc, New York, NY) before and after the twenty-nine subjects "gently" rubbed their closed eyelid on the cornea horizontally for 1 minute. Increases in the corneal surface asymmetric index and regularity indices were observed due partly to tear film alterations, but also due to corneal surface moulding. The induced corneal astigmatism averaged between 0.5 and 0.74 D and returned to baseline after five minutes.

The mechanical trauma of eye rubbing on the corneal surface has long been suspected to have a link with the development and/or progression of keratoconus. It has been proposed that habitual eye rubbing may cause a permanent change to the cornea (Jafri *et al.* 2004) with multivariate analysis suggesting that it is significantly associated with keratoconus (Bawazeer *et al.* 2000). However it should be noted that keratoconus and eye rubbing may be associated but not causally linked.

1.5.2 Tonometry

The two main techniques to measure the intraocular pressure (contact applanation and non-contact tonometry) both flatten the cornea as part of the measurement process.

Non-contact tonometry estimates the intraocular pressure by flattening the cornea with a jet of air. The interval of time to flatten is monitored and this is

transformed into the intraocular pressure measurement. Bowman and Carney (1978) measured corneal topography after five consecutive non-contact tonometry measurements using a photokeratoscope and no corneal distortion was observed. Similarly no change in refraction or visual acuity was found after non-contact tonometry (Augsburger and Polasky 1976). This indicates that healthy corneas recover quickly after non-contact tonometry deformation.

The corneal deformation during applanation tonometry is determined by the interaction between the external pressure applied and the intrinsic properties of the cornea. The estimation of intraocular pressure assumes that the Imbert-Fick law is upheld which states that the pressure within a sphere is approximately equal to the external force needed to flatten a portion of the sphere divided by the area that is flattened. For the standard applanation circular area with a radius of 1.53 mm, it is assumed that the surface tension of the tear film on a “normal” cornea will cancel out the resistance from corneal rigidity. However this is only applicable to surfaces that are perfectly spherical, elastic, and infinitely thin and it is now known that the cornea is not infinitely thin, elastic or homogeneous. Carney and Clark (1972) used a modified applanation tonometer probe to deliberately flatten corneas. The load was applied for between 30 and 180 seconds and the resultant corneal distortion was detected with a photokeratoscope. Small deviations in the central corneal surface were detected and recovery occurred within eight seconds after the retraction of the probe.

Biomechanical properties of the cornea influence the accuracy of intraocular pressure measurements. A mathematical model predicted that true intraocular pressure is measured by applanation tonometry for a cornea with radius of 7.8 mm, thickness of 0.536 mm, and Young’s modulus E=0.19 MPa (Liu and Roberts 2005). However variations away from these values decrease the accuracy of the intraocular pressure measurement. Using this model it was calculated that for the variation in corneal thickness and curvature in the normal population, the intraocular pressure measurement will vary by 2.87 mmHg and 1.76 mmHg respectively. Due to the large variation in measurements of Young modulus of the cornea (0.1 to 0.9 MPa), the intraocular pressure may be inaccurate by up to

17.26 mmHg. An increase in corneal stiffness with age of 16% per decade would lead to an overestimation of approximately 0.85 mmHg. This highlights the importance of corneal biomechanical properties in the measurement of intraocular pressure.

A number of new tonometry instruments have incorporated consideration of corneal parameters in the design to increase the validity of the intraocular pressure measurements. The Dynamic Contour Tonometer (SMT Swiss Microtechnology AG, Port, Switzerland) uses a contoured tip to conform the cornea to its inner curvature. This means that there is no bending or tangential forces acting on the area and so intraocular pressure measurement should be unaffected by corneal thickness or curvature (Francis *et al.* 2007). This appears to be the case for regular corneas, however further studies are required to validate the instrument for abnormal and irregular corneas (Punjabi *et al.* 2006).

The Ocular Response Analyser (Reichart Inc, Depew, NY) is a non-contact tonometer that estimates the viscoelastic properties of the cornea and takes this into consideration when estimating intraocular pressure (Laiquzzaman *et al.* 2006). The biomechanical properties are assessed by measuring the hysteresis or the ability of the cornea to absorb and dissipate energy using a bi-directional applanation process. The main measures of this instrument are corneal hysteresis (CH) and corneal resistance factor (CRT). So intraocular pressure measurements should be less influenced by corneal biomechanics using an ORA (Kotecha *et al.* 2006; Medeiros and Weinreb 2006). For this reason, it is particularly useful in situations where the biomechanical properties of the cornea are altered, for example after refractive surgery or for corneal conditions such as keratoconus (Pepose *et al.* 2007).

1.5.3 Contact Lenses

Wearing contact lenses causes changes to the cornea's shape, thickness and surface smoothness. There are many conflicting reports of the corneal topography changes from contact lens wear due to many different types of

contact lenses, wearing regimes, fitting protocols, adaptation times, time of measurements and instrumentation. Results have shown increasing mid-peripheral corneal curvature (Collins and Bruce 1993), decreasing central curvature (González-Meijome *et al.* 2003) or no significant corneal change (Carney and Bailey 1972; Yeniad *et al.* 2003).

A few decades ago corneal changes were very common due to hypoxia. However now with highly oxygen transmissible contact lenses, hypoxia is not as common, though corneal changes are still recorded. These are thought to be due to the mechanical action of the contact lens on the cornea (González-Meijome *et al.* 2003; Yeniad *et al.* 2004). It is likely that the formation of superior epithelial arcuate lesions (SEALs) when wearing these lenses also has a mechanical origin (Young and Mirejovsky 1993).

Soft tinted contact lenses can cause corneal changes corresponding to the annular tinted zone and clear pupil junction (Bucci *et al.* 1997; Voetz *et al.* 2004). Voetz *et al*. (2004) found a maximum change of 5 µm in corneal height after 1 hour of contact lens wear. Irregular astigmatism has also been reported after wearing soft tinted lenses (Schanzer *et al.* 1989) and so blurred vision and poor visual acuity are experienced.

Considering corneal regression after short-term wear of lenses, Voetz *et al.* (2004) found that corneal recovery following one hour of cosmetic tinted contact lens wear took between 2 to 3 hours. The regression of corneal changes after the long term wear of various contact lenses has also been investigated. The average time required for topography to stabilise after the removal of the lenses was 14.7 weeks (hard PMMA), 10.1 weeks (rigid gas permeable), and 5.2 weeks (soft contact lens) (Wilson *et al.* 1990). Similarly Wang *et al.* (2002) found regression times for various contact lens modalities to be 11.6 ± 8.5 weeks (soft extended-wear), 5.5 ± 4.9 weeks (soft toric), 2.5 ± 2.1 weeks (soft daily wear) and 8.8 ± 6.8 weeks (rigid gas permeable). An investigation of 42 subjects found that on cessation of soft contact lens wear, 62% had no significant corneal changes, 38% required 3 days to stabilise with all except two corneas stabilising by 14 days (Hashemi *et al.* 2008).

1.5.3.1 Orthokeratology

The corneal surface can be deliberately altered by orthokeratology contact lenses to temporarily reduce or eliminate myopia. This refractive technique was originally reported in the early 1960s, though it was not popular due to unpredictable refractive outcomes. Popularity increased in the 1990s when technology advances improved the reliability of the technique with better lens materials, designs and the introduction of videokeratoscopes to more accurately measure corneal topography. Current orthokeratology lenses are a reverse geometry design with a unique posterior lens contour. This creates a tear film layer, between the cornea and lens, which applies forces to the cornea. The technique has highest clinical efficacy for low and moderate myopia up to approximately 4 D, although higher corrections are often attempted in some Asian countries. It is not as effective for astigmatism with only half the reduction of the initial with-the-rule astigmatic error (Mountford and Pesudovs 2002).

Originally it was believed that the contact lenses caused an overall bending or flattening of the central cornea. However, over recent years it has been agreed that the primary corneal response to orthokeratology lenses is a central corneal thinning and a mid-peripheral thickening (Swarbrick *et al.* 1998; Nichols *et al.* 2000; Alharbi and Swarbrick 2003; Wang *et al.* 2003; Haque *et al.* 2004). Furthermore with the development of instruments such as the Pentacam, data of both the anterior and posterior corneal surfaces show primarily alteration of the anterior cornea rather than corneal bending (Tsukiyama *et al.* 2008). In contrast other work has reported a slight flattening of the posterior corneal surface which suggests corneal bending, though corneal oedema may have confounded this result (Owens *et al.* 2004).

Though at a cellular level it is still unclear exactly what changes take place. Cell migration has been suggested with epithelial cells moving away from the applied pressure. It has been observed in cats wearing steep silicone elastomer lenses that the epithelial cells under the lens thinned while there was thickening outside the lens edge (Holden *et al.* 1989). However it seems that cellular compression may be part of the mechanism of epithelial change as steep PMMA lenses can

create compression of all epithelial layers including broader and squashed basal cells (Greenberg and Hill 1973). While cellular compression seems to be involved, the mechanism of mid-peripheral thickening remains unexplained. Central epithelial thinning and mid-peripheral epithelial thickening have been confirmed histologically in primate (Cheah *et al.* 2008) and cat models (Choo *et al.* 2008). The amount of epithelial thinning was found to vary depending on wearing time for cats fit with orthokeratology lenses (Choo *et al.* 2008). This highlights the major role of the epithelium in orthokeratology changes.

The full effect and stability of orthokeratology is usually achieved after one week of overnight lens wear (Mountford 1998; Soni *et al.* 2003). Significant refractive changes can occur within minutes of lens insertion (Sridharan and Swarbrick 2003; Jayakumar and Swarbrick 2005; Lu *et al.* 2008) and there is generally a rapid initial recovery after lens removal which is dependent on the amount of corneal change (Polse *et al.* 1983), with the corneal changes associated with orthokeratology being fully reversible after cessation of lens wear (Kobayashi *et al.* 2008). The rapid response of the cornea is due to its viscoelastic properties and suggests that the mechanism of cellular change is something that can alter quickly in response to the applied pressure. This may be due to the structure of cells as cytoplasm (consisting of microtubules and microfilaments) which mathematical modelling suggests can store energy (Stamenovic 2005) and so cells can potentially alter and return to their original shape quickly after deformation. After wearing specially designed rigid gas permeable contact lenses, 95% recovery was achieved in 4, 7, and 8 hours after wearing the contact lenses for 1, 2 and 4 hours respectively (Horner *et al.* 1992). Hence, it has been suggested that the cornea will generally take twice as long to recover as the contact lens wearing period (Soni *et al.* 2004).

1.5.4 Biochemical response to applied force

The cornea can be subjected to a number of external forces including tension, compression, torsion, vibration and shear and to internal forces such as intraocular pressure and osmotic pressure (Tan *et al.* 2006). In response to

these forces the corneal cells may alter their shape, align perpendicular to the force, release extracellular matrix proteoglycans or increase protein and collagen synthesis. Biochemically, changes to the following proteins have been measured in response to applied force or during the corneal wound healing process. In human limbal epithelial cells, cyclic strain induces the synthesis of fibronectin and laminin V (Oh *et al.* 2006). It has also been shown that during contact lens wear, corneal epithelial cells release matrixmetalloproteinase-9 (MMP-9), a protein involved in the development and repair of tissue. The tears of contact lens wearing eyes show higher levels of MMP-9 than non contact lens wearing eyes and the levels increase with the length of lens wear (Papas *et al.* 2006). Also the transmembrane protein aquaporin-3 seems to facilitate cell migration in the re-epithelialisation of mice corneas (Levin and Verkman 2006) and during corneal wound healing, Wnt signalling proteins and MMP-12 regulate the proliferation of corneal epithelial cells to resurface defective areas (Lyu and Joo 2006). While changes in these chemicals have been found, the exact processes that occur from applied force are poorly understood.

1.6 Anterior eye morphology

1.6.1 Eyelid anatomy

The eyelids are thin, skin-covered mobile folds which act as an anterior physical barrier for the eye. The upper eyelid extends to the eyebrow where the skin is attached loosely to the periosteum, while the lower eyelid extends to the lower orbital margin where the skin passes into the skin of the cheek.

When the eye is open, the eyelids are separated by an elliptical space known as the palpebral fissure. The upper and lower eyelids meet at the medial and lateral canthi. The more rounded medial canthus supports a fleshy elevation of skin called the caruncle and lateral to this is a reddish semilunar fold, the plica semilunaris. The eyelids are supported internally by flat fibrous tissue sheets

called tarsal plates. The upper tarsal plate, semicircular in shape, is much larger than the lower plate, which is rectangular.

When the upper eyelid is raised, the skin forms a distinct fold, the superior palpebral sulcus at the border of the tarsal plate. The formation of this crease is due to the levator aponeurosis, a tendinous extension of the levator palpebrae superioris muscle which travels anteriorly and fuses with the orbicularis muscle. The corresponding lower palpebral furrow is less distinct because the lower lid does not move and therefore does not fold as much. When closed, the upper eyelid covers nearly the entire cornea while the lower eyelid rises only slightly.

The lid margins are relatively flat and from front to back are 1.95 ± 0.07 mm thick for the upper eyelid and 1.87 ± 0.06 mm for the lower eyelid (Hykin and Bron 1992). The posterior border is sharp edged while the anterior is round. From the anterior rounded edge project the eyelashes or cilia, except in the region which encircles the caruncle and plica. The posterior border of the lids lies closely against the globe. Anterior to this border are the Meibomian gland orifices and the grey line demarcating the change from external keratinised skin to the mucous membrane of the conjunctiva.

The main muscles of the eyelids are the orbicularis oculi and the levator palpebrae superioris. These are skeletal muscles which attach to the tarsal plates. The orbicularis oculi encircles the eye and extends up to the eyebrow where it interweaves with the frontalis muscle. Anatomically it can be divided into two main portions: an outer orbital component and an inner palpebral component.

1.6.1.1 Ethnic differences

The Oriental and Caucasian eyelids are similar anatomical structures but differ in the point of insertion of the retractor tendons. In Asian eyelids, the orbital septum fuses with the levator aponeurosis below the superior tarsal border rather than above as in the Caucasian eyelid. This means that orbital fat proceeds to the anterior tarsal surface resulting in a full or thickened eyelid (Jeong *et al.* 1999). Additionally the inferior extension of the orbital septum, beyond the superior

tarsal border, prevents anterior aponeurotic fibres from fanning toward the subcutaneous tissues to produce the normal eyelid crease (Doxanas and Anderson 1984; Jeong *et al.* 1999). Due to these anatomical differences eyelids can be classified as single (no crease whether the eyelid is open or closed), low eyelid crease (a crease when the eyelid is closed but not when open) and double eyelid (a crease is present when the eyelid is open and when it is closed) (Jeong *et al.* 1999). Asian eyes typically have a smaller aperture by approximately 1.0 mm horizontally and vertically (Lam and Loran 1991). Although only a small Asian sample was included in the study by Read *et al.* (2006), three main differences from Caucasian eyes were noted: smaller horizontal dimensions (both horizontal visible iris diameter and horizontal eyelid fissure), smaller upper eyelid to pupil centre distance and increased upslanting palpebral fissure (higher temporal canthus than the nasal canthus).

1.6.2 Eyelid movement

The opening and closing movement of the eyelids may be voluntary or reflex. Automatic blinking is most common and occurs at regular intervals and is a subconscious action controlled by the higher blinking centre in the cerebral cortex. Its primary function is to replenish the tear film by spreading the tears over the cornea. Spontaneous blinking occur approximately 12 to 15 times per minute (Davson 1972; Moses 1987). Reflex blinking may occur in response to external stimuli for protection due to proprioreceptive or light stimuli, concentration or from a change in fixation. The reflex closing mechanism is fast, occurring in less than 100 ms (Hung *et al.* 1977; Doane 1980). The rate of blinking decreases with eyelid squint by 50% and as blinking and squinting are controlled by the same muscle, some interaction is possible (Sheedy *et al.* 2005). Mean blink rates are significantly lower when performing tasks in downward gaze than for the same tasks completed in primary gaze (Cho *et al.* 2000).

While the same muscles are involved in opening the eyelids for blinking and upward gaze saccades, there are differences in the muscles used for blinking closure and downward gaze. Opening of the eyelids associated with both

blinking and upward saccades is achieved by activation of the levator superioris palpebrae. Eyelid movement associated with downward gaze shifts is from passive downward forces and inhibition of the levator palpebrae muscle. The orbicularis oculi is not involved in eyelid movement with downward gaze but it is involved in generating eyelid closure with a blink (Evinger *et al.* 1991). It is thought that the involvement of the orbicularis oculi muscle generates the backward and upward movement of the eye globe observed with reflex blinking, known as Bell's phenomenon (Evinger *et al.* 1984).

1.6.3 Age-related changes of the eyelids

The upper eyelid margin becomes more round and the vascularity increases with age (Hykin and Bron 1992). Changes occur in the distance from the eyelid margin to the palpebral sulcus. Eyelid parameters were measured for newborns through to individuals more than 60 years of age, and an increase in the eyelid crease height was observed between 21 to 40 years and then remained constant later in life (Cartwright *et al.* 1994). A higher skin crease with age was also reported in a study of 320 subjects aged between 10 and 90 years (van den Bosch *et al.* 1999). The lower eyelid was also considered and an increase in the position of the lower eyelid relative to pupil centre with increasing age. There is also a decrease in lower eyelid movement with age (Shore 1985), thought to be associated with the loss of eyelid tone. So there is evidence that the position and motility of the eyelids alters with age.

1.6.4 Marx's Line

Marx's line has been suggested to be the natural site of frictional contact between the eyelid margin and the surfaces of the bulbar conjunctiva and cornea. It is a line of squamous cells that extends along the entire length of the upper and lower lid margins and can be observed when stained with lissamine green or rose bengal. Scanning electron microscopy of rabbit eyelids has shown that there is a discrete zone of squamous cells immediately posterior to the tarsal gland orifices representing the mucocutaneous junction (Doughty and Panju 1995).

It is not known exactly why Marx's line stains. While fluorescein reveals corneal damage, lissamine green usually stains dead, membrane-damaged or degenerative cells and mucous proteins. Squamous epithelial cells are typically located within the body in regions that undergo contact with other surfaces, for example the cornea, skin and oral mucosa. So the anatomic features of Marx's line are consistent with tissue that is subject to mechanical trauma. There is some conjecture over this issue with another hypothesis that Marx's line is desiccated cells at the edge or base of the tear meniscus (Norn 1985).

In most subjects Marx's line is located posterior to the Meibomian gland orifices, but can occur anteriorly in a small percentage of people (Hughes *et al.* 2003). The anterior edge of this line tends to be well demarcated while the posterior border may take a slightly irregular course. Doughty *et al.* (2004) reported that Marx's line seems to be present in nearly all individuals, as 83 of 85 subjects had a prominent lissamine-stained line and it was just noticeable for the other two subjects. So it is an anatomical feature showing no obvious age or gender-related differences. In 40 subjects between the ages of 18 to 78 years, the average width of Marx's line was found to be 0.10 ± 0.09 mm (Hughes *et al.* 2003). Some ethnic differences have been observed with European subjects having a predominantly uniformly thin Marx's line and Arabic subjects having either consistently wide or narrow sections.

Sometimes adjacent posterior conjunctival tissue may also stain along with Marx's line. This has been termed lid-wiper epitheliopathy and tends to occur with soft contact lens wearers and dry eye sufferers. This staining is thought to occur if there is a compromise to the epithelium of the dynamic wiping surface. Korb *et al.* (2005) classified subjects with dry eye from tear break-up time, Schirmer test and the presence of corneal staining and found 76% of dry-eye symptomatic subjects and 12% of asymptomatic dry-eye subjects had lid-wiper staining. Lid-wiper epitheliopathy was present for subjects with dry eye symptoms but normal tear breakup time, Schirmer results and staining, suggesting that it may be an early manifestation and useful diagnostic tool for dry eye (Pult *et al.* 2008; Yan *et al.* 2008). Another investigation with contact lens

wearers found 80% of subjects with symptoms of dry eyes displayed lid-wiper staining compared with 13% asymptomatic dry-eye contact lens wearers (Korb *et al.* 2002). Additionally staining of feathery extensions from Marx's line has been reported for silicone hydrogel wearers who experience dryness symptoms (Varikooty *et al.* 2008). It has been suggested that exposure keratopathy, due to incomplete blinking, may increase the friction between the cornea and eyelids and result in lid-wiper epitheliopathy (McMonnies 2007). As Marx's line and lid-wiper epitheliopathy appear to be two different entities, care must be taken to differentiate them. Generally, lid-wiper epitheliopathy staining tends to be more posterior, diffuse and wider than Marx's line (Korb *et al.* 2005).

The laying down of the tear film layer during blinking by the eyelid wiper has been mathematically modelled (Jones *et al.* 2008). An outcome was that to achieve tear flow from under the eyelids, eyelid tension needs to be substantially higher during the closing phase than the opening phase and the eyelid margin may also need to alter.

1.7 Eyelids and the cornea

Although the cornea demonstrates remarkable stability under normal circumstances it can be influenced by the eyelids. Altered eyelid shape, thickness and position can occur due to disease processes and a high incidence of astigmatism is often associated with these conditions. Changes to the eyelids from the development, recession or surgical intervention of eyelid abnormalities may also produce changes to corneal astigmatism (Bogan *et al.* 1987). In downward gaze, the altered position of normal eyelids may produce topographical corneal distortions. These irregularities produce the visual symptom of monocular diplopia. There have been attempts to quantify the pressure of the eyelids on the ocular surface, however the results are inconclusive.

1.7.1 Abnormal eyelids and the incidence of corneal astigmatism

Ptosis is a condition when the upper eyelid is less than 2 mm from the middle of the pupil in primary gaze (Small and Meyer 2004). The incidence of astigmatism associated with ptosis is high, being reported at around 40% (Cadera *et al.* 1992; Beckingsale *et al.* 2003). However not only is there a higher incidence of regular astigmatism but also irregular astigmatism increases (Ugurbas and Zilelioglu 1999).

Along with altered eyelid position, the slant of the eyelids is also associated with astigmatism. Garcia *et al.* (2003) studied children with at least 1.5 D of astigmatism and found a statistically significant relationship between palpebral fissure slanting and both the amount and axis of corneal astigmatism. In conditions such as Down syndrome where up to 82% have upward slanting palpebral fissures, 60% have astigmatism (20% of which is greater than 3 D) (da Cunha and Moreira 1996). This is often oblique astigmatism with the right cylinder axis most likely to be approximately 135° and the left around 45° (Doyle *et al.* 1998). Other studies have linked the eyelids and astigmatism by noting the right-left symmetry of oblique astigmatism and have suggested that this is due to the mechanical action of the slanted eyelids on the cornea (Doyle *et al.* 1998; Haugen *et al.* 2001). Downward slanting of the palpebral fissure is common in Treacher Collins syndrome, with the severity of the facial and eyelid malformations showing a correlation with the presence of astigmatism (Wang *et al.* 1990).

Although the shape and position of the eyelids is normal in nystagmus, the rhythmic involuntary biphasic oscillation of the eyes moving against the eyelids appears to influence corneal astigmatism. In a cohort of 96 eyes with idiopathic nystagmus, 57.3% had with-the-rule astigmatism (Nathan *et al.* 1986). High frequencies of with-the-rule astigmatism have also been reported in other samples of subjects with nystagmus (Nathan *et al.* 1986; Wildsoet *et al.* 2000).

1.7.2 Abnormal eyelids and changes to corneal astigmatism

Corneal topography alters during the presence of eyelid masses such as chalazia (Nisted and Hofstetter 1974) and eyelid hemangiomas (Robb 1977; Plager and Snyder 1997). Cosar *et al.* (2001) presented a case report of a chalazion-induced area of central corneal flattening causing a decrease in vision. Most eyelid defects seem to place pressure on the cornea perpendicular to the negative cylinder axis, with significant correlations between the position of the eyelid mass and the cylinder axis (Robb 1977). Regression of the induced change has been observed with the resolution of the chalazia (Robb 1977) and the surgical resection of eyelid hemangiomas (Plager and Snyder 1997).

Additionally, there is ample evidence of the association between the eyelids and corneal astigmatism in relation to blepharoptosis surgery (Merriam *et al.* 1980). Among several cases, Anderson and Baumgartner (1980) reported a 7-year-old boy with 4 dioptres of with-the-rule astigmatism which regressed to 1.25 dioptres after ptosis surgery. Eyelid surgery can produce temporary corneal changes thought to be due to the repositioning of the eyelids placing abnormal pressure on the cornea (Merriam *et al.* 1980; Brown *et al.* 1999). After ptosis surgery, Holck *et al.* (1998) recorded that 72.4% of patients showed increased with-the-rule astigmatism, 13.8% increased against-the-rule astigmatism and 13.8% had no change compared to the preoperative astigmatism. Similarly 66% of children with congenital ptosis showed astigmatic changes after surgery, with 36% of these being greater than 0.75 D (Cadera *et al.* 1992). Lower eyelid ectropion surgery causes corneal topography changes with most showing an increase in with-the-rule astigmatism (Detorakis *et al.* 2005). However some of the surgery-induced corneal changes may be temporary, as post-operative astigmatic regression has been recorded. One study reviewed patients 12 months after surgery and all of the corneal changes were regressing towards the pre-operative magnitude and direction of astigmatism (Holck *et al.* 1998).

Gold weights are occasionally inserted into the eyelids in the treatment of facial paralysis to reduce the exposure of the ocular surface (Goldhahn *et al.* 1999; Mavrikakis *et al.* 2006). Implants alter the weight, height and contour of upper eyelids and so can influence the cornea. After this surgery, the mean with-the-rule astigmatism increased from 0.3 D to 1.7 D for 18 patients (Mavrikakis *et al.* 2006). However this change appears to be reversible, as the mean astigmatism of nine of these patients, who had the weight removed on recovery from the nerve palsy, reduced from 2.2 D of with-the-rule astigmatism to 1.0 D. Another example of eyelid surgery influencing the cornea, is a palpebral spring inserted into the upper lid reducing the corneal distortion that had been present with ptosis (Avni-Zauberman *et al.* 2008).

1.7.3 Normal eyelids in downward gaze and corneal changes

Considering the large number of reports of altered eyelid position in ptosis affecting corneal topography, it is not surprising that a lowered upper eyelid position associated with downward gaze in reading also causes topographical changes. As these changes are close to the corneal centre they can be easily captured by videokeratoscopes and can have a significant influence on corneal optics.

Buehren *et al.* (2003) measured the interpalpebral aperture to be 9.4 ± 0.9 mm in primary gaze reducing to 6.8 ± 1.0 mm when reading in downward gaze. Recently Read *et al.* (2006) studied anterior eye morphology in a number of vertical downward gaze angles. The average vertical palpebral aperture of 76 Caucasian subjects was 9.7 mm in primary gaze decreasing to 7.9 mm (20°down gaze) and to 6.4 mm (40° down gaze). Other eyelid morphometry changes occurred with down gaze including a downward tilt (toward temporal canthus) and flattening of the morphometry of both the upper and lower eyelid margins.

Altered corneal topography, specifically astigmatism, occurs with lid retraction and narrowed palpebral apertures (Wilson *et al.* 1982; Grey and Yap 1986;

Lieberman and Grierson 2000). Typically the direction of astigmatic change expected in relation to the mechanical effects of the eyelids on the cornea is in the 90°/180° direction (Robb 1977). Recently Han *et al.* (2007) agreed that deliberate narrowing of the palpebral aperture influences 90°/180° astigmatism more than the 45°/135° meridians.

The corneal changes measured after downward gaze have a clear association with the position of the eyelids during an assigned reading task (Golnik and Eggenberger 2001; Buehren *et al.* 2003; Collins *et al.* 2006). Typically tangential topography maps show a band of change across the cornea. Refractively, the change in corneal optics is a small hyperopic shift (flattening of the cornea) and an against-the-rule astigmatic alteration. In terms of best fit sphero-cylinder change in corneal topography, Buehren *et al.* (2003) found up to 0.37 D alteration in sphere, 0.41 D in cylinder and 30 degrees rotation of the axis. In terms of wavefront aberrations these wave-like distortions are mainly described by primary astigmatism (with-the-rule to against-the-rule change), vertical coma, and trefoil x 30 degrees (Buehren *et al.* 2003; Collins *et al.* 2006). Similarly Han *et al.* (2007) recorded changes in defocus, 90/180 astigmatism, vertical coma and spherical aberration between narrowed and wide-open eyelid positions.

These eyelid-induced corneal changes have been studied for a variety of reading conditions. Generally the eye movements associated with reading cause greater corneal changes than steady fixation tasks which have limited eye movement. Also greater angles of downward gaze cause larger corneal changes (Collins *et al.* 2006). Considering specific near tasks, reading and microscopy generally exhibit larger and more centrally located changes compared with computer tasks (Collins *et al.* 2006). In this study, 6 of the 9 subjects showed statistically significant corneal bands of distortion after reading, 5 subjects showed changes for the microscopy task and there were almost no changes after the computer task. The magnitude and location of the changes was related to the position of the eyelids during each of the tasks.

Vasudevan *et al.* (2007) measured the corneal topography changes of 19 subjects reading at 30° downward gaze using the Orbscan (Orbtek Inc., Salt

Lake City, UT, USA). However the changes recorded were much smaller than previous studies. A major difference in this investigation was that the reading task was interrupted by measurements over the hour period. Also the changes in corneal topography were analysed at a set corneal location for every subject rather than customising the analysis depending on the location of the eyelid-induced change. It is likely that both these factors resulted in smaller measured corneal changes compared to previous studies.

The regression of the corneal changes caused by the eyelids in downward gaze has also been investigated. It has been shown that corneal recovery is approximately equal to the length of time spent reading (Collins *et al.* 2005). However no matter how long the period of reading, rapid recovery occurs within the first 10 minutes after ceasing reading. This is in agreement with previous anecdotal reports. Knoll (1975) stated that the persistence of his own monocular diplopia after near work was dependent on the length of reading, but generally required several hours to recover (provided no further near work was undertaken). Golnik and Eggenberger (2001) reported that after a 95 minute task, symptoms resolved and topography returned to baseline within 60 minutes.

1.7.3.1 Monocular Diplopia

Monocular diplopia may be due to optical, structural or neurosensory anomalies, however the most common cause of monocular diplopia is corneal irregularity (Stampfer and Tredici 1975) from conditions such as map-dot-fingerprint dystrophy (Orndahl and Fagerholm 1998), keratoconus (Takei *et al.* 2001), pterygia (Walland *et al.* 1994), contact lens induced corneal warpage (Takei 2002), and decentralized or inhomogeneous laser surgery ablations (Orndahl and Fagerholm 1998; Hersh *et al.* 2000; Takei *et al.* 2001; Chalita *et al.* 2003). The corneal distortions caused by eyelid pressure often result in vertical monocular diplopia (Mandell 1966; Bowman *et al.* 1978; Carney *et al.* 1981; Goss and Criswell 1992; Ford *et al.* 1997; Golnik and Eggenberger 2001; Collins *et al.* 2005).

One of the first records of monocular diplopia was a case report of a 20 year-old student complaining of vertically doubled images after 1 hour of reading (Mandell 1966). The conclusion that the diplopia was due to a corneal anomaly was drawn from a pinhole test, keratometer mire distortions, steepening of the vertical meridian and the disappearance of the doubling when rigid gas permeable contact lenses were worn. Knoll (1975) described his personal experiences of primarily vertical monocular diplopia which he could induce in a matter of minutes by completing near work. The amount of diplopia seemed to be related to the length of reading and was easiest to discriminate when viewing a bright object on a dark background. His investigations showed that the symptoms could be prevented by supporting his upper eyelids with his thumbs during reading. Bowman and Carney (1978) published the first quantitative data of the corneal irregularity causing monocular diplopia using Clark's auto collimating photokeratoscope. There were superior corneal distortions that closely aligned with the position of the upper eyelid during reading. Using ray tracing, Carney *et al.* (1981) established a direct relationship with a strong correlation between the predicted position of the secondary images and the subjective report of monocular diplopia. Another case featured an individual who experienced monocular diplopia due to a narrow palpebral aperture when watching television in a reclined position (Goss and Criswell 1992).

Ford *et al.* (1997) used a videokeratoscope and found a change of 2.5 D between the areas of steepening and flattening for monocular diplopia symptomatic subjects, whereas there was no significant corneal topography change for the asymptomatic subjects. The development of corneal distortions and monocular diplopia seemed to be related to the palpebral aperture size during reading as the symptomatic group had statistically significant narrower palpebral apertures than the control group in downward gaze. Golnik and Eggenberger (2001) also showed that the changing eyelid position on the corneas was responsible as the subjects experienced monocular diplopia after reading in downward gaze but not after reading in primary gaze.

1.7.4 The pressure of the eyelids on the cornea

There have been several attempts to quantify eyelid pressure as its measurement has a number of applications including eyelid reconstructive surgery and the design of contact lenses as the eyelids are critical in determining the behaviour of the lens (movement, centration, rotation and distortion) on eye.

Eyelid pressure has been measured using modified scleral contact lenses (Table 1-3). The lens designed by Miller (1967) had a water-filled rubber balloon on the inner side and a catheter connected a pressure transducer on the outer side. The average change in pressure for 10 subjects was quantified as 2.8 mmHg for a light blink, 3.2 mmHg for a gentle blink, 10.3 mmHg for a deliberate blink and 51 mmHg for a hard squeeze. However a second scleral lens had to be worn to protect the cornea which meant that the total thickness of the scleral contact lens sandwich was 2.5 mm at the apex. This thickness would likely alter the normal relationship between the eyelids and the corneal surface. An aspect of the methodology that has been criticised is that there was no way to ensure that the balloon was filled with gas-free water, as any air present would inflate the readings (Lydon and Tait 1988). In their own investigation Lydon and Tait (1988) used a scleral shell with a silicone elastomer contact lens over the top to create a small chamber which was filled with sterile gas-free water. While the quantification of the eyelid pressure was not published they concluded that the lid pressures were “small”. A scleral contact lens system was also used to measure 21 subjects with average results of 1.7 mmHg for normal lid closure and 19.63 mmHg for a tight eyelid squeeze (Shikura *et al.* 1993). There was a large range in measured eyelid pressure for normal eyelid closure from -0.50 to 6.7 mmHg.

There have been indirect measures of eyelid pressure. A modified manometer and cannula apparatus was used to measure the change in pressure in the retro-bulbar space (Moller 1954). This is an indirect technique as it measures the force of the eyelids that has been dissipated through the entire eye rather than

Table 1-3: Eyelid pressure measurements

Reference	*Instrument*	*Number and Age of subjects*	*Mean measurement (reported units)*	*mmHg*
Moller (1954)	Manometer measuring intra-orbital pressure in the retrobulbar space (indirect measure)	n = 1	Gentle: 10 mm H_20 Voluntary blink: approx 20 mm H_20 Forced squeeze: 55 mm H_20	0.7 1.4 3.6
Miller (1967)	Scleral lens-rubber balloon combination filled with water, connected to a pressure transducer, 2.5mm thick at contact lens apex.	n = 10 17-35 yrs	Light: 2.8 ± 2.2 mmHg Gentle: 3.2 ± 1.2 mmHg Deliberate: 10.3 ± 2.3 mmHg Hard squeeze: 51 ± 14.6 mmHg	2.8 3.2 10.3 51
Lydon and Tait (1988)	Manometer system, scleral lens with attached silicone elastomer lens over the top to form a water-filled chamber	n = 9 20-35 yrs	"small"	-
Shikura, Yamaguchi, Nakajima (1993)	Contact lens shaped capsule filled with water	n = 42 (21 subjects)	Normal lid closure: 1.7 mmHg Tight squeezing: 19.63 mmHg	1.7 19.63

measuring the pressure between the cornea and eyelid surfaces. The results for voluntary blink and a forced eyelid squeeze were 1.4 and 3.6 mmHg respectively. Another indirect measure of the pressure influence of the eyelids is the change in intraocular pressure with blinking. Coleman and Trokel (1969) took direct intraocular pressure readings by inserting a needle into the anterior chamber of a subject who was to have the eye enucleated. The pressure measurements were 5 to 10 mmHg during normal blinking and greater than 70 mmHg for squeezing the lids.

These results indicate that although the pressure of the eyelids has significant influence on the cornea, its magnitude is small. The studies that directly measured eyelid pressure were disadvantaged by the complexity of the instrumentation and the techniques may not have been sensitive enough to accurately quantify small pressures. There is a wide variation in the measurements of eyelid pressure, as a number of subjective blinking and lid squeeze conditions have been considered. Some indirect techniques have been used but only give an estimate of the influence of the eyelids on the corneal surface.

1.7.4.1 Measurement of eyelid tension

If the eyelid is assumed to act like an elastic spring, its tension is related to the pressure it exerts on the corneal surface. A few studies have examined eyelid tension as it is thought to be related to rigid lens flexure (Ehrmann *et al.* 2001) and overnight RGP adherence (Swarbrick and Holden 1996).

From dynamic transducer measurements made during blinking on four subjects, the passive spring constant of the eyelid was estimated at 1.5 gm/mm (Hung *et al.* 1977). This was estimated by loading the upper eyelid with weights while the subject maintained 45° downward gaze. Vihlen and Wilson (1983) measured 100 subjects and found the average force to pull the upper eyelid away from its resting position to be 3.33 gm/mm. These subjects ranged in age from 20 to 80 years and the study reported a decrease in eyelid tension (elastic coefficient) with

increasing age. Also Evinger, Manning and Sibony (1984) measured the upper eyelid tension on three subjects to be 10 gm/mm while looking straight ahead, which reduced to 2.5 gm/mm in 40° downward gaze.

More recently a tensiometer was designed and used to investigate the difference in upper eyelid tension between Asian and Caucasian subjects (Ehrmann *et al.* 2001) and to quantify the tension of the lower eyelids (Francis *et al.* 2006). These studies found no difference in the upper eyelid tension between Asian and Caucasian subjects (Ehrmann *et al.* 2001) nor was there a decrease in lower eyelid tension with age (Francis *et al.* 2006). Although tension and pressure may be linked mathematically there are many assumptions involved to describe the eyelid as an elastic spring. So although eyelid tension is undoubtedly associated with eyelid pressure on the cornea, it is unlikely to be directly related to the pressure exerted by the eyelids on the corneal surface.

1.8 Rationale

There is extensive evidence that the eyelids exert pressure on the anterior corneal surface. Pressure from both abnormal eyelids due to pathology and normal eyelids in downward gaze can cause subtle, temporary corneal topography changes. Videokeratoscopes allow detailed investigation of the cornea after reading, showing bands of wave-like corneal distortion that run parallel to the eyelid margin. Yet little is known about how the eyelids contact the ocular surface and what pressure distribution exists between the eyelids and cornea. Figure 1-7 is a summary of the current state of knowledge of the contact between the eyelids and the cornea. The aim of this thesis is to provide further knowledge of the characteristics and magnitude of eyelid pressure on the ocular surface.

In contrast to previous studies that have used hour long near tasks, we are interested to investigate the corneal changes due to eyelid pressure after 15 minutes of near tasks. We hypothesise that eyelid pressure from short-duration tasks, which more closely replicate everyday near tasks, may still lead to

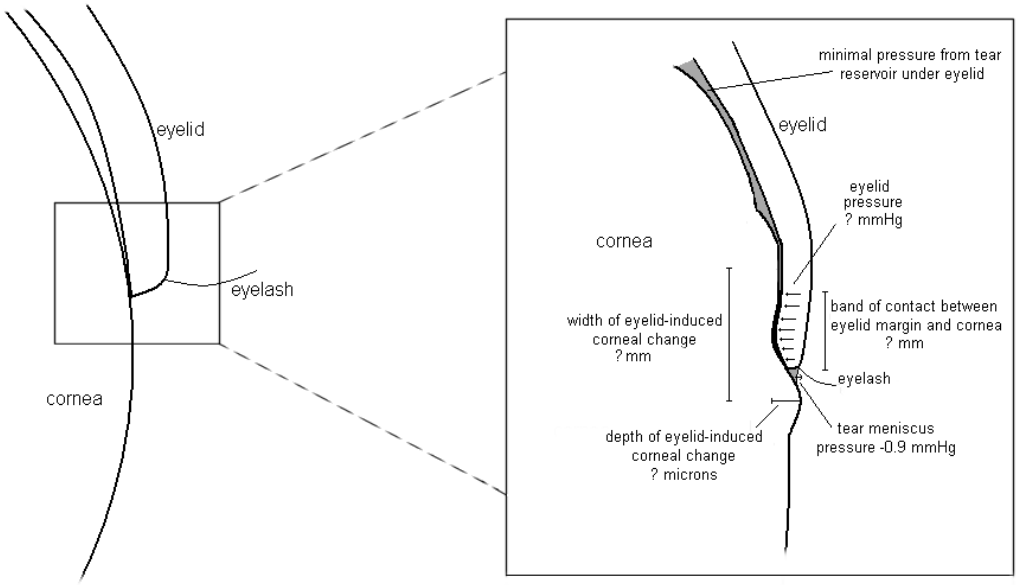

Figure 1-7: Schematic of current knowledge of the eyelid and cornea relationship. Corneal curvature and refractive changes due to the eyelids have been previously measured though the width and depth of the corneal changes are unknown. There is evidence that a band of the eyelid margin is the primary contact with the ocular surface and is likely to be wider than Marx's line width of 0.10 ± 0.09 mm (Hughes *et al.* 2003). The pressure of a static eyelid has not been previously reported but during blinking ranges from 1.7 to 51 mmHg (Miller 1967; Lydon and Tait 1988; Shikura *et al.* 1993). The tear meniscus is estimated to have an outward pressure of -0.9 mmHg (Jones *et al.* 2008).

measurable changes in the corneal shape and influence refraction. The role of eyelid morphology will be examined by analysing associations between the eyelid shape, tilt or position with the corneal refractive change after the near tasks. As Marx' line has been implicated in contact with the ocular surface, its width will also be examined for any association with the corneal changes.

The changes in elevation topography maps, which most closely represent the physical change of the cornea, will be considered. The corneal changes will be compared for different angles of downward gaze and different eye movement conditions (reading and steady fixation) and the relative effects of the upper and lower eyelids will also be considered. By analysing the characteristics of corneal change, inferences can be drawn about the relative eyelid pressure in these conditions.

While these eyelid pressure inferences will give some insight into eyelid-induced corneal changes, direct measurement of eyelid pressure would provide important further information. The three previous published attempts to measure eyelid pressure are somewhat inconclusive. This was largely due to the complex techniques using manometers and modified contact lenses, which were cumbersome when inserted into the eye. Alternative methods for eyelid pressure measurement using thin tactile piezoresistive sensors will be explored to allow the pressure to be measured directly between the eyelid and contact lens.

The contact region between the eyelids and cornea also needs consideration. Previous work suggests that a band of the eyelid margin is in primary contact with the ocular surface and Marx's line has been implicated as part of this region of contact. New techniques will be investigated to measure the region of contact. From these measurements of eyelid pressure and contact width, models of eyelid pressure could be developed. The results of these studies will improve our understanding of the influence, contact region and pressure distribution of the eyelids on the ocular surface.

Chapter 2: Corneal topography changes and eyelid morphometry during downward gaze

2.1 Introduction

The cornea is the principal refractive component of the eye and so the regularity and stability of its surface is important for clear vision. However, the topography of the corneal surface is not fixed and is known to be susceptible to the pressure exerted by the eyelids. Increased or altered pressure from abnormal eyelids can produce topographical corneal changes. Astigmatic changes from eyelid chalazia and hemangiomas are dependent on the size and location of the eyelid defect (Nisted and Hofstetter 1974; Robb 1977). Ptosis also causes changes in corneal astigmatism (Cadera *et al.* 1992; Beckingsale *et al.* 2003) with blepharoptosis surgery partially reversing the induced change (Anderson and Baumgartner 1980; Cadera *et al.* 1992; Holck *et al.* 1998; Brown *et al.* 1999).

The retraction or narrowing of normal eyelids influences corneal shape (Wilson *et al.* 1982; Grey and Yap 1986; Lieberman and Grierson 2000). Typically the change due to the mechanical effect of the eyelids on the cornea with a narrow aperture is to 90°/180° degree astigmatism (Grey and Yap 1986). In downward gaze the palpebral aperture is smaller (7.9 mm in 20° downward gaze and 6.4 mm in 40° downward gaze) than in primary gaze (9.7 mm) (Read *et al.* 2006). The altered position of the normal eyelids on the cornea in downward gaze has been found to have a clear association with bands of wave-like corneal topography change parallel to the eyelid margins (Buehren *et al.* 2001; Golnik and Eggenberger 2001; Collins *et al.* 2006). These corneal changes can be optically and clinically significant with up to 0.37 D alteration in sphere, 0.41 D in cylinder and 30 degrees rotation of the axis being recorded after 60 minutes reading (Buehren *et al.* 2003).

Corneal irregularity after reading has often been linked with the visual symptom of vertical monocular diplopia (Mandell 1966; Knoll 1976; Bowman *et al.* 1978;

Carney *et al.* 1981; Goss and Criswell 1992; Kommerell 1993; Ford *et al.* 1997; Campbell 1998; Golnik and Eggenberger 2001). While thorough testing determined that the monocular diplopia was of corneal origin it has only been with the use of modern videokeratoscopes that the causative corneal irregularities can be accurately studied.

Marx's line extends along both the upper and lower eyelid margins and can be visualized by staining with rose bengal or lissamine green vital dyes (Marx 1924; Norn 1980; Hughes *et al.* 2003). Squamous epithelial cells are typically located within the body in regions that undergo contact with other surfaces, for example, the cornea, skin and oral mucosa. Its anatomical features are consistent with tissue that is subject to mechanical trauma. The squamous cell phenotype of this tissue and staining properties of this region suggests that it is subject to mechanical contact and so may be involved in contacting the ocular surface (Parsons 1904; Hughes *et al.* 2003; Doughty *et al.* 2004). Doughty *et al.* (2004) reported that Marx's line seems to be present in nearly all individuals and is an anatomical feature with no obvious age or gender-related differences.

While it is known that the eyelids cause corneal changes, little is known about the distribution of eyelid pressure, the exact eyelid contact area or the biomechanics of the corneal changes. Previous investigations have considered eyelid-induced corneal changes in different downward gaze angles, eye movements and a variety of tasks including reading, microscopy and computer work (Collins *et al.* 2006; Collins *et al.* 2006). In this study a localised topographical analysis method was developed to determine the magnitude and width of the corneal changes for both the upper and lower eyelids after four downward gaze tasks, involving 2 angles of vertical downward gaze (20° and 40°) and 2 visual tasks (reading and steady fixation). This allowed the influence of the downward gaze angle and the role of eye movements on topographical change to be examined as well as the nasal, central and temporal variations. Analysing the eyelid-induced corneal changes for all these conditions allowed the relative eyelid pressure to be inferred.

Previous investigations have analysed corneal changes after reading sessions of one hour (Buehren *et al.* 2003; Collins *et al.* 2006). In this study the task length

was 15 minutes so that the corneal refractive changes could be assessed after task durations more commonly used in everyday life. Another objective of this study was to examine associations between the corneal topography changes and eyelid morphometry. Digital photographs were taken in downward gaze so that the shape and position of the eyelids were recorded. By comparing corneal changes and eyelid features, the role of eyelid morphometry in the production of the induced corneal changes was examined. Photographs were also taken of lissamine-stained Marx's line to assess whether its dimensions are associated with the eyelid-induced corneal changes.

2.2 Methods

2.2.1 Subjects

Eighteen young subjects, aged between 19 and 29 years with an average age of 23 ± 3 years, were recruited for this study. The subjects consisted of equal numbers of males and females and there were eight emmetropes (±0.25 D) and ten myopes (greater than -0.25 D). The average refractive error was -1.22 ± 0.66 D and ranged from +0.25 to -5.75 D with -0.75 D or less of astigmatism.

Within this cohort there were eight subjects of Eastern Asian origin (Chinese, Japanese, Korean, Malaysian or Thai) and ten with a Caucasian background. The subjects were predominantly staff and students of the Queensland University of Technology, School of Optometry. Only the left eye was tested for each subject to avoid issues associated with enantiomorphism in eyelid morphometry and corneal topography (Rabinowitz and Klyce 1993; Lam *et al.* 1995).

2.2.2 Preliminary screening

Testing was undertaken to screen subjects in relation to the inclusion and exclusion criteria of the study. This involved slit lamp biomicroscopy to examine the anterior eye, administering the McMonnies dry survey, non-invasive tear break up time (NIBUT) using the videokeratoscope mires, subjective refraction and visual acuity measurements.

Inclusion criteria for subjects included corrected acuity of 0.0 logMAR or better, normal ocular health (including clear corneas without scarring or opacities), a stable tear film, able to comply with eyelid eversion and no history of ocular surgery.

Conditions that excluded subject participation were active blepharitis, conjunctivitis, Meibomian gland dysfunction and dry eye, as they have the potential to alter eyelid morphometry, ocular surface health and the staining of the eyelid margin (Norn 1985; Korb *et al.* 2002; Korb *et al.* 2005). A diagnosis of dry eye was made on the basis of dry eye symptoms (McMonnies score ≥ 14) and reduced tear film stability (NITBUT < 10 secs). A NITBUT of less than 10 seconds has been found to have a diagnostic sensitivity and specificity of 82% and 86% (Mengher *et al.* 1986).

Various exclusion criteria were used to minimise previous topographical alterations from eyelid pressure and contact lenses. Subjects were excluded if they had a history of rigid gas permeable contact lens wear. Prior to testing, the subjects were instructed to refrain from soft contact lens wear in the preceding 32 hours (Hartstein 1965; Harris *et al.* 1975; Holden *et al.* 1985; Wilson *et al.* 1990; Swarbrick *et al.* 1998; Liu and Pflugfelder 2000) and to avoid any substantial reading on the morning of the experiment (Buehren *et al.* 2003; Collins *et al.* 2005; Collins *et al.* 2006).

2.2.3 Protocol

The research protocol was approved by the University Human Research Ethics Committee (Appendix 1) and adhered to the tenets of the Declaration of Helsinki. An information sheet was provided and written consent was obtained from each study participant.

The protocol was designed to allow investigation of the effects of eyelid pressure in four downward gaze conditions. This involved combinations of 2 downward gaze angles (20° and 40°) and 2 visual tasks (reading with gaze shifts and steady fixation without gaze shifts). A downward angle of approximately 25° has been reported for recreational and study-related reading (Hill *et al.* 2005). So the 20°

downward gaze conditions of this study most closely represent the vertical gaze angle usually adopted during reading, while the 40° conditions examine a more extreme angle. So the 4 conditions studied were reading at 20° downward gaze, steady fixation at 20° downward gaze, reading at 40° downward gaze and steady fixation at 40° downward gaze.

Each condition was tested in the morning on separate days, typically between 9 and 11 am, to minimise the influence of prior visual tasks on corneal topography.

2.2.3.1 Pre-task topography

Six baseline corneal topography measurements of the left eye were taken using the Medmont E300 Corneal Topographer (Medmont Pty. Ltd., Victoria, Australia). This videokeratoscope has a high level of accuracy with a RMSE of 2 µm for both spherical and aspherical test surfaces over a 7 mm diameter and small standard errors for precision (Tang *et al.* 2000). For normal human corneas the Medmont has also been reported to have a high level of repeatability (Cho *et al.* 2002). Each subject was instructed to blink, open their eyes wide and to maintain fixation on the instrument target while the image was captured. The instrument was then realigned between measurements. Maps with irregularities, for example due to tear film instability, were excluded. Only videokeratoscope images with an overall score (Medmont E300 calculates this score based on centration, distance and movement scores) of 97% or greater were accepted. The average score of all the measurements used in analysis was 98.5%.

2.2.3.2 Eyelid morphometry

Digital images of the anterior eye structure were recorded using a Canon 300D 6.3 megapixel SLR camera with a 100 mm macro lens. The camera was set to manual mode with an f-number of 32 and an exposure time of 1/60 second with an automatic flash. Three custom built camera mounts allowed images to be taken in primary gaze and 20° and 40° downward gaze (Figure 2-1 shows the 40° version).

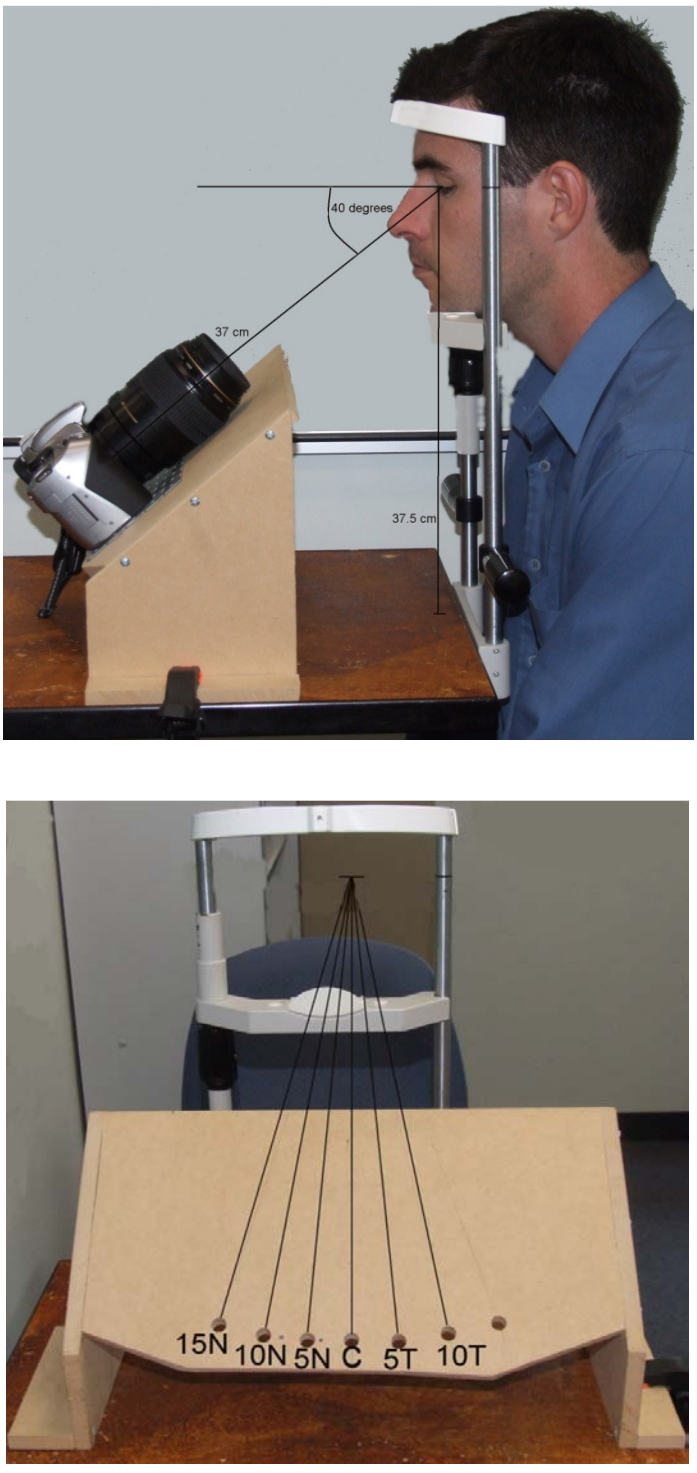

Figure 2-1: A) Subject fixating at the camera in 40° downward gaze B) Camera mounting positions on the platform at 15° nasal, 10° nasal, 5° nasal, central, 5° temporal and 10° temporal with respect to the left eye.

This set-up allowed the subject to be positioned in a head rest with their eye at a known height of 37.5 cm above the table. Horizontal adjustments could be made for intersubject variations of the inset of the eye. This means that when the camera was mounted at the chosen angle of either 20° or 40°, the camera was at a known distance of 37 cm from the eye. With the vertical height and angle of the camera fixed and the horizontal distance adjustable for fine tuning of alignment, every image had the same scale ratio (i.e. real eye to digital image scale).

The camera mounts not only allowed the camera to be fixed at the required vertical downward gaze angles of 20 and 40 degrees, but also to pivot horizontally around the centre of rotation of the left eye in order to capture images with the eyes in various horizontal gazes (Figure 2-1).

A total of 6 images per vertical gaze angle were taken, one for each horizontal angle (15° nasal, 10° nasal, 5° nasal, central, 5° temporal and 10° temporal). These angles encompass the approximate range of horizontal eye positions when viewing text with a width of 17 cm (A4 page) at a reading distance of 40 cm. It has been shown that head movements contribute only approximately 5% of the total head and eye movement with reading (Seo and Lee 2002), so it is predominantly eye movements that are responsible for horizontal gaze alteration during reading.

2.2.3.3 Visual tasks

The subject then completed one of the four 15 minute visual tasks. The order of the four tasks was randomised between subjects. For each of these tasks the subject was positioned in the head rest to ensure consistency of eye position and eyelid morphometry with the digital photography images (Figure 2-2).

With the standard fluorescent room lighting, illuminance was approximately 300 lux at the plane of the visual task. The visual stimulus was located approximately 40 centimetres from the eye with the reading text subtending a horizontal angle of 24 degrees. This is comparable to an A4 page at 40 centimetres. Three lines of N12 text (standard novel font size) were visible at any one time through a

Figure 2-2: Visual task positioned at 40° downward gaze, approximately 40 cm from the subject.

cut-out window and a mouse or keyboard was used to scroll the text to allow continuous reading throughout the 15 minute task. This set-up ensured that the subject's eye movements were primarily in the horizontal plane. During the 15 minute steady fixation tasks a fixation cross was visible in the centre of the cut-out window and subjects were encouraged to listen to music to aid concentration on this target. Subjects were instructed to blink naturally during all four tasks.

2.2.3.4 Post-task topography

Immediately following the near task, six topography measurements were captured. These measurements were taken within two minutes after the completion of the task, as there is a sharp decline in the magnitude of eyelid-induced corneal distortions immediately following the cessation of the near task (Collins *et al.* 2005).

2.2.3.5 Marx's line

A lissamine green impregnated strip, wetted with two drops of sterile saline was applied to the superior and inferior bulbar conjunctiva of the left eye. To aid even distribution of the dye, the subject was instructed to blink a few times and to lightly rub the eye through the closed eyelid. Images of Marx's line were captured using the Canon 300 D digital SLR camera and a 100 mm macro lens. A fluorescent lighting ring was mounted on the end of the macro lens to obtain even illumination. The camera was manually focused at the setting 0.31 m with an f-number of 2.8 while the exposure time was automatically optimised by the camera and typically was about 1/60 of a second. To view Marx's line, the upper eyelid was everted, holding the eyelashes while avoiding finger contact with the eyelid margin. The lower eyelid was rotated away from the globe to expose the inferior palpebral conjunctiva. With the level of focus at 0.31 m, the camera was moved until Marx's line was in focus, which standardized photography between the subjects. A horizontal width of approximately 14 mm of the eyelid margins was photographed.

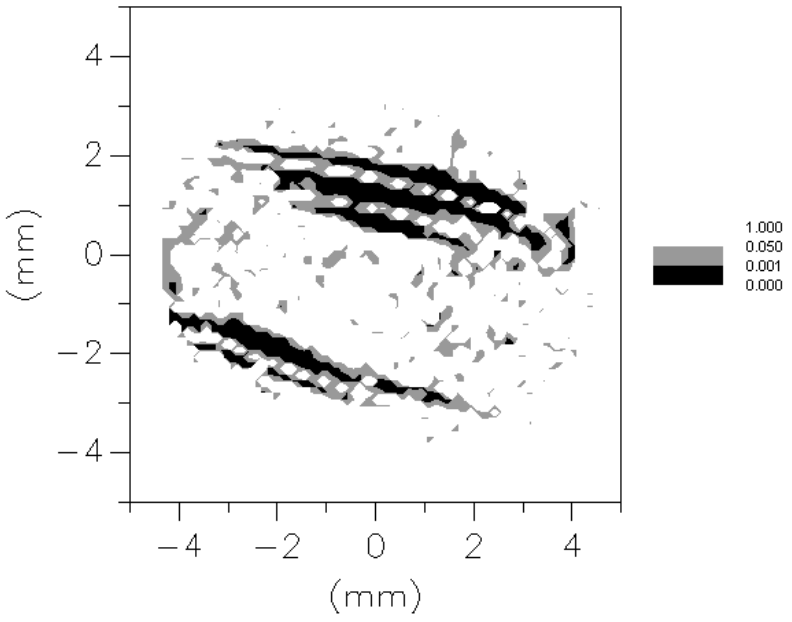

Figure 2-3: Significance map based on t-test at all points within the map. Highly significant regions ($p<0.001$) are shaded black, $p<0.05$ grey and $p>0.05$ white.

Table 2-1: Subjects with bands of significant topography changes induced by the eyelid within the central 6 mm.

Total subjects = 18	*Downward gaze angle 20°*		*Downward gaze angle 40°*	
	Reading	Steady fixation	Reading	Steady fixation
Upper eyelid-induced change	18	14	17	18
Lower eyelid-induced change	7	3	16	13

2.2.4 Data analysis

Following data collection corneal height, tangential power and refractive power data were exported from the videokeratoscope. The mean number of maps exported per condition was 6 and ranged from 4 to 7 maps. Corneal topography data were analysed using custom written software. For each subject and condition the data were averaged by interpolating into 300 common meridians, with a radial point spacing of 0.13 mm. This spacing minimises the required interpolation, as it is similar to the spacing of the data points exported from the Medmont E300 videokeratoscope.

To examine eyelid-induced corneal changes after the visual tasks, tangential power and elevation difference maps were calculated by subtracting the average pre-task topography map from the average post-task map for each subject. Significance maps were generated by performing a two-tailed t-test on every point of the tangential power difference maps (Buehren *et al.* 2001). This enabled areas of the cornea with significant changes to be located (Figure 2-3).

Inspection of the tangential difference significance maps enabled determination of the tasks and individual subjects that demonstrated significant ($p<0.05$) horizontal bands of eyelid-induced change within the central 6 mm of the cornea. This diameter was chosen for analysis as it maximised the corneal area analysed but minimised missing data. Every subject showed a band like change across the superior cornea after at least 2 of the 4 task conditions. For the inferior eyelid induced changes, all but 2 subjects had bands of significant change after one or more of the tasks. Table 2-1 shows the number of subjects with horizontal bands of significant corneal change from the upper and lower eyelids for each of the tasks.

2.2.4.1 Localised elevation analysis

The following procedure was developed to analyse the localised eyelid-induced corneal topography changes. The elevation difference topography maps were chosen for analysis as they most closely represent the physical corneal change. The most distinct feature of an eyelid-induced corneal change is the valley or

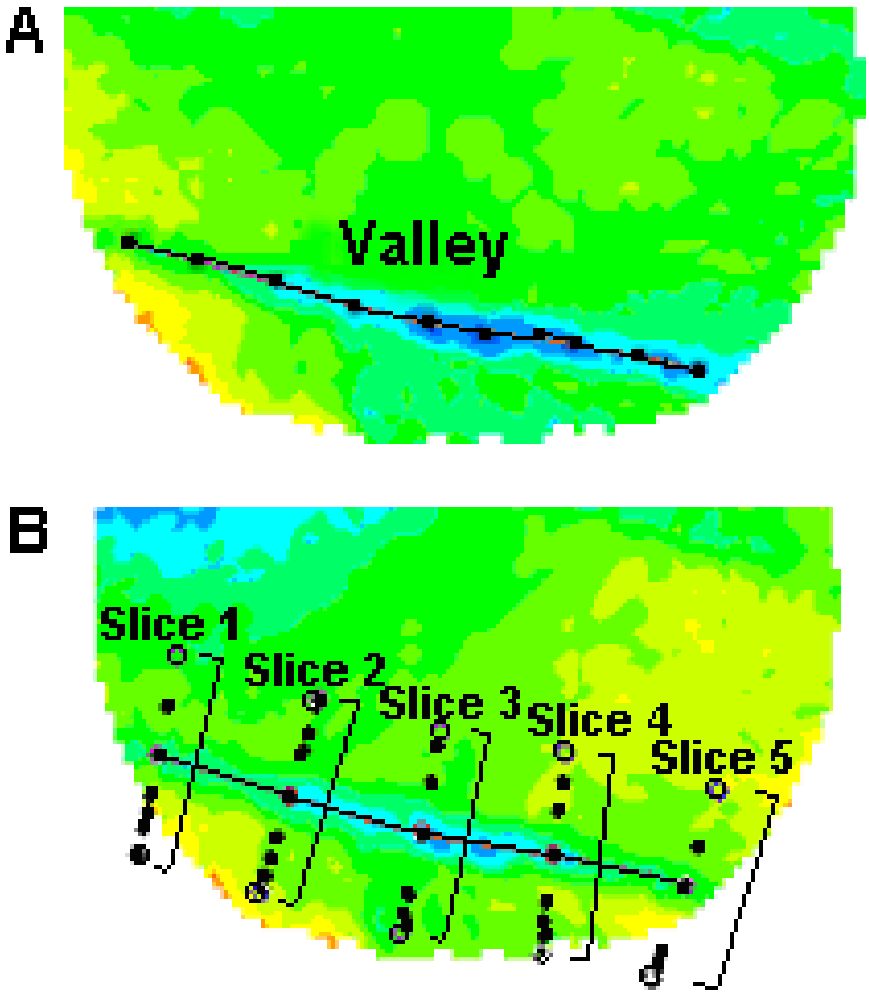

Figure 2-4: A) Points selected along valley and fit with a 4th order polynomial fit, B) plane removed and 5 cross-sections (for viewing simplicity) fit normal to the valley line, 2 mm width and peaks and valleys (zero slope points) indicated by filled circles. Open circles define the start and end of each cross-section and along with the first and last cross-section, form the limits of the analysed localised region.

depression, so this was chosen as the reference point. User-selected points were chosen along the valley and these fit with a 4th order polynomial function (Figure 2-4A).

Cross-sections of data were taken perpendicular to the polynomial function, extending 1 mm either side. The spacing between the cross-sections was 0.05 mm, which is the approximate spacing of Medmont data at 2 mm from videokeratoscope map centre (the average distance from the centre to the eyelid-induced valley). Therefore the number of cross-sections taken depended on the horizontal extent of eyelid-induced corneal change. The limits of these cross-sections define the localised area under consideration (refer to open circles and first and last cross-sections in Figure 2-4B).

Across the 2 mm of each cross-section, 16 points were interpolated with a spacing of 0.13 mm, replicating the Medmont topographer's normal radial spacing of data points. Each cross-section was fit with a 9th order polynomial function, which was the lowest order found to minimise the fit error and so closely represented the original data. The maxima and minima (peaks and valleys) were determined by locating when the first derivative of the fit was equal to zero. The peaks and valley of corneal change for each cross-section are evident in the cross-sectional data (Figure 2-5) and indicated as filled circles in Figure 2-4B.

As a measure of the magnitude of the eyelid-induced corneal change, peak-to-valley amplitudes were calculated from the difference topography maps (Collins *et al.* 2005). An example of a tangential difference map with an upper eyelid induced corneal change and the corresponding cross-section of data for the 90 meridian are shown in Figure 2-6. Peak-to-valley amplitudes were calculated from the valley towards the centre of the cornea (central peak-to-valley) and from the valley towards the edge of the cornea (peripheral peak-to-valley). The distance from the central peak to the peripheral peak (peak-to-peak width) was used as an approximation of the width of corneal change.

The peak-to-valley amplitudes and peak-to-peak widths for each subject and condition were saved in an output file along with the original x, y and z coordinates of the valley and the corresponding cross-section number.

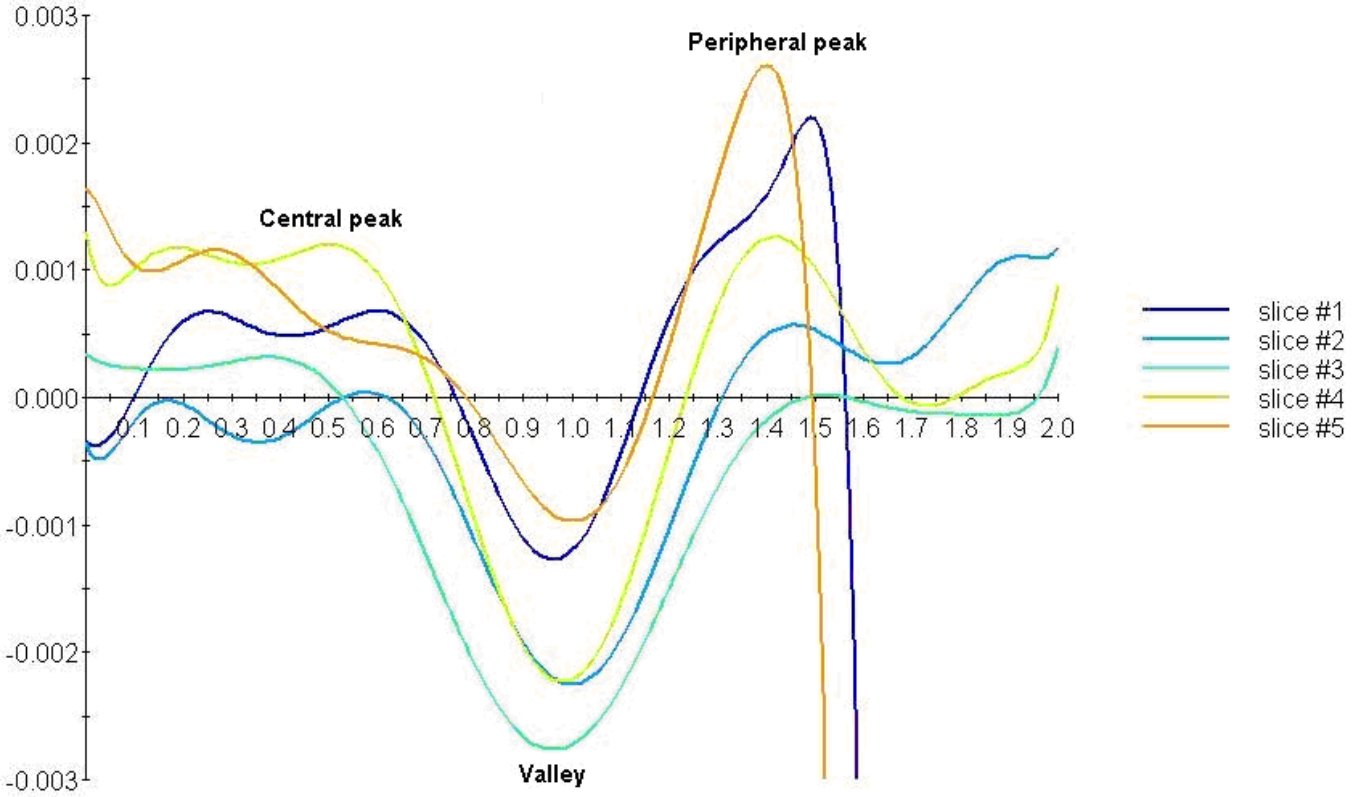

Figure 2-5: Five cross-sections of data from central cornea (left) to peripheral cornea (right) and cross-section 1 (nasal) through to 5 (temporal).

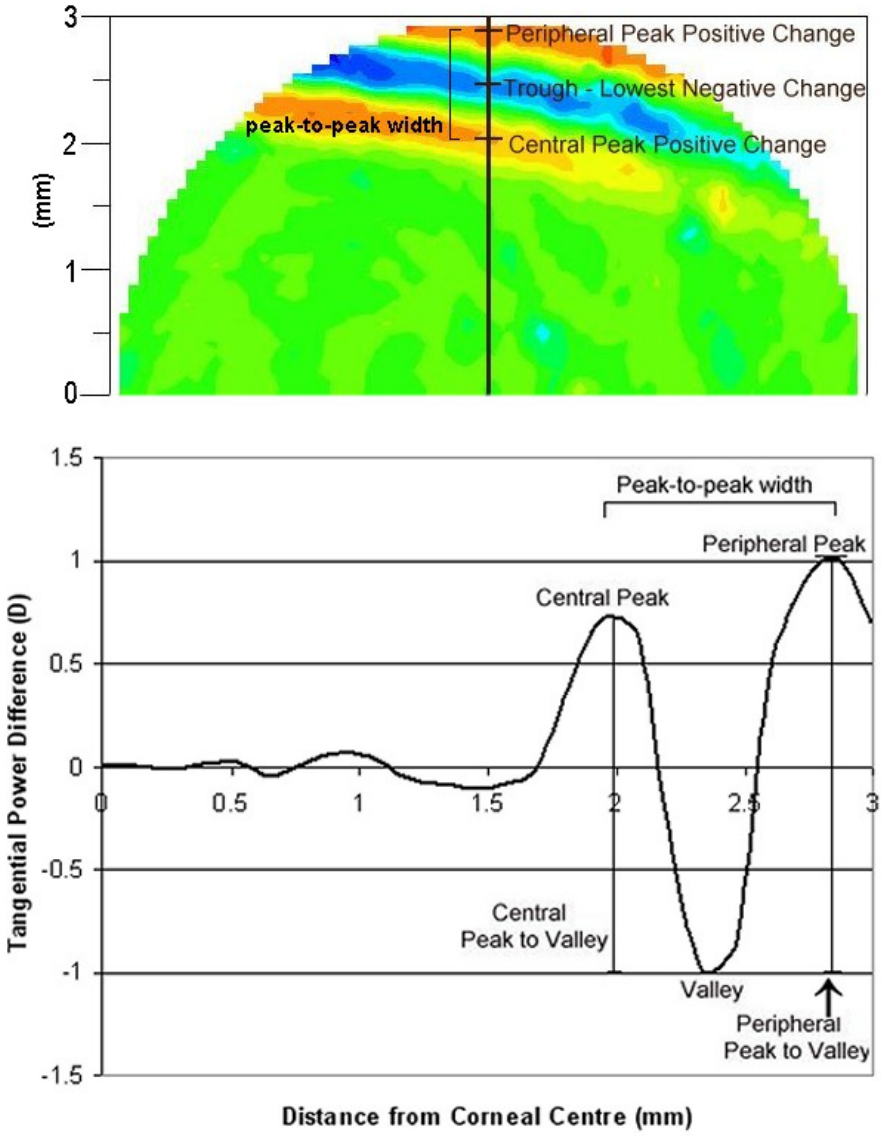

Figure 2-6: Tangential difference map (average of a subject's post-task maps minus the average of the pre-task maps) with the peaks and valley indicated. The 90° meridian cross-section shows the central and peripheral peak-to-valley amplitudes and the peak-to-peak width.

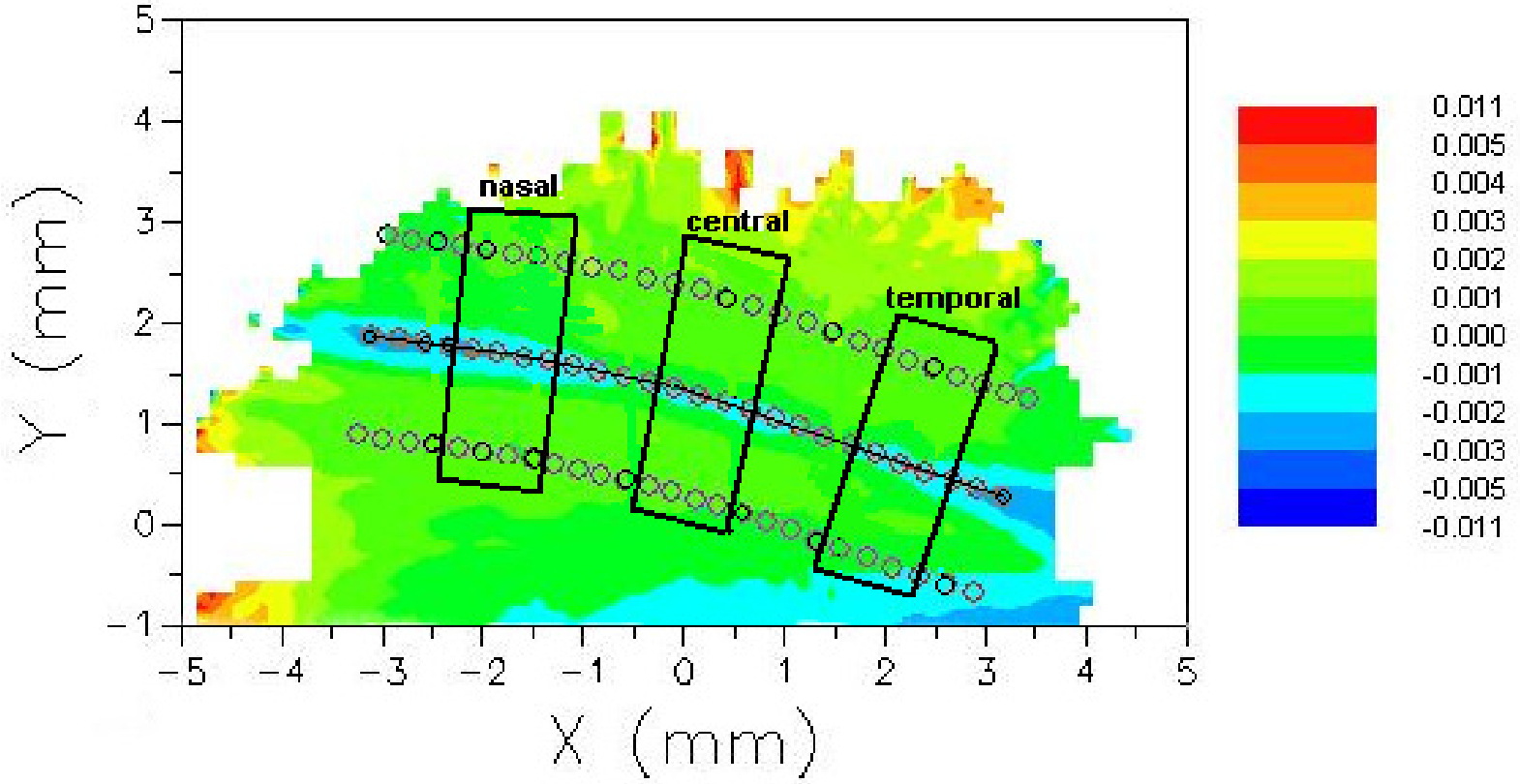

Figure 2-7: Data averaged in 3 corneal regions of 1 mm width: nasal, central and temporal.

Some subjects had narrow palpebral apertures and couldn't open their eyes wide enough so eyelash shadows often interfered with the image captured by the corneal topographer. For these subjects the eyelid-induced changes were usually at the edge of the topography map. Data was only analysed for subjects with eyelid-induced corneal changes that were not in close proximity to the edge of the captured topography map. This ensured the integrity of the polynomial fit to the elevation data. So the averages only included data from subjects that demonstrated distinct eyelid-induced changes that could be analysed (Table 2-2).

Three corneal regions within the central map were defined relative to the videokeratoscope centre as nasal (-2.5 to -1.5 mm), central (-0.5 to 0.5 mm) and temporal (1.5 to 2.5 mm). Approximately 20 cross-sections within each of these areas were averaged to obtain mean values for each region (Figure 2-7).

The central and peripheral peak-to-valley amplitudes were compared using mixed linear analysis and their relationship examined by a Pearson's product moment correlation. The ideal method to analyse the effect of the downward gaze angle, type of visual task, corneal region and central peak-to-valley amplitude versus peripheral peak-to-valley amplitude, would be to apply a repeated measures MANOVA. However there was a high correlation between central and peripheral peak-to-valley amplitudes, so the multicollinearity assumption was violated and central and peripheral peak-to-valley amplitudes could not be combined in one analysis. Also few subjects had data for every condition and every corneal region, so the number of observations varied for each subject. A mixed linear model was used to take into account the differing amount of data per subject by including subject identity as a random factor.

Using the mixed linear model, the effect of downward gaze angle, visual task and corneal region were investigated for the central peak-to-valley amplitudes due to the upper eyelid. For the lower eyelid, there were no changes in the central cornea captured by the topographer for the 20° downward gaze conditions. So the effect of the type of visual task and corneal region were examined for the 40° downward gaze conditions. The changes due to the upper and lower eyelids were also only compared for the 40° downward gaze tasks using Pearson's correlation.

Table 2-2: The number of subjects (total n = 18) that had complete eyelid-induced changes that were analysed and the number of subjects that demonstrated changes at the edge of the topography map and so were not analysed.

Task condition	*Upper eyelid-induced corneal change*		*Lower eyelid-induced corneal change*	
	Analysed	Not analysed (incomplete change)	Analysed	Not analysed (incomplete change)
20° reading	9	5	0	0
20° steady fixation	10	2	0	0
40° reading	13	4	11	4
40° steady fixation	17	0	11	3

Mixed linear analysis was applied to the widths of corneal change (central peak to peripheral peak width) for both the upper and lower eyelid-induced corneal changes. Correlations were investigated between the peak-to-peak widths of the 20° and 40° tasks and between the widths after the reading and steady fixation tasks.

2.2.4.2 Refractive corneal change

The change in refractive power (post-task minus pre-task) was calculated along with the average change for each condition for the 18 subjects. A best-fit sphero-cylinder was fit to each pre-condition and post-condition refractive map for 4 mm and 6 mm diameters using the method of Maloney *et al.* (1993). These corneal diameters were chosen to simulate average pupil sizes in photopic and mesopic conditions. The sphero-cylinder best-fit process was calculated around the videokeratoscope axis. The calculated best-fit sphero-cylinders from the average refractive power maps were used to examine the influence of eyelid-induced corneal changes in terms of higher order aberrations. The best-fit sphero-cylinder was subtracted from the corresponding average refractive power map to leave the residual error at every data point. The RMS error (RMSE) was calculated for each map, using the data points in the residual error topography map, to provide a single value estimate of corneal higher order aberrations.

Some topography data within the selected corneal diameters was missing due to shadows from the eyelashes. Approximately 0.05% and 0.81% of the data was missing for the 4 mm and 6 mm analysis diameters respectively, which would not have any significant influence on the results. During the best-fit process, if a data point was missing the calculation was made using the available points in that meridian.

For statistical analysis, the sphero-cylindrical change was separated into vector components M (best sphere), J0 (difference between vertical and horizontal meridians) and J45 (oblique astigmatism) using power matrices (Harris 2000). The vector changes were analysed with one-sample t-tests to indicate which changes were significant compared to baseline.

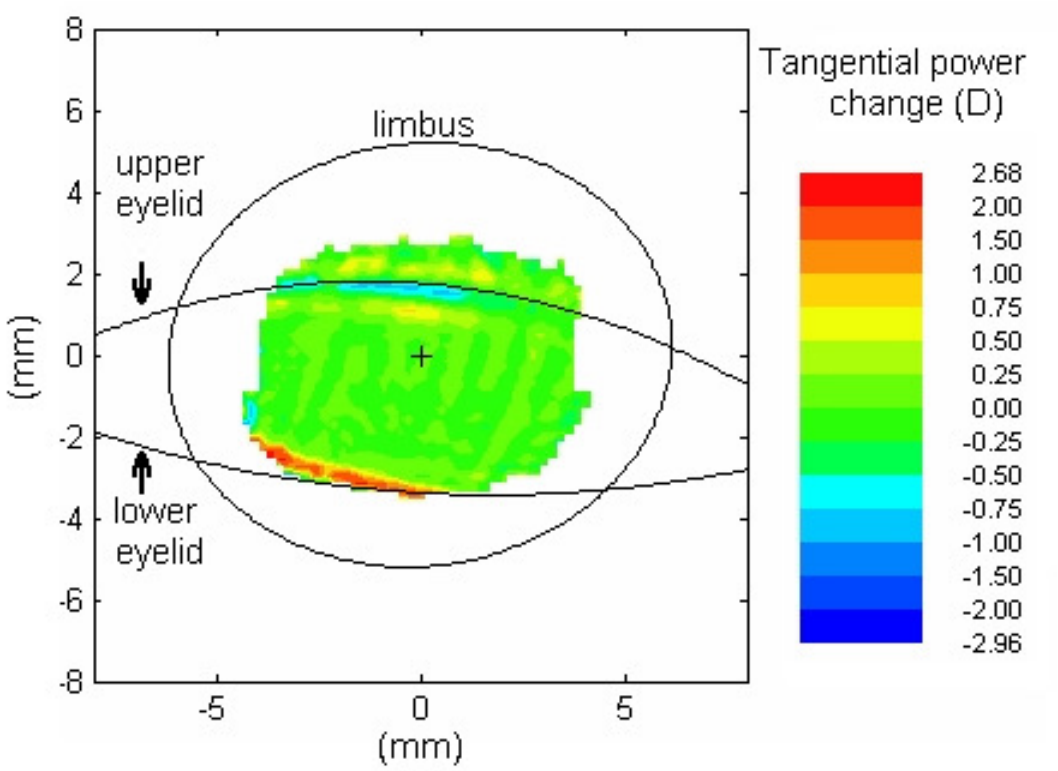

Figure 2-8: Relationship between the position of the eyelids and the induced corneal topography change. Tangential power difference map (post-task minus pre-task) after 40° downward gaze steady fixation task overlaid with the eyelid morphometry in 40° downward gaze (subject 5).

The combined change of these vector components for each condition were analysed using a MANOVA with two repeated within-subject factors (downward gaze angle and type of visual task). The difference between pre-task and post-task RMSE was analysed with 2-sample t-test for each condition. The changes in RMSE were analysed for the four conditions with a two-way repeated measures ANOVA. The change in vector components was also analysed for a correlation with spherical refractive error.

2.2.4.3 Anterior eye morphometry

The digital images of the anterior eye anatomy in primary gaze and 20° and 40° downward gazes were analysed with custom written software to approximate the morphometry of the limbus, upper and lower eyelid contour and eyelid movement during simulated reading (Iskander *et al.* 2004; Read *et al.* 2006). As the camera was manually focused and positioned at a known distance from the eye, each image had a resolution of 68.7 pixels per mm. For the limbus and pupil outlines, 10 and 8 points respectively were used for the ellipse functions fit to the outlines.

For the upper and lower eyelid margin, a total of 9 points were selected which were then fit with a polynomial function $Y= AX^2 + BX + C$ (Malbouisson *et al.* 2000), with respect to the limbus centre. This method has been previously used and the terms describe different aspects of the eyelid with A being the curvature, B the angle or tilt and C the distance from the geometric corneal centre (Read *et al.* 2006). The corneal changes were matched to the eyelid morphometry in downward gaze (Figure 2-8). The palpebral aperture size was estimated by adding coefficient C for the upper and lower eyelids. The eyelid parameters (A, B, C and palpebral aperture size) were analysed for correlation with the change in corneal astigmatic vectors J0 and J45 and the spherical component, M.

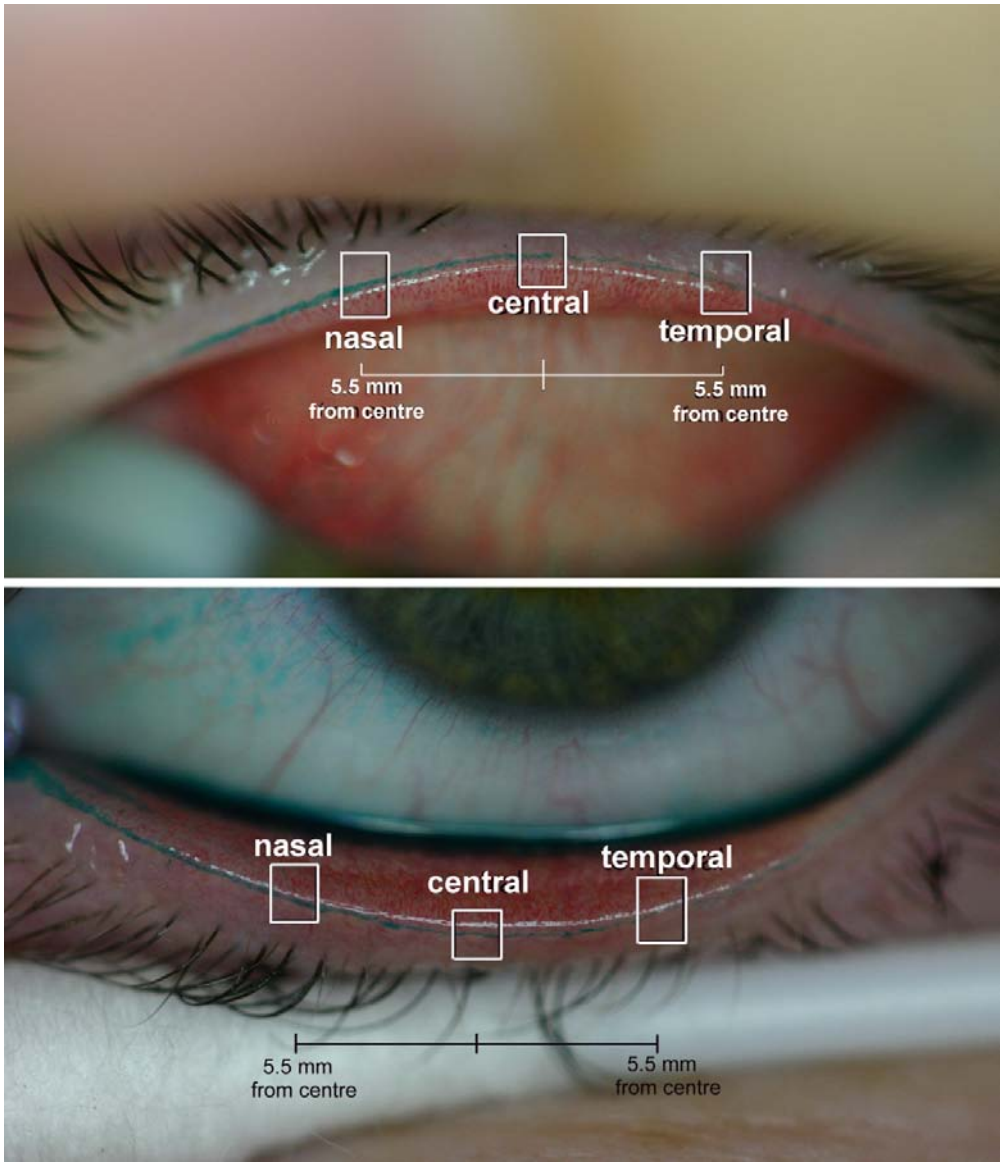

Figure 2-9: Marx's line stained with lissamine green for the upper eyelid (top panel) and lower eyelid (bottom panel), with the nasal, central and temporal regions indicated.

Custom-written software was used to measure the width of Marx's line (using the Euclidean distance between user selected limits) from the digital photographs of the upper and lower eyelid margins in nasal, central and temporal regions (Figure 2-9). The macro lens allowed high magnification and a resolution of approximately 137.8 pixels per mm for these images. Five measurements of width were made at each of these three regions and the averages calculated. For both eyelids the average standard deviation between repeated measures of Marx's line width was approximately 20% of the mean (about 0.02 mm). There were small variations in the width of Marx's line between nasal, central and temporal locations. However the error associated with estimating Marx's line width was of similar magnitude to the regional variations, so only the central Marx's line width was used in subsequent analyses. Associations between the central Marx's line width and the corneal topography peak-to-peak widths and peak-to-valley amplitudes for the steady fixation conditions were investigated with Pearson's correlations.

2.3 Results

2.3.1 Central versus peripheral peak-to-valley amplitudes

For the upper eyelid there was a highly significant difference between the central and peripheral peak-to-valley amplitudes (mixed linear analysis, $p<0.001$), with the peripheral peak-to-valley amplitudes on average being larger than the central peak-to-valley amplitudes (Figure 2-10). For the lower eyelid-induced corneal changes there was no statistical difference between the central and peripheral peak-to-valley amplitudes (Figure 2-11).

The central and peripheral peak-to-valley amplitudes were highly correlated for both the upper and lower eyelid-induced changes ($R^2=0.69$, $p<0.001$). Due to this strong correlation, further analyses were conducted only using the central peak-to-valley amplitudes. The peripheral peak-to-valley amplitudes also had

Upper eyelid: Elevation peak-to-valley amplitudes

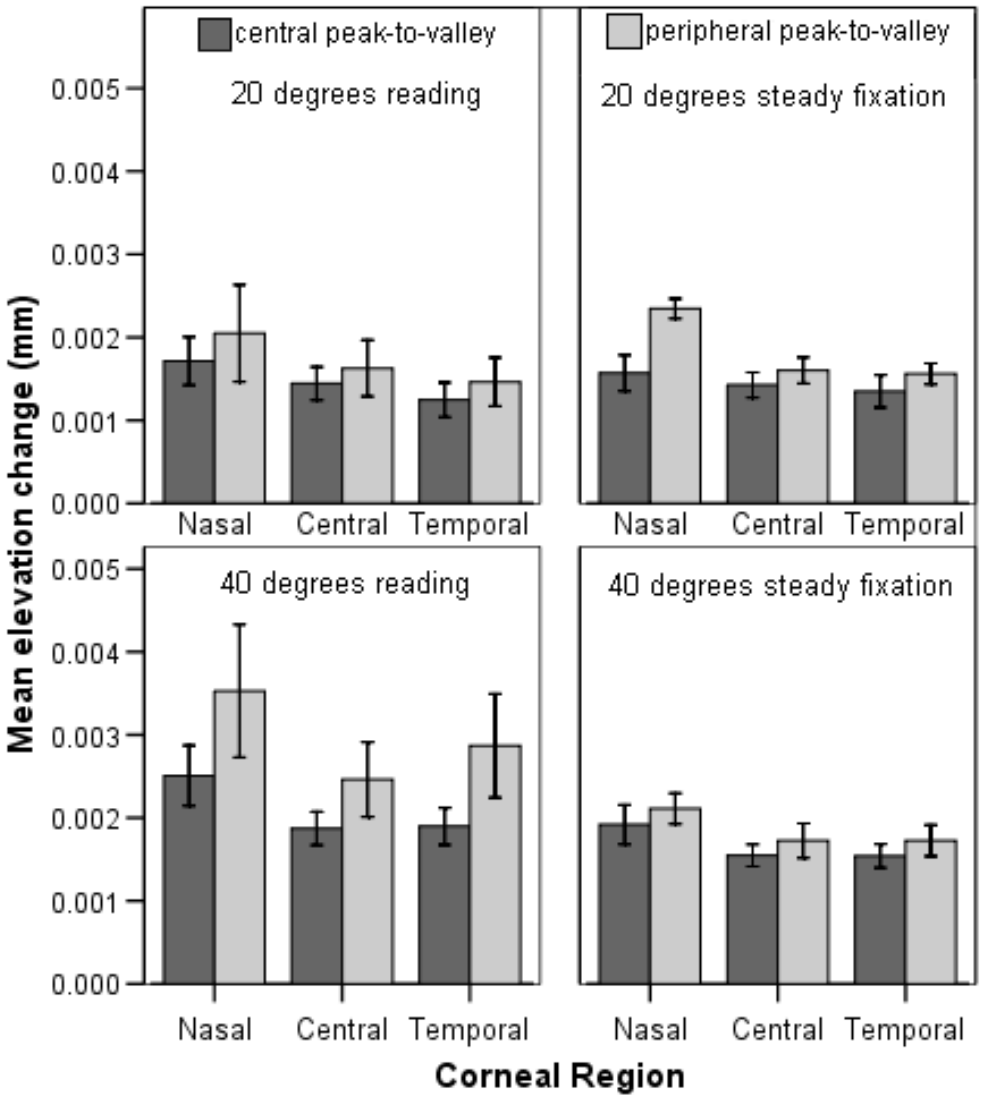

Figure 2-10: Group mean change in elevation peak-to-valley amplitudes due to the upper eyelid over nasal, central and temporal regions. Error bars ± 1 SE.

Lower eyelid: Elevation peak-to-valley amplitudes

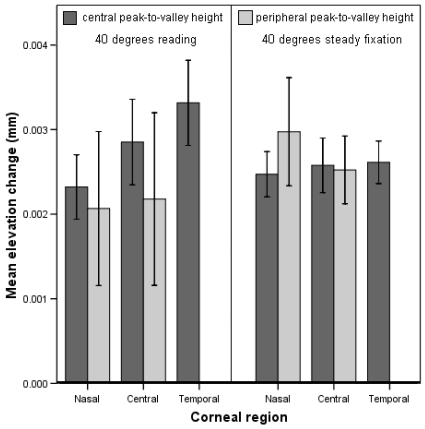

Figure 2-11: Group mean elevation peak-to-valley amplitudes due to the lower eyelid over nasal, central and temporal regions. Error bars ± 1 SE. There was data from only one subject for the peripheral peak-to-valley height in the temporal region, so an average and standard error was not calculated.

Table 2-3: Elevation peak-to-valley amplitudes. Results of mixed linear analysis for the upper and lower eyelid-induced elevation peak-to-valley amplitudes. P value of the F statistic is shown and ** = highly significant at p<0.001. Factors incorporating downward gaze angle for the lower eyelid are blank as there was only data for one angle, 40° downward gaze.

	Upper eyelid	*Lower eyelid*
Downward gaze angle (20° vs. 40°)	(<0.001)**	-
Type of visual task (Reading vs. Steady fixation)	(<0.001)**	0.883
Corneal region (Nasal vs. Central vs. Temporal)	(0.001)**	0.136
Angle and task interaction	0.300	-
Angle and region interaction	0.598	-
Task and region interaction	0.697	0.178

data for fewer subjects, as shadows from the eyelashes and nose reduced the corneal topography area captured.

For the 40° tasks, there were statistically significant differences in peak-to-valley amplitudes between the upper and lower eyelids, with the lower eyelid causing greater elevation change ($p<0.01$). There was also some weak evidence of an association between the magnitude of corneal changes induced by the upper and lower eyelids for an individual, with a positive correlation coefficient, $r=0.52$ ($R^2=0.27$, $p<0.1$).

2.3.2 Peak-to-valley amplitudes of corneal change

The mean peak-to-valley amplitudes were calculated for all conditions, corneal regions and for both eyelids. In the central corneal region the mean upper eyelid-induced central peak-to-valley amplitudes were 1.4 ± 0.6 m (20° reading, n=9), 1.4 ± 0.5 m (20° steady fixation, n=10), 1.9 ± 0.7 m (40° reading, n=13), and 1.5 ± 0.5 m (40° steady fixation, n=17) (Figure 2-10). The corresponding peripheral peak-to-valley amplitudes were larger than those for the central cornea for each condition: 1.6 ± 0.8 m (n=5), 1.6 ± 0.3 m (n=5), 2.5 ± 1.4 m (n=9), and 1.7 ± 0.8 m (n=14) respectively (Figure 2-10).

For the lower eyelid there were no corneal changes within the area captured by the videokeratoscope for the 20° tasks. For the 40° reading and 40° steady fixation tasks, the mean lower eyelid-induced central peak-to-valley amplitudes were 2.8 ± 1.5 m (n=11) and 2.6 ± 1.1 m (n=2) and the peripheral peak-to-valley amplitudes were 2.2 ± 1.4 m (n=11) and 2.5 ± 0.8 m (n=4) respectively (Figure 2-11).

All the within-subject factors (downward gaze angle, type of task and corneal region) were found to have a significant influence on the central peak-to-valley amplitudes for the upper eyelid. The corneal changes after 40° downward gaze were larger than after 20°, changes after reading were larger than those following steady fixation and nasal corneal changes were larger than the central and temporal regional changes (Figure 2-10 and Table 2-3).

However this was not the case for the region affected by the lower eyelid. Analysis of the 40° tasks showed that neither the type of visual task nor the corneal region (nasal, central or temporal) were statistically significant factors in the elevation change (Table 2-3 and Figure 2-11). However the angle of downward gaze was critical for the lower eyelid-induced changes as there were no changes evident within the corneal area captured by the videokeratoscope after 20° tasks for any subject.

2.3.3 Peak-to-peak width of corneal change

The mean distances from the central peak to the peripheral peaks due to the upper eyelid were 1.3 ± 0.2 mm (for the 20° reading, n=5 and 20° steady fixation, n=5 conditions) and 1.4 ± 0.2 mm (for the 40° reading, n=9 and 40° steady fixation, n=14 conditions) (Figure 2-12). The mean lower eyelid peak-to-peak widths were 1.4 ± 0.3 mm and 1.2 ± 0.1 for the 40° reading (n=2) and 40° steady fixation conditions (n=4) respectively (Figure 2-13). The mixed linear analysis showed that the downward gaze angle was the only significant factor ($p<0.01$) affecting the upper eyelid-induced peak-to-peak width.

The widths after the 20° tasks were on average slightly smaller than those due to the 40° downward gaze tasks. There were no statistically significant differences in the peak-to-peak widths due to the type of visual task (reading versus steady fixation) or between the corneal regions (nasal, central or temporal) for either the upper or lower eyelid.

The upper eyelid peak-to-peak width for the 20° steady fixation task was significantly correlated with the peak-to-peak width for the 40° steady fixation task ($R^2=0.60$, $p<0.01$). There were no significant correlations between the widths of change for the 20° and 40° reading tasks or between the widths due to reading and steady fixation.

Upper eyelid: Elevation peak-to-peak width

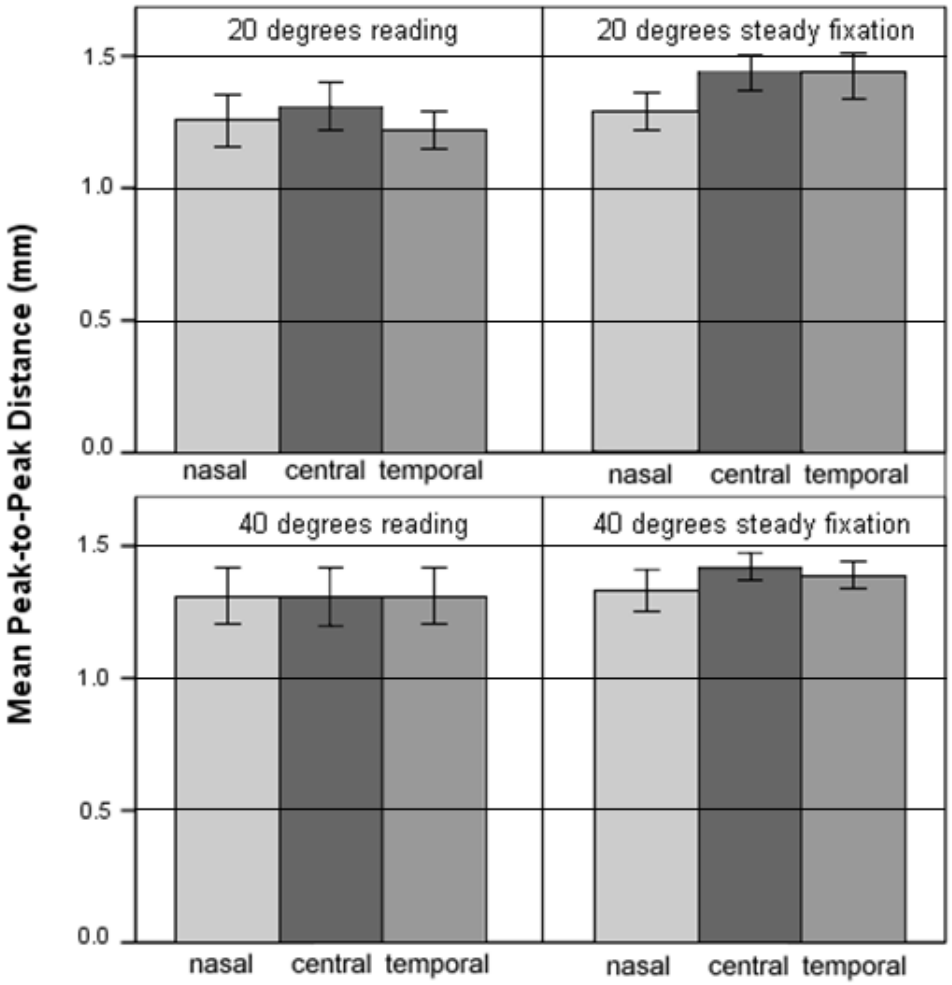

Figure 2-12: Group mean peak-to-peak widths for the upper eyelid-induced changes in nasal, central and temporal corneal regions. Error bars ± 1SE.

Lower eyelid: Elevation peak-to-peak width

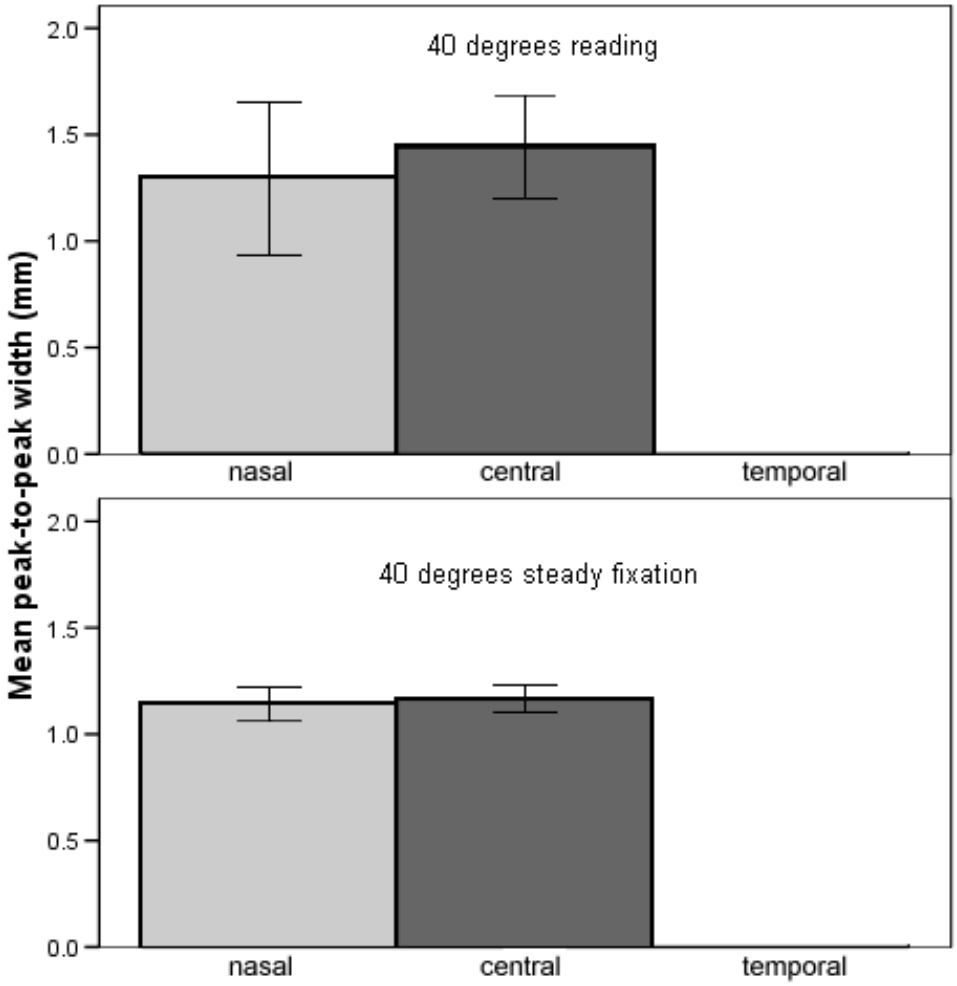

Figure 2-13: Group mean peak-to-peak widths for the lower eyelid- induced changes in nasal, central and temporal corneal regions. Error bars ±1 SE. There was data from only one subject for the temporal region for both 40° reading and steady fixation, so an average and standard error were not calculated.

2.3.4 Corneal refractive changes

The group means and standard deviations for the changes in vector components (M, J0 and J45) for each of the task conditions and for the 4 and 6 mm pupil diameters are presented in Table 2-4 and the 6 mm means graphed in Figure 2-14. The consistent direction of astigmatic change for all task conditions was against-the-rule (positive J0) and was statistically significant ($p<0.05$) for all conditions and over both analysis diameters. Spherical corneal changes reached statistical significance for the 40° tasks over both 4 and 6 mm diameters ($p<0.001$). The change in the oblique component of astigmatism (J45), although small, was closer to 45° for the 20° tasks and closer to 135° for the 40° tasks.

A repeated measures MANOVA examining the combined changes in M, J0 and J45 within 6 mm, found the downward gaze angle (20° versus 40°) to be a significant factor ($p<0.001$) with the 40° downward gaze producing larger corneal changes than 20°. The significance of downward gaze angle on the individual refractive vectors was M ($p<0.001$), J0 ($p<0.001$) and J45 ($p<0.01$). However there was not a significant difference between the changes due to reading and steady fixation.

For a clinical interpretation of the corneal changes the mean sphero-cylindrical corneal changes were considered. Over a 4 mm pupil diameter the group mean sphero-cylindrical changes were +0.06/-0.07x97 and +0.05/-0.09x109 for the 20° downward gaze reading and 20° downward gaze steady fixation conditions respectively. The group mean changes were substantially larger for the extreme 40° downward gaze reading and 40° steady fixation conditions, being +0.33/-0.30x84 and +0.24/-0.25x87 respectively. Similar refractive changes were measured over 6 mm pupil diameter: +0.06/-0.07x97 D (20° reading), +0.05/-0.07x95 D (20° steady fixation), +0.29/-0.28x93 D (40° reading) and +0.25/-0.26x88 D (40° steady fixation).

Table 2-4: Group mean changes and standard deviations of M, J0, and J45 within 4 and 6 mm corneal diameters for each condition. M represents the spherical corneal power, J0 is the 90/180° astigmatic power and J45 is the 45/135° (oblique) astigmatic power. Comparison of vector change with no change (0 D) using t-tests (* = significant, $p<0.05$ and ** = highly significant, $p<0.001$).

Pupil size (mm)	*Downward gaze angle (degrees)*	*Task*	*M (D)*	*J0 (D)*	*J45 (D)*
4	20	reading	0.02 ± 0.05	(0.03 ± 0.07)*	0.01 ± 0.06
		steady fixation	0.01 ± 0.09	(0.04 ± 0.06)*	(0.03 ± 0.05)*
	40	reading	(0.18 ± 0.16)**	(0.15 ± 0.15)**	-0.03 ± 0.09
		steady fixation	(0.12 ± 0.10)**	(0.13 ± 0.08)**	-0.01 ± 0.05
6	20	reading	0.02 ± 0.06	(0.03 ± 0.06)*	0.01 ± 0.06
		steady fixation	0.02 ± 0.09	(0.04 ± 0.05)**	0.02 ± 0.04
	40	reading	(0.16 ± 0.10)**	(0.14 ± 0.10)**	(-0.03 ± 0.06)*
		steady fixation	(0.11 ± 0.09)**	(0.11 ± 0.07)**	-0.02 ± 0.05

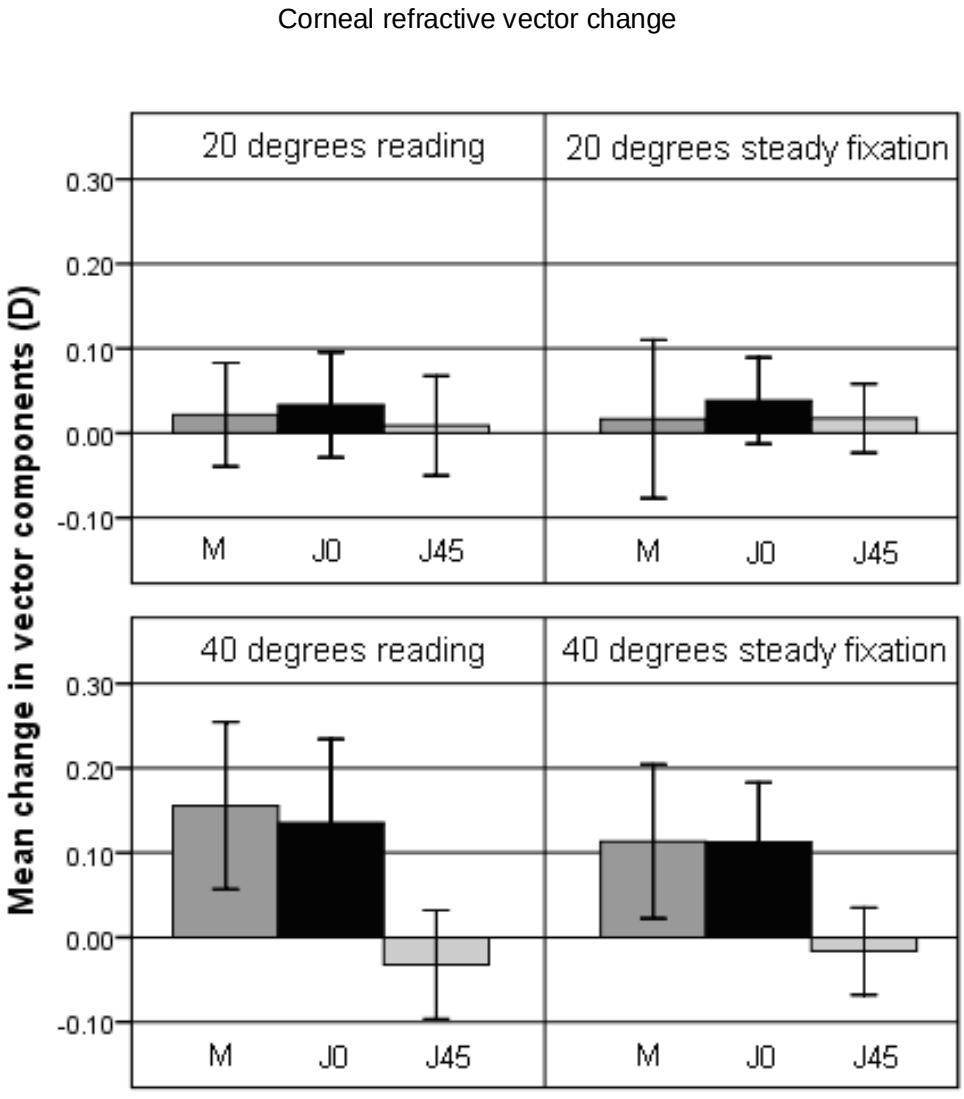

Figure 2-14: Group mean change in M, J0, J45 and B within a 6 mm corneal diameter and the standard deviation for each condition.

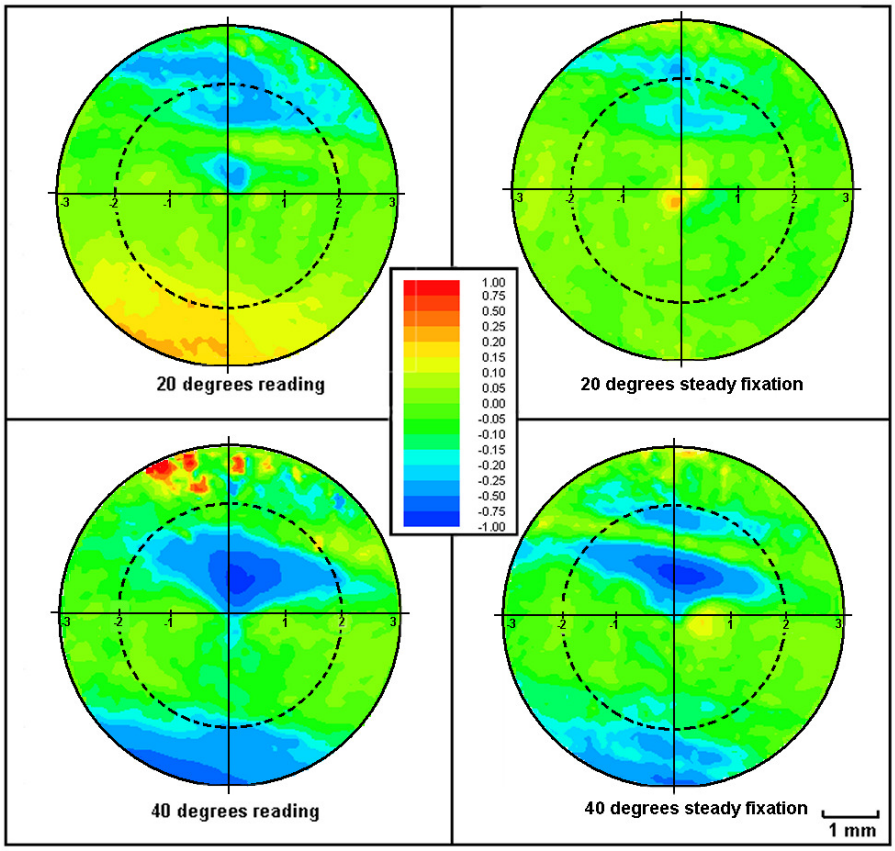

Figure 2-15: Mean refractive power difference maps for each task condition. Outer circle 6 mm corneal diameter; inner dashed circle 4 mm diameter.

Over both analysis diameters the astigmatic changes for the 40° tasks were approximately 0.25 D, reaching clinical significance. While the group sphero-cylindrical changes for the 20° were smaller, individually there were often clinically significant changes. Over the 4 mm analysis diameter, the maximum sphero-cylindrical changes were +0.29/-0.29x81 D (20° reading) and +0.30/-0.24x88 D (20° steady fixation). The mean refractive power difference maps (for all 18 subjects) highlight the corneal regions that experienced the greatest refractive change for each of the conditions (Figure 2-15).

The corneal RMSE, which represents the higher order aberrations, increased post-task for all conditions (Table 2-5). Similar to the refractive vector analysis, the downward gaze angle was a significant factor affecting the change in RMSE ($p<0.01$) (40° downward gaze greater than 20° downward gaze), but the type of visual task was not a significant factor. Results from two-tailed paired t-tests between pre-task and post- task RMSE show that the increase in RMSE was significant for all conditions except the 20° steady fixation condition, when analysed for both 4 and 6 mm corneal diameters (Table 2-5).

2.3.5 Anterior eye morphometry

The eyelid anatomy was overlayed with the topography maps to observe the relationship between the eyelid and the corneal changes (Figure 2-8). While overlaying the topography and eyelids is useful to observe their relationship, no statistical analysis was conducted due to the variability of the topography area captured.

As there was no statistical difference in the peak-to-peak width between the reading and steady fixation conditions or between corneal regions (nasal, central, temporal), no further analysis was conducted on the eyelid morphometry in the various horizontal angles of gaze.

Table 2-5: Mean corneal refractive RMSE change (high order aberrations) for the four task conditions within 4 and 6 mm corneal diameters. Comparison of pre-task versus post-task RMSE with t-tests (* = significant at p<0.05 and ** = highly significant at p<0.001).

Pupil size (mm)	*Downward gaze angle (degrees)*	*Task*	*RMSE change (D)*	*p-value*
4	20	reading	0.07	(0.016)*
		steady fixation	0.02	0.535
	40	reading	0.20	(0.022)*
		steady fixation	0.22	(<0.001)**
6	20	reading	0.06	(0.002)**
		steady fixation	0.03	0.35
	40	reading	0.13	(0.003)**
		steady fixation	0.16	(<0.001)**

2.3.5.1 Eyelid morphometry and corneal refractive change

The vector J0 which described most of the corneal refractive change was not significantly correlated to any of the eyelid parameters. Despite small average changes in M and J45, significant correlations were found with some of the upper and lower eyelid morphometry parameters after the 40° tasks.

The change in the best sphere, M, had a statistically significant correlation with the 40° lower eyelid curvature (coefficient A) after the 40° reading task (R^2=0.22, $p<0.05$) (Figure 2-16). This indicates that straighter lower eyelids were associated with greater changes in best sphere than curved lower eyelids. The best sphere change after the 40° steady fixation task was correlated with the 40° downward gaze upper eyelid curvature (R^2=0.40, $p<0.01$) (Figure 2-16). However, in this case a curved eyelid produced a greater best sphere change.

The change in vector J45 after the 40° reading task was correlated with the tilt of the lower eyelid at 40° (R^2=0.28, p=0.025) (Figure 2-17). A downward slant of the lower eyelid (down towards the temporal) produced a negative J45 change, while an upward slanting eyelid was more likely to produce a more positive J45 change.

For the 40° steady fixation condition, there was some evidence that the palpebral aperture size was associated with the change in best sphere (R^2=0.29, p=0.077), with a narrow palpebral aperture more likely to be associated with a larger refractive change.

There were no correlations between the corneal refractive changes and the subject's spherical refractive errors for either change in M (r=-0.05, p=0.67), change in J0 (r=-0.09, p=0.46) or change in J45 (r=-0.20, p=0.10). So there does not seem to be an association between the degree of refractive error and magnitude of the corneal change.

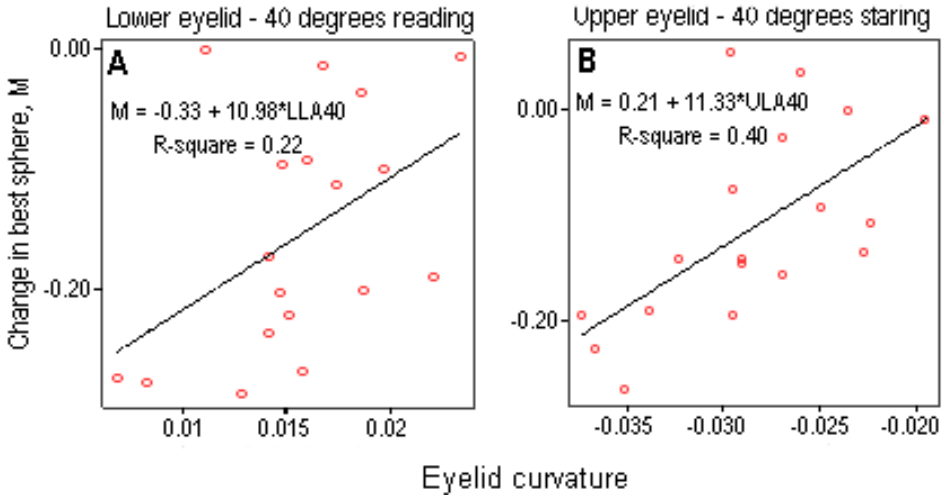

Figure 2-16: Correlation between the change in best sphere, M and the lower eyelid curvature (A, left panel) and the upper eyelid curvature (B, right panel).

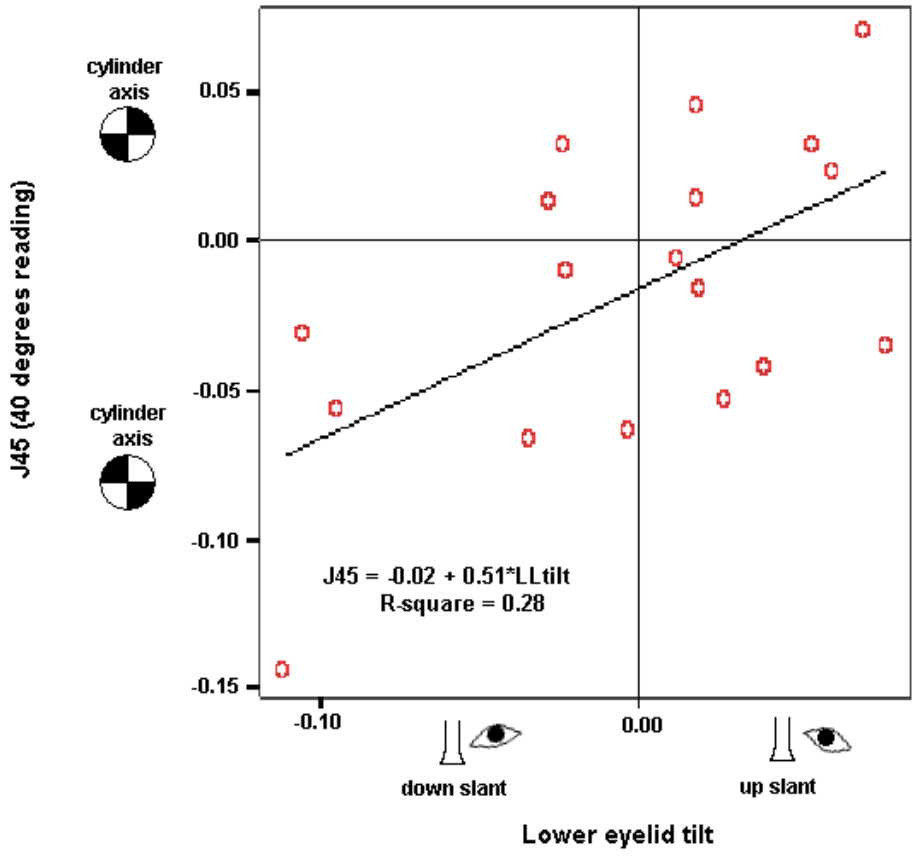

Figure 2-17: Correlation between the change in J45 and the lower eyelid tilt.

2.3.5.2 Marx's line width

The average width of Marx's line centrally for the upper eyelid was 0.11 ± 0.05 mm and 0.13 ± 0.10 mm for the lower eyelid (Figure 2-18). There were no statistically significant correlations between the widths of the upper and lower eyelid central Marx's line, or between the Marx's line width and the peak-to-peak width of corneal change for either eyelid. There was however, some evidence of an association between the upper eyelid Marx's line width and the peak-to-valley amplitudes. A positive correlation for the 40° steady fixation task (R^2=0.32, $p<0.05$) indicated that a wider Marx's line was associated with a deeper corneal change. There was also a positive correlation for the 20° steady fixation condition peak-to-valley amplitudes and Marx's line width (R^2=0.14) though this did not reach statistical significance. So there was evidence of an association between Marx's line and eyelid-induced corneal changes.

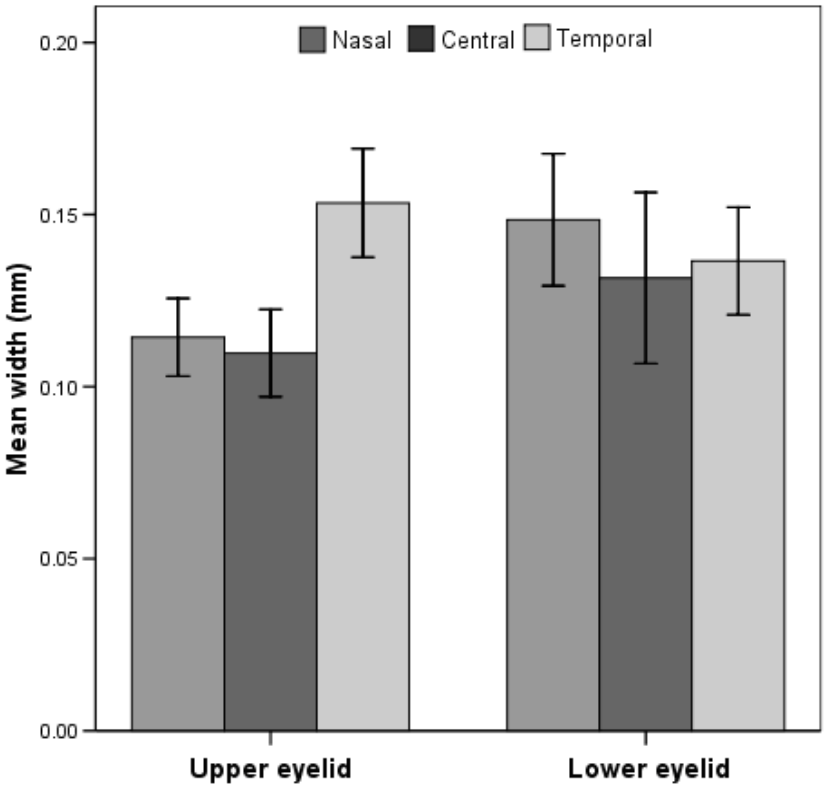

Figure 2-18: Group mean Marx's line width for the upper and lower eyelids at nasal, central and temporal locations. Error bars ±1 SE.

2.4 Discussion

Significant corneal refractive changes occurred for short (15 minutes) periods of downward gaze. The average astigmatic change was in the direction of against-the-rule astigmatism (i.e. with-the-rule astigmatism decreased or against-the-rule astigmatism increased), which is the direction of astigmatic change recorded by others that have measured eyelid-induced corneal changes (Buehren *et al.* 2003; Collins *et al.* 2006). For the 40° conditions the sphero-cylindrical changes were in the order of 0.25 D, which is substantial considering that this change occurred after only 15 minutes of reading or steady fixation. As the magnitude of eyelid-induced corneal changes increases with the length of time spent reading (Collins *et al.* 2005), a greater change could be expected for longer reading durations. The cumulative effect of multiple near tasks over the course of a day may also increase the magnitude of corneal changes, as diurnal changes to the cornea have been found in adults whose work involved significant reading (Read *et al.* 2005).

There are two main differences in the protocol used in this study compared to previous work. The subjects were positioned in fixed angles of downward gaze rather than adopting a natural reading posture and the task duration was 15 minutes compared to 60 minutes used in previous research. The refractive changes after the 20° downward gaze conditions of this study are comparable with previously measured corneal sphero-cylindrical changes after reading (Collins *et al.* 2006). This suggests that in the natural reading posture used in previous research, the eye's vertical downward gaze angle was on average approximately 20°. This is consistent with other investigations concerning visual posture that have recorded an average 26.3° downward eye gaze during reading (Hill *et al.* 2005). In contrast the 40° downward gaze conditions produced larger changes than both the 20° tasks and compared to prior work despite the shorter task duration. For large downward gaze angles such as 40°, both the upper and lower eyelids are in contact with the central 6 mm of the cornea. So it can be expected that in comparison to the 20° conditions, when usually only the upper eyelid is in contact with the central cornea, the corneal refractive changes will be larger.

Similar to previous reports the presence of the eyelids on the corneal surface in downward gaze caused wave-like corneal distortions (Buehren *et al.* 2001; Buehren *et al.* 2003; Collins *et al.* 2005; Read *et al.* 2005; Collins *et al.* 2006; Collins *et al.* 2006). The average elevation central peak-to-valley amplitudes ranged from 1.4 to 2.8 µm. As longer reading periods have been shown to cause larger corneal changes (Collins *et al.* 2005), this result for 15-minute tasks is comparable to the 4 µm mean recorded for one hour reading sessions (Buehren *et al.* 2003).

The magnitude of the downward gaze angle has a significant impact on the induced corneal change. For the upper eyelid, elevation peak-to-valley amplitudes were 25% larger for the extreme 40° conditions compared with the 20° conditions. It is the altered relative position of the eyelids and the eye globe with downward gaze that changes the location and magnitude of the induced corneal change. Centrally, the upper eyelid was on average 0.6 mm closer to the videokeratoscope centre for the 40° tasks compared with the 20° tasks. It is doubtful whether the corneal biomechanical properties would alter enough over this small distance to make the corneal tissue more susceptible to eyelid pressure and account for the 25% increase in corneal change. It is more likely that at the increased downward angle, the upper eyelid exerts higher pressure on the ocular surface. This increased pressure may be due to the eyelid resting closer to the centre of the cornea on a region of “higher cornea” nearer to the apex.

However Collins *et al.* (2006) have previously discussed that this would only be valid if there was no change in the antero-posterior position of the eye with downward gaze. It is well known that the eye globe retracts on blinking with the contraction of the orbicularis oculi (Doane 1980; Collins *et al.* 1992). In contrast a downward gaze lid saccade is achieved almost exclusively by the passive elastic forces of the ocular tissues and the relaxation of the levator palpebrae superioris muscle with no involvement of the orbicularis oculi (Davson 1972). As these eyelid movements have different mechanisms it is unlikely that the globe would retract with a downward eyelid saccade. The antero-posterior position of the eyes has been previously studied but no relationship was found between the exophthalmus data and the degree of topographic change (Collins *et al.* 2006). There is also a possibility that extraocular muscles may influence the corneal shape at larger downward gaze angles. However this seems

unlikely, as previous studies have failed to conclusively show a change in corneal shape with convergence (Fairmaid 1959; Löpping and Weale 1965; Mandell and St Helen 1968). Therefore it seems that eyelid pressure on the cornea seems to be greater when the eyelid is closer to the corneal centre in larger downward gaze angles.

In contrast, despite the lower eyelid changes being further from the videokeratoscope centre (2.7 mm compared with 1.5 mm for the upper eyelid), the corneal changes due to the lower eyelid were deeper than those from the upper eyelid. The lower eyelid has previously been shown to produce larger corneal changes than the upper eyelid following 45° downward gaze tasks, although the position of the eyelids on the cornea was not considered (Collins *et al.* 2006). These findings suggest that at large downward gaze angles the lower eyelid pressure on the corneal surface is greater than that of the upper eyelid.

Typically eyelids induce a valley of corneal change (corresponding closely to the eyelid margin) (Buehren *et al.* 2003), with corneal tissue redistributed either side of this depression. There was high correlation between the central and peripheral peak-to-valley amplitudes. For the upper eyelid, corneal changes were greater peripherally compared with centrally. There is little known about the exact area of contact between the eyelid margin and the cornea. The upper eyelid margin has been described as a lid-wiper (Korb *et al.* 2002), aiding tear film distribution during blinking. Mathematical modelling of the upper eyelid's blinking action suggests that the margin needs to change angle during opening and closing to effectively distribute tear fluid (Jones *et al.* 2008). The shape or angle of the upper eyelid margin as it contacts the cornea could result in unequal tangential forces and asymmetrical tissue distribution. In contrast, the lower eyelid induced symmetrical peak-to-valley profiles with equal peaks either side of the valley and its movement during blinking is primarily in the horizontal direction (Doane 1980). Alternatively the pressure of the tear meniscus may be also be involved in the peak-to-valley corneal change (Mountford 2004). This force acts in a direction away from the cornea (opposite to eyelid pressure) (Jones *et al.* 2008) and so may pull the cornea at the location of the eyelid margin.

There was also no statistical difference in the peak-to-valley amplitudes between the reading and steady fixation conditions for the lower eyelid. While for the more mobile upper eyelid, reading-associated movements increased the peak-to-valley amplitudes by 3% and 25% for 20° and 40° tasks respectively. Increases of between 17 and 35% have been recorded for 1 Hz eye movements compared with a steady fixation control for 15-minute visual tasks (Collins *et al.* 2006). The increased depth of change for the reading task may be due to kinetic friction between the upper eyelid and the ocular surface.

While the upper eyelid peak-to-peak widths of the 20° and 40° steady fixation conditions were correlated, there were no significant correlations between the widths of the reading tasks. This indicates that the eye movements during reading produced more random spatial changes of the corneal surface. This was confirmed by the generally larger standard deviations of corneal change associated with the reading conditions compared with the steady fixation tasks.

The lower eyelid-induced corneal changes were consistent across the cornea with no regional variations in peak-to-valley amplitude or peak-to-peak width, suggesting similar eyelid pressure is applied across the cornea. In comparison to the lower eyelid, the corneal changes due to the upper eyelid were wider and shallower. For the upper eyelid while the width of corneal change was constant across the cornea, there was an increased depth of change nasally compared with the central and temporal cornea. It is possible that changes in the position and angle of the eyelids and canthi in downward gaze (Read *et al.* 2006) may influence the regional pressure that the upper eyelid exerts on the cornea. However a highly elastic eyelid could be expected to wrap consistently to the underlying ocular surface.

While the pressure of the eyelids is a major factor in the induced corneal change, corneal factors may also be involved. There was a moderate positive correlation between the upper and lower eyelid peak-to-valley amplitudes after the 40° downward gaze tasks. Subjects with a large upper eyelid-induced change were more likely to have a large lower eyelid-induced change. This indicates that certain individuals may

be more susceptible to pressure from the upper and lower eyelids due to either the cornea's mechanical properties or from common anatomical features of the eyelids.

The results are from a sample of eighteen subjects and may be not representative of a larger population. The subjects in the study had a range of refractive errors but this factor was not correlated with the corneal changes we found. However other factors such as ethnicity and eyelid tension may contribute to differences in the corneal change between individuals.

Corneal refractive changes were analysed over both 4 and 6 mm corneal diameters to simulate photopic and mesopic pupil sizes. Similar changes were seen over both analysis diameters. Examination of the difference corneal topography maps revealed that in 40° downward gaze only the upper eyelid-induced changes were within the central 4 mm diameter, while both the upper and lower eyelid-induced changes were within the central 6 mm. This accounts for the comparable refractive changes over the 4 and 6 mm analysis diameters.

Using the assumption that greater than 1/8 D change would alter the subjective refractive outcome by at least 0.25 D, the group mean refractive change for the 20° tasks was not clinically significant. Though for both the 20° reading and steady fixation conditions, 8 of the 18 subjects had spherical corneal changes greater than 1/8 D. For the 40° conditions, the group mean sphero-cylindrical changes were in the order of 0.25 D, which is a clinically significant change. The maximum corneal sphero-cylindrical change observed at this downward gaze angle was +0.87/-0.75x90 D.

Using wavefront aberration analysis, the wave-like corneal distortion can be described primarily as a change in vertical coma, trefoil x30 and 90/180 astigmatism (Buehren *et al.* 2003; Collins *et al.* 2006). In this study the change in RMSE provided an estimate of the change in higher-order aberrations. While there was less than 0.1 D RMSE change for the 20° tasks, the largest group mean change was 0.23 D (4 mm corneal diameter, 40° steady fixation condition). Compared to baseline, RMSE increased by a mean of 28% for the 15-minute 40° tasks. The corneal distortions described by higher-order aberrations may be responsible for the visual symptom of monocular diplopia that has

been reported after downward gaze reading (Mandell 1966; Bowman *et al.* 1978; Carney *et al.* 1981; Goss and Criswell 1992; Kommerell 1993; Ford *et al.* 1997; Golnik and Eggenberger 2001).

There was evidence that the morphology of the eyelids is associated with the induced corneal changes. In particular, the J45 astigmatic changes after the 40° tasks were correlated with the lower eyelid tilt. The important influence of the lower eyelid on corneal topography has been previously highlighted with an association between lower eyelid tilt and the natural axis of corneal astigmatism (i.e. not after reading) in a group of 100 young subjects (Read *et al.* 2007). So not only does eyelid pressure cause temporary corneal changes but also the cumulative effect may be associated with the natural astigmatism of young healthy subjects. The shape of the eyelids (eyelid curvature) showed correlations with the magnitude of best spherical change (vector M). A narrow palpebral aperture (eyelid position) was associated with larger corneal changes, as previously reported (Buehren *et al.* 2005). These associations are moderate and account for between 20 to 40% of the variation in corneal refractive change. This suggests that other factors are involved that were not measured in this investigation, such as eyelid tension and corneal modulus.

Due to its anatomical structure, it is thought that Marx's line is the natural site of frictional contact between the eyelid margin and the surfaces of the bulbar conjunctiva and cornea. The average width of the upper eyelid Marx's line in this group of subjects was 0.11 ± 0.05 mm, which is a similar to the previous report of 0.10 ± 0.09 mm (Hughes *et al.* 2003). There does not appear to be any previous published values reporting the width of the lower eyelid Marx's line. A width of 0.13 ± 0.10 mm in this study suggests that it has similar dimensions to the upper eyelid.

While there was no association evident between Marx's line width and the peak-to-peak width of the corneal change, there was a positive association with the depth of corneal change. This indicated that a wider Marx's line was associated with a greater depth of corneal change. While the same force distributed over a wider area would result in less pressure, this finding suggests that subjects with greater eyelid pressure on the globe have a wider Marx's line and deeper corneal changes. While this association was

evident for the 40° steady fixation conditions when eyelid pressure was stable on the corneal surface, it was not significant for the 40° reading condition when eye movements resulted in more random spatial changes.

It has been noted that the staining of Marx's line can be confused with surrounding additional eyelid margin staining. This has been termed lid-wiper epitheliopathy and is common in contact-lens wearing (Korb *et al.* 2002) and dry eye patients (Korb *et al.* 2005). All care was taken to exclude subjects from this study who had dry eyes and to differentiate Marx's line from lid-wiper epitheliopathy on the marginal eyelids. However if some subjects had marginal dry eye and decreased tear lubrication between the eyelids and the cornea, then there may be increased friction between the surfaces resulting in a wider estimation of Marx's line width. Another potential explanation of this association could be that subjects with greater eyelid pressure on the globe have wider Marx's line and deeper corneal changes.

This study and previous work (Collins *et al.* 2006) have reported increased corneal changes with reading tasks (involving horizontal eye movements) compared with steady fixation tasks. The increased corneal change with eye movements suggests that there could be increased kinetic friction between the eyelid and the cornea during reading which would most likely affect the epithelium. It is possible that the cellular mechanism associated with orthokeratology corneal changes may also be responsible for eyelid-induced corneal changes. Extensive research has established that orthokeratology lenses cause central epithelial thinning and mid-peripheral stromal thickening (Swarbrick *et al.* 1998; Alharbi and Swarbrick 2003; Wang *et al.* 2003). Although the cellular mechanism behind this change is unknown, possibilities include epithelial cell redistribution, increased cell mitosis, cell compression and stromal remodelling (Choo *et al.* 2008). It is unlikely that eyelid-induced corneal changes would be due to the redistribution of entire epithelial cells as surface epithelial cells have an individual thickness of about 4 µm (Bron *et al.* 1997) and the elevation changes in this study were between 0.4 to 5.3 µm.

Recent work using a cat model suggests that cell compression and deformation are most likely the changes occurring from short-term orthokeratology contact lens wear

(less than 8 hours). The small height changes observed in this study could be due to epithelial cell compression, involving structural alteration of epithelial cells with maintenance of the cell numbers. Similar changes have been seen with rigid contact lenses bearing on rabbit corneas where there was cell compression at all epithelial levels including the widening or flattening of the basal cells (Greenberg and Hill 1973; Choo *et al.* 2004; Choo *et al.* 2008). The topographical analysis method used in this study did not allow us to determine whether there was tissue redistribution (i.e. if displaced tissue from the trough equalled the tissue deposited in the peaks) or whether there was cellular compression with intercellular fluid transfer. Future analysis of conservation of cell volume and epithelial layers would add valuable information in determining the corneal response to eyelid pressure.

There are other similarities between eyelid-induced corneal changes and orthokeratology corneal changes that make the suggestion of a similar mechanism plausible. They both seem to have a similar time-course of action and regression. The corneal changes in this study occurred after 15 minutes of eyelid pressure and corneal curvature changes have been recorded after only 10 minutes of orthokeratology lens wear (Sridharan and Swarbrick 2003). Additionally the regression of corneal change due to orthokeratology lenses takes 4.2, 6.6 and 8.2 hours after 1, 2 and 4 hours of lens wear respectively (Horner *et al.* 1992). In comparison, a study of the regression of eyelid-induced corneal changes after reading concluded that it generally took about the same amount of time as was spent reading for the corneal changes to return to baseline (Collins *et al.* 2005).

Another possibility is that corneal swelling due to hypoxia under the eyelid may contribute to the corneal changes measured in this study. The mean corneal oedema due to a closed eyelid during sleeping has been measured to be approximately 3-4%, equivalent to approximately 20 µm (Mertz 1980; Holden *et al.* 1983; du Toit *et al.* 2003). Using optical coherence tomography it has been shown that the change is predominantly stromal but there are also epithelial changes proportional to its thickness (Feng *et al.* 2001). However it is not known whether localised corneal hypoxic changes (under the eyelid) could occur after 15 minutes of downward gaze. The analysis of the

central and peripheral peak-to-valley amplitudes in our data do not suggest that greater corneal changes occurred under the eyelids.

Eyelid-induced corneal changes were not evident for all subjects in every measurement condition. The combined topography procedure completed for five subjects supports the conclusion that this is most likely due to the location of the eyelid on peripheral cornea (Appendix 2). It was demonstrated that the absence of eyelid-induced corneal changes within the central topography maps often was due to the limits of the topography area captured rather than there being no eyelid-induced corneal change.

The steady fixation conditions tested in this experiment provided a measure of the eyelid-induced corneal changes with no eyelid or globe movement, apart from regular blinking. During the steady fixation task conditions eyelid movement was limited as there were no horizontal or vertical gaze shifts. However there were still eyelid movements associated with blinking that may have influenced corneal topographical changes. The blink rate in downward gaze is between 1.4 and 14.4 blinks/minute for normal adults (Doughty 2001), which is slightly reduced compared with primary gaze due to less exposure of the ocular surface (Cho *et al.* 2000; Doughty 2001). However as a typical blink lasts 0.26 seconds (Doane 1980) less than 7% of the total time is spent blinking, so natural variations in blink rate are unlikely to influence the corneal changes.

The 6 to 10 µm thick tear film (Doane 1980) overlying the cornea influences the measurement of corneal topography (Buehren *et al.* 2001; Németh *et al.* 2001; Zhu *et al.* 2007). Placido-based videokeratoscopes, such as the Medmont, rely on reflection from the precorneal tear film layer to determine corneal topography, so the measurement can be affected by tear film inconsistencies. It is possible that in this experiment tears may have pooled in the depression of eyelid-induced corneal change resulting in an underestimation of the true peak-to-valley amplitudes. However, it is interesting to note that the tear layer did not appear to totally fill the corneal depression. One possible explanation is that if eyelid pressure alters the microvilli and glycocalyx on the corneal surface then perhaps the tears may temporarily not cover the cornea in this region. To investigate this, the tear layer of 4 subjects was examined using fluorescein

after downward gaze. Immediate inspection of the tear film layer (without blinking) revealed that the tears were mainly concentrated within the palpebral aperture space. There was an absence of tears close to the prior position of the eyelid margins similar to the “black lines” in the tear film that occur at the eyelid margins for incomplete blinks (Miller *et al.* 2002). However within three blinks the tear film was spread uniformly over the ocular surface. As subjects were instructed to blink several times before videokeratoscopy measurements it is unlikely that measured corneal topography changes were changes in the tear film. Nor does it appear that local eyelid pressure alters the ability of the tears to spread across the corneal surface. Although the tear film is quite stable in between the build-up and break-up phases, (Németh *et al.* 2001; Iskander *et al.* 2005; Zhu *et al.* 2007) it is not known how the tear film forms over a distorted cornea. There are other corneal topography instruments that do not rely on reflection from the overlying tear film such as the PAR CTS (PAR vision systems, New Hartford, NY, USA) (raster photography), Pentacam (Oculus Inc., Dutenhofen, Germany) (Scheimpflug imaging) or Humphrey-Zeiss Optical Coherence Tomographer (Carl Zeiss Meditec, Jena, Germany). However the current resolution of these instruments is insufficient to measure eyelid-induced corneal changes such as those reported here (Tang *et al.* 2000; O'Donnell 2005; Hashemi and Mehravaran 2007).

In summary, we have shown that eyelid tilt, curvature and position are influential in the magnitude of eyelid-induced corneal changes. These corneal changes are optically and clinically significant considering that the magnitudes were approximately 0.25 D group mean change after only 15 minutes of the downward task and can be much larger for individual subjects. This offers a possible explanation for some of the variation in refraction observed from day-to-day. When high accuracy in refraction required, sustained tasks performed in downward gaze should be avoided for at least 30 minutes prior to assessment and if not, the refraction should be qualified in terms of the prior visual tasks.

Several inferences about the pressure of the eyelids on the cornea can be drawn from the analysis of the corneal topography changes in this study. It appears that the degree of downward gaze alters the upper eyelid pressure on the cornea. In large angles of downward gaze, when the lower eyelid is in contact with the central cornea, its pressure

is greater than that of the upper eyelid despite being further from the corneal centre. Reading-associated eye movements increase the depth of corneal change, presumably as a result of kinetic friction. An association between the width of Marx's line and the depth of corneal change was observed and is evidence that it is likely to be the point of frictional contact between the cornea and eyelids. Also certain individuals experience greater eyelid-induced corneal changes due to either more susceptible corneas or certain eyelid anatomical features (eyelid curvature, tilt or position). The ability to directly measure eyelid pressure would enable confirmation of these eyelid pressure inferences and lead to better understanding of the mechanism of these corneal changes.

Chapter 3: Development of an eyelid pressure measurement technique

3.1 Introduction

It has been shown that pressure from the eyelids can alter the corneal surface. There have been three published studies over the past five decades where the authors have designed systems to attempt to measure eyelid pressure (Miller 1967; Lydon and Tait 1988; Shikura *et al.* 1993). These techniques have used modified contact lenses attached to manometers. The manometers are usually u-shaped tubes filled with liquid with either end exposed to different pressures. The liquid column rises or falls with the change in liquid level representing the applied pressure of the eyelid. These devices were used to measure eyelid pressure while the subjects performed "gentle" or "forced" blinks, and static eyelid pressure was not reported. The contact lens-manometer devices were quite thick (up to 2.5 mm), so the validity of the measurements was limited by the unnatural thickness of the device. This Chapter outlines the development of a technique to measure eyelid pressure using thin piezoresistive pressure sensors. The pressure units used in this chapter are psi, since this is the units most commonly used by engineers and are also the units used to rate the sensors.

3.1.1 Tekscan pressure sensors

In 1987, Tekscan Inc. (Boston, MA, USA) introduced multiplexed array piezoresistive tactile sensors (T-scan) to measure the forces in the mouth during occlusion. These piezoresistive sensors contain piezoresistive ink which changes in response to mechanical deformation. Following the T-scan other sensors were designed to measure stresses under the foot during gait (F-Scan) and between the articulating surfaces of the knee (K-Scan). These sensors consist of two Mylar sheets which are layered with a conductive material (silver) and pressure-sensitive ink. The layers are created by a printing process with one layer having rows and the other layer columns to

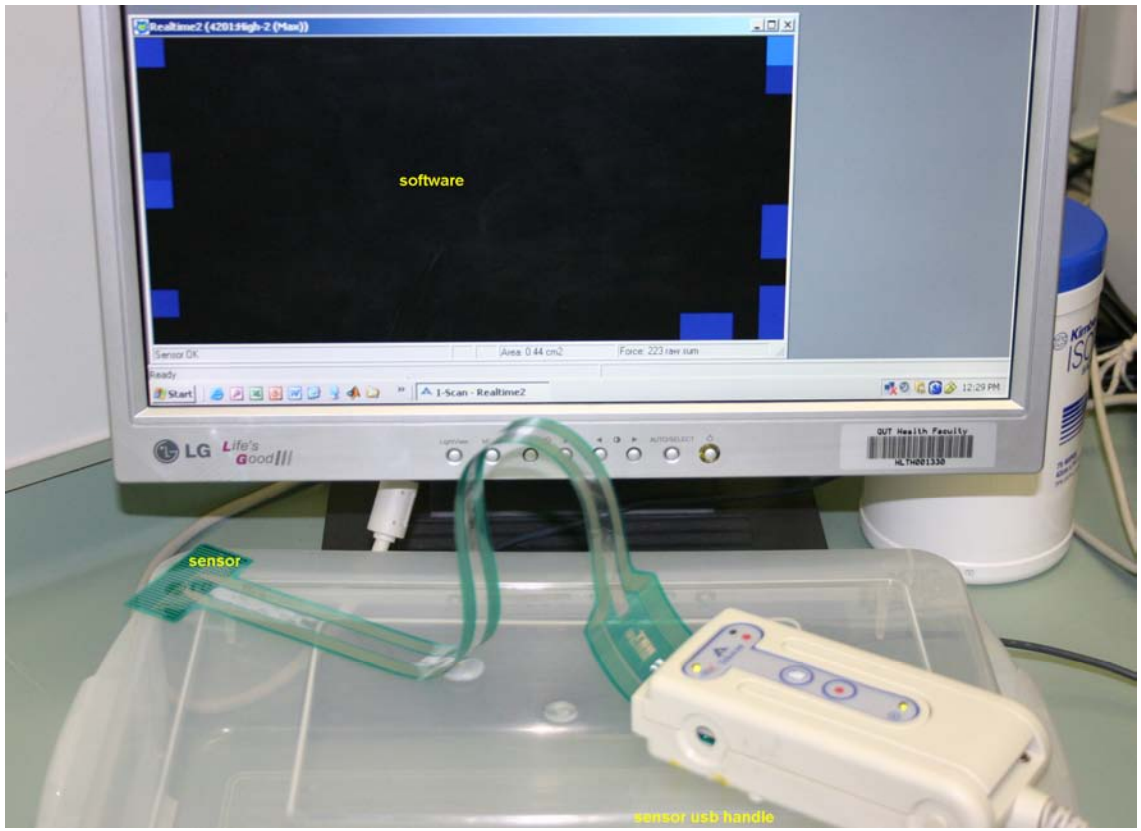

Figure 3-1: A Tekscan sensor model #4201 inserted in the handle and connected to the computer via USB connection with the output displayed on the monitor.

create a matrix when they are laminated together. At the junction of each row and column is a pressure sensing cell or “sensel”. The spacing of these sensels is varied depending on the application, but can be as close as 0.5 mm. The electrical resistance of each sensel varies inversely with the applied pressure. The raw digital output of the sensors extends from 0 to a value of 255. Output from a sensor is sent to the computer through a USB port (Figure 3-1). Software is supplied to control the sampling rate and gain with the data displayed dynamically. There are also options for graphing the output against time or position, and data can be exported in ASCII format for further processing. Tekscan software allows capture of video footage using a DV camera connected to the computer via firewire. A trigger starts the data and video capture. They can be synchronised (to allow for the delay in computer processing) using an LED which lights up in the video frame to mark the start of the data capture. The video is captured at 30 Hz while the maximum capture frequency of the pressure data is 9.84 Hz.

Tactile pressure sensors (I-scan) made by Tekscan Inc (Boston, MA, USA) were chosen for this application as they are thin and are available in various physical dimensions and pressure sensitivities. The labelled pressure range of the sensor is determined after manufacture by loading the sensor with various known pressures. The pressure sensitivity of Tekscan sensors varies with the upper pressure limit being as low as 5 psi or as high as 25 000 psi. Sensor model #4201 (Appendix 3) was selected for this study as it is thin (0.17 mm), has a low pressure range of 5 psi and good sensitivity. It is also suitable as it is non-toxic, waterproof so that tears do not influence measurements and is able to conform to the surface of the eye. Additionally its size and shape can be altered by trimming the edges. To be able to use these sensors to measure eyelid pressure, the sensors needed to be trimmed, resealed and attached to a custom designed contact lens. A calibration apparatus was constructed to calibrate the sensor output into real pressure units. To understand the output response of the sensor, the properties drift, hysteresis, compressibility, precision and the influence of temperature and curvature were examined. From these results, criteria on the best way to use the sensors were developed. Also an *in vivo* measurement apparatus was developed to place the sensor-contact lens combination accurately and safely on the eye to measure eyelid pressure.

3.2 Sensor-contact lens combination

It has been reported that curving Tekscan sensors can cause both an offset and decreased sensitivity of the sensor's output (Ferguson-Pell *et al.* 2000). Therefore for the output to result only from the applied pressure to the sensor and not curvature changes, it must be fastened in a set shape on a non-flexible surface. So the pressure sensor was attached to a specially designed rigid contact lens.

3.2.1 Contoured Surfaces

When pressure sensors are applied to contoured surfaces they are placed under stress which impacts their output (Buis and Convery 1997). Tekscan sensors can be used on curved surfaces although the inability to conform to highly contoured surfaces has been noted (Polliack *et al.* 2000). It is very difficult to curve the sensors in two planes (spherical curvature) but bending in one plane is more achievable (Woodburn and Helliwell, 1996). So within limits, Tekscan sensors may be used on cylindrical, spherical or sphero-cylindrical surfaces but it is necessary to take into account the induced offset and to calibrate under the same curvature conditions (Maurer *et al.* 2003). The effect of convex cylindrical surfaces with radii between 8.0 and 51.7 mm was investigated for Tekscan flexiforce sensors rated at 9 psi with loads up to 1 psi (Ferguson-Pell *et al.* 2000). Curvature caused an offset in output at zero pressure, with an inverse relationship between offset and radius of curvature. This offset dramatically increased for curves with a radius of less than 32 mm and there was also a substantial decrease in the sensor's sensitivity. So curvature not only introduced an offset to the measurement but it also altered the properties of the sensor.

The effect of curvature on the model #4201 Tekscan sensor was investigated for cylindrical radii of between 10 and 54 mm and pressure loads of between 0 to 0.5 psi. The sensor was fastened onto segments of flat PVC various convex curvature radii: 10, 13, 17, 22, 28, 34, 40, 44, 54 mm. The output of the sensors was recorded without a load and after loads of approximately 0.1, 0.2 0.3, 0.4 and 0.5 psi applied for 1 minute. The flatter curvatures were measured first so that the sensor did not retain any "curvature memory". For each curvature the output pressure was plotted against the input pressure (Figure 3-2). The significance of curvature on the offset

and sensitivity of responses was determined by plotting the output pressure and output/input (sensitivity) respectively versus the radius of curvature (Figure 3-3).

It was observed that as the radius of curvature decreased the initial offset increased (with no load). Examining the sensitivity of the sensor, it was similar for radii between 17 and 54 mm and was slightly increased compared to the flat condition. For smaller radii of curvatures (10 and 13 mm), there was difficulty maintaining the sensor in contact with the PVC surface, as previously reported for highly curved surface (Polliack *et al.* 2000). While the sensitivities were higher for these curvatures, the raw outputs approached the upper limit of the sensor. Based on this experiment it was decided that the smallest radius of curvature that could be used with the model #4201 Tekscan sensors was 17 mm.

It has been noted that in addition to an output offset, the response of the sensor also alters with induced curvature (Polliack *et al.* 2000). An extensive investigation of the impact of curvature was conducted by Polliack *et al.* (2000) who attached an F-socket sensor to a variety of contours on the leg stump of amputees. The sites at which the sensor was attached ranged in radius of curvature from cylinders of 17 to 50 mm and spherical surfaces of 54 to 100 mm radii. The sensors behaved differently in terms of hysteresis and drift when used on contoured surfaces compared to being loaded while flat. While the hysteresis error decreased for the contoured surfaces, the drift error increased (Table 3-1). These relatively large errors for hysteresis and drift resulted from a large range of dynamic loads and long load times (up to 20 minutes) that were considered. They concluded that the sensor should be preferably used for static conditions and its properties should be validated in the same physical conditions as the measurement.

Table 3-1: Average errors of drift and hysteresis for flat and contoured sensors.

	Flat surface	*Contoured Surfaces*
Hysteresis error (%)	41.88 ± 14.9	24.0 ± 19.2
Drift error (%)	11.9 ± 6.05	33.2 ± 26.5

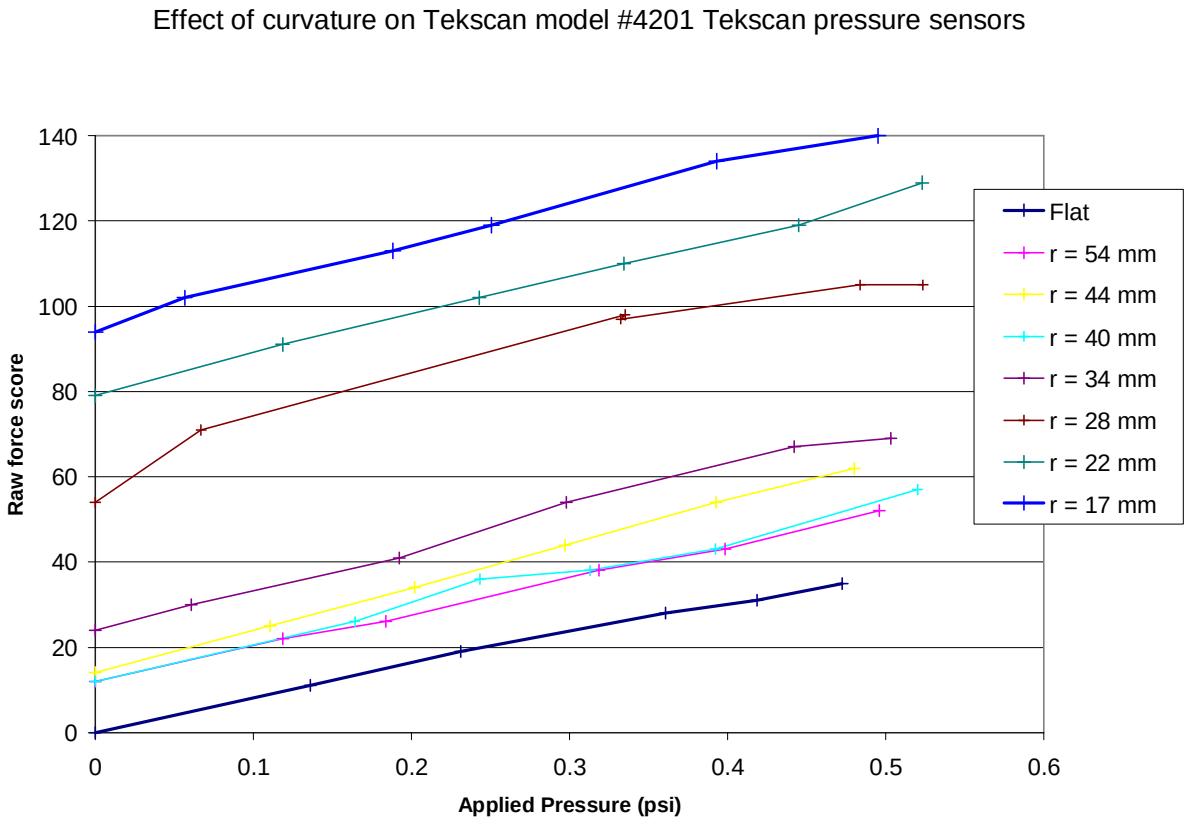

Figure 3-2: The effect of curvature on the output of a model #4201 Tekscan pressure sensor with loads of 0.1 psi to 0.5 psi (0.1 psi steps) loaded for 1 minute. There was increasing raw score output with decreasing curvature (initial offset, no load).

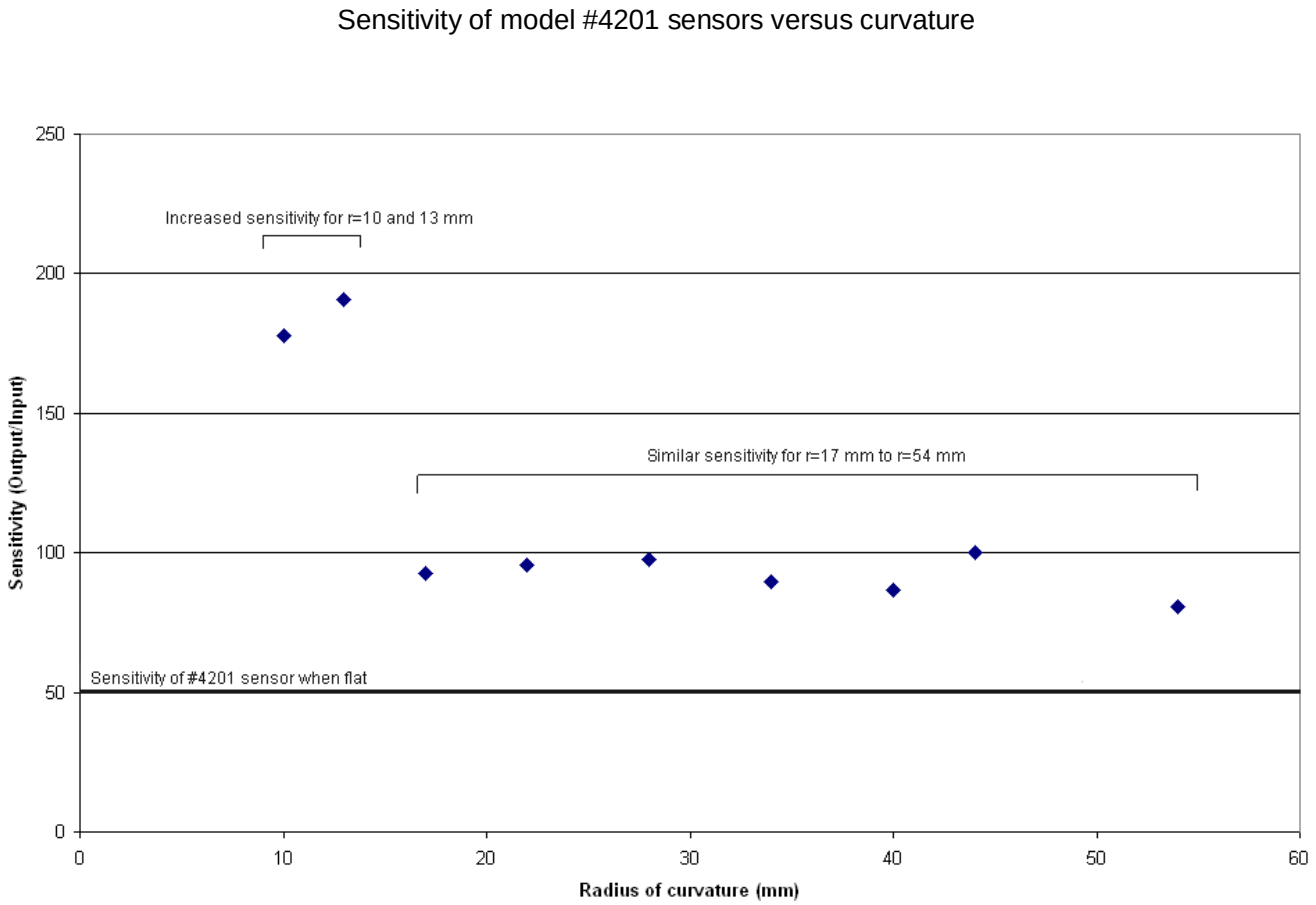

Figure 3-3: Sensitivity (output/input) of a model #4201 Tekscan sensor for various curvatures (r = 10 to 54 mm) for loads between 0 to 0.5 psi.

3.2.2 Carrier lens parameters

The investigation of the effect of curvature on the pressure sensors revealed that a relatively flat area was required on the contact lens surface to mount the model #4201 Tekscan sensor. To visualise how a flat area could be incorporated into the front contact lens surface, some initial designs were developed (Figure 3-4 and Figure 3-5).

A generic back surface curvature was used with the central and peripheral curvature values based on the average of 100 healthy young subjects with a radius of 7.8 mm and prolate eccentricity of Q = -0.25 (Read *et al.* 2006). The curvature of the cornea and sclera around the limbus cannot be measured by any current technique, but it is known that it is flatter than the cornea so the contact lens curvature was flattened for the final peripheral curve. The large contact lens diameter of 13.5 mm was chosen so that the lens edge would be past the limbus and would maximise stability of the contact lens on eye. So the initial contact lens was ordered with the following parameters:

Optic zone radius / lens diameter / optics zone radius / peripheral curve radius x peripheral curve width

$$7.8 / 13.5 / 8.0 / \begin{matrix} 9.5 \times 1.25 \\ 11.0 \times 1.5 \end{matrix}$$

Due to excessive edge lift (Figure 3-6), the peripheral curves were altered:

$$7.8 / 13.5 / 8.0 / \begin{matrix} 9.0 \times 1.0 \\ 10.0 \times 1.0 \\ 11.0 \times 0.75 \end{matrix}$$

Pilot studies with the 13.5 mm diameter lens on eye revealed that the lower eyelid would generally sit over the lower edge of lens but would sometimes slide off and push on the lower edge of the lens. A 15 mm diameter lens was better with both eyelids maintaining their position on the contact lens.

The lens order for the 15 mm contact lens which fitted well was:

$$7.8 / 15.0 / 8.0 / \begin{matrix} 8.8 \times 1.0 \\ 9.8 \times 1.25 \\ 11.0 \times 1.25 \end{matrix}$$

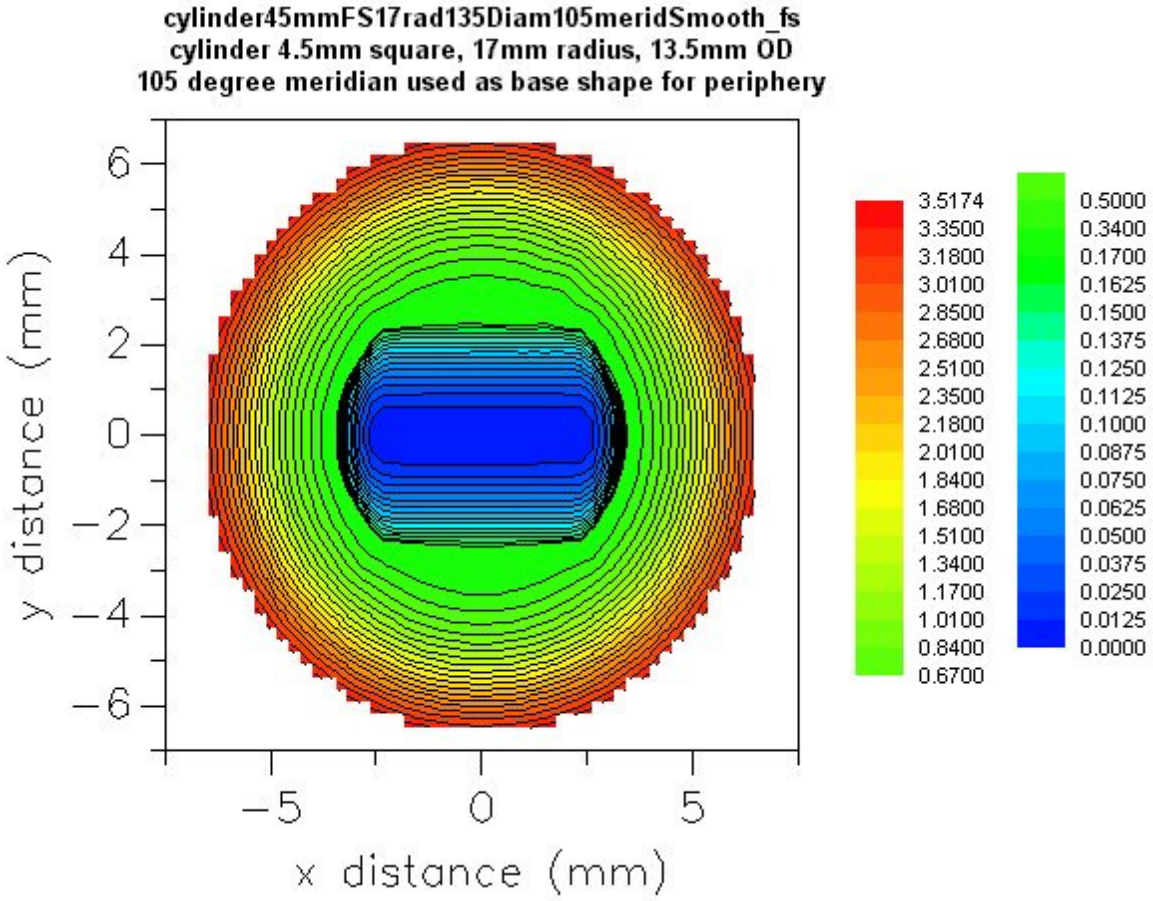

Figure 3-4: Trial contact lens design with “flat” central area with a cylindrical radius of 17 mm and lens diameter of 13.5 mm.

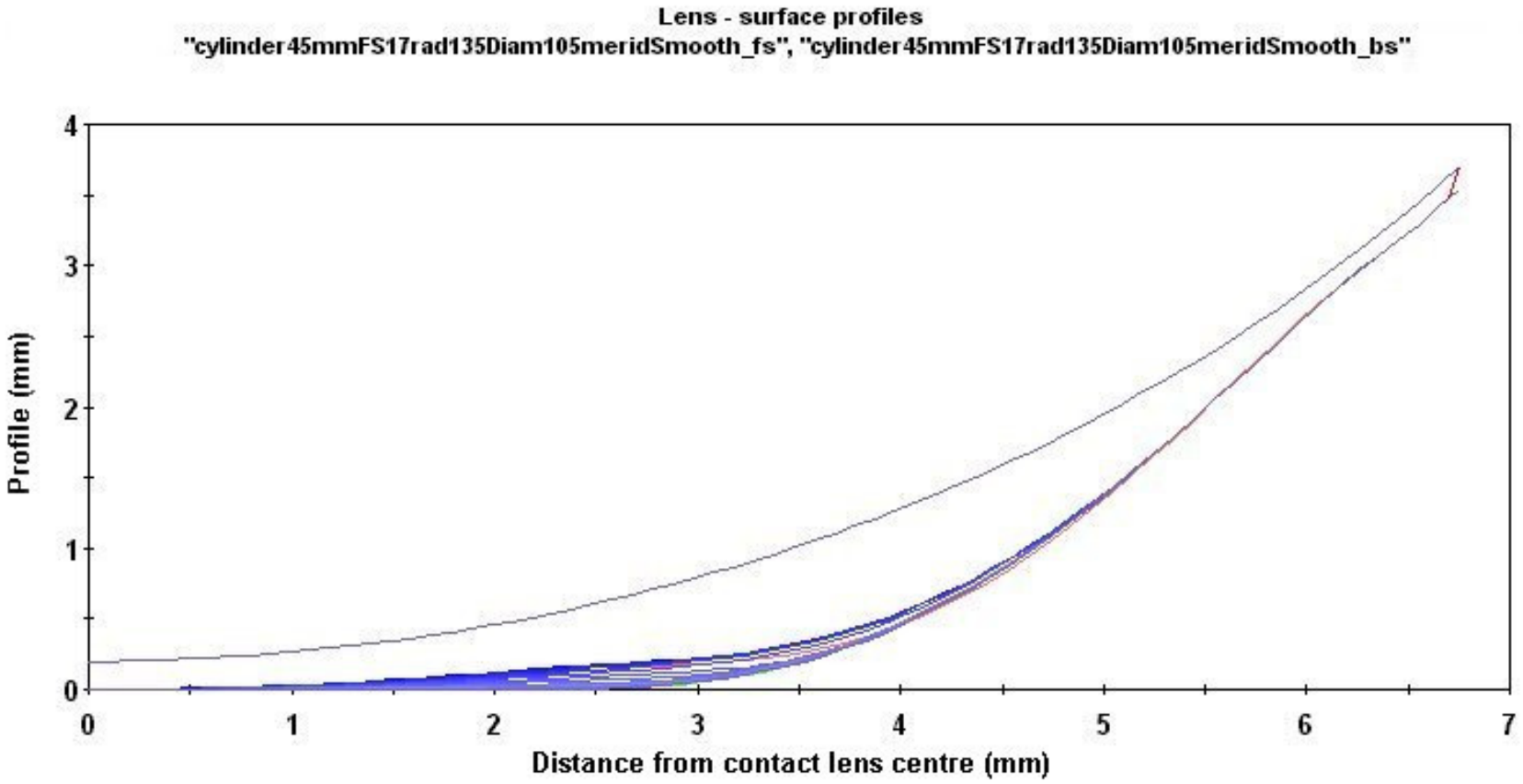

Figure 3-5: Profile of the trial contact lens design from lens centre to edge (24 equally spaced semi-meridians) showing that a “flat” area of cylindrical radius (17 mm) can be created centrally with relatively smooth peripheral curves.

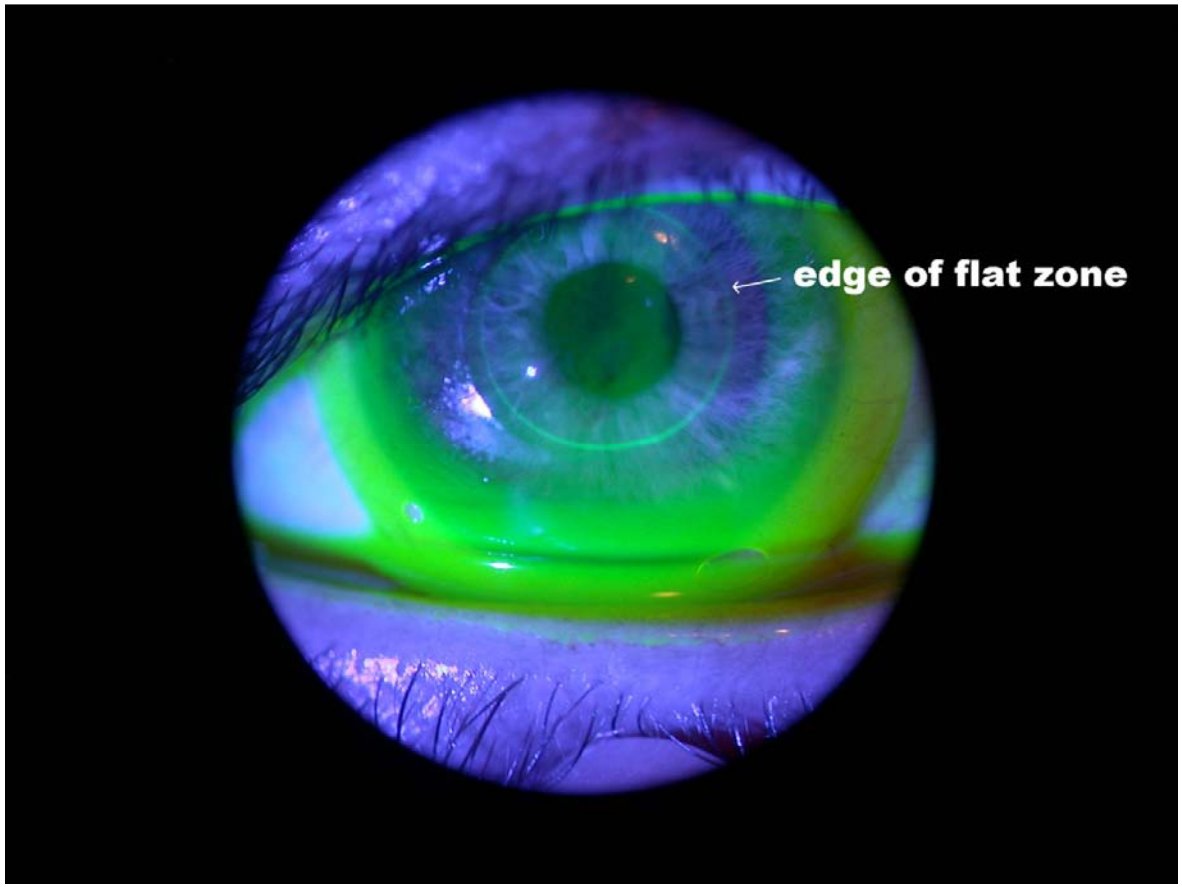

Figure 3-6: Fit of original lens ordered with excessive edge lift. Junction between the central “flat” area and the first peripheral curve is visible.

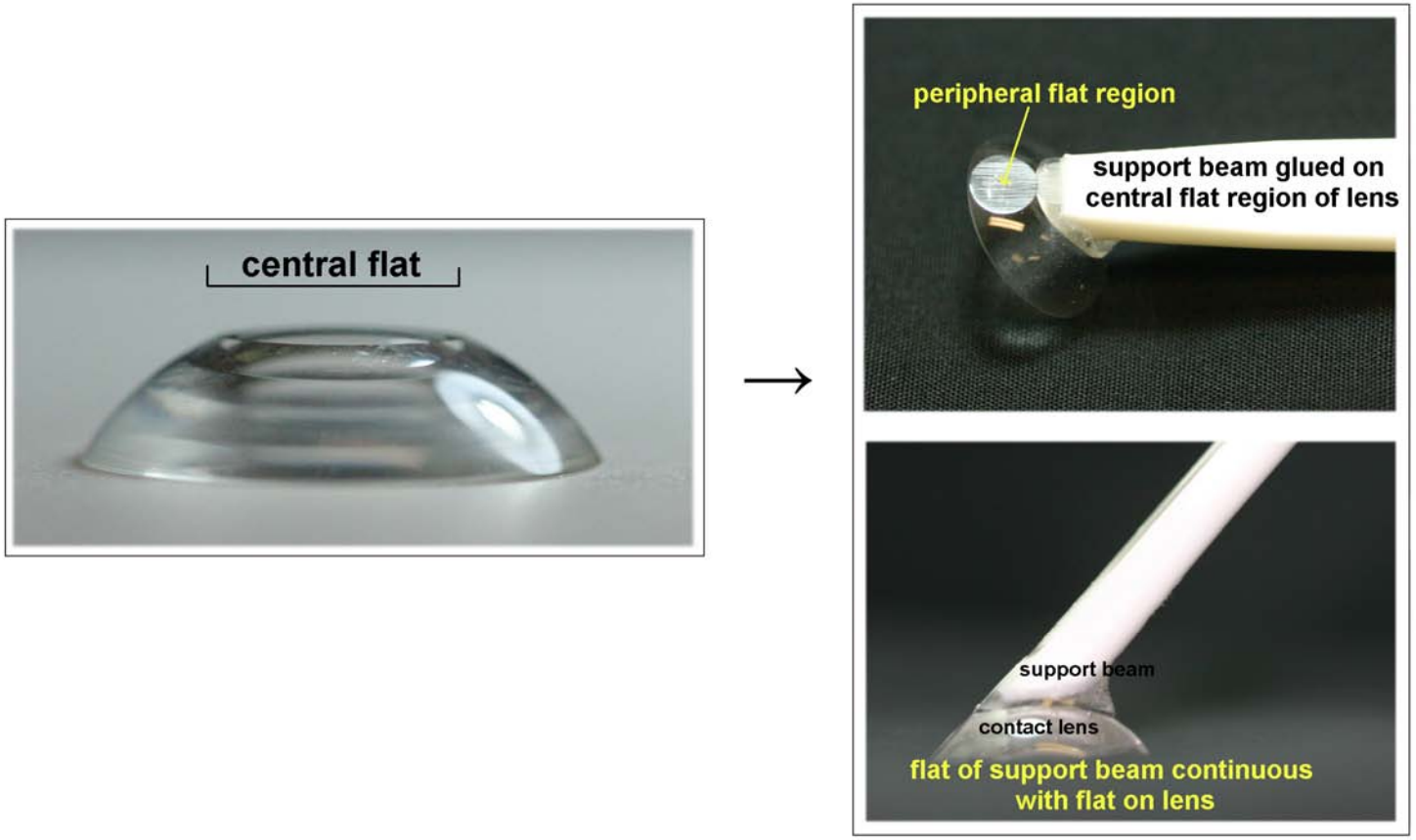

Figure 3-7: Original lens with central flat region (left). Support beam glued to central flat region of lens with peripheral flat region continuous with support beam (right).

The front surface of these contact lenses was manufactured with a flat central area of 6 mm diameter, to which the sensors could be adhered, while the periphery was designed to have a normal as possible lens edge so that the eyelids could still easily slide over the contact lens surface. While the central flat area was initially trialled (as it could be easily manufactured), this region needed to be in the lens periphery so that the eyelid margin in its usual resting position would be in direct contact with the sensor. While contact lenses could be manufactured with a flat central area, the flat peripheral area had to be filed by hand (Figure 3-7). Exactly where the peripheral flat area was located was decided based on the eyelid morphology data of Read *et al.* (2006). The upper eyelid is on average 3.6 mm, 3.3 mm and 3.1 mm from corneal centre for primary gaze, 20˚ and 40˚ downward gaze respectively. While the lower eyelid is on average 6.1 mm, 4.6 mm and 3.3 mm from corneal centre for primary gaze, 20˚ and 40˚ downward gaze respectively. Considering that the dimensions of the sensor to be attached to the contact lens were approximately 3 mm by 3 mm, it was decided that the flat area should be located between 3 mm to 6 mm from the centre of the contact lens.

A few measures were applied to ensure limited flexure of the contact lens. The minimum acceptable contact lens centre thickness was considered in terms of lens flexure. Lenses of centre thickness 0.2 mm, 0.5 mm and 1 mm had peripheral thicknesses of 0.7 mm, 1 mm and 1.3 mm respectively at 4.5 mm from the contact lens centre. These thicknesses reduced to approximately 0.3 mm, 0.5 mm and 0.7 mm respectively after filing to create the flat region. This is well above the recorded critical minimum centre thickness of a PMMA contact lens to avoid lens flexure of 0.13 mm (Harris and Chu 1972). Also surface tension of the post-lens tear fluid layer has been found to maintain lens shape rather than create lens flexure (Corzine and Klein 1997). For this reason when the contact lenses were positioned on the eye, it was verified using the front and side cameras that the tear layer filled behind the lens. Since the sensors are known to be are sensitive to curvature changes, the sensor-contact lens combination was placed in the calibration device with rubber bands over the edges of the lens (to simulate the eyelids resting on the lens surface) (Figure 3-8). No change in the sensor output was recorded, suggesting that the sensor-contact lens combination was not susceptible to flexure or curvature artefacts.

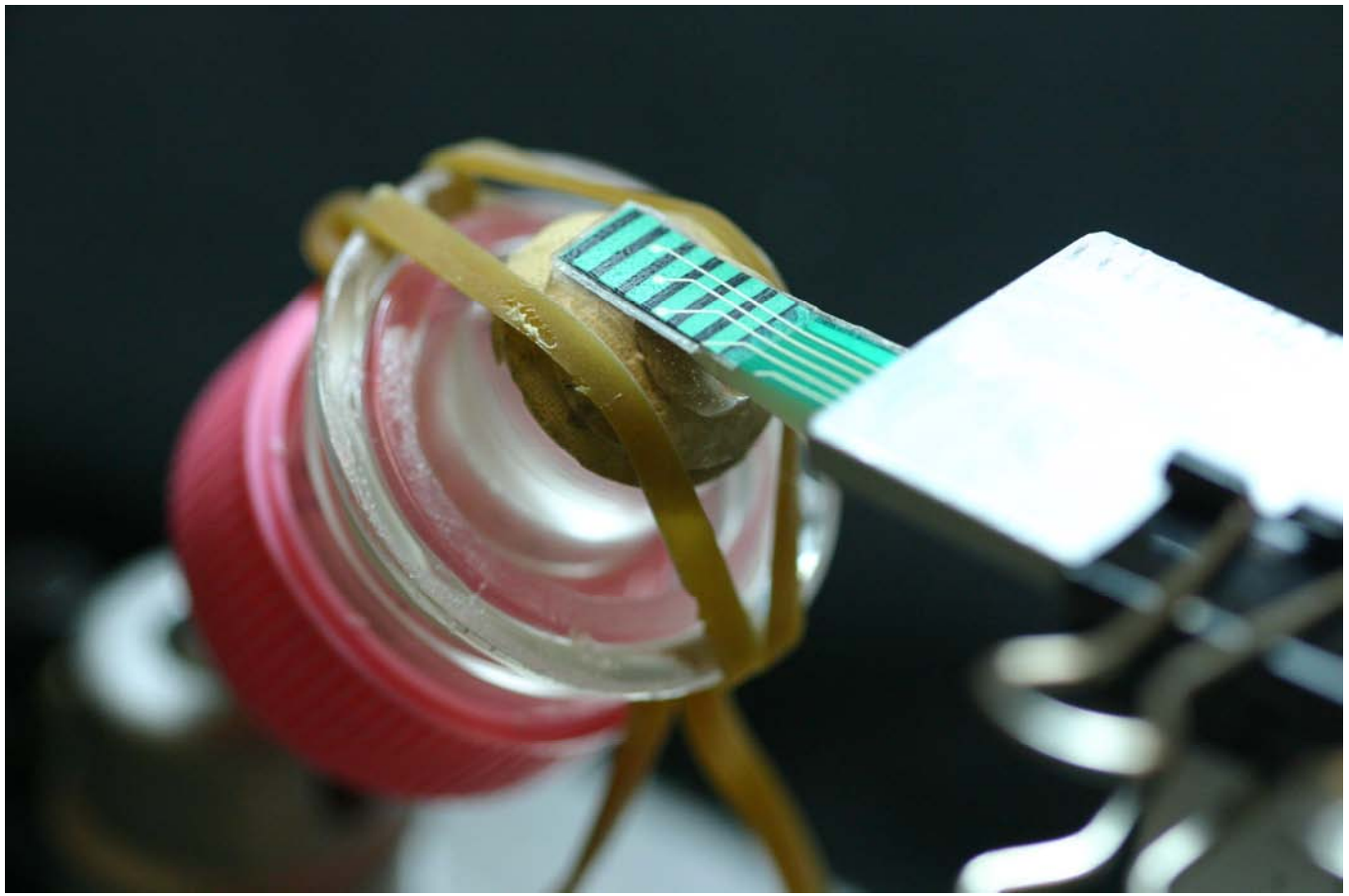

Figure 3-8: The sensor-contact lens combination in the rubber band holder simulating eyelids on the lens. There was no output change with the rubber bands so it can be assumed that there was no flexure of the contact lens surface over the region to which the sensor was attached.

3.2.3 Fixing the sensor to the contact lens

The following is the process of attaching the sensor to a rigid contact lens with a plastic support beam. Once the method of successfully assembling a sensor-contact lens combination was determined, rigs were made so that repeatable combinations could be produced (Figure 3-9).

1. So that the contact lens could be stabilised on the eye (without movement or rotation), a support beam was required. This was determined after trials of inserting the sensor-contact lens with no support beam. The lens and active part of the sensor would try to rotate against the sensor tail causing false readings. The support beam was placed on the angled holder and ground using a mounted rotary tool so that the end would be flat against the central flat area of the contact lens when held at that angle (Figure 3-9). One of the initial versions of the sensor-contact lens had the sensor flat on the lens with a bend in the sensor to then run along the support beam perpendicular to the contact lens (Figure 3-10). However this resulted in shearing effects with the back and front Mylar sheets of the sensor shifting against each other, particularly when the sensor was clamped in position (Figure 3-11).

2. The support beam was clamped at the other end of the holder (on a slide mechanism) and positioned so that the ground flat end was in contact with the central flat of the contact lens (Figure 3-9). The plastic support beam was then moved away from the contact lens using the slide mechanism so that the glue could be applied to the end of the beam. It was then placed back on the contact lens surface and left to set for at least one hour. A toxicity test has been previously conducted on this type of glue (Appendix 4).

3. The contact lens-support beam combination was then clamped on the flat ledge of the contact lens holder so that a flat area could be ground on the lens periphery (Figure 3-9). With the plastic beam held horizontal, the lens was ground using the mounted rotary tool so that the flat area was continuous onto the contact lens surface. Alternatively this peripheral flat region could be created with a file moved along the support beam. The filed region on the contact lens could then be polished using a polishing attachment on the rotary tool.

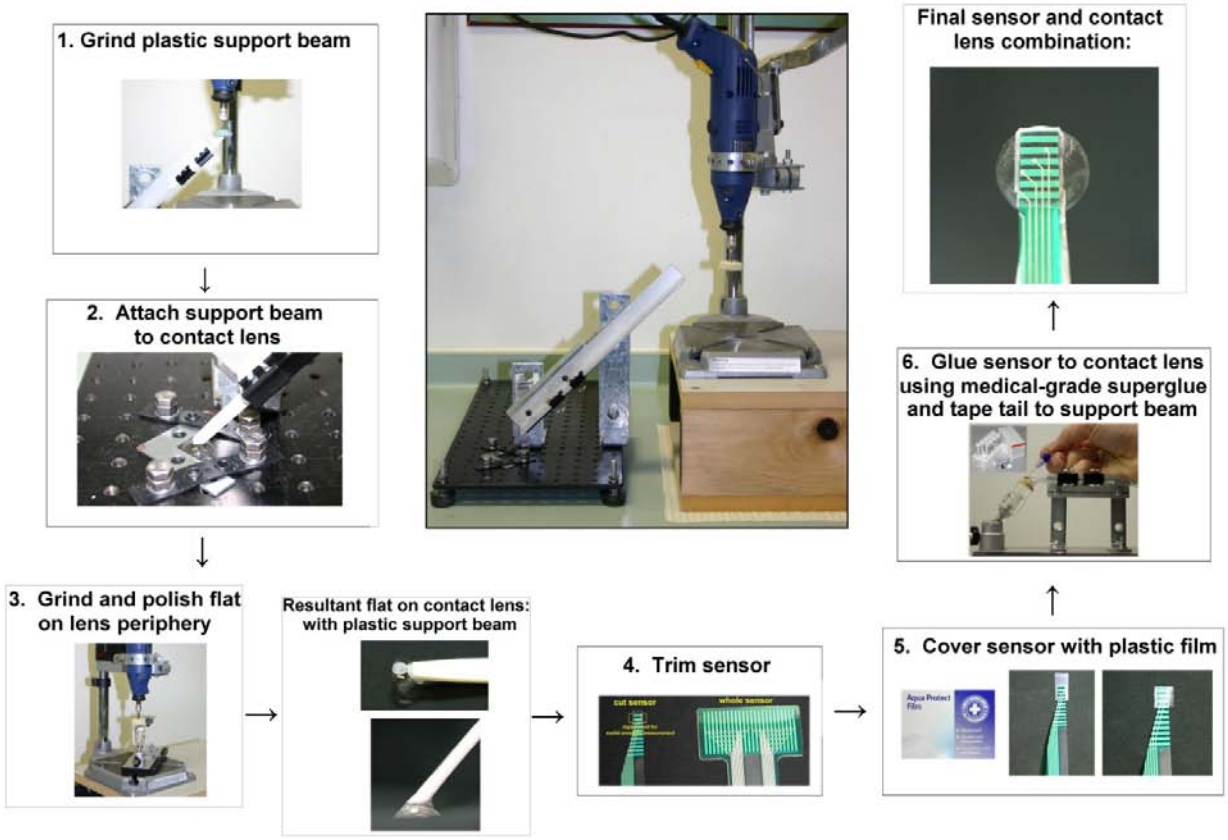

Figure 3-9: Constructing the sensor-contact lens combination: 1) Grinding plastic support beam, 2) Gluing support beam to contact lens using araldite, 3) Grinding and polishing a peripheral flat area on the lens, 4) Trimming the sensor, 5) Covering the sensor with aqua-film tape and 6) Gluing the active part of the sensor to the peripheral flat lens area and taping the tail to the support beam.

4. To attach the sensor to the contact lens it needed to be trimmed to the appropriate size of 9 cells (3 rows by 3 columns) that were to be attached to the contact lens (Figure 3-9).

5. Trimming the sensor meant that it was no longer sealed so a layer of aqua protect film was placed around the entire sensor (Figure 3-9). This medical tape known also as “second skin” is used to cover the point of insertion of intravenous drips, is water and bacteria proof, very thin and flexible. This tape was also appropriate as it can be disinfected using mediswabs (70% isopropyl alcohol) as per the standards for optometric equipment that comes in contact with the eye (Ethics approval – Appendix 5). While the application of the tape was observed to alter the sensitivity of the sensor, this did not influence the measurements as calibration was performed after the tape had been applied to the sensor. The example in Figure 3-12 shows the same pressure being applied with the raw score being higher when the sensor was enclosed in tape. This is most likely due to the tape pulling the two layers of the sensor closer together.

6. The tail of the sensor was fastened to the plastic support beam using double sided tape. While the active part of the sensor was adhered to the contact lens surface using Histoacryl, a medical cyanoacrylate, which has FDA approval (Figure 3-9). It is typically used to seal skin wounds such as lacerations and incisions and has been used for corneal wounds (Leung *et al.* 2005). It was applied in a very thin layer using a precision needle. Output of the sensor was compared with and without it being glued to the contact lens and there was not much difference between the two conditions (Figure 3-13). However it was thought best to fasten the sensor to the contact lens so there would be no possibility of sensor shape changes influencing the measurements.

Figure 3-10: The initial bent sensor-contact lens combination (left) which resulted in shearing effects between the layers of the sensor and the flat sensor-contact lens combination (right) with the sensor lying continuously flat from the contact lens surface onto the support beam.

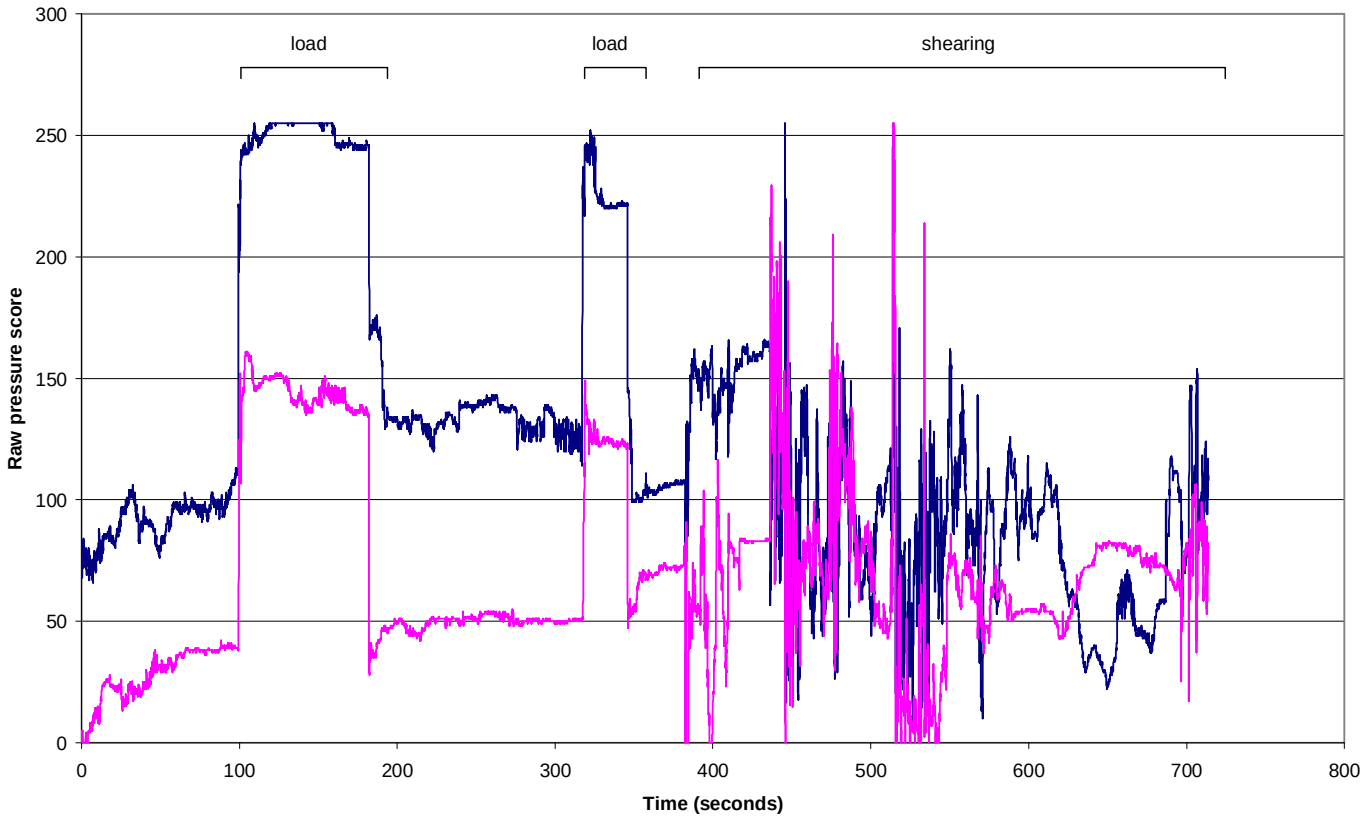

Figure 3-11: Data from two pressure cells. Pressure load applied twice then a metal clamp was applied to the sensor tail and support beam resulting in shearing between the sensor layers and noisy sensor output.

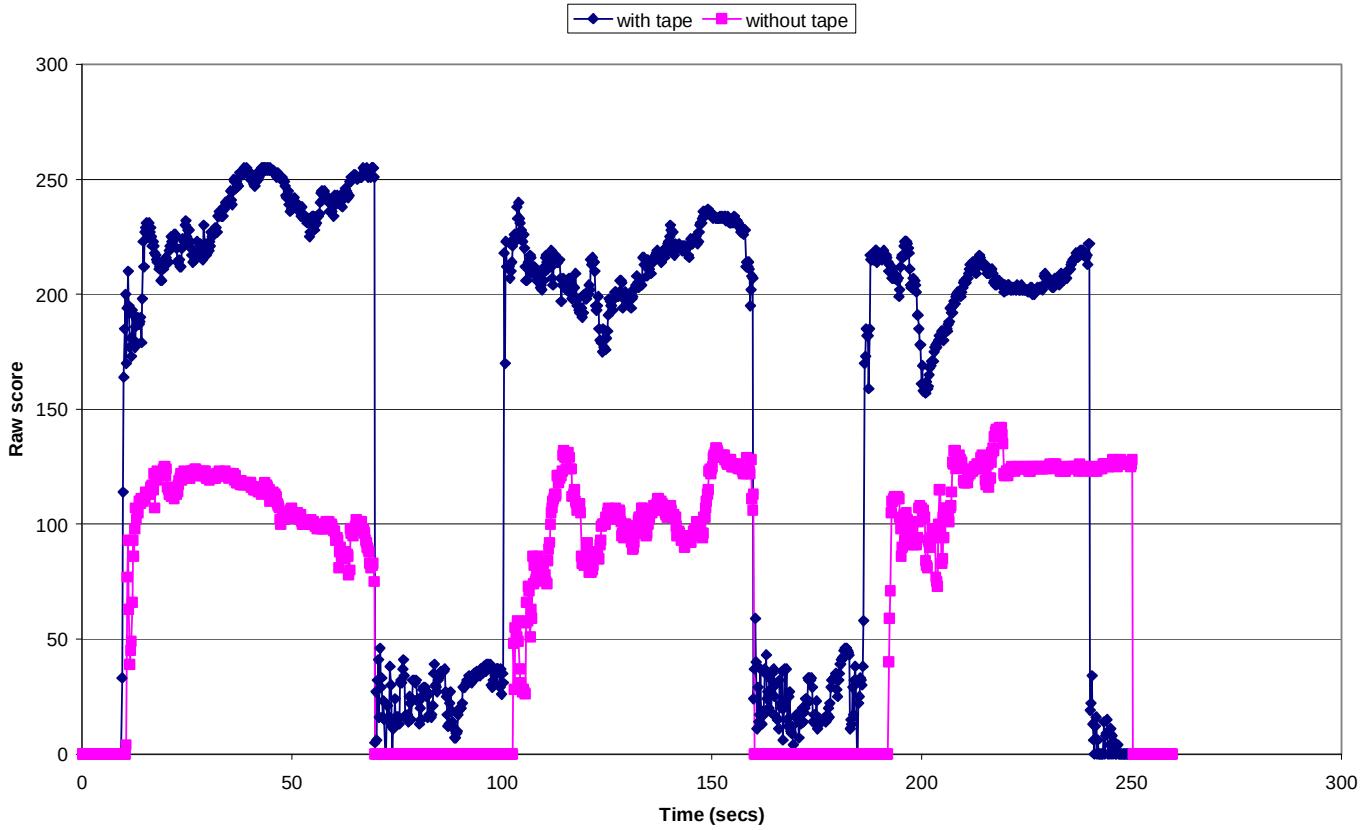

Figure 3-12: The raw score output of 0.15 psi applied three times to a sensor before and after it has been enclosed in aqua film tape.

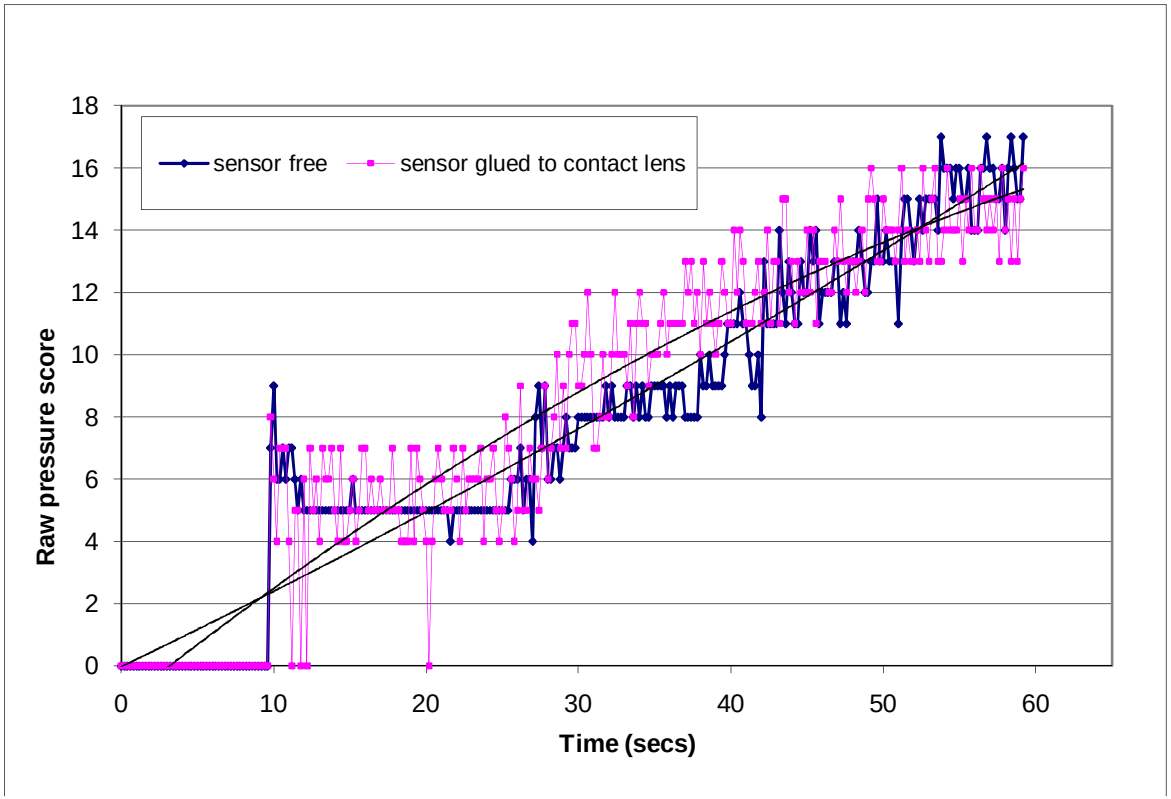

Figure 3-13: Similar output (fit with 2nd order polynomials) with and without the sensor being glued to the underlying contact lens for approximately 50 seconds after loading.

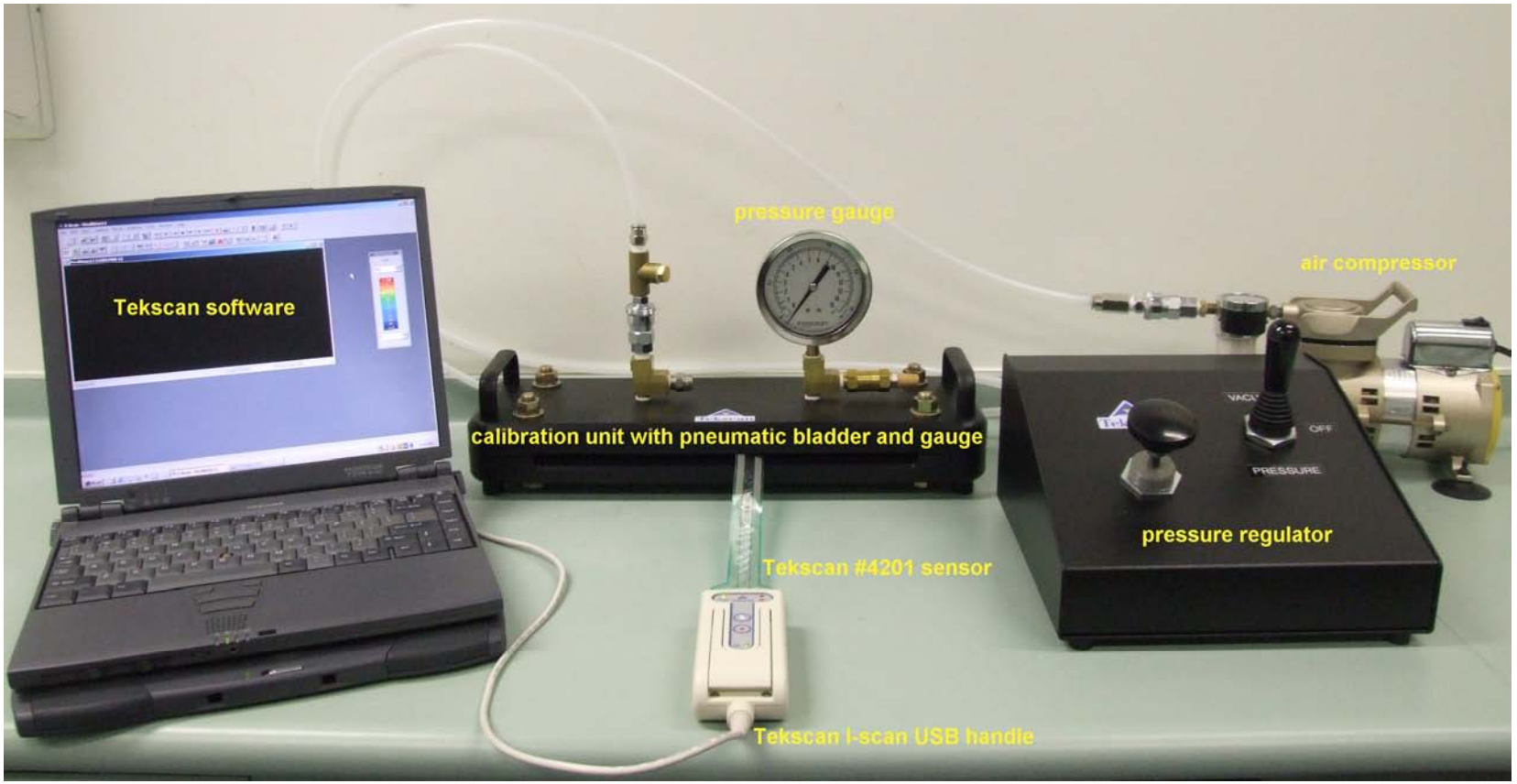

Figure 3-14: Tekscan pneumatic calibration unit. Air flow from right to left from the air compressor through the pressure regulator to the calibration unit which consists of a bladder to apply the pressure and a 0 to 15 psi pressure gauge. The sensor is connected to the computer via a USB handle so that the output can be viewed using the Tekscan software.

3.3 Development of a calibration system

3.3.1 Tekscan pneumatic calibration system

A pneumatic calibration unit was purchased with the I-scan pressure measurement system from Tekscan Inc. (Boston, MA, USA), to produce a calibration curve to convert the raw digital output from the sensor into actual pressure units. It uses a pneumatic bladder, controlled by a pressure regulator, to apply known pressures to the inserted sensor (Figure 3-14).

Tekscan recommends a dual procedure consisting of equilibration and calibration. Equilibration aims to minimise the variation in the output across the cells of a given sensor. This step is needed as each sensor is unique and the pressure-sensitive ink is not entirely uniform throughout the whole sensor. Pressure cells within a sensor vary in their sensitivity. By applying a uniform load, a scaling factor can be applied to each cell so that its value is equal to the average digital output for all the loaded cells. The scaling factors vary depending on the applied load so equilibration needs to be conducted over a large range of pressures. The Tekscan software allows equilibration for up to 9 different pressure levels and a linear fit is used to extrapolate the scaling factors for other loads. To examine the Tekscan equilibration procedure, loads of 0.1, 0.2, 0.3 and 0.5 psi were applied to a sensor and the average and standard deviation of the raw scores across all 264 cells were calculated. The variation in output (standard deviation) between the cells of the sensor was reduced after equilibration (Figure 3-15).

The second stage of calibration converts the raw digital score into standard pressure units. Loads of known pressures are evenly applied to the sensor and the raw score is recorded. These data may be fit with a linear calibration where interpolation is made between a zero load and the known calibration load. Alternatively, a 2-point power law calibration involves applying two different loads and the interpolation is based on a power law. For this fit, Tekscan recommends that the two loads be approximately 20% and 80% of the maximum expected test load.

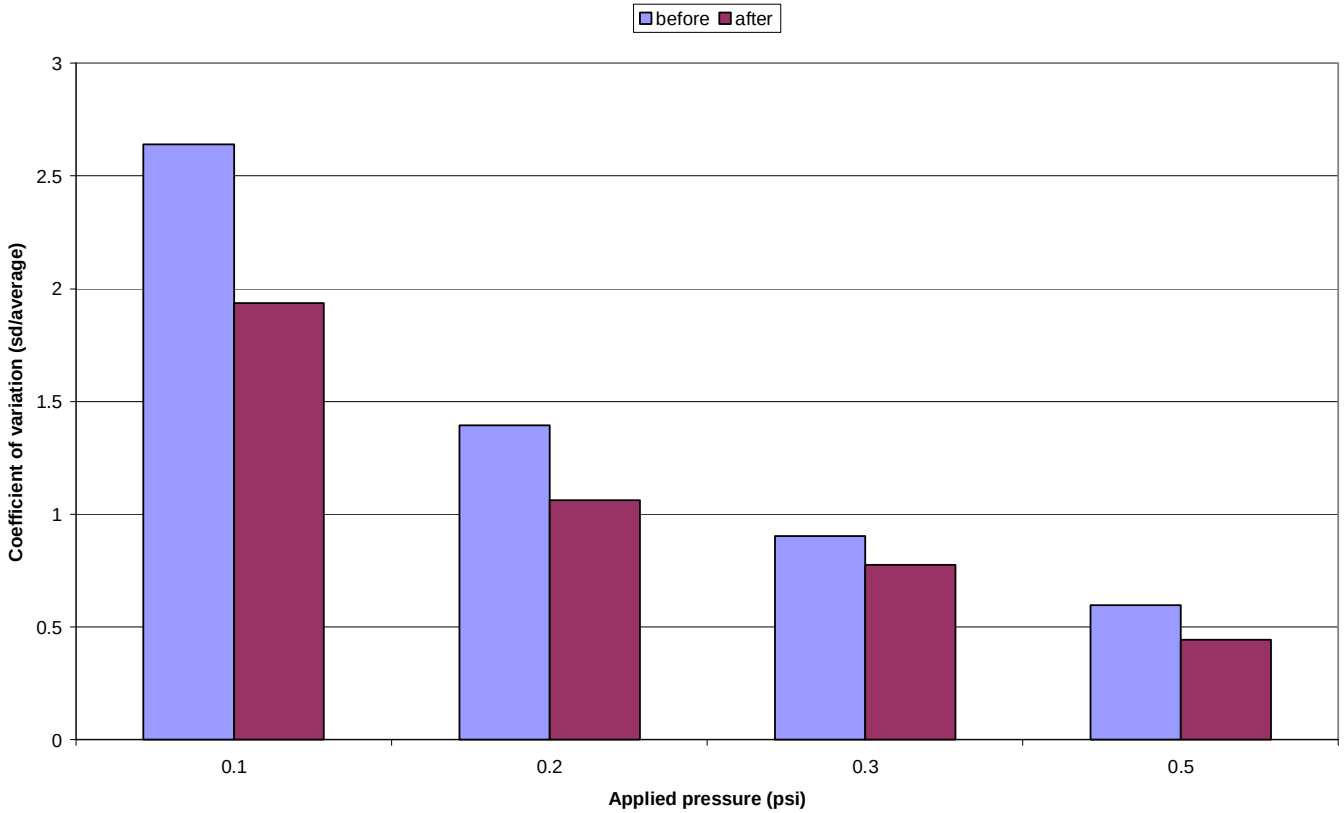

Figure 3-15: Variation between cells of a pressure sensor is decreased (lower coefficient of variation) after equilibration for 0.1, 0.2, 0.3 and 0.5 psi loads.

However the Tekscan calibration unit and software could not be used for the eyelid pressure application. First the calibration unit had a narrow gap (approximately 1 mm) which only allowed flat sensors to be inserted into the apparatus, whereas we needed to calibrate sensors attached to contact lenses that can have an apex to edge depth of up to 0.5 cm. Another potential problem was that it was not designed to conform to the surface of a sensor at low pressures compared to elastic eyelids which wrap to the sensor's surface. Sensor output is sensitive to surface conditions (Luo *et al.* 1998), so it is important to mimic measurement conditions during calibration. For these reasons an alternative calibration system was required.

3.3.2 Pneumatic balloon calibration system

A pneumatic calibration system using an elastic balloon was developed (Figure 3-16 and Figure 3-17). Air from the compressor passed through the pressure regulator to inflate a balloon to a known pressure. The size of the balloon was limited by a plastic container which enabled the pressure of the system to be increased. The balloon applied pressure to the sensor inserted at the bottom of the plastic container. This calibration system allowed the thicker sensor-contact lens combination to be calibrated.

It was confirmed that the elastic surface of the balloon conforms to the sensor better than the pressure applying element of the Tekscan calibration system. This was examined by calibrating and measuring for two different loads (0.5 and 1.5 psi) using both systems. Four measurements were considered: balloon calibrated and balloon measured; balloon calibrated and Tekscan measured; Tekscan calibrated and Tekscan measured and Tekscan calibrated and balloon measured. The average calibrated output of the loaded pressure cells was plotted against the applied load (input pressure) (Figure 3-18).

It was obvious that the accuracy was greatest when the same system was used for both calibration and measurement. The output pressure was underestimated when the sensor was calibrated using the balloon system and then measured with the Tekscan calibration system. In contrast, the output was overestimated for the Tekscan calibrated and balloon measured condition. This is what would be expected if the balloon's elastic nature enabled it to more closely conform to the sensor when

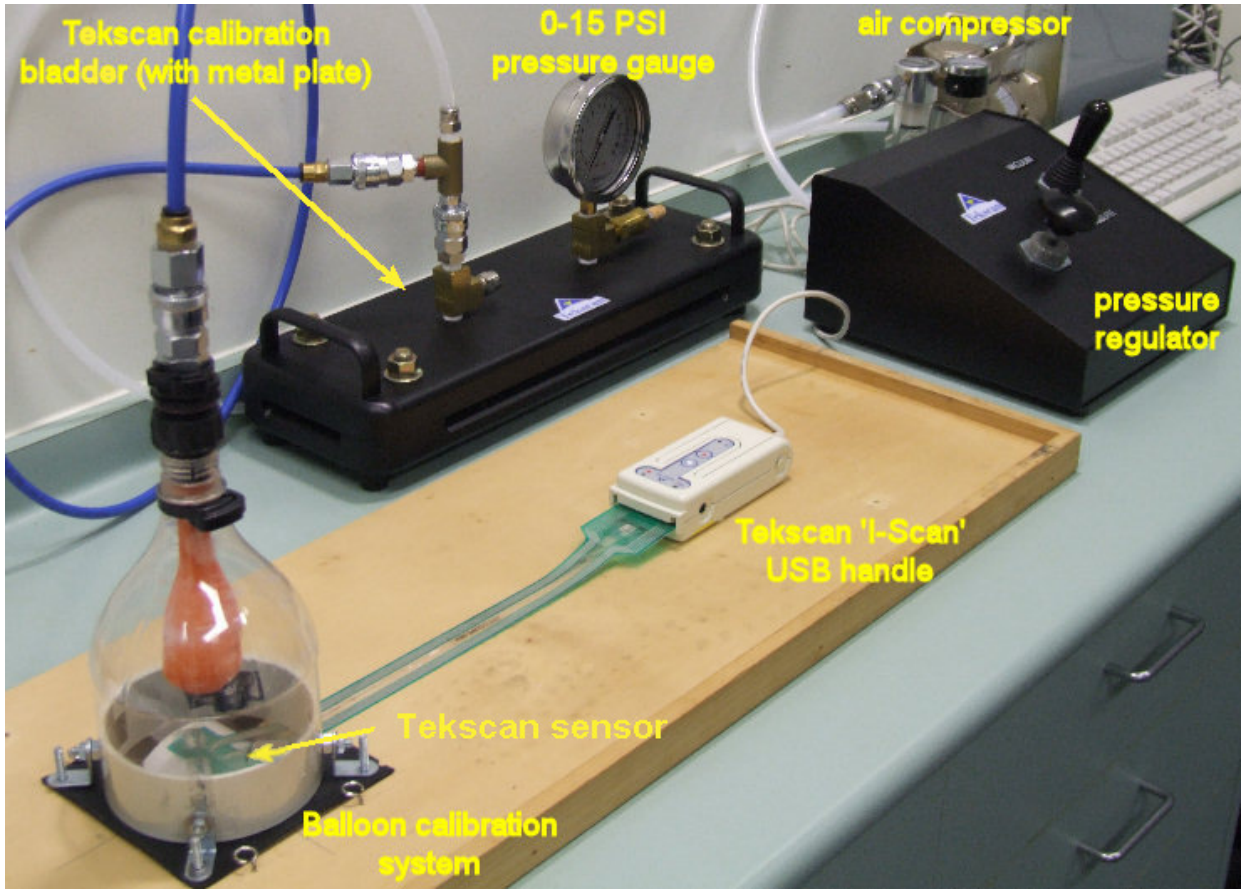

Figure 3-16: "Balloon" calibration system. Air flows from the air compressor through the pressure regulator to inflate a balloon to a certain pressure. This pressure is applied to the sensor at the base of the container.

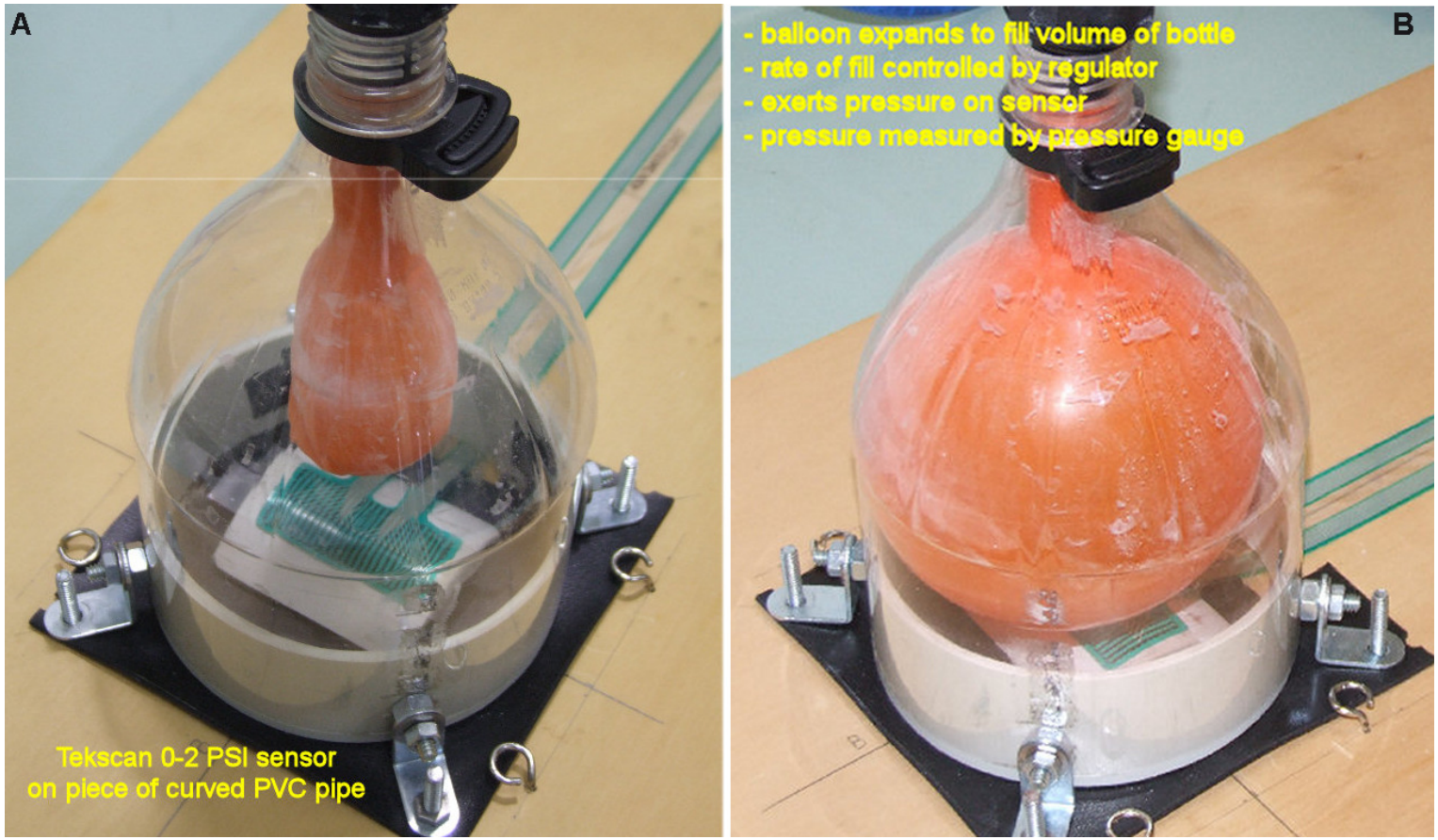

Figure 3-17: "Balloon" calibration system. Balloon expands to fill the volume of the bottle at the pressure determined by the regulator, and exerts pressure on the inserted sensor. Here the sensor is attached to a piece of PVC pipe to simulate a curved contact lens surface.

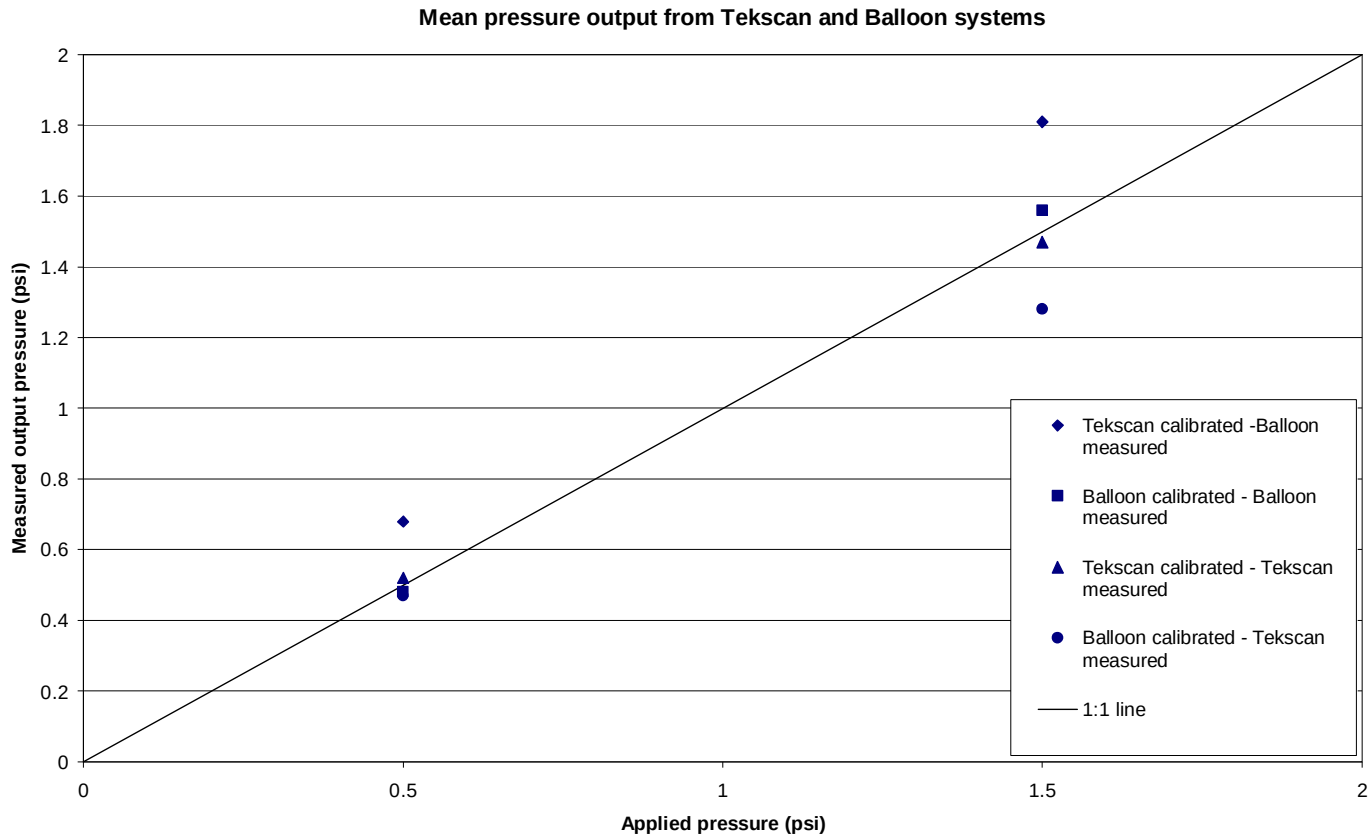

Figure 3-18: Mean pressure of loaded cells of sensor after four measurement conditions: 1) Tekscan calibrated – balloon measured; 2) balloon calibrated – balloon measured; 3) Tekscan calibrated – Tekscan measured; and 4) balloon calibrated – Tekscan measured.

there are small depth differences between individual pressure cells. So if a sensor is calibrated by the balloon but then the measurement is taken with the Tekscan calibration system, fewer sensels are loaded leading to an underestimation of the pressure. The reverse is true for the condition when the sensor is calibrated with the Tekscan calibration system and the measurement is made with the balloon system. In this case fewer cells would be loaded for the calibration compared to the measurement and so the pressure load is overestimated. This highlights the importance of the calibration being performed with an interface material that has similar compliance to the test conditions (Wilson *et al.* 2006).

To further examine this hypothesis, the standard deviations of the average pressure of the loaded cells were considered. The balloon calibrated conditions had smaller standard deviations than the Tekscan calibrated conditions (Figure 3-19), indicating that the pressure cells were more evenly loaded. This is further evidence that the balloon conforms better to the surface of the pressure sensors.

However after further testing the balloon calibration system did not seem to be ideal. It could not be verified that the pressure inside the balloon, determined by the regulator, was transferred by the balloon to the underlying sensor. Also there was a lower pressure limit due to a certain pressure being required to initially fill the balloon. This was 0.3 psi for a normal balloon or 0.2 psi for a giant balloon. From a literature review and initial trial measurements of eyelid pressure, it was expected that we would have to calibrate for pressures less than 0.2 psi. A weight system was considered, however there were a few disadvantages with this approach. Particularly the mass would have to have to be applied over a known area of active sensor area (approximately 9 mm^2). Any small errors in determining this area would significantly alter the pressure calculations.

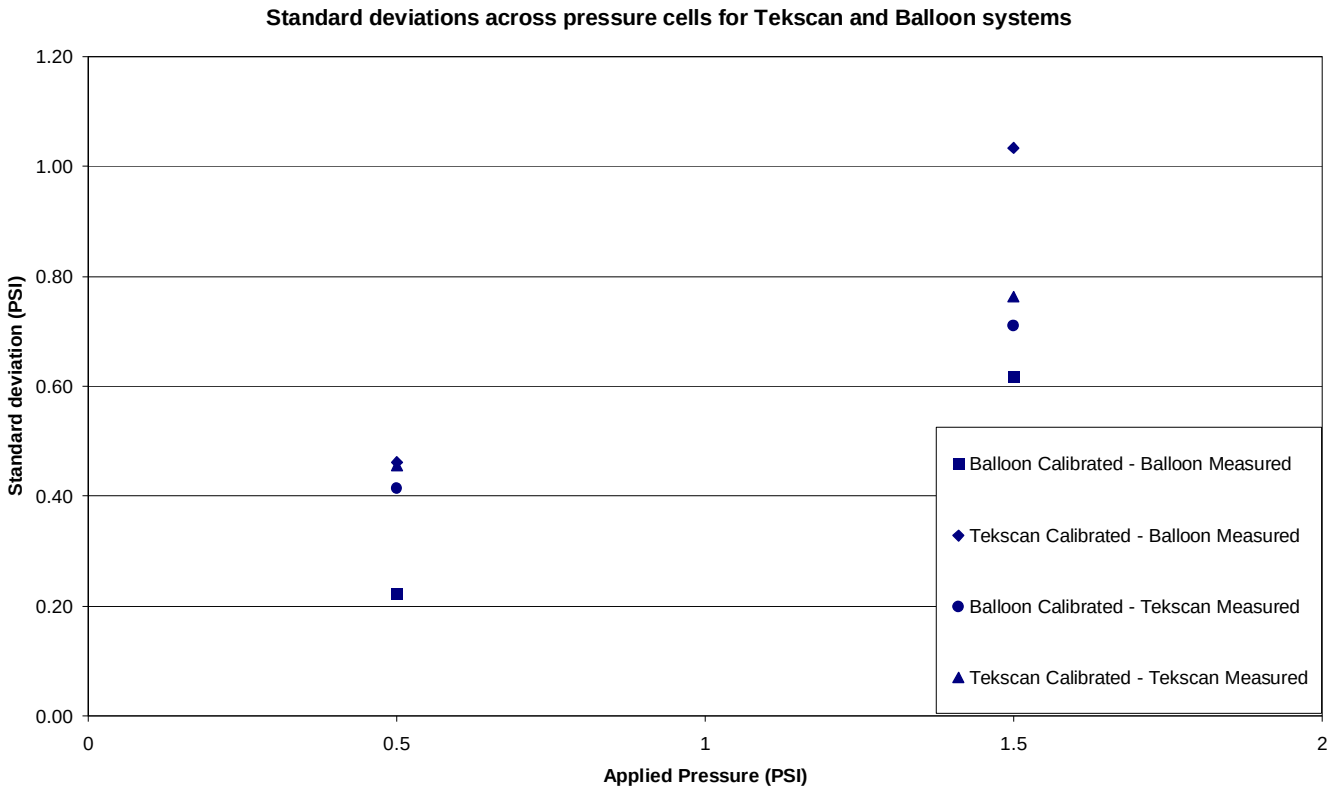

Figure 3-19: Standard deviation of loaded pressure cells of the model #4201 Tekscan sensor from after measurement conditions: 1) balloon calibrated – balloon measured; 2) balloon calibrated – Tekscan measured; 3) Tekscan calibrated – Tekscan measured; and 4) Tekscan calibrated – balloon measured.

3.3.3 Hydrostatic pressure calibration system

A hydrostatic pressure calibration system was designed using a known height of water load placed on the sensor (Figure 3-20). Compared to weights, the area of the tube does not matter as the pressure is determined solely by the height of water. So as long as a cell is completely covered by the load it has the known pressure applied. A clear tube was used so that the water height was visible. A piece of plastic film was fastened over the end of the tube to be the contact between the water column and the sensor. The flexible nature of the plastic meant that it would conform to the surface of the sensor. The plastic tube was clamped to a microscope stand so that the stage height adjustment could be used to gently lower the column of water onto the sensor.

The pressure of a known height of water was calculated using the following equations:

Height of water (m) x Density of water (997.296 kg/m^3 @ 24°C) = Mass pressure (kg/m^2)

Mass pressure (kg/m^2) x Acceleration (9.79 m/s^2 @ 27° latitude) = Applied pressure (N/m^2)

To convert to psi: Applied pressure (N/m^2) divided by 6894.76

So a 7.04 cm water column height at a room temperature of 24°C at 27° latitude applies 0.1 psi to the underlying surface. It was estimated that loads up to 0.5 psi might be needed during calibration which would required a tube length of tube of 35 cm.

During the pilot stage, a slight modification enabled verification of the pressure applied by this calibration apparatus (Figure 3-20). The water column tube was placed on a balance so that the total force could be measured while the Tekscan software indicated the area of the sensor that was loaded. A load of 14 grams measured on the balance applied over 2 cm^2 of the sensor is 0.1 psi, as calculated by the 7 cm column of water. So it was confirmed that the pressure from the water column height was acting on the underlying sensor. Compared with the balloon calibration system, this hydrostatic method allowed small loads (for example less than 0.1 psi) to be applied to the sensor.

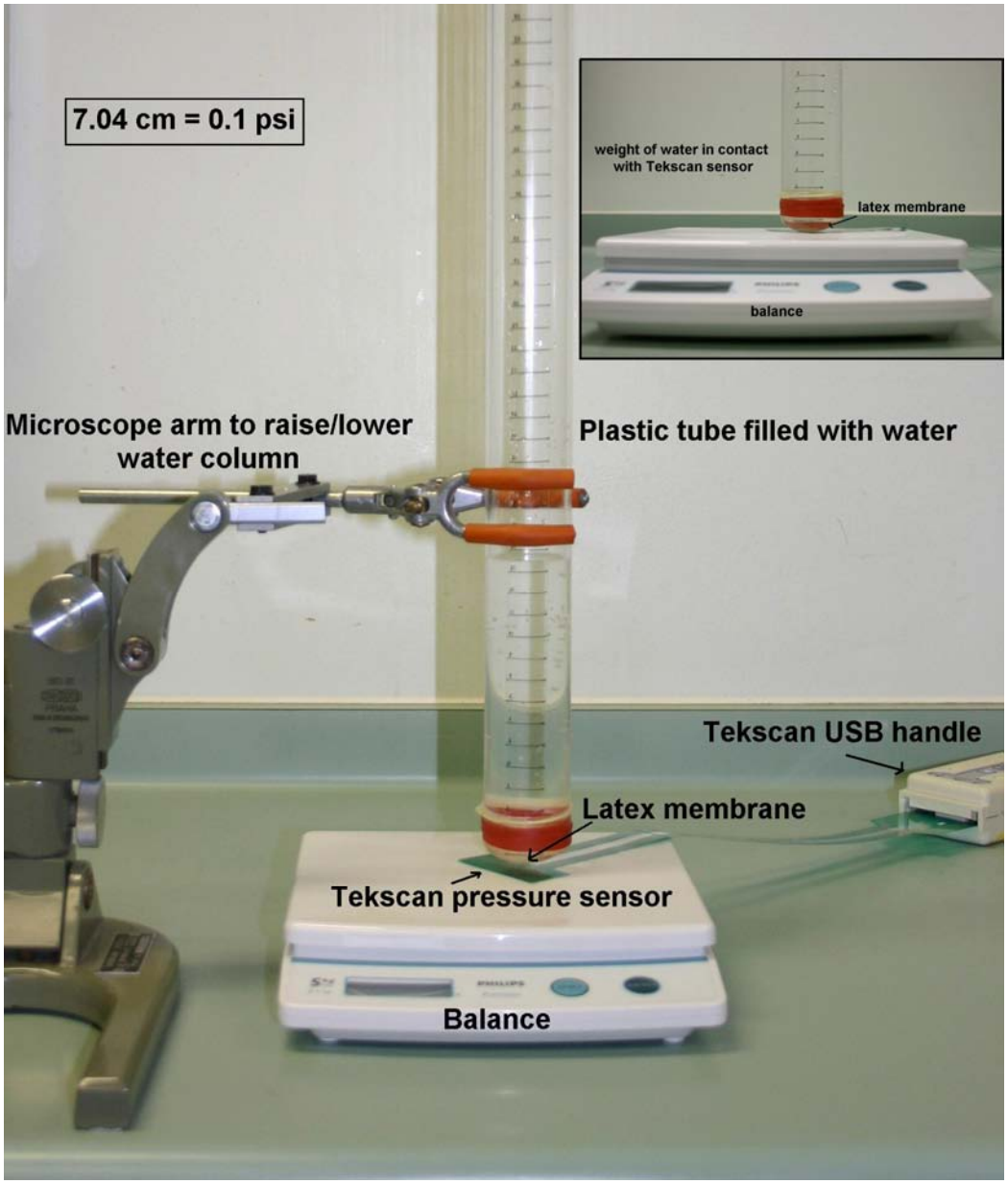

Figure 3-20: Hydrostatic pressure calibration system. A column of water of known height can be gently placed onto the sensor using the microscope height adjustment. The balance mass and Tekscan sensor area loaded enabled verification of the water column height pressure. Inset shows the height of water in contact with the Tekscan sensor.

One of the main issues that arose during testing was the amount of sag of the contact membrane. The system was most reliable when the sag of the membrane was kept to a minimum (as flat as possible) so that it closely matched the curvature of the sensor on the contact lens. With a large sag in the membrane, the positioning of the sensor in relation to the membrane became critical and pressure cells located under the edge of the membrane did not get loaded at the same time as the central cells. With a membrane that was relatively flat with little sag, the cells were loaded at approximately the same time and so the positioning of the sensor-contact lens beneath the membrane became less critical.

A modification that decreased the noise of the calibration was not to use the microscope arm when placing the tube in contact with the sensor (Figure 3-21). It was thought that vibrations may have been transferred and possibly amplified by the microscope arm to the water column and onto the sensor. So the sensor was positioned in a holder with the contact lens positioned in the centre of and at the same height as the contact between the calibration tube and a base piece of tube. The water column could be lowered to rest on the base tube, with only the water column height acting on the sensor via the plastic film. The output from repeated loads of the same pressure was more consistent than previous measurements (Figure 3-22).

The only disadvantage compared to the previous pneumatic systems was that loads could not be easily altered as the water tube needed to be filled up or emptied rather than turning the air pressure regulator knob. While this was not a serious issue for calibration with static loads, this system could not be used for dynamic calibrations or to assess sensor properties such as hysteresis.

The raw score output from the final water calibration system was compared to the Tekscan pneumatic system for pressures between 0.1 to 0.3 psi (in 0.05 psi steps) (Figure 3-23). There was a difference between the two systems thought to be due to the inability of the Tekscan calibration system to conform to the sensor's surface, resulting in a lower output. Higher pressures (0.5 and 1 psi) were also loaded to the sensor using both systems with similar results at the higher pressure of 1 psi.

Final water column height calibration system

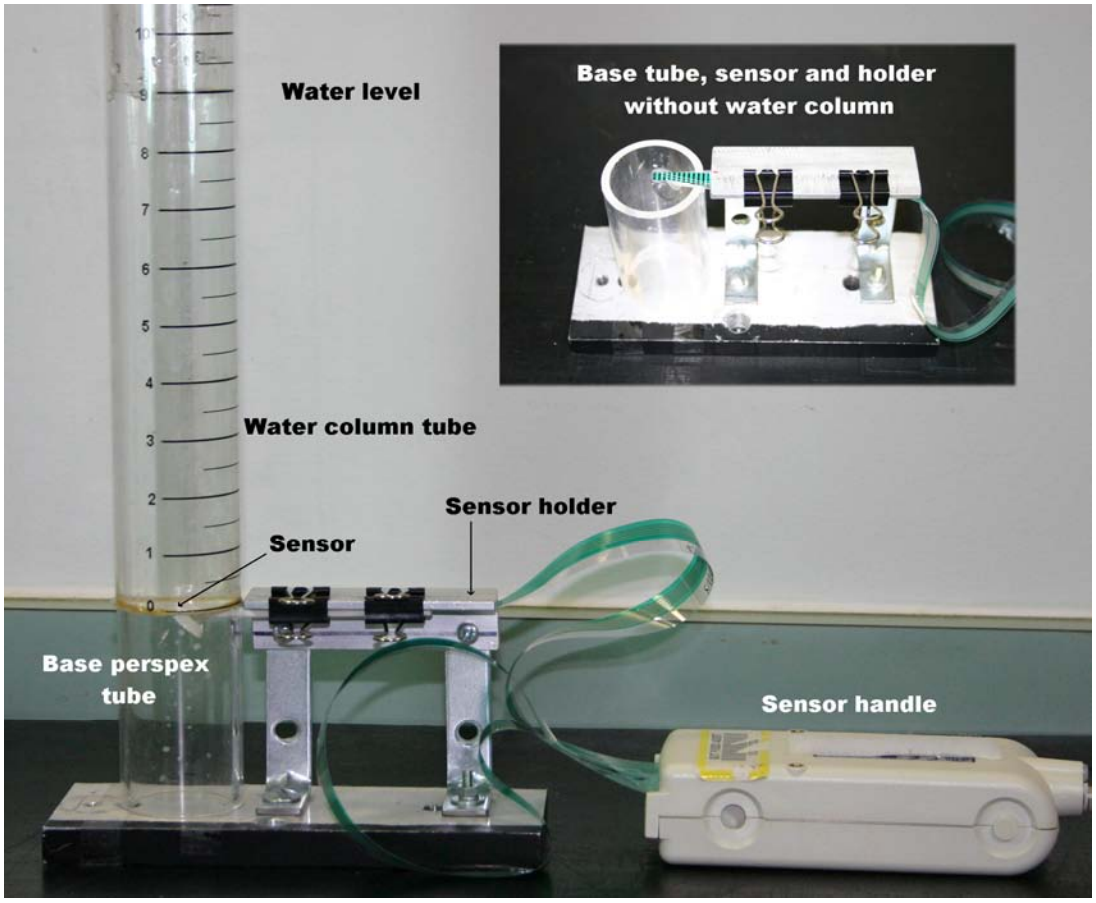

Figure 3-21: Final water column height calibration system. Inset shows system without water column in place.

Figure 3-22: Output using the final calibration system with loads of 0.1 psi (yellow) and 0.5 psi (pink) each applied three times for approximately 1 minute.

Comparison of water column and Tekscan pneumatic calibration systems

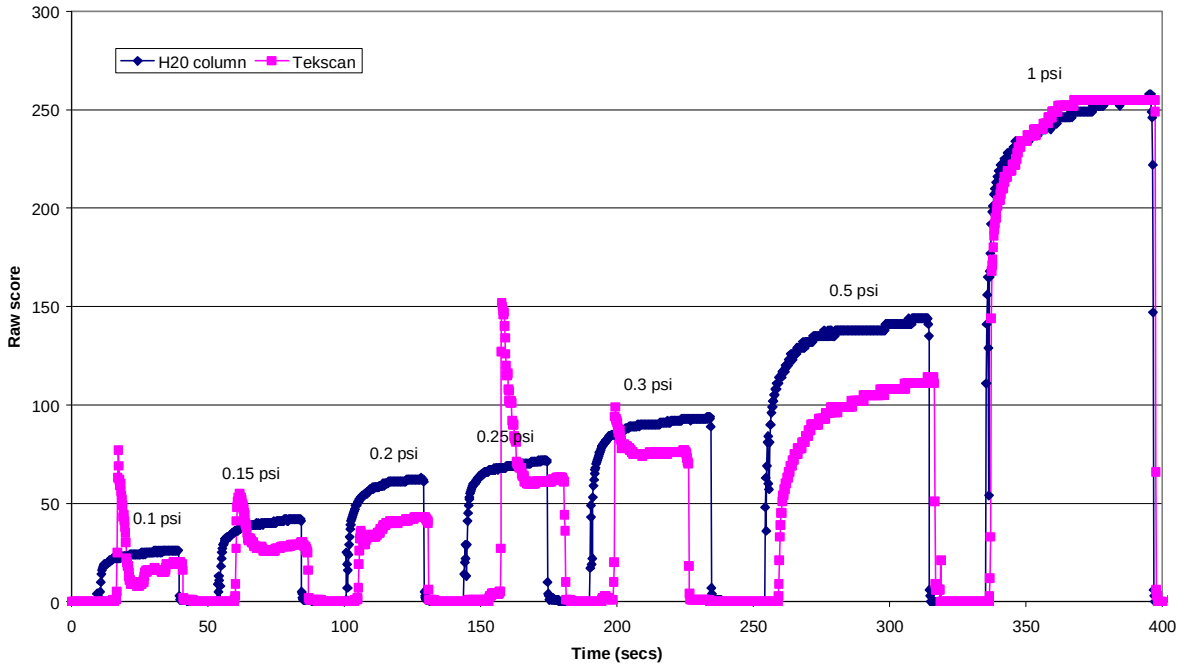

Figure 3-23: Comparison of water column height and Tekscan calibration systems, with lower output for the Tekscan system for applied pressure between 0.1 and 0.5 psi. The peaks for the Tekscan data at the start of the lower pressure loads are due to a higher initial pressure being required to open valves in the pneumatic system.

The advantages of the hydrostatic water column calibration system compared with previous methods were: the thicker sensor-contact lens combination could be calibrated; a plastic film was used as contact to conform to the sensor surface (more closely resembling an eyelid); the calculated pressure being applied to the sensor was confirmed and no lower pressure limit was imposed by the calibration apparatus.

3.3.3.1 Calibration process

The Tekscan software could not be used for calibration as it requires at least 25% of the 264 pressure cells of the model #4201 sensor to be loaded, so a custom calibration process was developed. The Tekscan software employs a dual procedure of equilibration and calibration which applies scaling factors to each cell then calibrates based on the average raw score of the cells. However as the pressure cells would not be simultaneously loaded during eyelid pressure measurement, the customized calibration was designed with each cell being individually calibrated. Custom calibrations have been used for other applications of Tekscan sensors and typically 3 or 10 point polynomial fits were found to be more accurate than either the linear (at 20% or 80% of the measurement load) or the power law options provided by the Tekscan software (Brimacombe *et al.* 2005). A 3 and 10 point polynomial best fit the pressure data over a 0 to 1.6 psi range (Figure 3-24). However for loads between 0.1 and 0.3 psi (in the lower range of the sensor) the data was best fit with a straight line (Figure 3-25).

The calibration process involved applying loads of 0.02, 0.03, 0.04 0.05, 0.06, 0.08, 0.10, 0.12, 0.15 and 0.19 psi (1, 1.5, 2, 2.5, 3, 4, 5, 6, 8 and 10 mmHg) on two occasions each. The raw score data was averaged for each load between 10 and 30 seconds after loading. The first 10 seconds was ignored as it was found that the response is variable (see drift section 3.4.1) and up to 30 seconds to match to the eyelid pressure measurement time. The input pressure was plotted against the raw score value and the data fit with a best fit line providing a calibration equation (for example Figure 3-26). It was noted that during calibration some vibrations could alter the response of the sensor. For example if the drawer of the bench on which the calibration system was positioned was closed, a jump in the pressure reading of the pressure cells was observed (Figure 3-27).

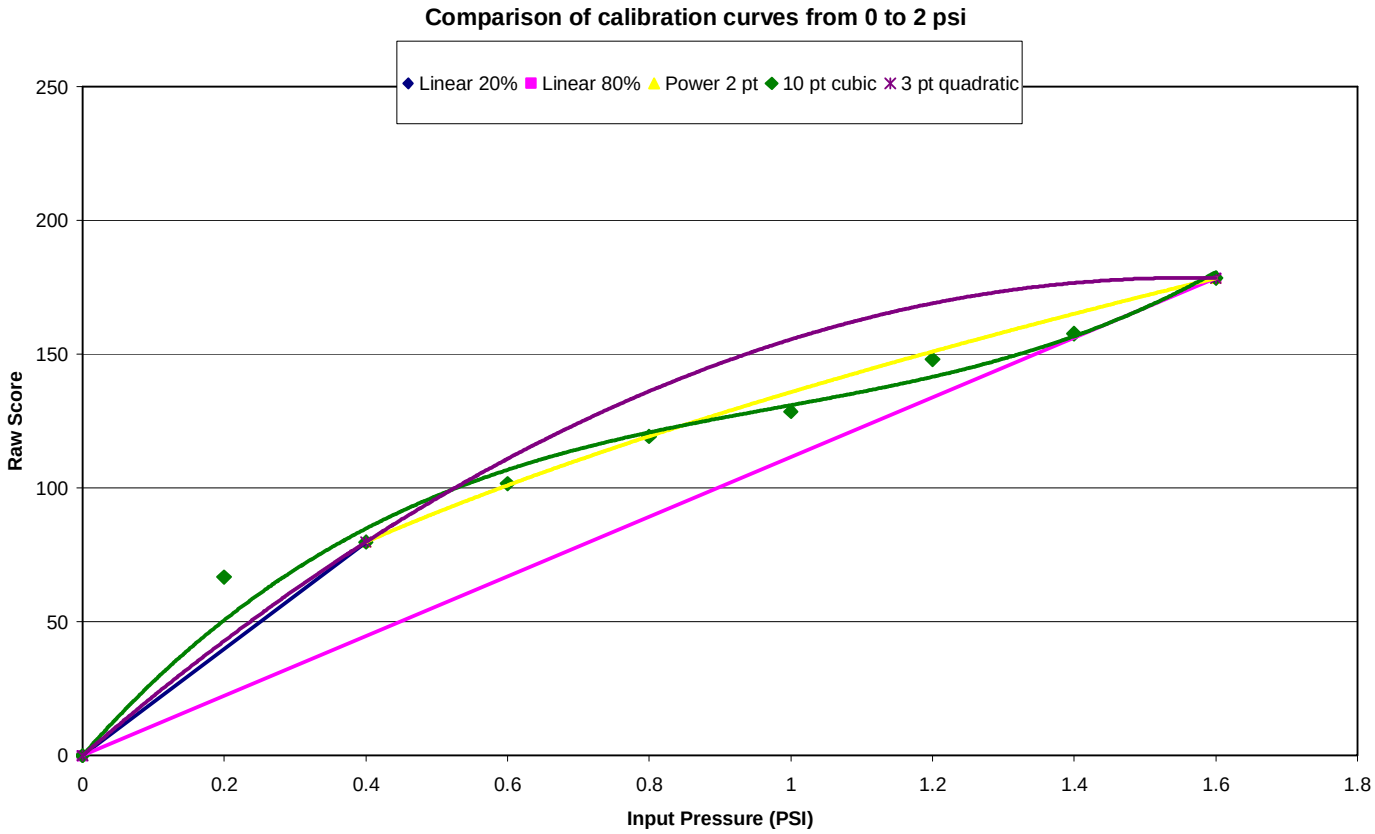

Figure 3-24: Example of calibration: raw score versus applied pressure of between 0 to 1.6 psi (0.2 steps), and 5 different fits to this data.

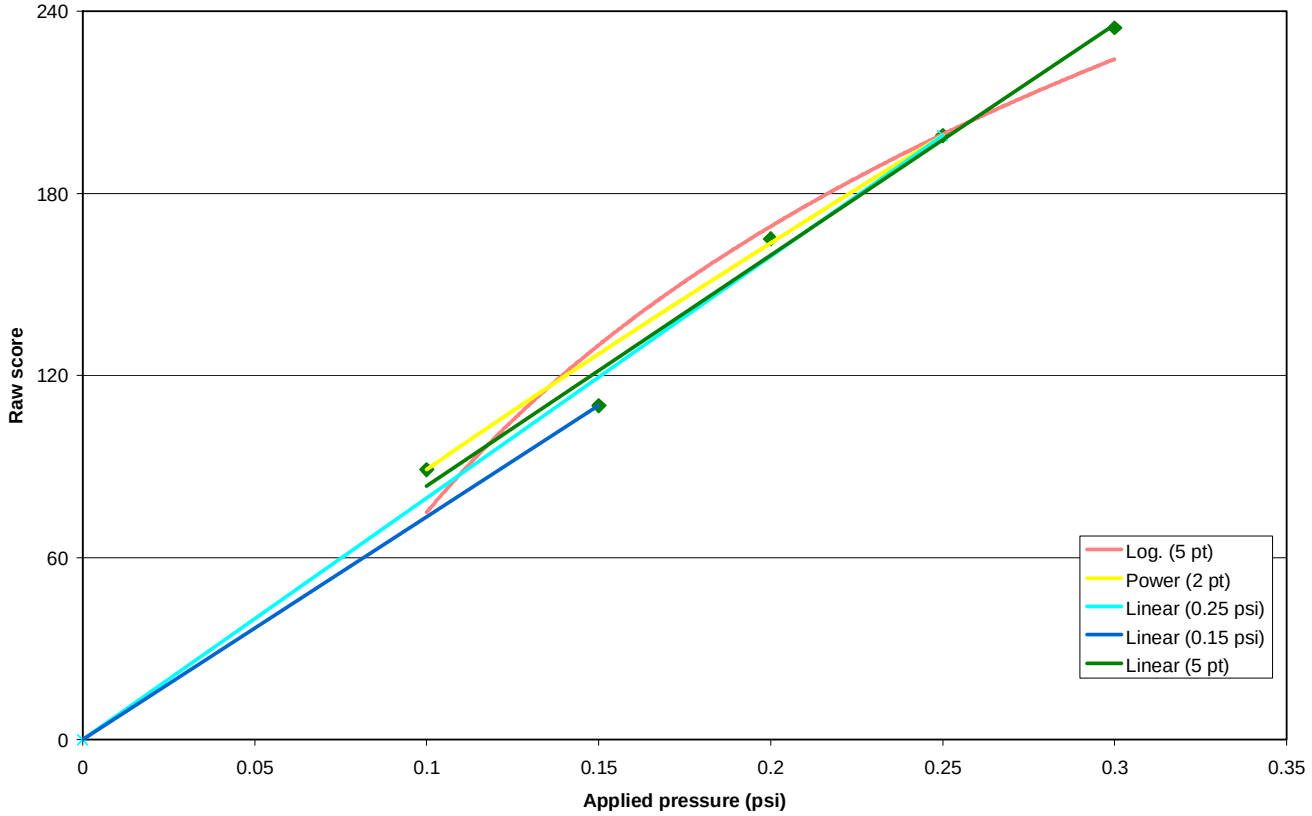

Figure 3-25: Example of calibration: raw score versus applied pressure of 0.1, 0.15, 0.2, 0.25 and 0.3 psi. Fit with the following curves: 5 point logarithmic, 5 point linear, 2 point power (0.1 and 0.25 psi), 0.25 psi linear, and 0.15 psi linear curve.

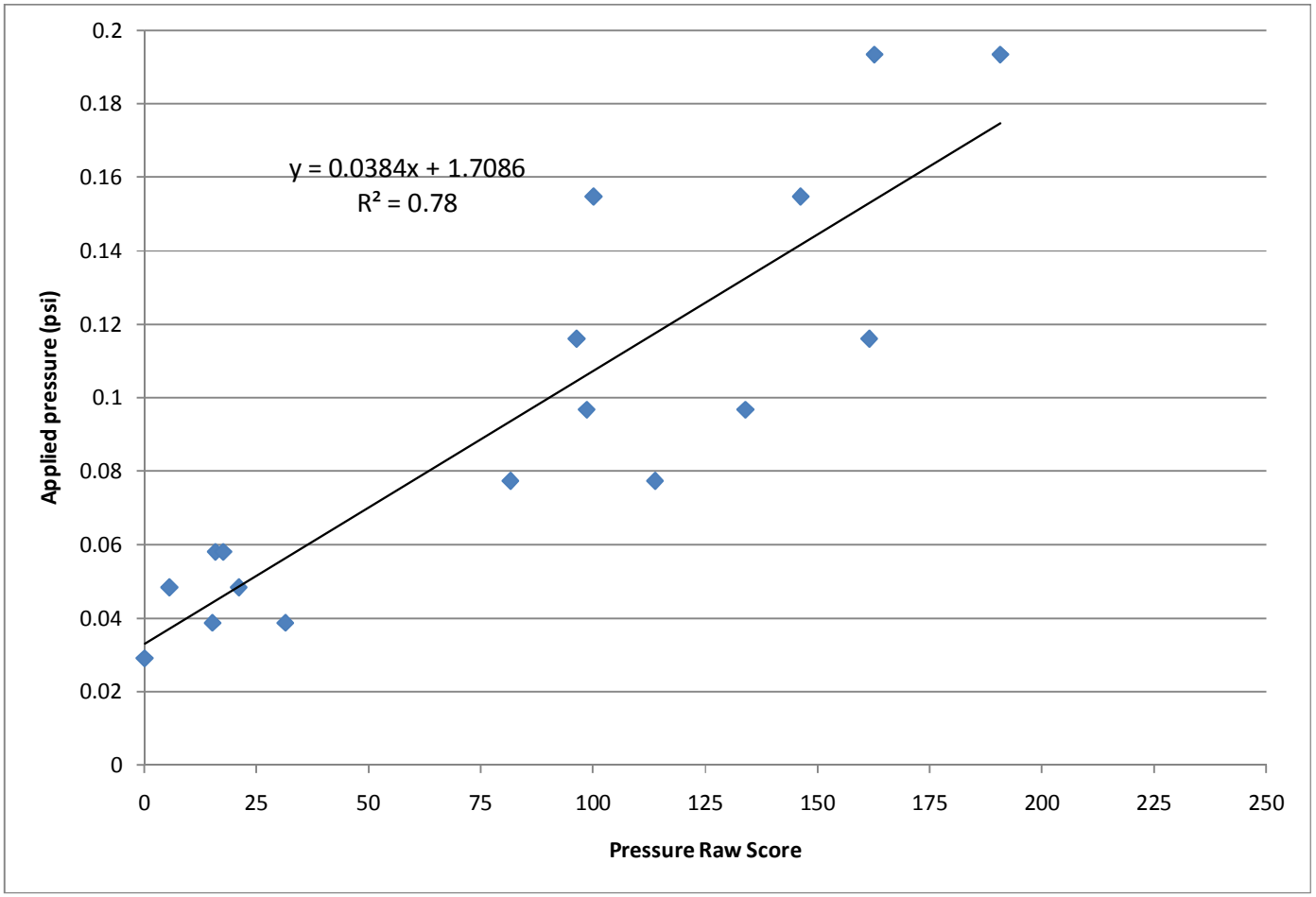

Figure 3-26: Calibration data for 1 cell with applied pressure between 0.03 and 0.19 psi, coefficient of determination, $R^2 = 0.78$.

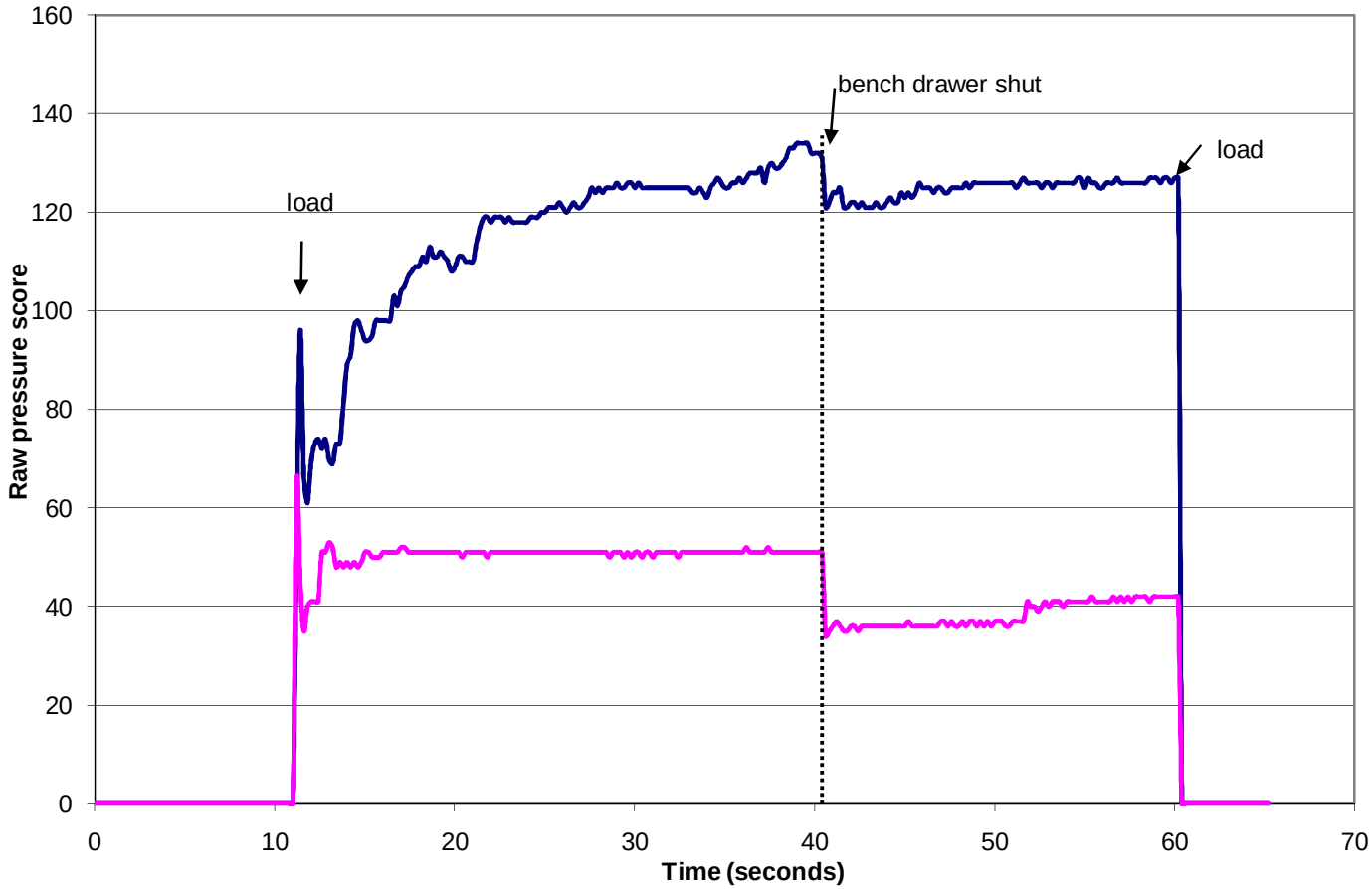

Figure 3-27: Change in output in both pressure cells corresponding to bench drawer being closed.

3.4 Sensor performance characteristics

The output response of various piezoresistive sensors used in biomedical applications has been investigated. When considering these studies it must be noted that the results are for different sensors with different pressure ranges and measurement loads. It is unlikely that a sensor rated to 9 psi and tested with loads up to 1 psi will respond in the same way as a sensor rated to 2 psi and loaded at its maximum pressure. Various properties of Tekscan sensor model #4201 were assessed with the sensor attached to the rigid contact lens and plastic support beam (replicating measurement conditions).

3.4.1 Drift

Drift is the change in sensor output while a static load is maintained. Initially when a load is applied the output usually underestimates the pressure but increases until it reaches a steady state (Figure 3-28). The Tekscan I-scan instrument manual states that "among other things, the sensor design, the sensor sensitivity, the interface material, the applied load, and environmental conditions may influence the drift". It also states that in a worst case scenario the drift is less than 3% per logarithmic time. It is thought that this property is due to the piezoresistive ink (Otto *et al.* 1999).

An evaluation of Tekscan K-scan sensors recorded an initial underestimation of the pressure which crossed over to overestimation after approximately 30 seconds (Otto *et al.* 1999). The relative errors due to drift of an F socket sensor were -8.5% after 1 minute, 3.6% after 2 minutes and 5.3% after 3 minutes (Maurer *et al.* 2003). Drift errors have been investigated over longer time periods on a variety of pressure sensors and can be expressed as drift error % = (Initial Sensor Response – Later Sensor Response / Initial Sensor Response) x 100.

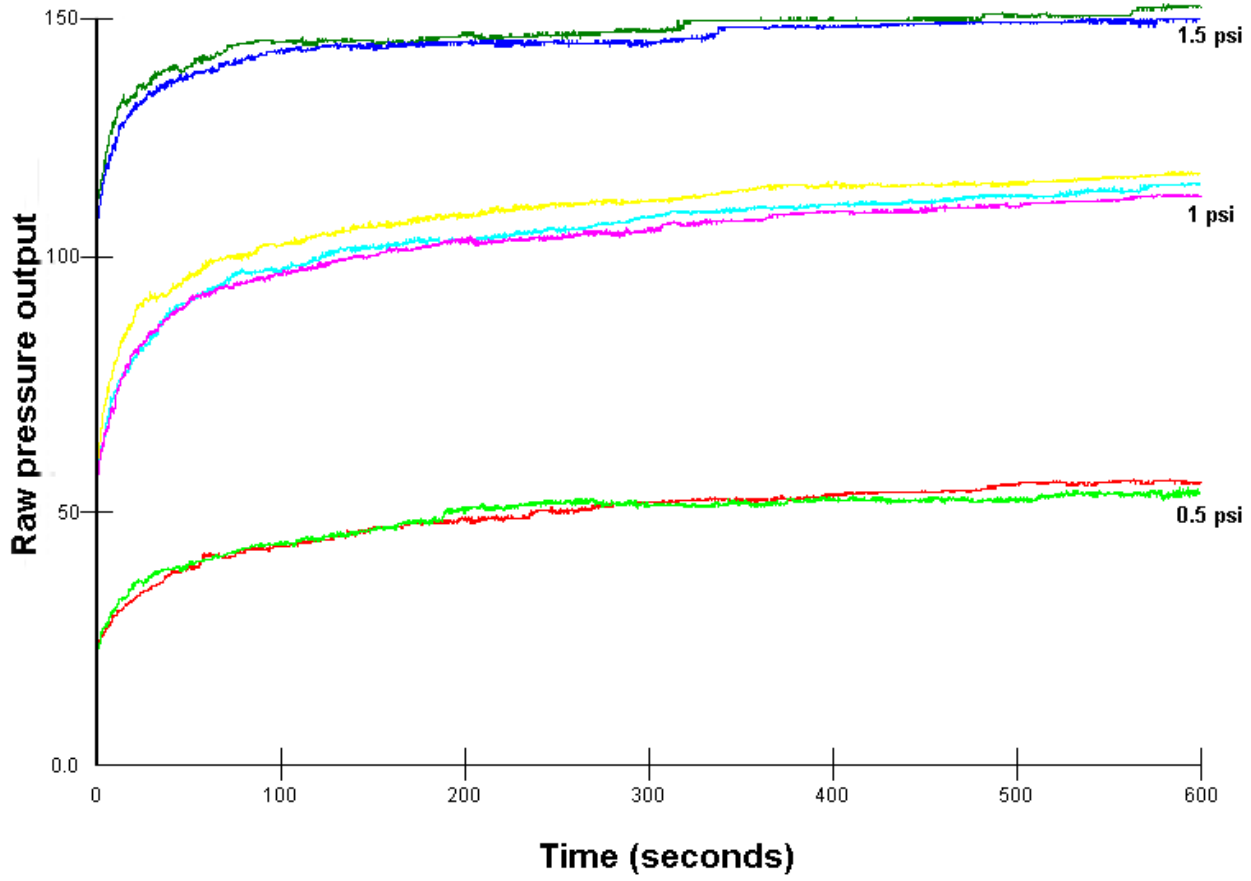

Figure 3-28: Drift curves for repeated measurements of three different loads. The load is applied at time = 0 and the output continues to increase with time.

To compare drift between studies, the drift percentage is divided by the log of time and values vary from 0.55 to 6.4 % per log time (Table 3-2). Two drift trials were conducted to evaluate drift over long-term (days) and short-term (seconds) time periods. First output was measured every minute for 64 hours. It was found that the measurement increased continuously until a relatively stable level was reached after around 15 hours (Figure 3-29).

In the second experiment, five loads (0.1, 0.2, 0.3 0.4 and 0.5 psi) were applied on three separate occasions and the pressure recorded at 9.8 Hz for 1 minute. The shorter 1-minute loading time was considered similar to the loading time likely to be used when measuring eyelid pressure. Although there was continuous increase in the output, it was most stable 10 seconds or more after loading (Figure 3-30). After this there was only a small amount drift or creep in the sensor output up to the 1 minute (required for eyelid pressure measurement).

While for the longer trial (64 hours) the output took approximately 15 hours to stabilize, when a shorter time period is considered (approximately 1 minute which is similar to an eyelid pressure measurement), drift is not as influential. Though for greatest accuracy to minimise the influence of drift the first 10 seconds of data after loading should be disregarded, the sensor should be conditioned prior to every use and the mean output for both the calibration and measurement data should be calculated over the same time frame after loading.

Table 3-2: Drift Errors for a Variety of Sensors

Reference	*Sensor Type*	*Pressure Rating (psi)*	*Load (psi)*	*Time Period (secs)*	*Drift Error %*	*Drift Error % per Log Time*
Woodburn and Helliwell (1996)	F-scan	181	72.5	900	19	6.4
Polliack et al. (2000)	F-socket	101	20 & 60	1200	average 11.9	3.9
Polliack et al. (2002)	Novel Electronics test sensor	88	20 & 60	1200	average 4.4	1.4
Ferguson-Pell et al. (2000)	Flexiforce	9	0.6	7200	2.5	0.65
			1		1.7	0.55
Otto et al. (1999)	K-scan	(not stated)	725	10 800	25	6.2
			1450		12	3.0

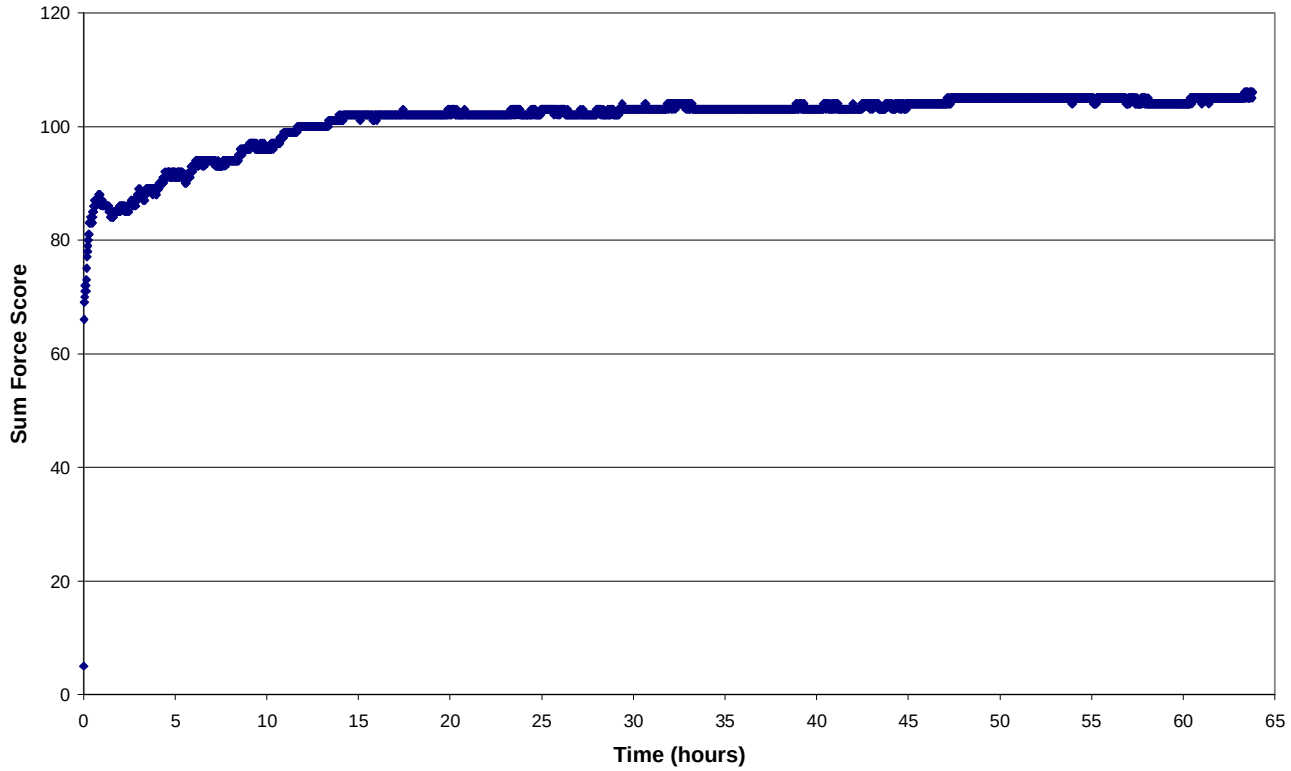

Figure 3-29: Drift of sensor output with constant load over 64 hours.

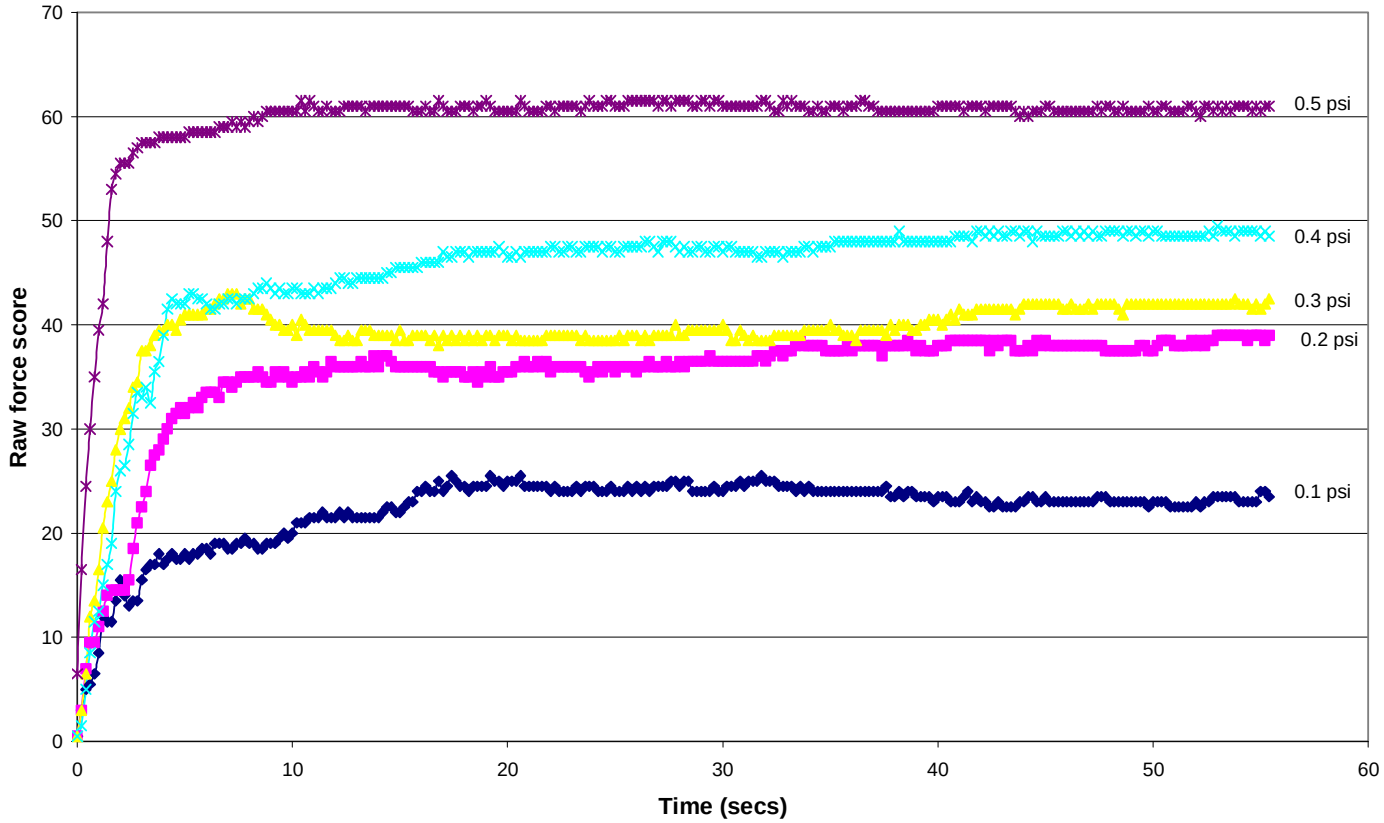

Figure 3-30: Drift curves for loads of 0.1, 0.2, 0.3, 0.4 and 0.5 psi measured for approximately 55 seconds after loading.

3.4.2 Hysteresis

Sensors experience hysteresis, which is the difference in output response during increased and decreased loading, at the same applied force (Figure 3-31). The Tekscan manual states that the contribution of the sensor to hysteresis is between 0 to 5%. While a similar value (5.4 ± 2.5%) was measured for a Tekscan Flexiforce sensor (Ferguson-Pell *et al.* 2000), other results for various sensors are 8.3% (Nicolopoulos *et al.* 2000), 12.93 ± 4.63% (Polliack *et al.* 2002) and some higher values of up to 21% (Woodburn and Helliwell 1996) and 36% (Hachisuka *et al.* 1998). Hysteresis is dependent on the frequency of the loading and unloading (Nicolopoulos *et al.* 2000) and greater hysteresis tends to occur with larger load ranges (Buis and Convery 1997). It is also dependent on the material of the surface that is applying force to the sensor. Hysteresis cannot be totally accounted for during the calibration process, but the best way to minimise its effects is to mimic the intended measurement conditions during calibration.

The difference in the sensor's output for loading and unloading conditions was examined (Figure 3-32). This was conducted using the pneumatic system, as loaded can be easily increased or decreased. The loads were increased and then decreased in 0.1 psi steps from 0 through to 0.6 psi. The percentage difference between loading and unloading conditions for the application loads was between 0.3% and 10.6% which is comparable to previous reports (Table 3-3).

Table 3-3: The hysteresis at each of the applied loads.

Load (psi)	*Hysteresis (%)*
0.1	10.6
0.2	6.1
0.3	2.2
0.4	6.4
0.5	0.3

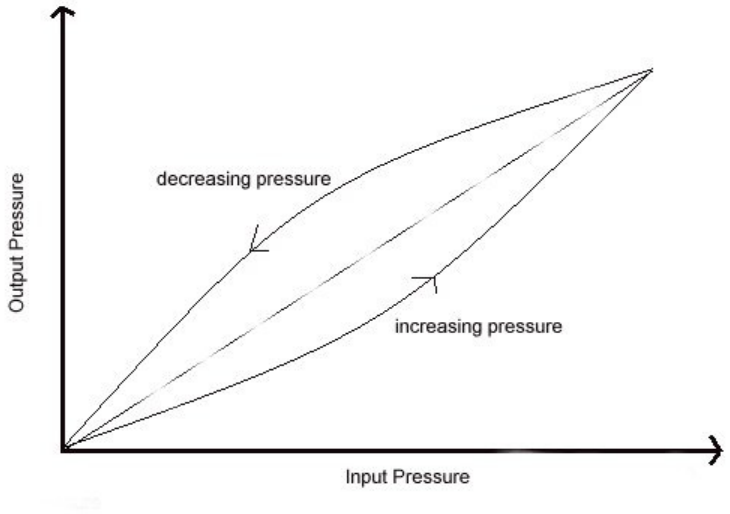

Figure 3-31: Schematic hysteresis plot showing output for increasing and decreasing applied pressure.

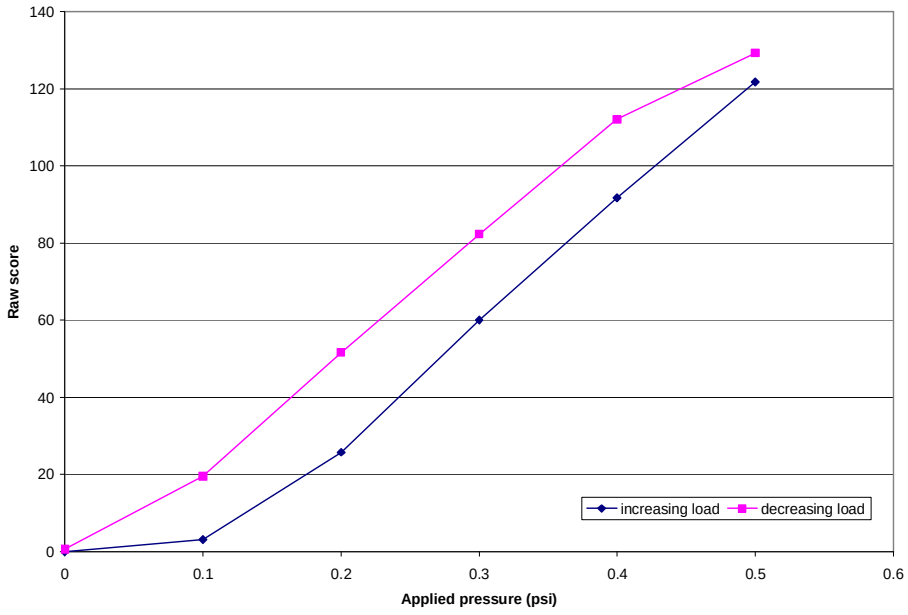

Figure 3-32: The output difference between loading and unloading for loads of 0.1, 0.2, 0.3, 0.4 and 0.5 psi using the Tekscan pneumatic calibration system.

3.4.3 Compressibility

The amount of compression of the sensor over its full pressure range was measured using a micrometer (Figure 3-33). The sensor was placed under the plunger and the micrometer zeroed just prior to the plunger making contact with the sensor (while its output was still zero). The plunger was then lowered in 1 micron steps and the output readings recorded in the Tekscan software. Measurements were made until the sensor reached its maximum output (raw score equal to 256). The start and end of the micrometer readings indicate the amount of compression that occurred over its active output range. The sensor had an initial thickness of 170 µm and approximately 74 µm of compression occurred to produce its maximum pressure output (Figure 3-34).

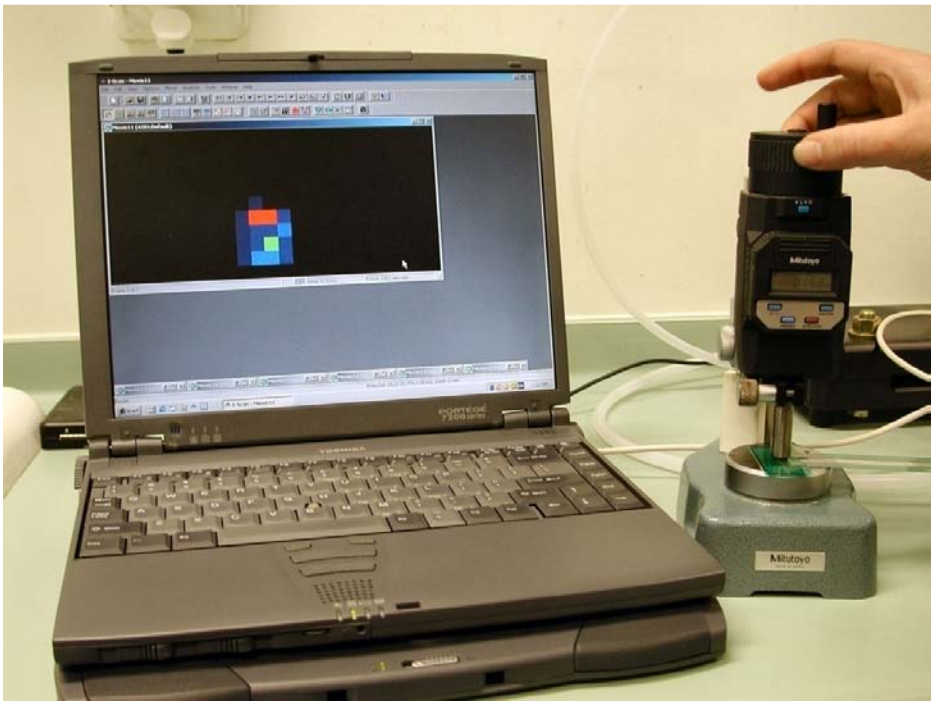

Figure 3-33: Measurement of compression of model #4201 sensor with micrometer, with sensor output shown on laptop screen.

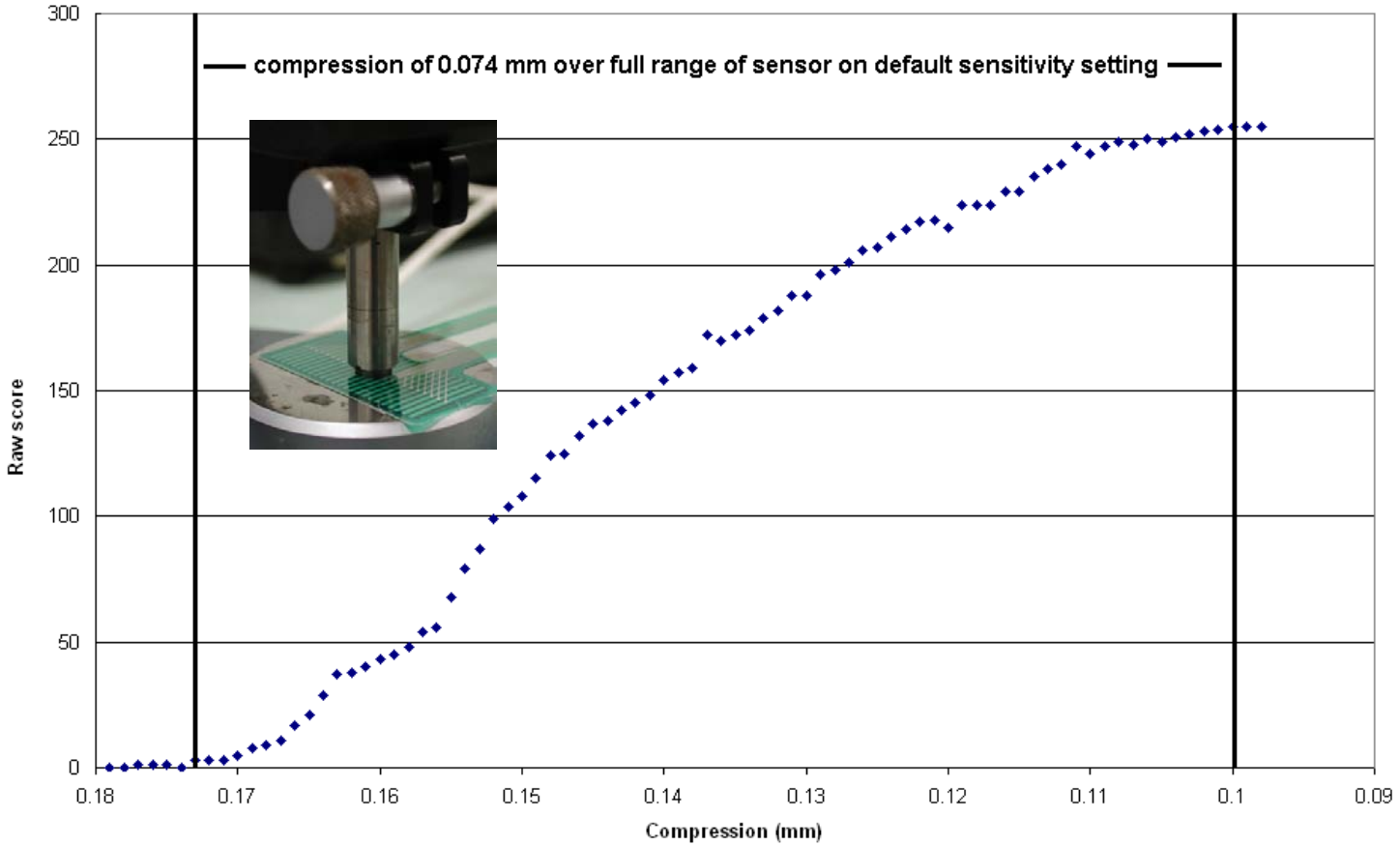

Figure 3-34: Average pressure raw score from initial thickness of 0.174 mm to 0.1 mm when the maximum raw score was reached.

Figure 3-35: Water-filled balloon in incubator in contact with temperature and pressure sensors.

3.4.4 Temperature

The sensor manufacturer states that its I-scan sensors are temperature sensitive and typically measurements can vary by up to 0.45% per degree Celsius. The best control method for temperature is to calibrate the sensor at the same temperature as the application. This principle has been adopted in a study measuring foot pressure, by keeping the room temperature close to the skin surface temperature (Ferguson-Pell *et al.* 2000; Randolph *et al.* 2000). The effect of temperature has also been investigated by calibrating and measuring at different temperatures (Hachisuka *et al.* 1998). While the sensor output at 20°C (room temperature) was found to be greater than at 37°C (body temperature), the difference in the output was not statistically significant.

The effect of temperature on Tekscan model #4201 sensor was investigated by placing a water-filled balloon in contact with pressure and temperature sensors inside an incubator (Figure 3-35). Four studies with different protocols were conducted.

1. Measurements of pressure output and temperature were made over 7 hours for a load under stable room temperature conditions (between 21°C and 23°C) and for the same load but with temperature decreasing from 40°C to 25°C. The output for the load at room temperature was consistently higher than the decreasing temperature, however both trials followed similar curves (Figure 3-36). Any potential differences between the two conditions were largely obscured by the drift property of the sensor.

2. In a second experiment pressure measurements were taken at 30.3 second intervals and temperature every 5 minutes, as the temperature was increased from 23˚C (room temperature) in hourly increments for 4 hours up to 39˚C. The room temperature, increasing incubator temperature and pressure sensor output were analysed (Figure 3-37). The stable room temperature and step increases in the incubator temperature can be seen. There was a cyclic nature to the incubator temperature, most likely related to the heating element switching on and off. The pressure sensor output slightly increased with increasing temperature, although there seemed to be a delay in the response.

3. In a third trial, measurements were made without a load on the sensor while temperature was increased and then decreased (Figure 3-38). Even without a load, the sensor responded and recorded output for increasing temperature. However over the 17˚C temperature increase, there was only an average raw score increase of 0.3 out of 256 for each cell.

4. Lastly a trial was conducted where loads of 0.15, 0.2, 0.25 and 0.3 psi were applied and measured in the incubator for room temperature (23˚C) and at an average ocular surface temperature (36˚C) (Holden and Sweeney 1985; Morgan *et al.* 1993; Purslow *et al.* 2005; Purslow and Wolffsohn 2007). When comparing calibration curves at 23°C and 36°C, the error associated with calibrating at 23°C but measuring at 36°C, was a slight overestimation of pressure (average 2.5%).

From these results it was concluded that temperature does not have to be taken into account in the calibration and measurement of eyelid pressure. Only small errors were recorded when a measurement was taken at ocular surface temperature but calibrated with data recorded at room temperature. It is also questionable whether the sensor would heat up to ocular surface temperature while on the eye as the piezoresistive conductive ink inside the sensor is covered with Mylar plastic layers. Mylar (polyester) is known for its excellent temperature resistance, with a coefficient of thermal conduction of 0.0001 and so should act as an insulator for the pressure sensitive ink. Unlike these experiments where the whole sensor was placed in the incubator for a number of hours, for eyelid pressure measurements the sensor-contact lens combination is only in contact with the eye and eyelids for a few minutes. Furthermore heat from the eye would be absorbed by the Perspex contact lens, further limiting the influence of temperature variations on the sensor. Therefore the effect of temperature on the Tekscan sensors reported by this study is most likely an overestimation of its influence.

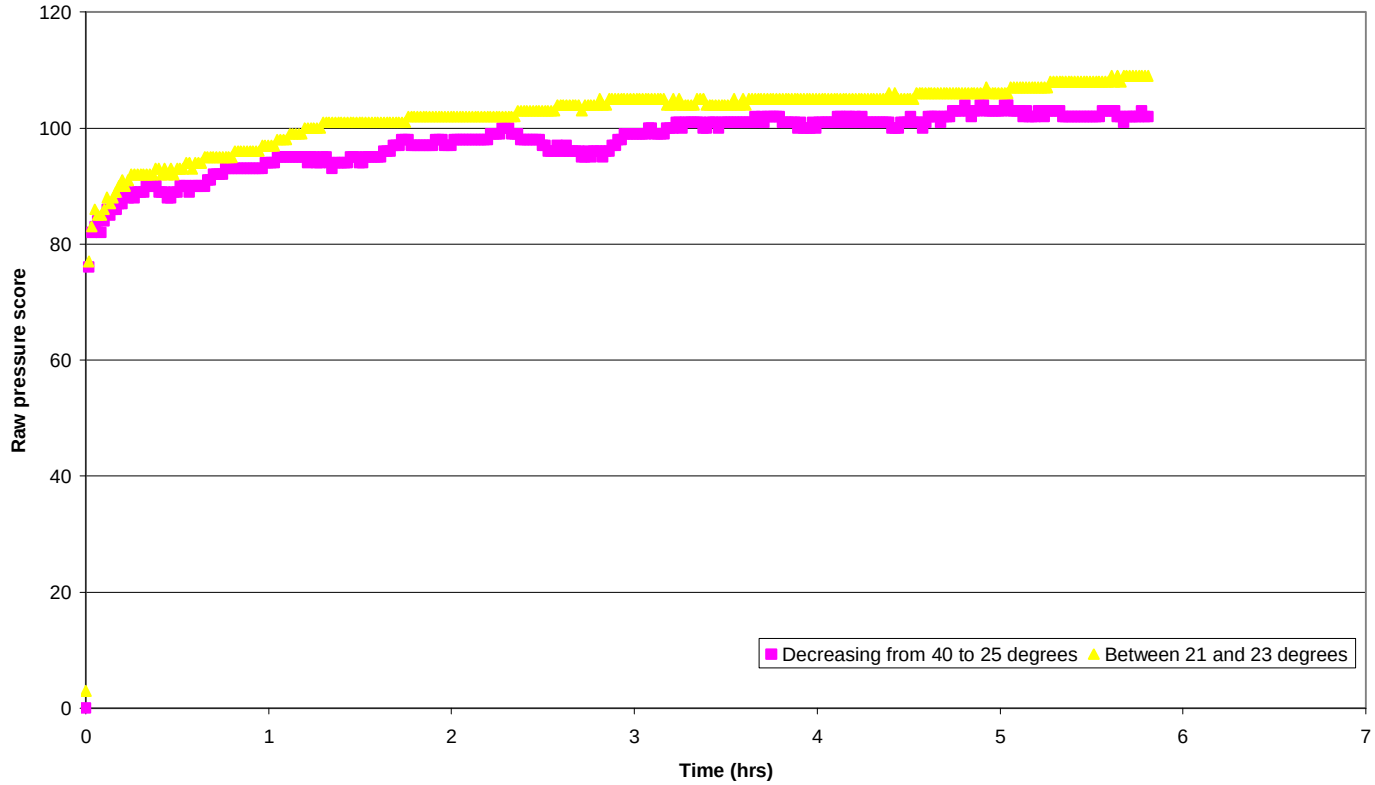

Figure 3-36: Temperature experiment 1: Static load output for stable room temperature conditions (21-23°C) and for decreasing temperature from 40°C to 25°C.

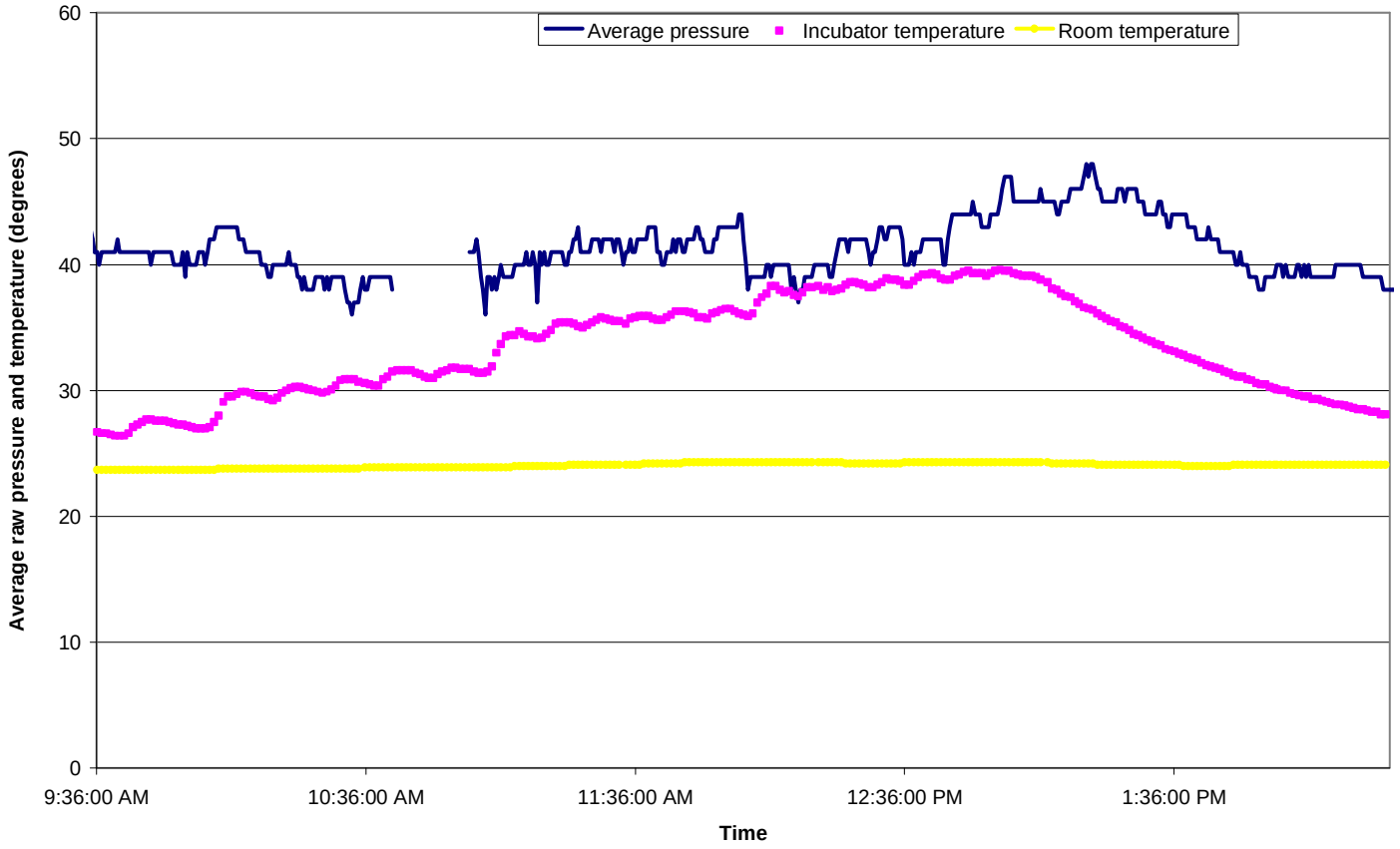

Figure 3-37: Temperature experiment 2: Pressure output for a static load with incremental increases in incubator temperature.

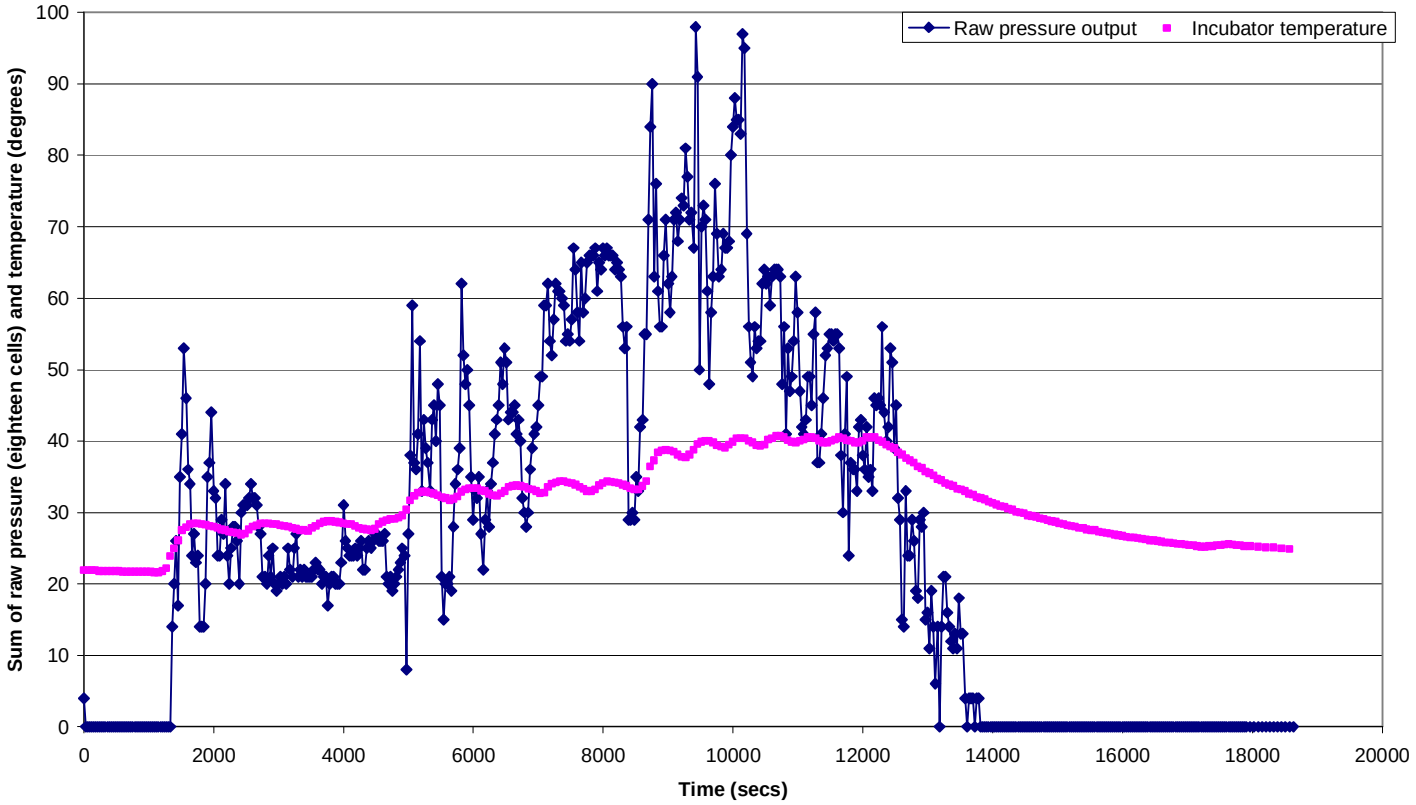

Figure 3-38: Temperature experiment 3: Pressure output with no pressure load as the temperature of the incubator was increased in increments.

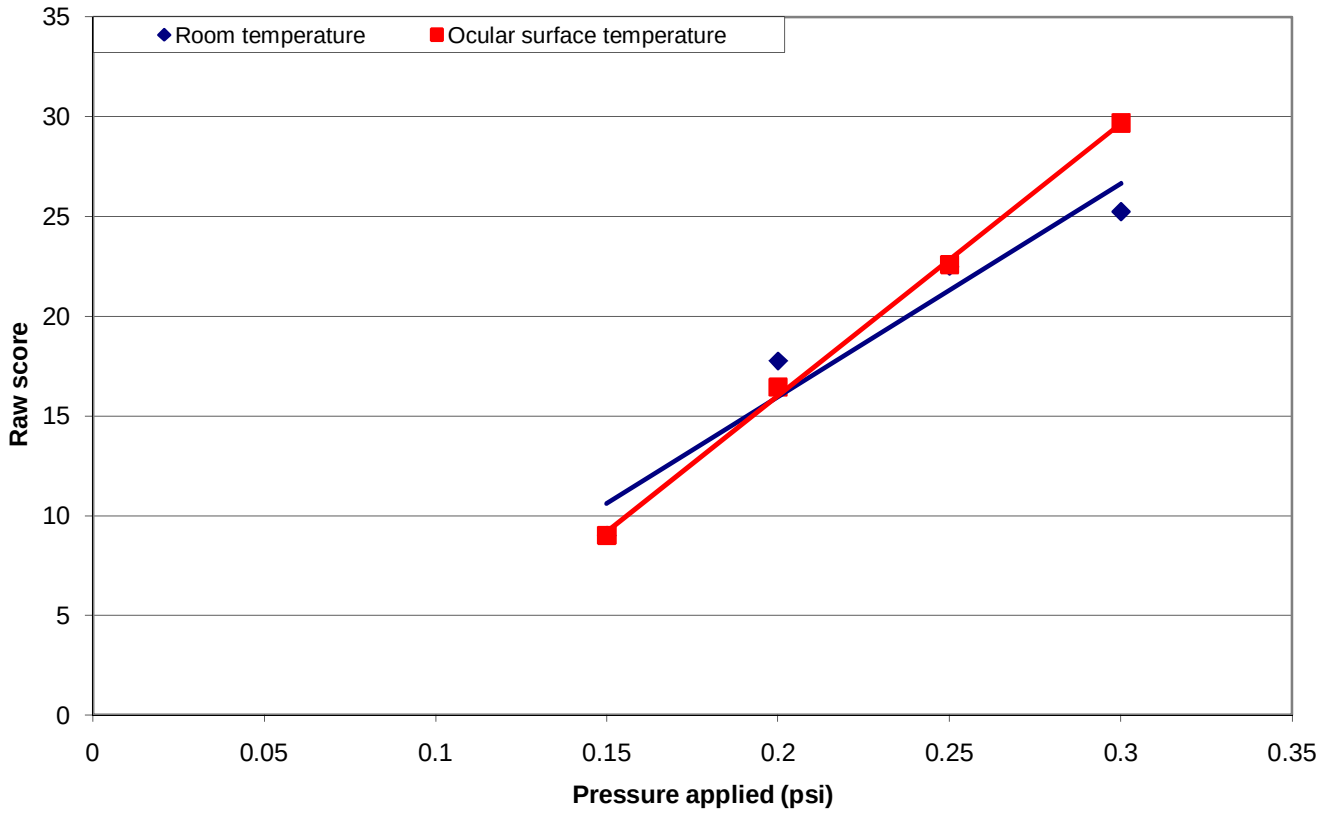

Figure 3-39: Temperature experiment 4: Difference in raw score output between the calibrations performed at room temperature (23°C) and at an average ocular surface temperature (36°C).

3.4.5 Precision

Precision is the ability for the sensor to respond the same way with the same load. Measurements with Tekscan sensors have been found to be very repeatable with small coefficients of variation. An average coefficient of variation was 8.5% for F-socket sensors, being at a minimum around the calibration pressure (Polliack *et al.* 2000). So repeatability is dependent on the accuracy of the calibration process. Loads of 0.2, 0.6 and 1 psi were measured 20 times on a 9 psi rated flexiforce sensor with coefficients of variation of 6.6%, 3.2%, and 2.3% (Ferguson-Pell *et al.* 2000). The greater variation for the lowest pressure may be due to the fact that a 0.2 psi load is in the bottom 3% of this sensor's range. Tekscan recommends that care should be taken when measuring in the bottom 15% of a sensor's range. Similar to drift, the repeatability of a sensor is said to be improved by conditioning (i.e. pre-loading with pressure) the sensor prior to use. A precision of within 4% to 8% has been recorded for force, pressure and area measurements of Tekscan sensors (Wilson *et al.* 2006). Precision was estimated with trial loads of 0.5, 1 and 1.5 psi applied randomly eight times each using the Tekscan pneumatic calibration system. The average raw scores were 97.5 ± 1.8, 139.1 ± 4.2 and 177.4 ± 1.6 respectively so the coefficient of variation were between 1 and 3 %.

3.4.6 Conditioning

The Tekscan I-scan manual recommends that sensors that are new or have not been used "for a length of time" should be "exercised" by loading them three to five times. For best results it is advised that the load be 20% greater than the maximum load to be applied in testing and should involve materials of similar compliance to the application. The benefits of conditioning are reduction in drift and hysteresis and an improvement in precision. Studies using Tekscan sensors usually apply this technique (Ferguson-Pell *et al.* 2000; Wilson *et al.* 2003; Wilson *et al.* 2006). It is thought that pre-stressing the sensor reduces the plastic creep of the sensor during actual measurement and applying a relative uniform pressure over the entire sensor may help control variation in output with location.

Preconditioning the sensor showed evidence of regulating the measurement response (Figure 3-40). Three 0.15 psi loads were applied using the hydrostatic calibration system to a sensor that had not been conditioned. Conditioning was then performed using four loads of 0.5 psi and the load of 0.15 psi was again applied and measured three times. The response of the sensor was variable prior to conditioning whereas after conditioning, the application and removal of loads are obvious with more consistent responses for the three loads.

The importance of the magnitude of the conditioning load and length of time between conditioning and measurement were examined by conditioning with loads of 0.2, 0.5 and 1 psi applied and breaks of 10, 30 and 60 minutes. After conditioning with 0.2 psi, the output for the 0.15 psi measurement took longer to reach a stable level compared with conditioning with the 0.5 psi or 1 psi loads (which gave similar results) (Figure 3-41). There was no significant effect of the length of the interval between conditioning and measurement (10, 30 or 60 minutes), on the stability of the output response. From these results it was concluded that model #4201 sensors should be optimally conditioned with four loads of 0.5 psi for 1-minute (with 30-second intervals between loads), less than 60 minutes prior to use.

3.5 Conditioning and calibration standards

Based on the preliminary experiments examining sensor responses, the following process was adopted before using model #4201 (5 psi) Tekscan sensors to measure eyelid pressure *in vivo*.

1. Condition the sensor using a pressure of 0.5 psi by loading it four times for 1 minute with 30 seconds break in between loads. This procedure is to be completed no more than 60 minutes prior to using the sensor.
2. The sensor should then be calibrated. Calibration loads should be applied and averaged over a similar length of time as the expected measurement duration. For loads less than 0.19 psi (10 mmHg) a line best fits the data.
3. The sensor-contact lens combination should be disinfected with a 70% alcohol swab and allowed to air dry before insertion into the eye, according to the infection control standards for optometric equipment that comes in contact with the eye (Ethics approval – Appendix 5).

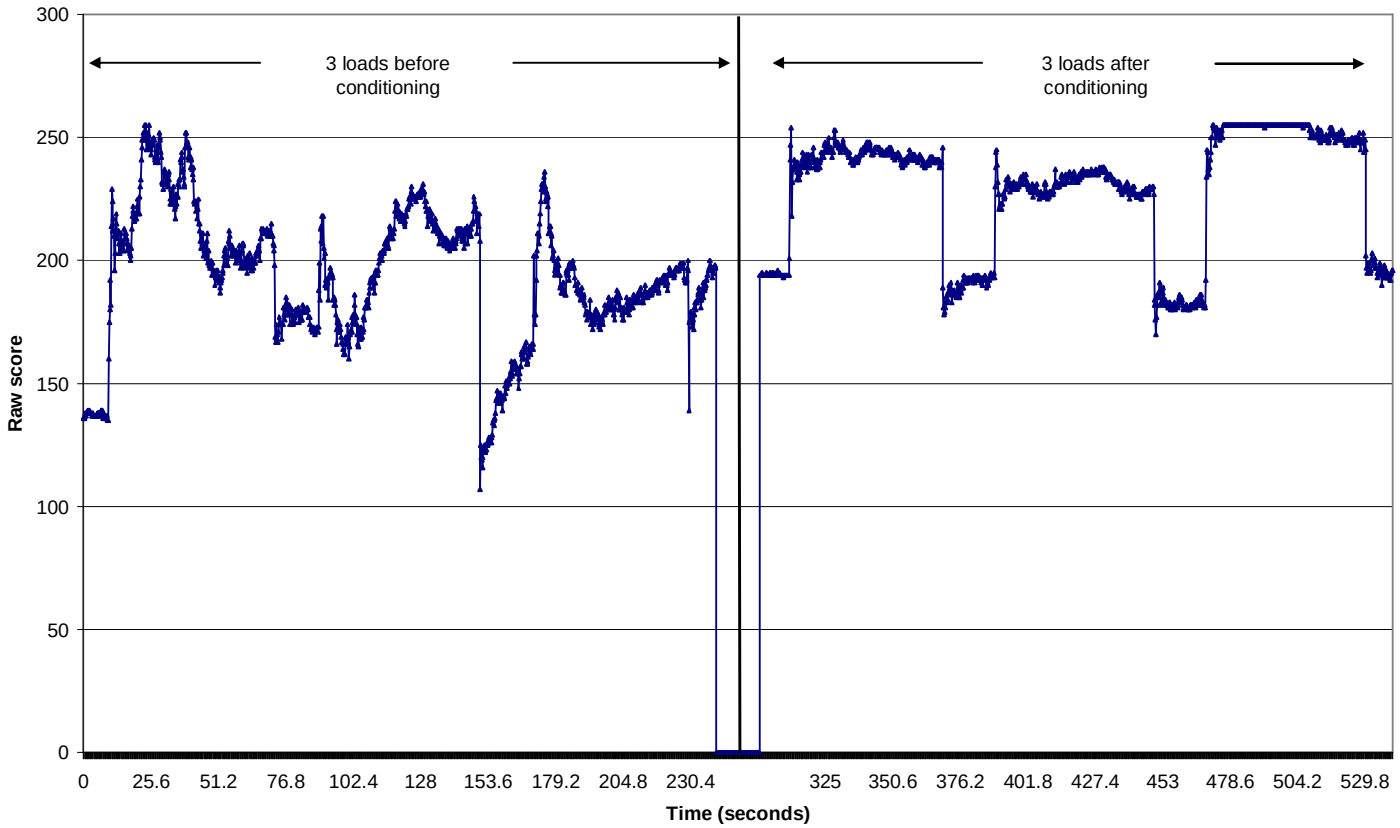

Figure 3-40: Six loads of 0.15 psi: three applied before conditioning and three applied after conditioning.

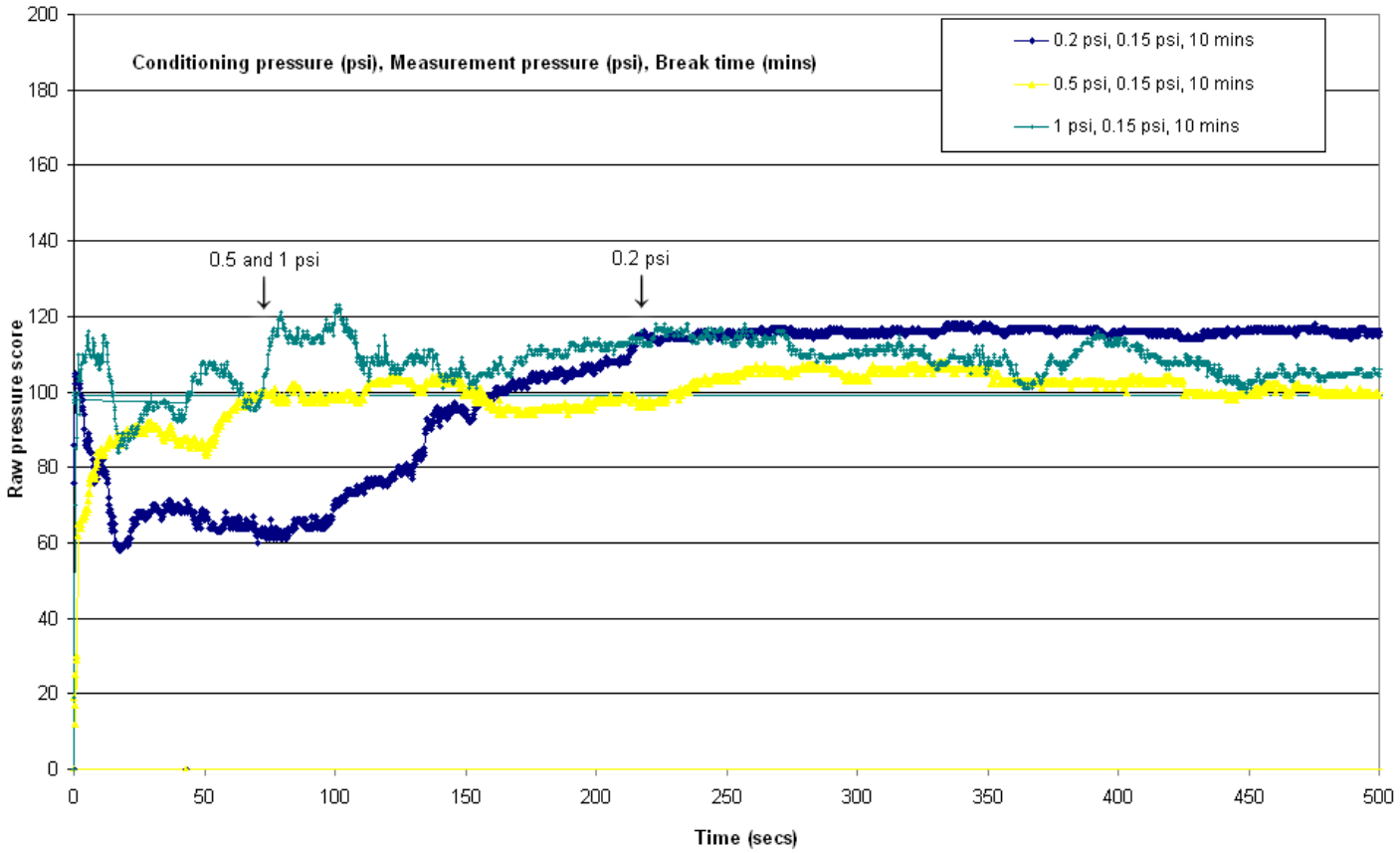

Figure 3-41: Measurement loads (0.15psi) after conditioning with 0.2, 0.5 and 1 psi. Measurements that were conditioned with either 0.5 or 1 psi stabilized earlier than the measurement that was conditioned with 0.2 psi.

3.6 Eyelid pressure in vivo measurement apparatus

3.6.1 Initial trials

Before a method was developed to attach the sensor to a rigid contact lens, initial measurement trials were conducted with the sensor attached to a smooth metal spatula (Figure 3-42). This figure shows the apparatus used for this measurement with the spatula-sensor held with a ball joint so that the position and angle could be altered for insertion under the upper eyelid. The patient was positioned in a head rest and the measurement recorded by a video camera so that the eyelid's position with respect to the sensor could be tracked through the measurement. The LED was controlled by the trigger box so that when data collection was triggered the LED would light up in the recorded video. The video frame when data collection can be then identified and the pressure data and video can be synchronized. With the flat spatula, it was quite difficult to position the sensor flush against the cornea and sclera. It was obvious that the sensor needed to be attached to a contact lens, but this trial did show that the model #4201 sensor was capable of measuring eyelid pressure (Figure 3-43). This measurement showed an increase in sensor output which remained stable while the eyelid rested on the sensor. The spikes in the data correspond with attempted blinks which were similar to a strong twitch of the eyelids.

3.6.2 In vivo measurement apparatus

The final apparatus used to measure eyelid pressure was constructed based on preliminary arrangement used for the early trials with the sensor attached to the spatula. The entire apparatus was attached to a slit-lamp biomicroscope base (Figure 3-44 and Figure 3-45). This allowed the position and height (x, y, and z planes) of all the equipment could be adjusted simultaneously and the sensor to be accurately placed under the eyelid margin. The plastic support beam (attached to the sensor-contact lens combination) was fastened to a ball joint and its orientation could be easily altered independent of the video cameras. The two video cameras provided front (en face) and side recording of the sensor-contact lens being placed onto the eye. A head movement guide was attached to the head rest and placed on the subject's temples so that they had some feedback if they moved their head.

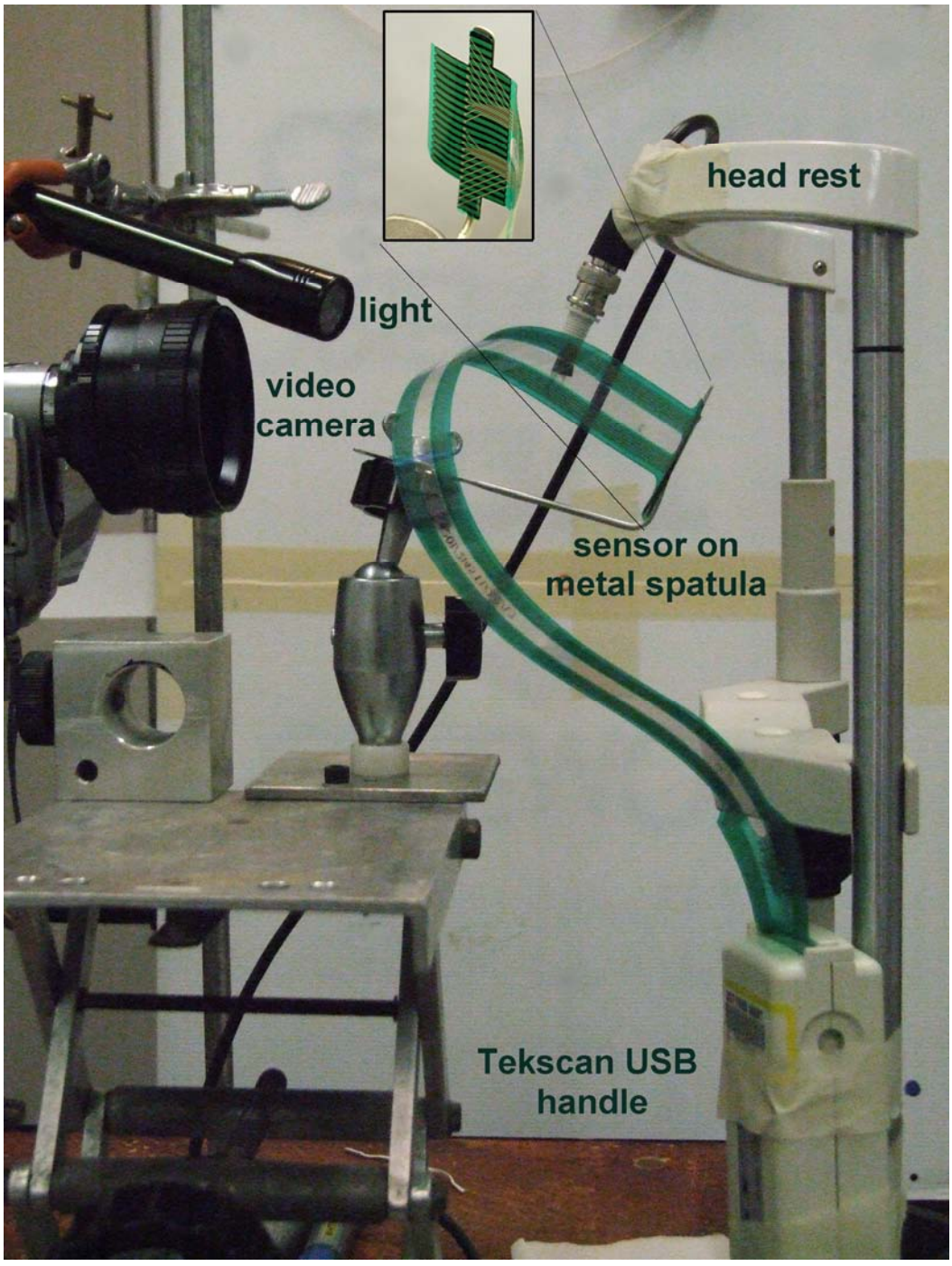

Figure 3-42: Measurement apparatus used for initial trials using the sensor attached to a metal spatula.

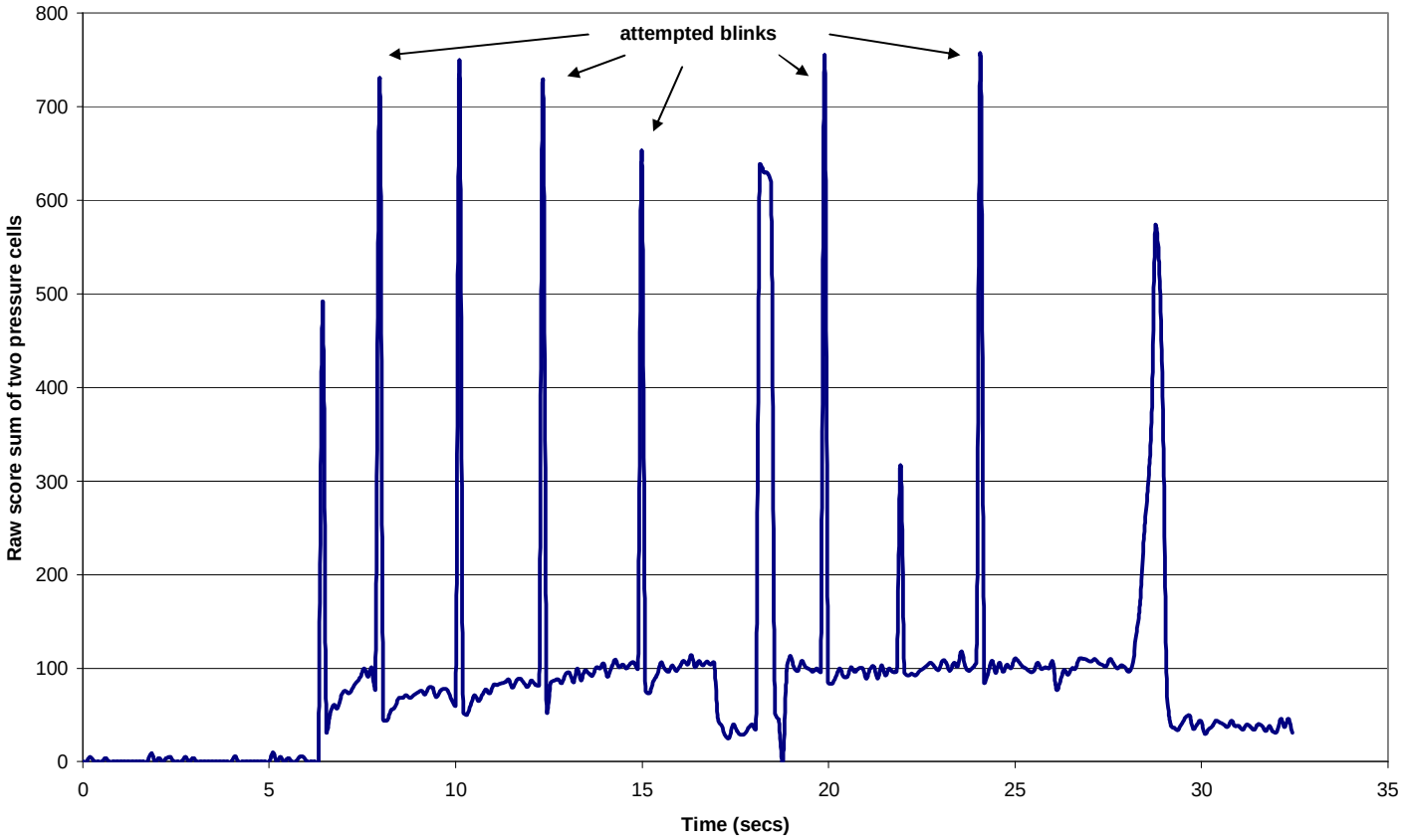

Figure 3-43: Early pressure measurement using the sensor attached to metal spatula. This demonstrated that the sensor could measure eyelid pressure with spikes representing attempted blinks.

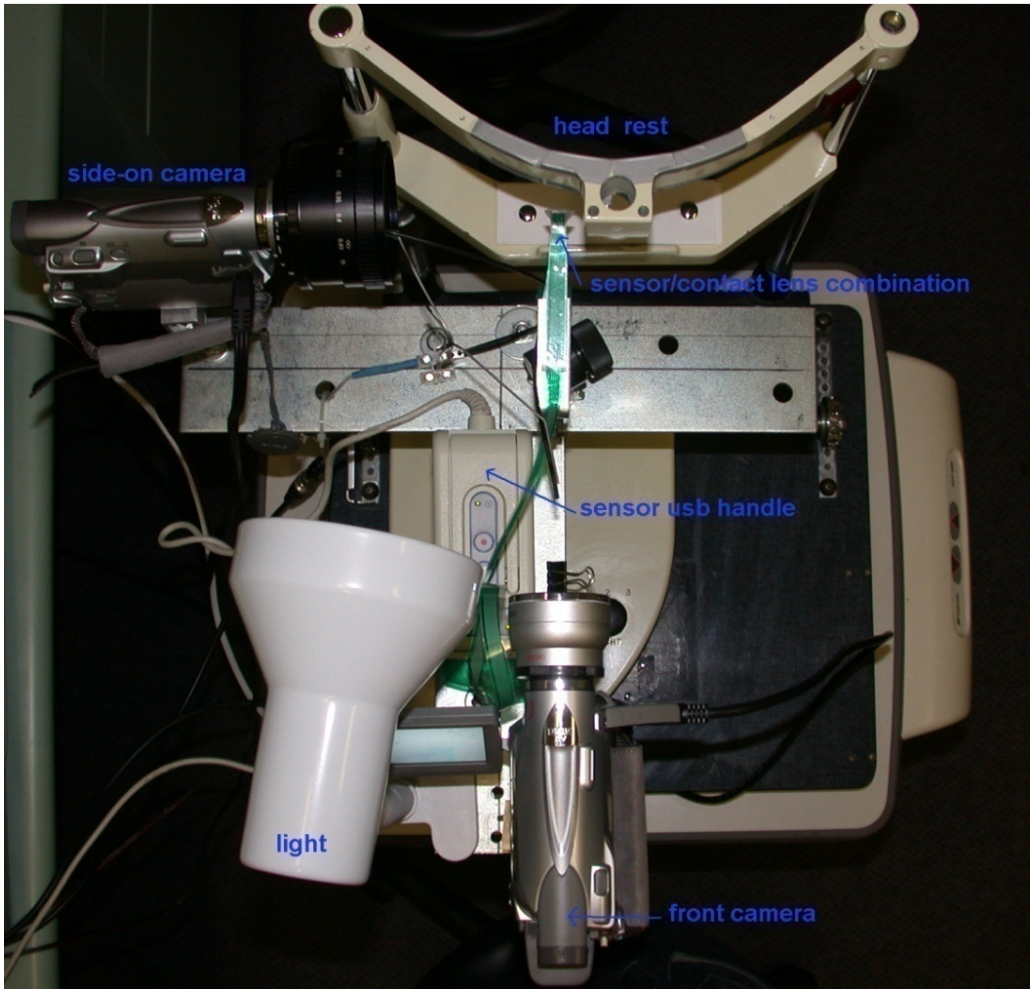

Figure 3-44: Measurement apparatus for eyelid pressure measurements (top-down) view.

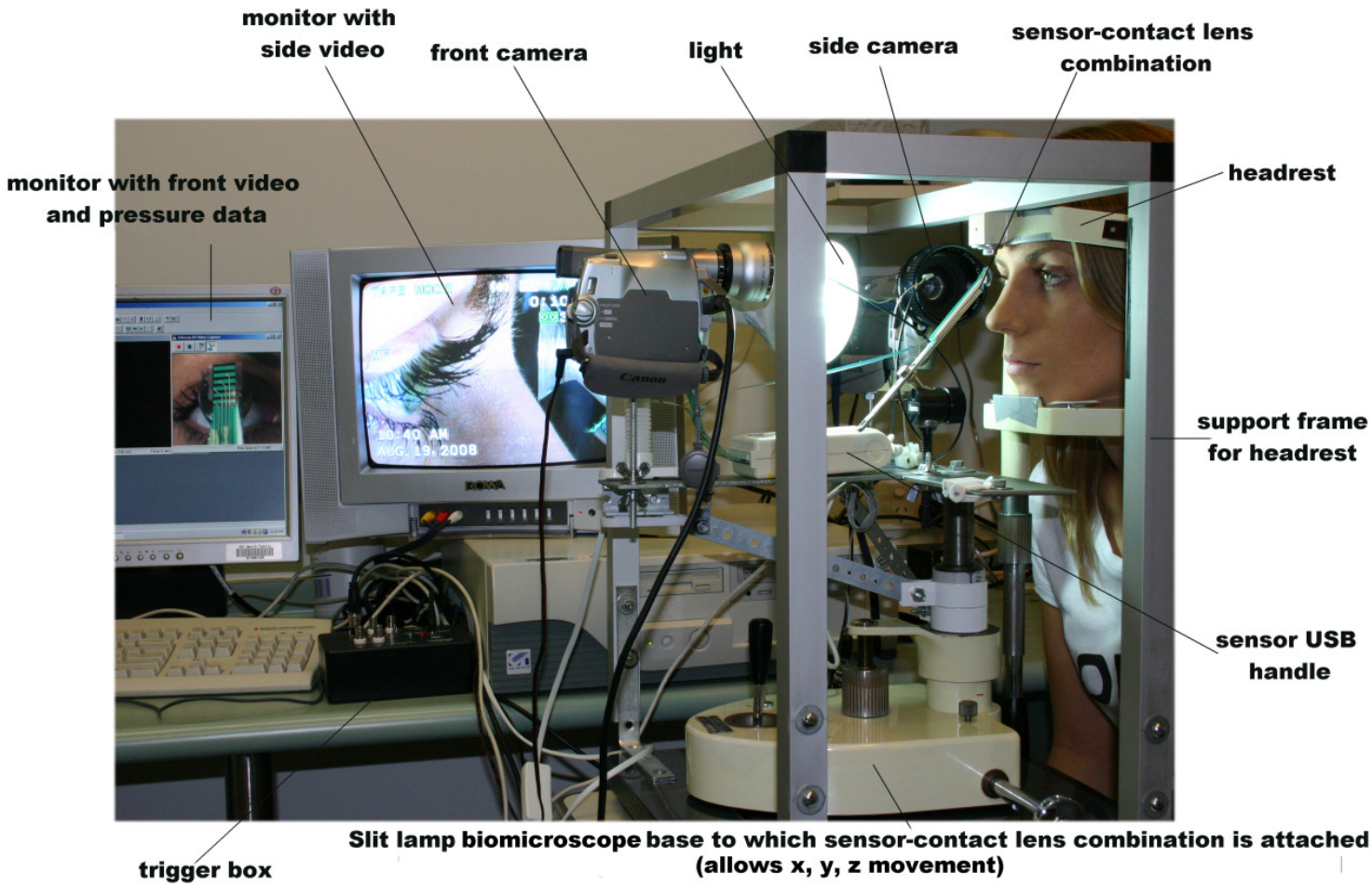

Figure 3-45: Apparatus for eyelid pressure measurements.

Via a firewire cable, the front camera was connected to the computer and to the Tekscan software so that it was synchronised with the pressure data. The side camera was connected to a monitor so that the image could be viewed as the contact lens was placed on the eye. A split LED system meant the trigger caused a LED in front of each camera to light at the beginning of the data collection. Initially a fluorescent ring light was used to provide extra illumination for the video capture. However it was found that this electrically interfered with the pressure sensor output, with erratic variations in the data. The fluorescent ring light was replaced with a desk lamp which could be positioned further away from the sensor. There was also electrical interference if the sensor tail was in contact with the LCD panel of the video cameras so the sensor tail was positioned away from the video cameras.

3.7 Examples of eyelid pressure measurements

This research was approved by the university Human Research Ethics Committee and all subjects gave informed consent before participation (Appendix 5). Sample eyelid pressure readings when the upper lid was placed on the sensor and removed three times showed an obvious and consistent response of the sensor (Figure 3-46). A frequency analysis of eyelid pressure signals demonstrated that intra-measurement dynamic variation is likely to have a physiological origin (Appendix 6). Another measurement example was the effect of tightening the upper eyelid (Figure 3-47), which is achieved by a technique similar to the lid-pull technique for removing a rigid contact lens. The sensor output shows that the pressure applied by the eyelid significantly increases when the eyelid was pulled (Figure 3-47).

Several techniques were developed to calibrate and measure eyelid pressure using piezoresistive sensors. These included designing the sensor-contact lens combination which involved a custom contact lens, trimming the sensor, resealing the sensor and attaching it to a support beam. A custom built calibration device was also required to enable small pressure to be loaded onto the sensor-contact lens combination. The output response of the sensor was examined so that a protocol for eyelid pressure could be designed appropriately. Also an *in vivo* measurement apparatus was built to enable easy and accurately positioning of the sensor-contact lens onto the eye. Trials using this equipment provided evidence that the technique is able to measure eyelid pressure.

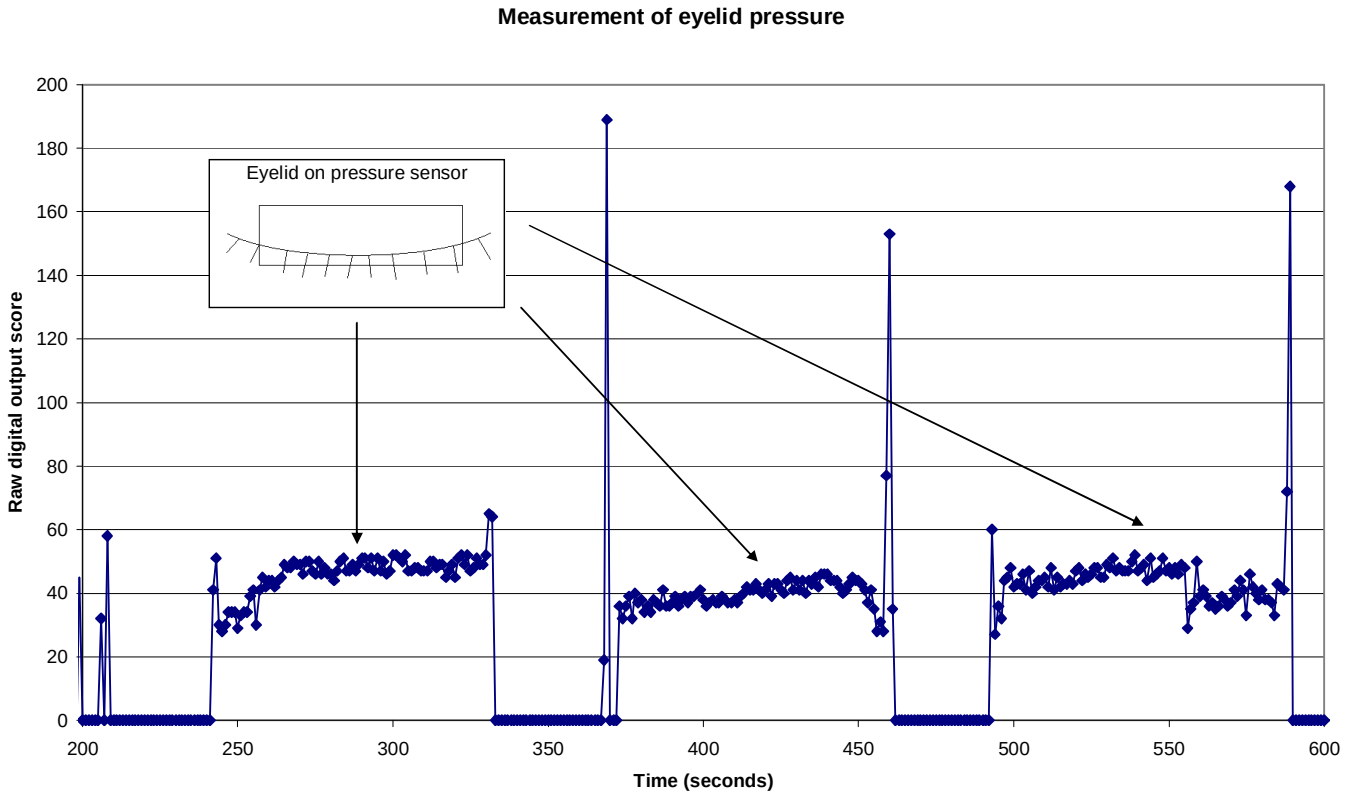

Figure 3-46: An eyelid pressure measurement with the eyelid being placed on and off the sensor three times.

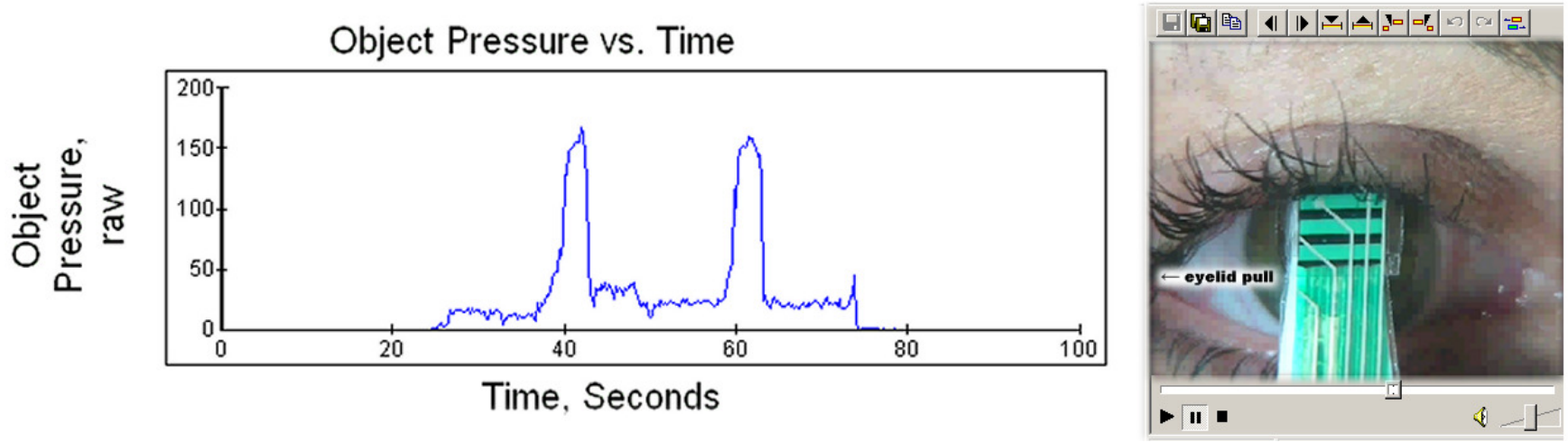

Figure 3-47: Eyelid pulled twice to increase applied pressure.

Chapter 4: Upper eyelid pressure against the eye

4.1 Introduction

It is known that corneal topography changes occur from eyelid abnormalities such as chalazia, hemangiomas and ptosis. The increased or altered pressure on the cornea from these eyelid conditions primarily alters corneal astigmatism. The pressure from healthy eyelids when the palpebral aperture is narrowed also causes corneal distortions (Buehren *et al.* 2001; Buehren *et al.* 2003; Collins *et al.* 2006; Collins *et al.* 2006; Shaw *et al.* 2008). In Chapter 2 we measured these corneal changes that are bands of wave-like distortion and are located approximately parallel to the eyelid margin.

Attempts to measure eyelid pressure have used modified scleral contact lenses attached to manometers. The lens designed by Miller (1967) measured the average change in pressure for 10 subjects as 2.8 mmHg for a light blink. Lydon and Tait (1988) used a scleral shell with a silicone elastomer contact lens but did not publish values for eyelid pressure only concluded that the lid pressure was "small". An apparatus similar to Miller's scleral-balloon system was used to measure 21 subjects with average results of 1.7 mmHg for normal lid closure (Shikura *et al.* 1993).

The eyelids are in close contact with the ocular surface but the exact area of contact (i.e. pressure distribution) between the two surfaces is unknown. Previous investigations suggest that the eyelid margin is the main region of the eyelid in contact with the ocular surface. X-ray examination of an individual has shown close contact between the upper eyelid and cornea only in the marginal eyelid region (Kessing 1967). This region has been termed the lid-wiper, an area of the marginal conjunctiva thought to be involved in the distribution of the tear film layer during blinking (Korb *et al.* 2002). A portion of the eyelid margin is known as Marx's line. This narrow line of squamous cells extends along the entire length of the upper and lower eyelids and can be visualised by staining

with lissamine green or rose bengal vital dyes (Marx 1924; Norn 1985; Hughes *et al.* 2003). The squamous cell phenotype suggests it is a tissue subject to mechanical contact and so may be the primary site of contact between the ocular surface and the eyelid. Increased staining in the region surrounding Marx's line in dry eye subjects also suggests enhanced frictional contact of this region with the ocular surface (Korb *et al.* 2002; Korb *et al.* 2005).

In Chapter 3 an eyelid pressure measurement technique was developed using relatively thin (0.17 mm) pressure sensors mounted on a contact lens, which gave a thickness of about 0.7 mm at the region where the eyelid contacted the sensor. This study aimed to use this system to measure the pressure of the central region of the upper eyelid for a group of young normal subjects. Static eyelid pressure was measured with the upper eyelid resting on the ocular surface without any movement such as blinking. While psi pressure units were used in Chapter 3, in this chapter mmHg were used as this is the pressure unit commonly used in eye research and clinical practice for other ocular pressure measures. For reference, 1 psi is equal to 51.7 mmHg. Measurements were also taken of the morphology of the eyelids and two methods were used to estimate the width of contact between the eyelid margin and the ocular surface. The combined data of eyelid pressure and estimated contact width were used to propose three models of eyelid pressure distribution on the ocular surface.

4.2 Methods

This research was approved by the University Research Ethics Committee (Appendix 5) and adhered to the tenets of the Declaration of Helsinki. Written consent was obtained from each study participant after they had read an information sheet.

4.2.1 Clinical considerations with technique

Chapter 3 has outlined the technical details of calibrating and mounting the piezoresistive pressure sensor on a contact lens. However a number of clinical issues needed to be addressed before measurements were taken. These

included standardising the insertion procedure, controlling subject fixation during the measurement and assessing the repeatability of the measurements.

4.2.1.1 Insertion procedure

The contact lens needed to be placed evenly on the eye. The tear film filling behind the contact lens could be seen in both the front and side video cameras and guided the placement of the lens centrally onto the eye (Figure 4-1).

4.2.1.2 Subject fixation

To obtain a stable measurement of eyelid pressure the subject was required to maintain constant fixation during the measurement with limited eye or eyelid movement. Steady fixation was difficult for the subjects if the non-measurement eye remained open, due to attempted blinking from tear film breakup and reflex twitching from seeing the approaching contact lens. Fixation was improved by inserting artificial tears or anaesthetic eye drops in the non-measurement eye to increase the time before tear breakup. However while the instillation of eye drops increased tear breakup time and therefore the possible measurement time, the subject could still see the approaching contact lens. The most stable measurements were achieved when the non-measurement eye was manually held closed by the subject. With the non-measurement eye closed and the vision of the measurement eye partially occluded by the sensor-contact lens combination, subjects were instructed to maintain fixation in the direction of the lower edge of the front video camera (approximately 10° downward gaze). This method resulted in relatively stable fixation of the measurement eye with less eyelid twitches so the sensor output was more consistent.

4.2.2 Eyelid pressure methodology

The technique to measure eyelid pressure was based on the conclusions of previous authors that a narrow band of the upper eyelid margin has the main pressure contact with the cornea (Kessing 1967; Korb *et al.* 2002; Doughty *et al.* 2004). So a region of the model #4201 sensor (3 cells by 3 cells, approximately 5 mm by 5 mm) was calibrated to measure eyelid pressure.

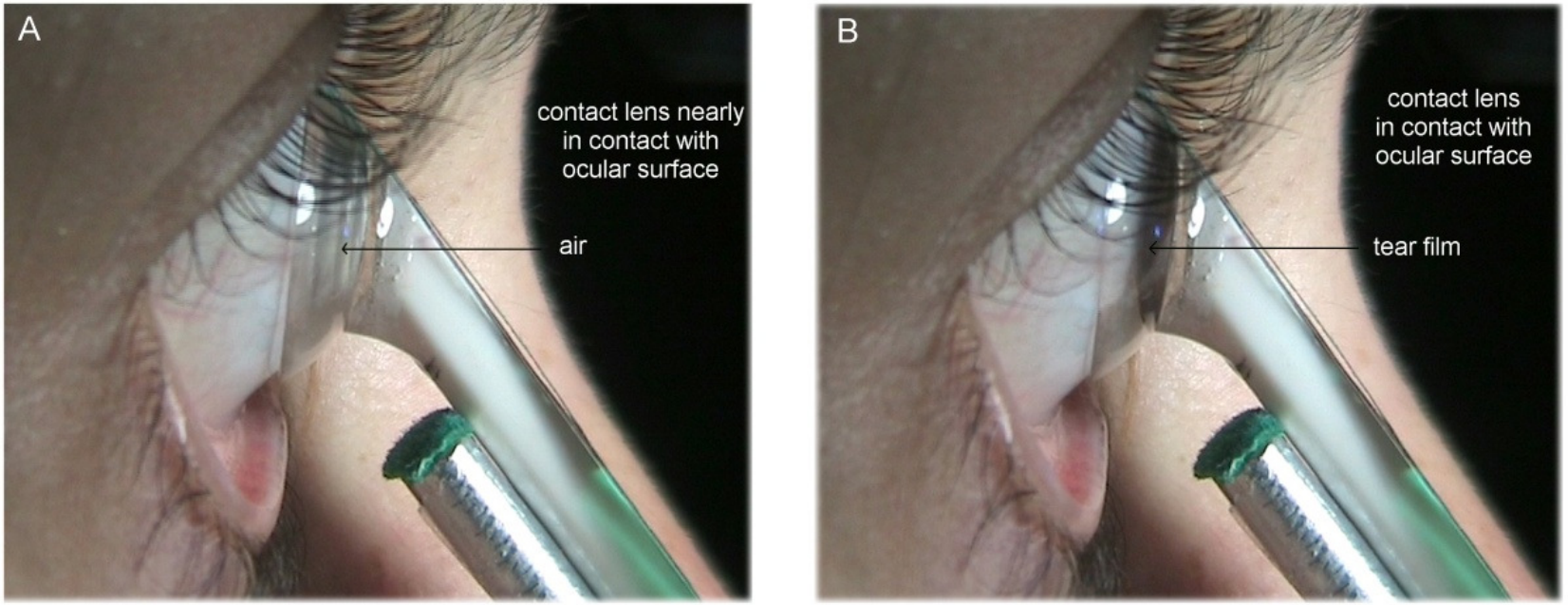

Figure 4-1: Side view of sensor-contact lens combination A) just before contact with the ocular surface and B) contacting the ocular surface with the tear film filling behind the contact lens.

From the results in Chapter 3, it was determined that a sensor could be used for measurement within an hour after it has been calibrated. Two drops of 0.4% benoxinate were used to anesthetise the cornea and eyelid. Subjects fixated at the lower edge of the front video camera and held their left eyelid closed while the eyelids of the measurement eye (right) were lifted away from the globe. The sensor-contact lens combination was then placed on the cornea using the adjustment of the slit-lamp biomicroscope base. The video cameras (front and side views) were used to guide the positioning of the contact lens on the cornea to achieve an even tear film filling between the cornea and contact lens back surface. The eyelids were then released so that the lower eyelid rested on the lower edge of the contact lens and the upper eyelid made contact with the pressure sensor.

The position of the eyelid on the sensor is critical. This example shows two eyelid pressure measurements in which the eyelid was lifted off the sensor during the recording (Figure 4-2). Later in the measurement the upper eyelid began to move upward off the active part of the sensor and although the visible edge of the eyelid margin appeared to be just in contact with the upper region of the cell, the output was zero.

The region of the eyelid contacting the sensor cannot be directly viewed during measurement due to the curved nature of the eyelid margin and eyelashes (Figure 4-3). So controlled eyelid movement was needed during a recording so that the active sensor would be loaded at some stage during the measurement. Eyelid movement was achieved by letting the eyelid drift naturally or by moving the contact lens vertically using the slit-lamp biomicroscope vertical control. As the response in the first 10 seconds after loading tends to be noisy (described in Chapter 3), this portion of the recording was not analysed. So the aim was to record at least 20 seconds of data with the eyelid in contact with the active region of the sensor, so that there would be 10 seconds of data that could be analysed.

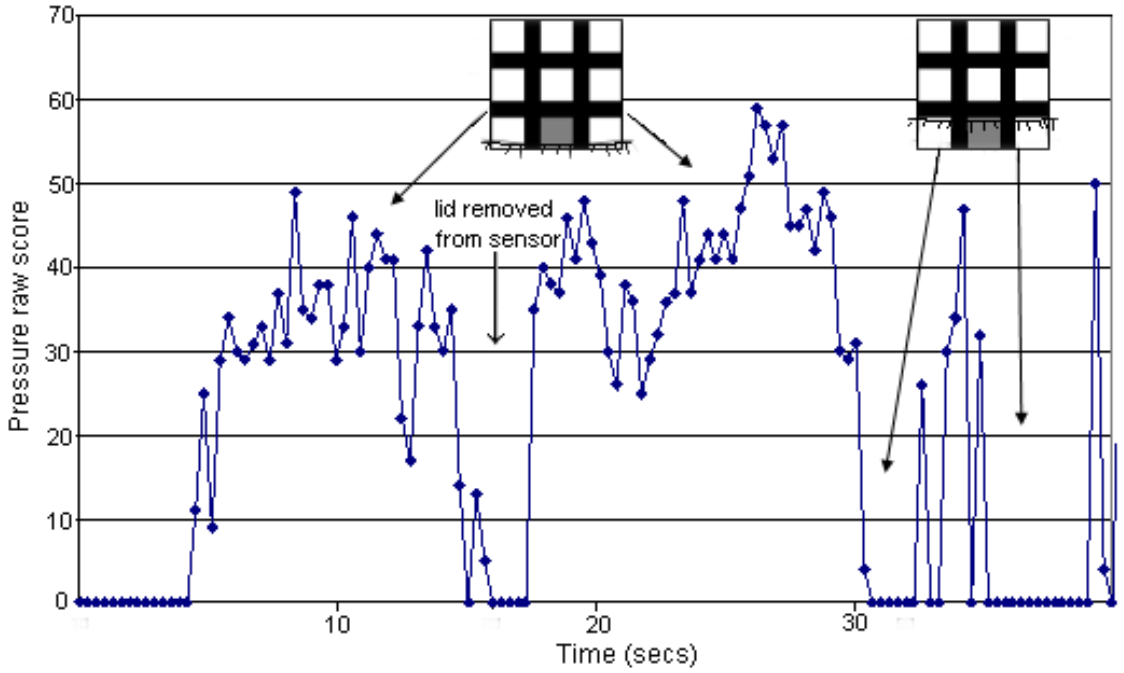

Figure 4-2: Eyelid pressure measurement for the lower middle pressure cell (shaded grey). The other pressure cells are white and the black regions indicate the inactive regions of the sensor. Two recordings with the eyelid covering nearly the entire lower sensor row (eyelid lifted between measurements). When the eyelid moved upward and the eyelid margin appeared to be only just in contact with the lower row, the output was zero.

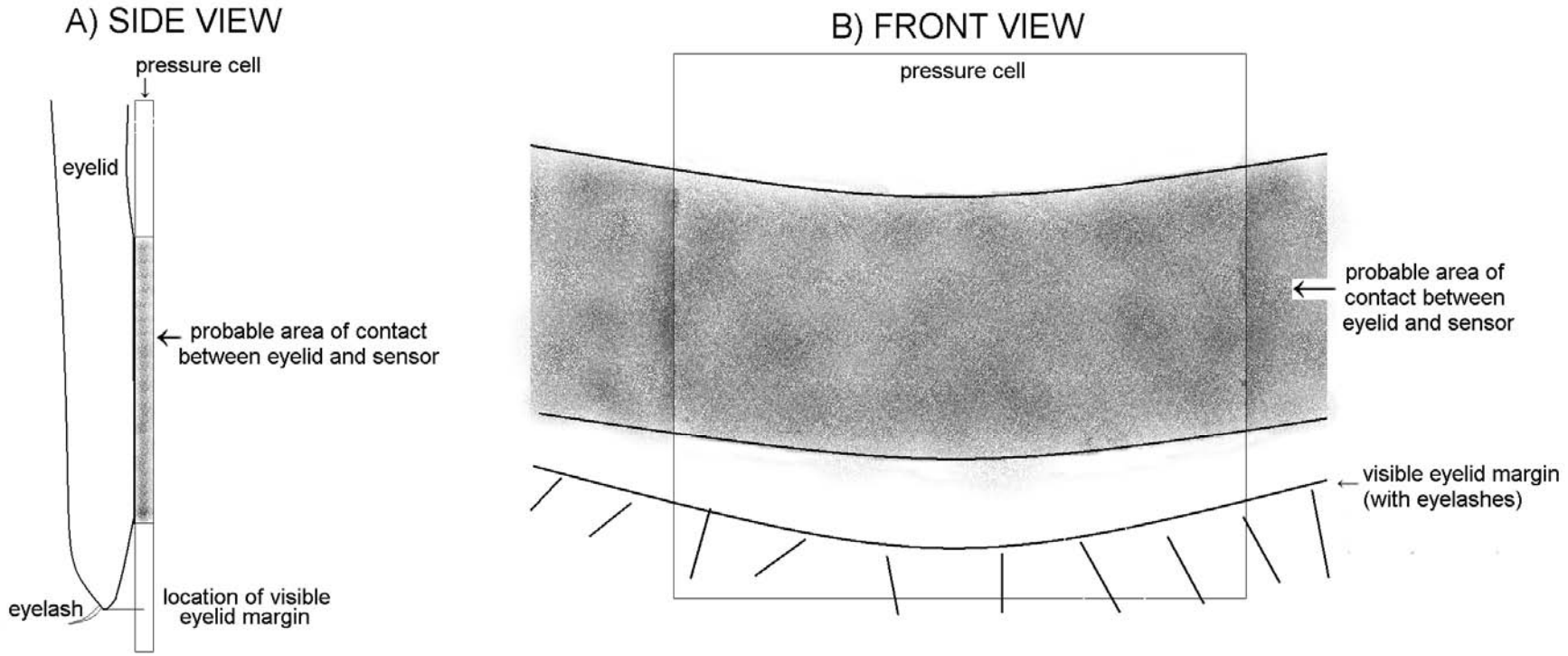

Figure 4-3: Schematics of the eyelid contacting the pressure sensor: A) side and B) front views.

The Tekscan software has various sensitivity settings: low 1, low 2, low 3, default, mid 1, mid 2, high 1 and high 2. These settings alter the ratio between the excitation voltage (Vtest) and reference voltage (Vref) in the Tekscan sensor. The default sensitivity setting has a higher ratio Vtest/Vref than the lower sensitivity settings. As the relationship between these settings is not simply a linear scaling factor, calibrations can only be applied to measurements made on the same setting. The exponential relationship between the raw score and sensitivity setting for a pressure of 25.9 mmHg measured 1 minute after loading can be seen in Figure 4-4. Using the model #4201 5 psi (258.9 mmHg) pressure sensors, the sensitivity needed to be on the maximum level (high 2) setting to measure eyelid pressure, which is in the lower range of the sensor.

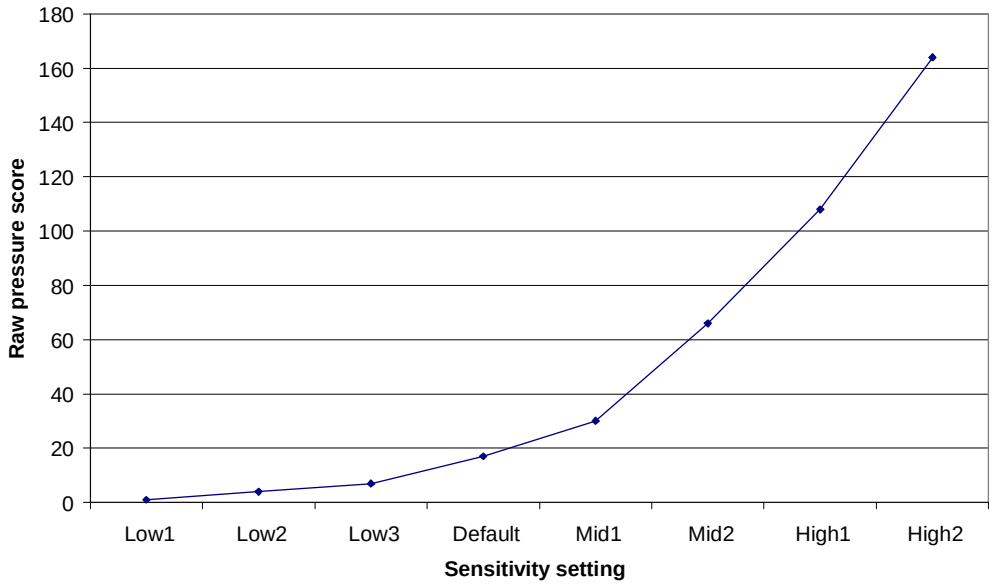

Figure 4-4: Raw pressure scores for a load of 25.9 mmHg measured at each of the sensitivity settings.

4.2.3 Repeatability of eyelid pressure measurements

The repeatability of eyelid pressure measurements was assessed in a number of ways including lifting the eyelid without removing the sensor-contact lens from the

eye, removing and reinserting the sensor-contact lens in the same session (between measurements), between days and between sensors. Conditioning and calibration were completed as per the guidelines outlined in Chapter 3. The subject was experienced with the technique so as there was limited twitching and movement of the eyelid during measurement.

Eyelid pressure measurements were taken on the same subject for 5 pressure cells on 3 different sensor-contact lens combinations (#24, #25 and #43). The position within the table indicates the cell position (row and column) within the sensor (Figure 4-5). For example #43 results are for sensor #43 and the pressure cell in the top right position. The eyelid pressure measurements have been averaged for the eyelid being placed on and off the sensor (without removal of the lens from eye). For example the two measurements for sensor #43 are 1.6 ± 0.8 mmHg which is the first measurement averaged for 3 eyelid placements (number in brackets) and the second measurement was 2.8 ± 0.4 mmHg also averaged for three eyelid placements. There is a table of results for each day the measurements were made (panels A and B of Figure 4-5).

Not surprisingly, the least variability was observed between lifting the eyelid on and off the sensor without removing the sensor from the eye and measurements taken in the same session with removal of the lens, followed by between measurements between days, while the most variability occurred between different cells of different sensors.

There was a consistent bias with cells on the left hand side recording higher pressure than the middle column, which in turn had higher readings than the right hand cells. This is unlikely to be a real observation, as the eyelid is elastic and so can be assumed to exert relatively even pressure across its length. It is more likely to be an artefact of the eyelid wrapping around the edges of the sensor onto the curved contact lens surface. So it was decided that data would only be considered from cells in the middle column, which should have the least error from the eyelid wrapping around the edge of the sensor. Based upon the results of these pilot studies, at least 2 and up to 5 x 20-second recordings (5 Hz) were taken for each subject, with the eyelid located in the active region of the sensor.

A) Eyelid pressure: day one

	Left column	Middle column	Right column
Top row	X	X	#43 1.6 ± 0.8 (2) 2.8 ± 0.4 (3)
Middle row	#24 7.4 ± 0.9 (3) 6.6 ± 3.4 (2)	X	X
Bottom row	#25 7.9 ± 0.8 (3) 6.9 ± 0.8 (3)	#25 3.1 ± 0.2 (3) 2.8 ± 0.2 (3)	#25 0.2 ± 0.2 (3) 0.3 ± 0.2 (3)

B) Eyelid pressure: day two

Top row	X	X	#43 n/a 0.8 ± 0.1 (2)
Middle row	#24 5.2 ± 0.2 (2) n/a	X	X
Bottom row	#25 6.0 ± 1.4 (2) 5.6 ± 1.4 (3)	#25 4.9 ± 0.1 (2) 4.6 ± 0.3 (3)	#25 1.9 ± 1.0 (2) 0.9 ± 0.2 (3)

Figure 4-5: Mean eyelid pressure measurements of 5 pressure cells from sensors #24, #25 and #43. Each measurement is the mean and standard deviation from lifting the eyelid on and off the sensor 2 or 3 times (number in brackets). The measurements within a box represent the whole sensor-contact lens combination was removed from the eye. A) Eyelid pressure results from day 1 and B) from day 2. The same subject's right eye was used for all measurements. Units are arbitrary as the final calibration has not been completed.

4.2.4 Protocol

4.2.4.1 Subjects

Eleven subjects were recruited from the staff and students of the Queensland University of Technology School of Optometry. There were 7 female and 4 male subjects of Caucasian (n = 6), Indian (n = 4) and Iranian (n = 1) ethnicity with a mean age of 28 ± 3 years (range 22 to 33 years). Subjects had a best corrected acuity of 0.00 logMAR or better with a mean spherical refractive error of +0.10 ± 0.39 D and the mean astigmatism was -0.20 ± 0.31 D.

4.2.4.2 Preliminary assessment

To confirm that all the inclusion and exclusion criteria were satisfied, all subjects underwent a preliminary eye examination. Due to eyelid pressure instrument restrictions, the right eye was investigated for all subjects. Slit-lamp biomicroscopy confirmed the anterior eye inclusion criteria including a clear and healthy cornea with no evidence of dry eye, Meibomian gland dysfunction, blepharitis, entropion, ectropion, chalazia or ptosis. Dry eye was defined as a score of ≥ 14 on the McMonnies dry eye symptom survey and a non-invasive tear break up time of < 10 seconds using projected mires. Subjective refraction, using the maximum plus for best visual acuity criteria, was used to confirm refractive status. Since there is evidence that rigid contact lens wear can lead to slight ptosis (van den Bosch and Lemij 1992) and there are anecdotal reports of ptosis from soft contact lenses (Nemoto *et al.* 2008), all contact lens wearers were excluded from the study. Subjects also had no history of ocular surgery or injury.

4.2.4.3 Eyelid pressure measurement

Conditioning and calibration of the piezoresistive sensors were completed as per the guidelines in Chapter 3 (see calibration example, Figure 3-26). Linear calibration equations for sensor #25 were calculated for each subject (Table 4-1). The coefficient of determination (R^2) ranged from 0.68 to 0.96, with an average of 0.77.

Table 4-1: Calibration equations for sensor #25

Subject Number	Calibration equation Pressure (mmHg) = a * Raw score + c	R^2
1	y = 0.042x + 1.209	0.96
2	y = 0.032x + 1.982	0.71
3	y = 0.031x + 1.280	0.68
4	y = 0.040x + 1.909	0.84
5	y = 0.038x + 1.709	0.78
6	y = 0.032x + 1.833	0.69
7	y = 0.036x + 2.284	0.84
8	y = 0.063x + 1.521	0.69
9	y = 0.041x + 1.635	0.80
10	y = 0.041x + 2.018	0.73
11	y = 0.058x + 1.192	0.75

Up to five eyelid pressure measurements (at 5 Hz) were taken until at least two, and preferably three successful measurements were captured (that is, with the eyelid in the correct position on the sensor for at least 20 seconds). The eyelid pressure measurements were taken with two sensors (#25 and #26). Results were incomplete (not all subjects measured) for sensor #26 as during swabbing with the mediswab some alcohol seeped into the sensor. This ruins the conductivity of the sensor and it is then no longer sensitive to pressure. There were 37 recordings taken for the 11 subjects with sensor #25. Six of these measurements were not analysed as either the eyelid position was unstable (3 measurements), the eyelid did not reach the active part of the sensor (2 measurements), or the video did not record (1 measurement). The remaining 31 recordings were analysed, and averaged for each subject (mean 2.8 recordings at 5 Hz per subject). There was a mean of 60 data points (equivalent to 12 seconds) for each eyelid pressure recording, giving a mean of 168 pressure readings per subject. At the conclusion of the experiment, fluorescein was instilled in the eye and the integrity of the anterior eye was checked prior to the subject leaving.

Calibration equations were calculated with Matlab according to the process outlined in Chapter 3, with a linear fit to the calibration data. As the region of the eyelid contacting the sensor cannot be visualized during measurement, the position of the eyelid margin was recorded during the measurement (front video). This was exported to jpeg images at 5 Hz to match the eyelid pressure measurements and the eyelid position relative to the lower edge of the pressure cell was determined with custom-written image processing software (Figure 4-6).

A Matlab macro was used to filter the sensor pressure data dependent on eyelid margin position with respect to the pressure cell. Similar to calibration data, the first 10 seconds of loading (of eyelid pressure) were discarded due to the initial noisy sensor response. Outliers (> 1.96 standard deviations from the mean) were removed, most likely due to eyelid twitches. Assuming that the maximum pressure value occurs when the eyelid is in the correct position on the sensor, half of the power of the maximum pressure was used to obtain a lower boundary limit (upper half criterion). This is equivalent to $\sqrt{2}/2$ of the signal's maximum amplitude or the logarithmic -3 dB criterion commonly used in acoustics and the half width point

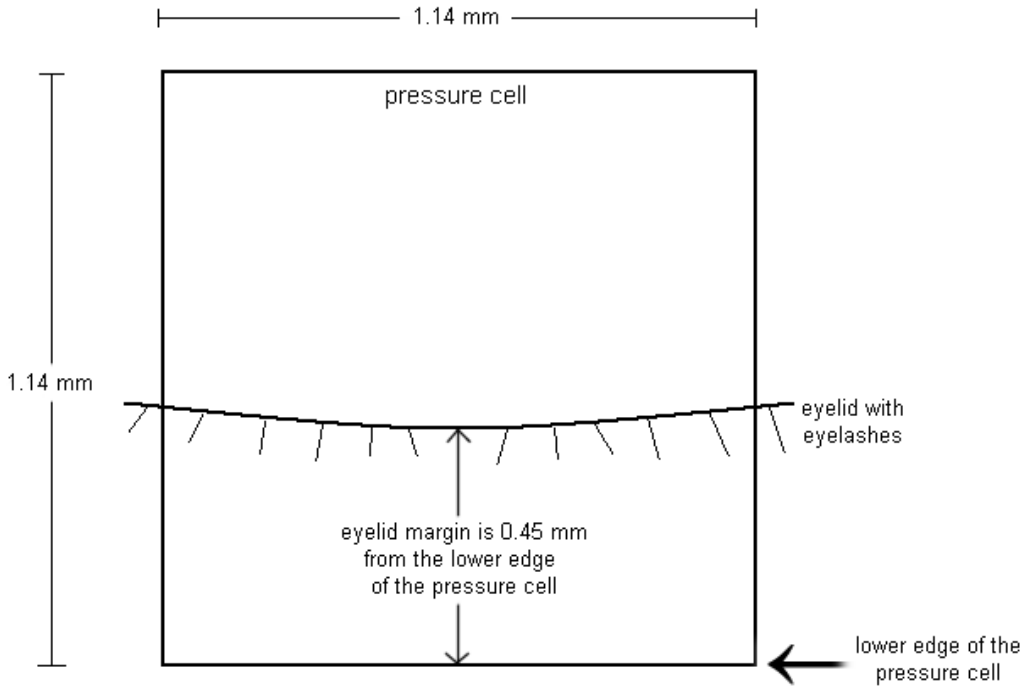

Figure 4-6: Eyelid margin position relative to the lower edge of the pressure cell. A pressure cell is 1.14 mm by 1.14 mm so in this example the visible eyelid margin is +0.45 mm (above) the lower edge of the cell. A negative eyelid position would indicate that the eyelid margin was lower than the edge of the pressure cell.

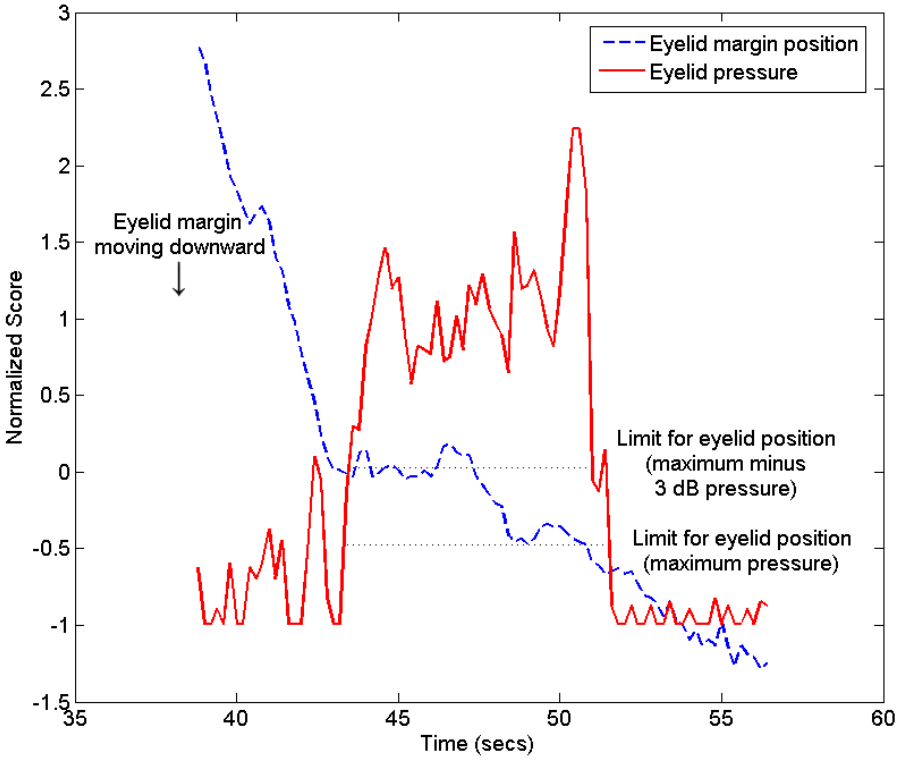

Figure 4-7: Normalised values for eyelid pressure measurement (red solid line) and the corresponding eyelid position (relative to the lower edge of the pressure cell, blue dashed line). The dotted lines give the critical eyelid boundary positions corresponding to the maximum and half power limits. For this example the visible eyelid margin was between -0.72 and -0.46 mm below the edge of the cell during valid pressure readings. The total eyelid movement during the measurement was -1.14 (below) to +0.97 (above) mm relative to the lower edge of the pressure cell. The mean raw score (prior to calibration) corresponding to the critical eyelid range was 79.69 ± 28.46 based on 32 data points.

spread function used in retinal image metrics (Thibos *et al.* 2004). The raw scores within the upper half criterion were averaged and the mean raw score converted to actual pressure units (mmHg) using the calibration equation for that sensor-contact lens combination.

An example of an eyelid pressure measurement and the corresponding eyelid position is shown in Figure 4-7. While the eyelid moved steadily down the sensor during the measurement (blue line), the corresponding pressure measurement was an approximately a step function (red line). Eyelid pressure is zero (-1 on the graphed normalised scale, after time = 52 secs) when the primary contact point of the eyelid has moved down past the pressure cell. As pressure is no longer measured by the sensor, it suggests that a band of the eyelid margin applies pressure to the ocular surface while the remaining eyelid applies very little pressure.

The maximum eyelid pressure (after outliers are removed) was used as this pressure is assumed to occur when the eyelid is in the correct position on the sensor. To check that this analysis protocol wasn't overinflating the eyelid pressure values, the average raw score was manually determined from the eyelid pressure signals. The mean raw score calculated using the upper half criterion was plotted with the manual raw score. This comparison shows a correlation of $R^2 = 0.62$, indicating a high degree of agreement between the methods (Figure 4-8). Similarly a Bland-Altman plot (difference versus mean) of the two measures did not show any bias (Figure 4-9). It was concluded that the average of the raw scores using the upper half criterion did not elevate pressure outcomes.

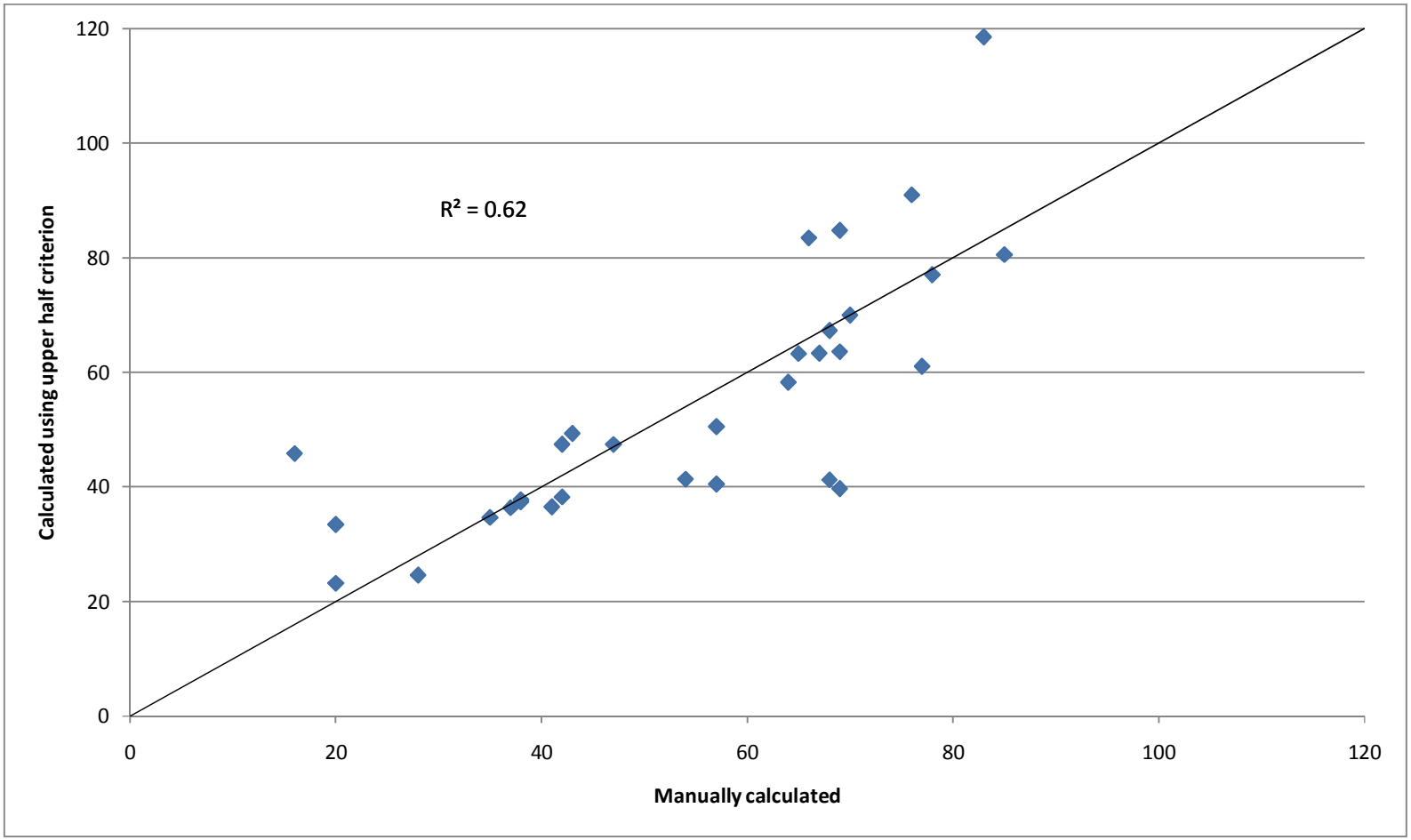

Figure 4-8: Raw scores calculated using the upper half criterion versus manual ($R^2 = 0.62$). Line represents 1:1.

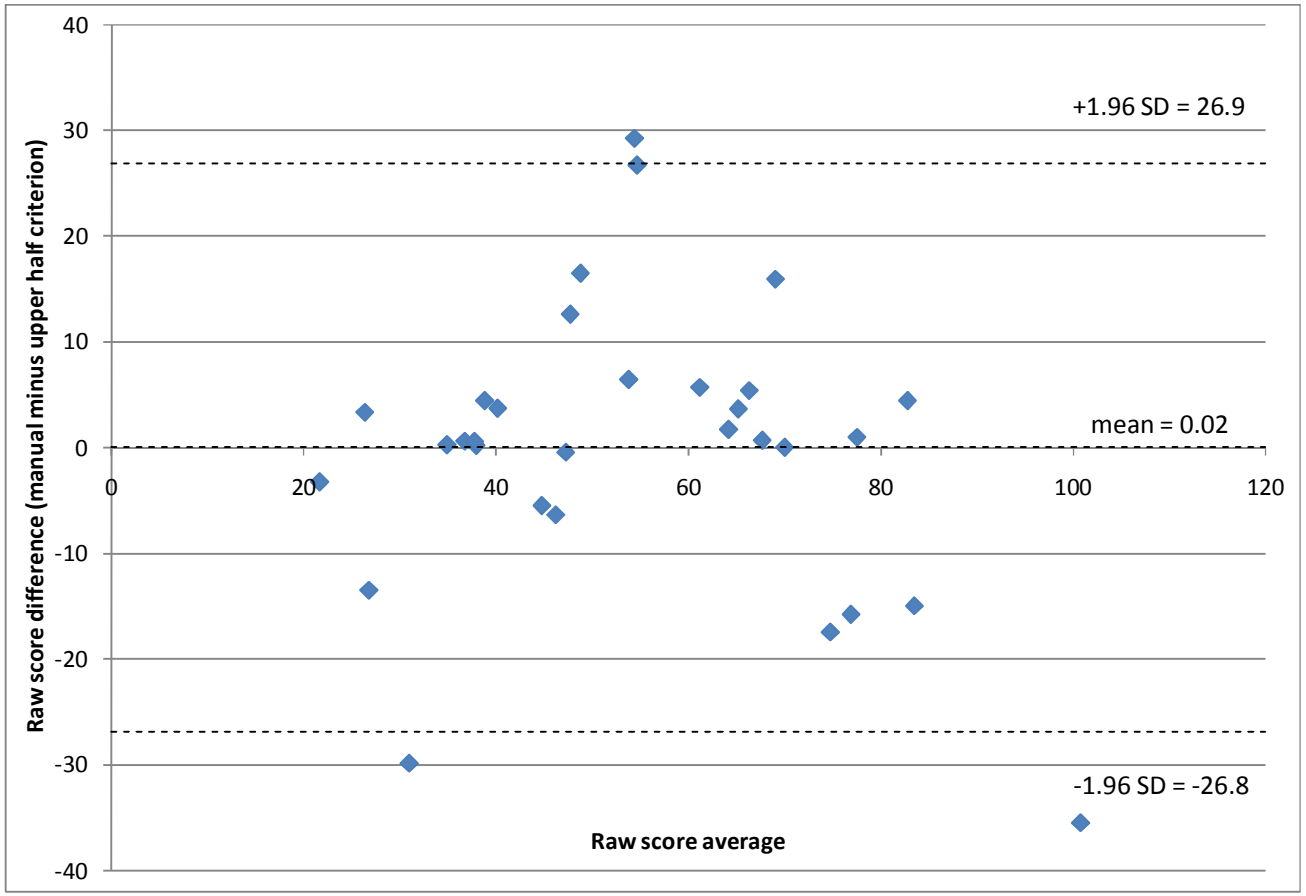

Figure 4-9: Bland Altman plot. Difference in raw scores (manually calculated score minus the upper criterion average) versus mean score for the two methods.

4.2.4.4 Pressurex-micro imprint

As the whole pressure sensor is loaded by the water column during calibration applying this to measurement data assumes that this is the case during an eyelid pressure measurement. However evidence from the work of Kessing (1967), Korb *et al.* (2002) and Doughty *et al.* (2004), suggests that contact occurs between the upper eyelid and ocular surface in a narrow band. To estimate the contact region Pressurex-micro (Sensor Products Inc., Madison, New Jersey) was sourced. This is pressure sensitive paper consisting of outer plastic protective layers and inner carbon and adhesive layers (Figure 4-10). The adhesive layer is exposed then the carbon layer placed in contact with it. Pressure applied results in a carbon imprint on the adhesive layer. It is mainly used to visualise the pressure distribution between opposing surfaces, for example during laminating or between industrial rollers. The specifications suggest a minimum pressure sensitivity of 103.4 mmHg or 2 psi, however much lower pressures were recorded in trials of known pressures (down to 4.6 mmHg), when the applanation surface was wet. This explains why eyelid margin pressure could be measured despite its pressure being lower than the minimum quoted pressure sensitivity of the paper.

Segments of Pressurex-micro paper were adhered to the flat area of the custom contact lenses with double-sided adhesive tape (Figure 4-10). Measurements were taken within half an hour of the adhesive and carbon layers being placed together, as the carbon layer becomes more difficult to remove with time. The subject's eye was anaesthetized (0.4% benoxinate) and the contact lens placed on the eye as per the protocol for eyelid pressure measurements. The upper eyelid was placed on the pressure sensitive paper for about 10 seconds during which time the subject was instructed to try to refrain from blinking. The eyelid was then lifted away from the paper and the contact lens removed from the eye. Removing the carbon layer revealed the carbon imprint of the eyelid pressure on the adhesive layer. Five separate contact imprints were collected for each subject.

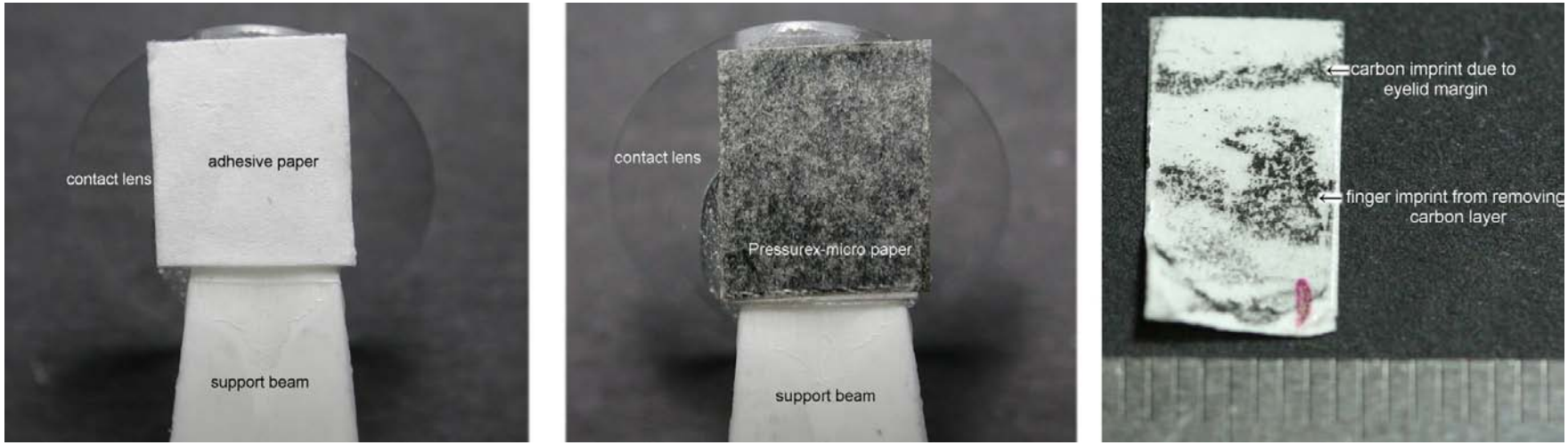

Figure 4-10: Example of Pressurex-micro adhesive paper: A) adhesive layer attached to the contact lens, B) carbon layer placed in contact with the adhesive layer and C) carbon imprint on the adhesive layer after exposure to eyelid margin pressure and removal of the carbon layer.

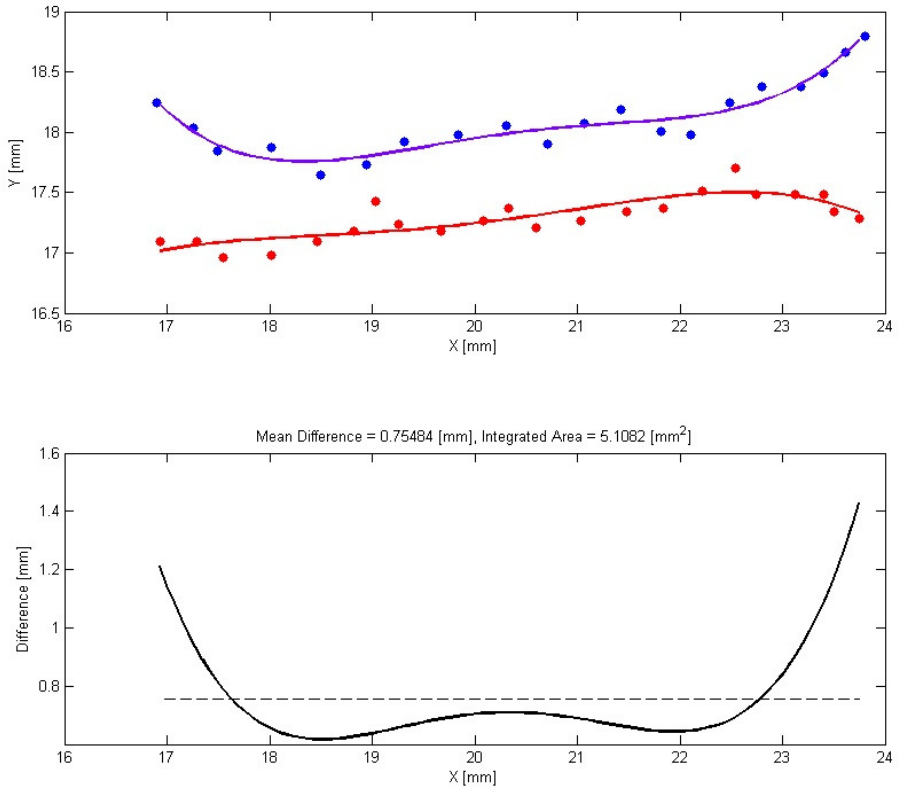

Figure 4-11: Example analysis of contact imprint width. Top panel: blue dots (upper boundary) and red dots (lower boundary). Bottom panel: width of imprint, with the mean equal to 0.75 mm for this subject (dotted line)

From the five imprints taken for each subject the best two or three images were chosen for analysis. Sometimes the measurements did not work due to moisture from the tears causing the carbon paper to stick to the adhesive layer and making it difficult to remove. Images of the carbon imprints due to the contact between the eyelid and the contact lens were analysed in Matlab (Figure 4-11). Points were chosen along the upper edge of the imprint and fit with a 4^{th} order polynomial. This was repeated for the lower edge of the imprint and then the mean distance between the upper and lower boundaries (imprint width) was calculated. The widths of the imprints were averaged for each subject.

4.2.4.5 Marx's line

It has been previously suggested that Marx's line is likely to be the anatomical region that represents frictional contact between the eyelids and ocular surface (Parsons 1904; Hughes *et al.* 2003; Doughty *et al.* 2004). Lissamine green was applied to the superior and inferior sclera of the right eye for each subject using an impregnated strip wetted with two drops of sterile saline and the excess fluid allowed to run off. The eyelids were pulled away from the globe a few times and the closed eyelid lightly rubbed to aid even distribution of the dye. Digital images of the upper eyelid Marx's line were captured as per the protocol of Chapter 2 using the Canon 300D 6.3 megapixel Digital SLR Camera with a 100 mm macro lens and mounted fluorescent lighting ring to obtain even illumination. To view Marx's line the upper eyelid was everted by gripping the eyelashes without contacting the eyelid to expose the palpebral conjunctiva. The camera was set to a manual focus of 0.31 m and positioned at a distance where Marx's line was in focus. The clearest image of Marx's line was chosen for analysis for each subject. The macro lens allowed high magnification and a resolution of approximately 137.8 pixels per mm. The width of central Marx's line was analysed with custom software, similar to the eyelid-cornea contact imprints. Points were chosen along the upper and lower boundaries over a 6 mm central portion of the eyelid. Each boundary was fit with a 4^{th} order polynomial and the average distance between the boundaries (mean Marx's line width) was calculated for each subject (Figure 4-12).

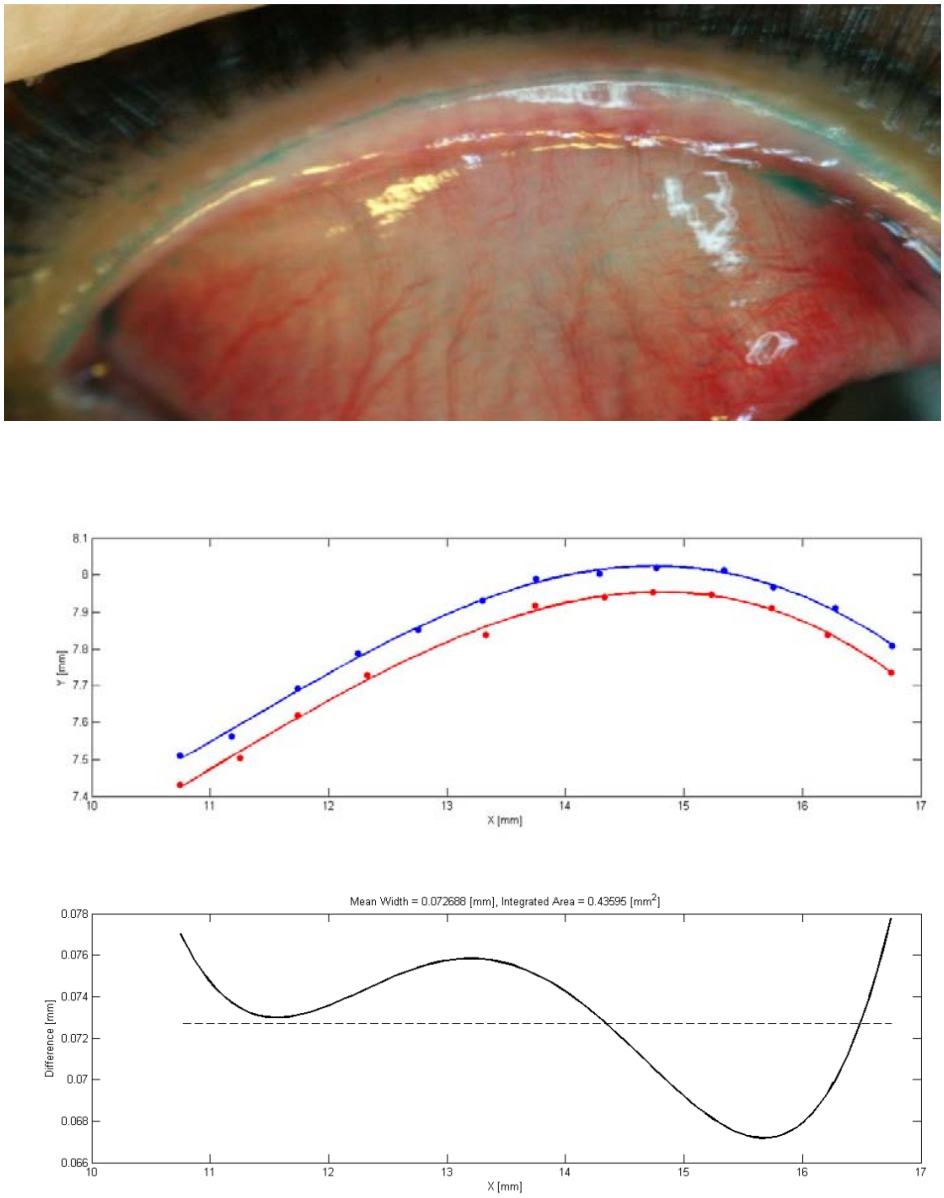

Figure 4-12: Photo of upper eyelid lissamine-stained Marx's line (top panel) and its analysis of Marx's line over the central 6 mm (lower panel). The blue dots indicate the upper boundary of Marx's line and the red dots the lower boundary. The mean difference (Marx's line width) is equal to 0.073 mm for this subject (lower panel, dotted line).

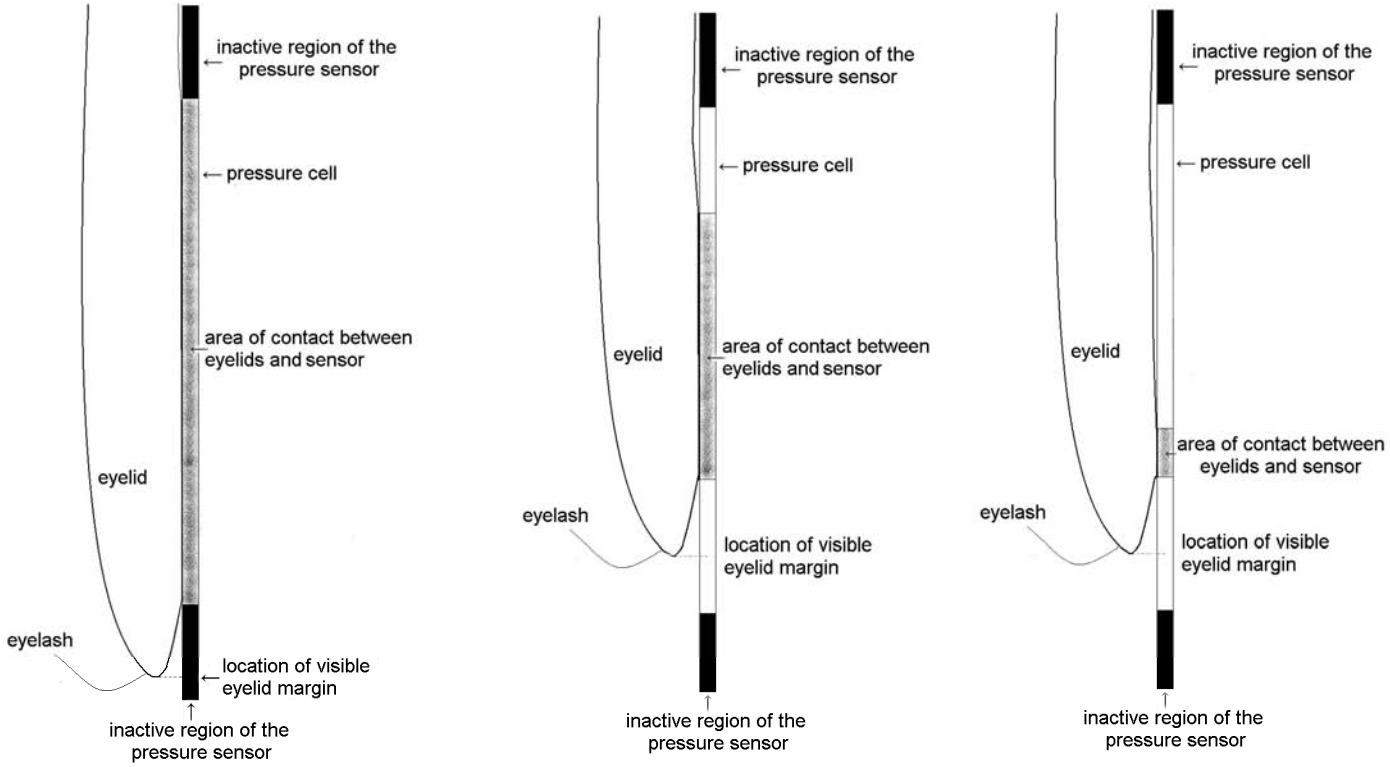

Figure 4-13: Possible models of eyelid contact with the pressure cell: A) the eyelid contacts the “whole cell”, B) contact is over the “imprint width” determined by Pressurex-micro imprint and C) contact over “Marx’s line” width determined by digital photography.

4.2.4.6 Eyelid and sensor contact width

We propose three possible models of contact between the eyelid and ocular surface and so three possible eyelid pressure models. If the eyelid contacts the ocular surface over a width more than or equal to 1.14 mm (pressure cell width), the calculated pressure from calibration is the "whole cell" eyelid pressure (Figure 4-13A). However if the width of primary contact between the eyelid and cornea is smaller than the pressure cell width (< 1.14 mm), then the calibrated pressure needs to be scaled according to the contact region. The sensor pressure measurements can be adjusted for contact area as the pressure cell acts as a force sensor with the output dependent on the total force applied, even if the cell is only partially loaded. The other two models are that the pressure acts over the width measured by the Pressurex-micro paper ("imprint width" eyelid pressure) (Figure 4-13B) or that the pressure acts over Marx's line width ("Marx's line" eyelid pressure) (Figure 4-13C). For example, assuming that the Pressurex-micro width imprint represents the contact between the cornea and the eyelid margin, this width of contact was applied to the "whole cell" eyelid pressure reading to calculate the "imprint width" eyelid pressure. *"Imprint width" eyelid pressure = "Whole cell" eyelid pressure * (1.14 / imprint width)* The standard deviation was calculated by propagating the errors associated with the "whole cell" eyelid pressure readings (EPwc) and imprint width measurements (IW). *Error = "Imprint width" eyelid pressure * √ ([error EPwc / EPwc] ² + [error IW / IW] ²)* The same process was used to calculate "Marx's line" eyelid pressure, using the width of Marx's line from digital photography as the assumed contact width.

4.2.4.7 Eyelid morphometry

A Canon 300D 6.3 megapixel Digital SLR camera with a 100 mm macro lens was used to obtain digital images of the eyelids in primary gaze and 20° downward eye gaze (approximately the range of possible gaze angles during eyelid pressure measurement). The same camera mounts as previously described in Chapter 2 were used (Shaw *et al.* 2008), with the camera set to AV mode (aperture specified as 10) and a ring light for extra illumination. The camera was manually focused and a scale included allowing calibration of the image during later analysis. The digital images for primary gaze and 20° downward gaze were

analysed using custom software with the limbus, pupil, and upper and lower eyelid contour being defined. A scale for calibration was included to allow for the calculation of the anterior eye parameters using Cartesian coordinates with the limbus centre used as the centre for the polynomial functions fitted to the eyelid shape. For the limbus and pupil outlines, 8 points were used for the ellipse functions fit to the outlines. For the upper and lower eyelid margin, a total of 9 points were selected which were then fit with a polynomial function $Y= AX^2 + BX + C$ (Malbouisson *et al.* 2000), with respect to the limbus centre. This method has been previously described with the terms describing different aspects of the eyelid morphology with A being the curvature, B the angle or tilt and C the distance from the geometric corneal centre (Read *et al.* 2006). The horizontal eyelid fissure is the distance between the nasal and temporal canthi and the palpebral aperture size was estimated by adding coefficient C for the upper and lower eyelids.

4.2.4.8 Association between variables

Marx's line width, the Pressurex-micro imprint width and the upper eyelid tilt and position in primary and 20° downward gaze were analysed using Pearson's product-moment correlation to investigate associations with eyelid pressure, along with any association between the imprint width and Marx's line width.

4.3 Results

Eyelid pressure was calculated based on the three models of contact between the sensor and eyelid: whole cell, imprint width and Marx's line. These pressure estimates along with the raw score values for each measurement can be seen in Table 4-2. The mean "whole cell" eyelid pressure was 3.8 ± 0.7 mmHg, ranging from 2.8 to 5.1 mmHg (Figure 4-14). The Pressurex-micro imprints showed a defined band of higher pressure between the eyelid and the ocular surface. The mean width of the contact imprints was 0.60 ± 0.16 mm with a range from 0.33 mm to 0.84 mm (Table 4-2 and Figure 4-15). When eyelid pressure was scaled for each subject using the contact imprint width, the mean "imprint width" eyelid

pressure for the 11 subjects was 8.0 ± 3.4 mmHg with a range from 4.4 to 14.4 mmHg (Figure 4-16 and Table 4-2). The mean Marx's line width was 0.09 ± 0.02 mm (Table 4-2). When the "whole cell" eyelid pressure was adjusted for Marx's line width for each subject, the mean "Marx's line" eyelid pressure was 55 ± 26 mmHg with a range from 32 to 115 mmHg (Figure 4-17 and Table 4-2).

Associations between eyelid pressure calculated using the three models and eyelid characteristics (position, shape and curvature, palpebral aperture and horizontal eyelid fissure) in primary gaze or 20° downward gaze were investigated. There were no significant correlations other than between "Marx's line" eyelid pressure with the position of the upper eyelid in 20° downward gaze ($R^2 = 0.37$, $p = 0.05$) (Table 4-3).

The "imprint width" eyelid pressure ranged from 4.4 to 14.4 mmHg which was larger than expected so two subjects with extreme measurements were repeated (Table 4-4), with comparable results for both the eyelid pressure and Pressurex-micro contact imprint width.

Table 4-2: Eyelid pressure using the three models: whole cell, imprint width and Marx's line. Raw scores are the values obtained from the pressure sensor prior to calibration. Imprint width was derived from the Pressurex-micro imprints and Marx's line width from digital images.

Subject number	*Raw scores*	*"Whole cell" eyelid pressure (mmHg)*	*Imprint width (mm)*	*"Imprint width" eyelid pressure (mmHg)*	*Marx's line width (mm)*	*"Marx's line" eyelid pressure (mmHg)*
1	41, 63, 40	3.21 ± 0.55	0.55 ± 0.20	6.6 ± 2.6	0.073	50 ± 8
2	81, 119, 91	5.07 ± 0.63	0.40 ± 0.05	14.4 ± 2.4	0.075	77 ± 19
3	41, 67	2.94 ± 0.58	0.74 ± 0.08	4.5 ± 1.0	0.089	38 ± 8
4	77, 58, 85	4.87 ± 0.55	0.62 ±0.05	9.0 ± 1.2	0.048	115 ± 25
5	35, 47, 51	3.41 ± 0.32	0.39 ± 0.05	9.9 ± 1.5	0.120	32 ± 5
6	70, 83, 38	3.85 ± 0.74	0.62 ±0.13	7.0 ± 2.0	0.094	46 ± 9
7	61, 41, 49	4.10 ± 0.35	0.65 ± 0.25	7.2 ± 2.8	0.083	56 ± 6
8	46, 47, 25	4.00 ± 0.80	0.33 ± 0.04	13.7 ± 3.2	0.090	50 ± 15
9	23, 34	2.81 ± 0.30	0.73 ± 0.01	4.4 ± 0.5	0.097	33 ± 5
10	36, 37, 37	3.52 ± 0.02	0.84 ± 0.23	4.8 ± 1.3	0.118	34 ± 5
11	63, 64, 38	4.39 ± 0.84	0.72 ± 0.10	7.0 ± 1.7	0.064	79 ± 19
Mean	-	3.8 ± 0.7	0.60 ± 0.16	8.0 ± 3.4	0.09 ± 0.02	55 ± 26

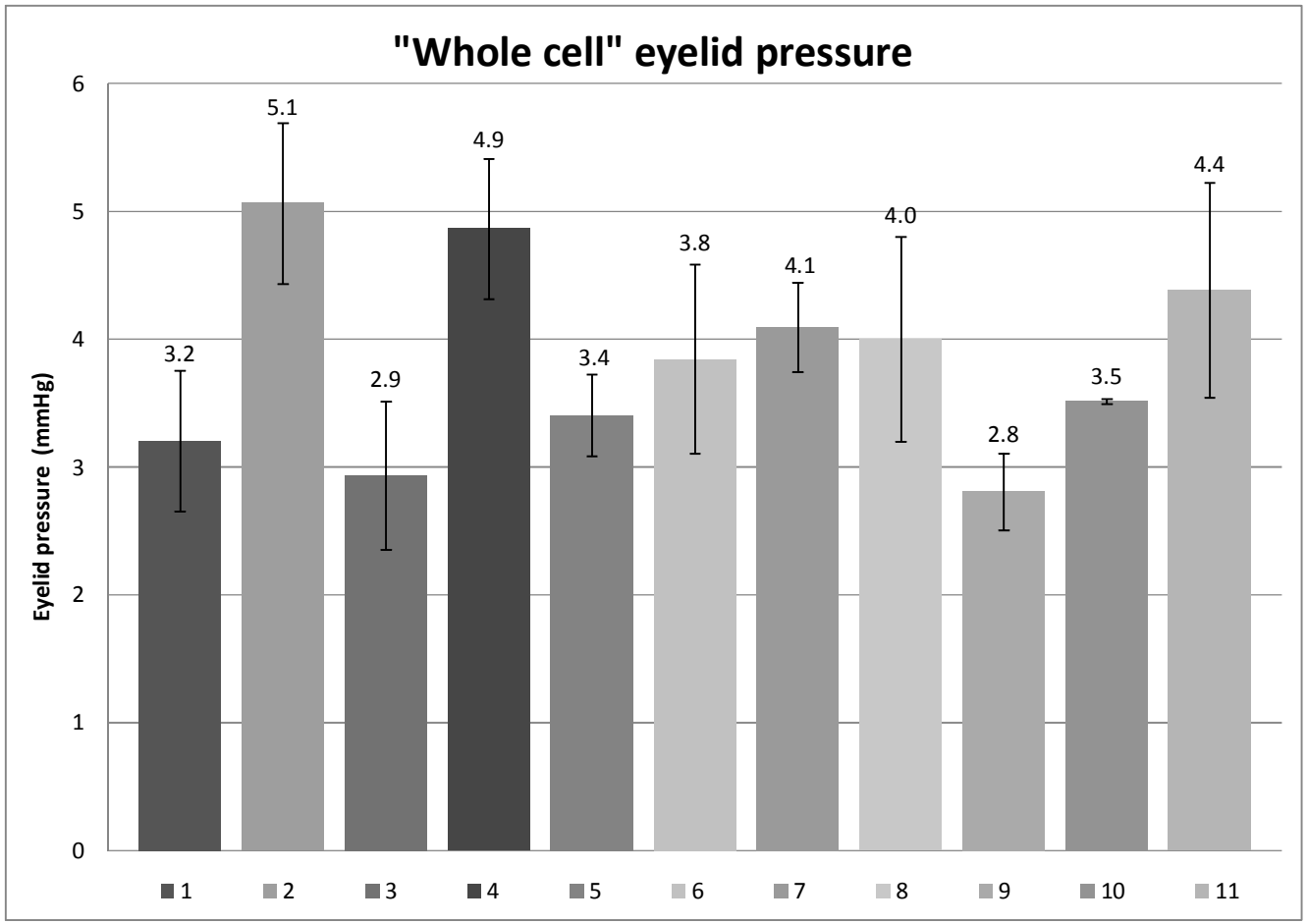

Figure 4-14: Mean eyelid pressure assuming the whole pressure cell was loaded for each of the 11 subjects. Error bars are ± 1 SD.

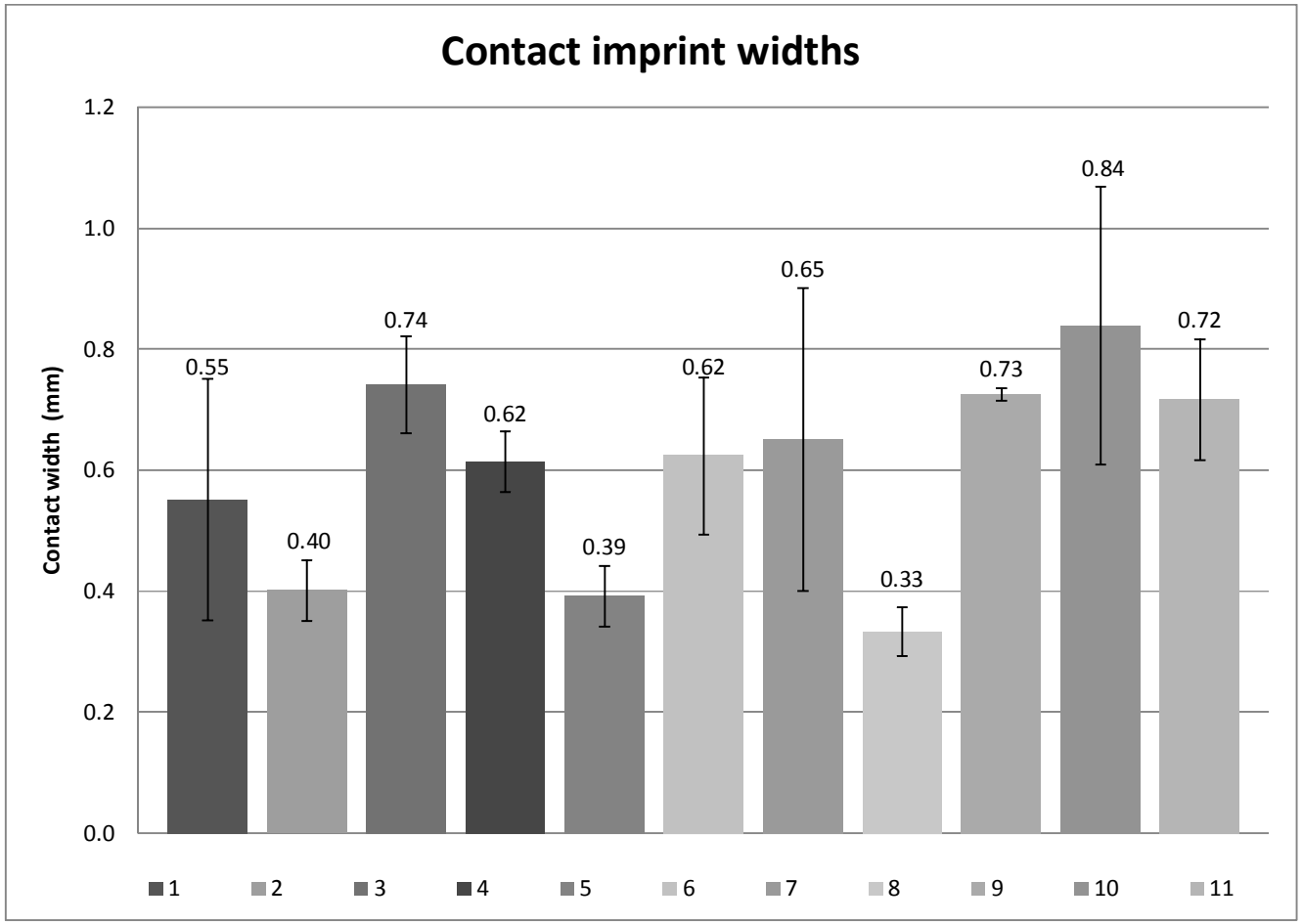

Figure 4-15: Mean contact imprint width for each subject from Pressurex-micro paper. Error bars are ± 1 SD.

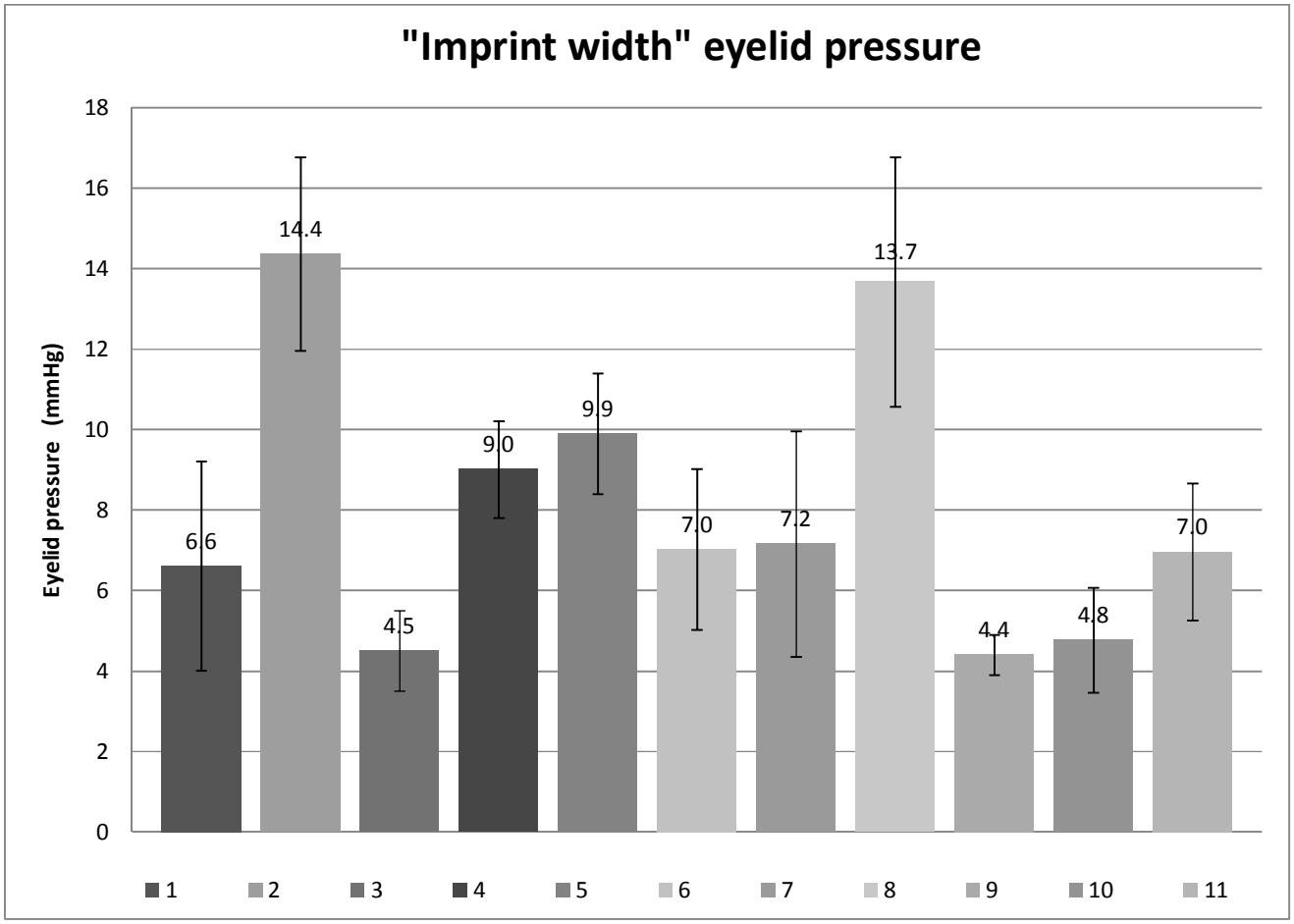

Figure 4-16: Mean “imprint width” eyelid pressure for each subject calculated using the Pressurex-micro imprints. Error bars are ± 1 SD.

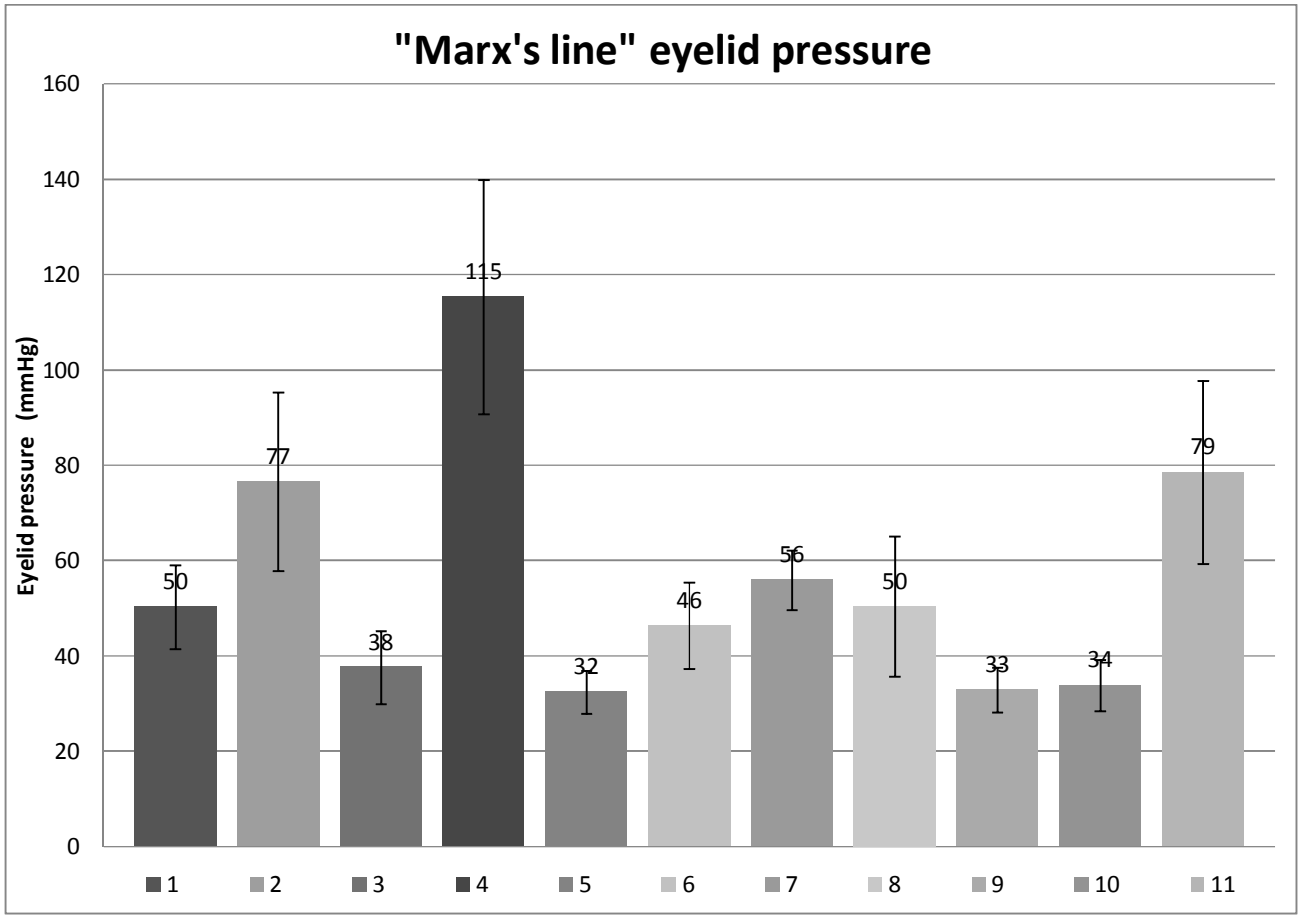

Figure 4-17: Mean eyelid pressure for each subject adjusted for Marx's line width contact with the pressure sensor. Error bars are ± 1 SD.

Table 4-3: R^2 values for Pearson's correlations between the three models of eyelid pressure and eyelid parameters in primary and 20° downward gaze (* = significant at $p<0.05$).

	Primary gaze					*20° downward gaze*				
	Eyelid Position, C	*Eyelid Tilt, B*	*Eyelid Curvature, A*	*Palpebral aperture*	*Horizontal eyelid fissure*	*Eyelid Position, C*	*Eyelid Tilt, B*	*Eyelid Curvature, A*	*Palpebral aperture*	*Horizontal eyelid fissure*
"Whole cell" eyelid pressure	0.07	0.06	0.04	0.16	0.03	0.26	0.00	0.17	0.01	0.11
"Imprint width" eyelid pressure	0.00	0.04	0.03	0.25	0.00	0.04	0.00	0.00	0.14	0.03
"Marx's line" eyelid pressure	0.02	0.09	0.12	0.02	0.00	(0.37)*	0.01	0.23	0.07	0.00

Table 4-4: Eyelid pressure and imprint width measurements repeated for subjects 2 and 3.

Subject number	*Raw scores*	*"Whole cell" eyelid pressure (mmHg)*	*Imprint width (mm)*	*"Imprint width" eyelid pressure (mmHg)*
2	81, 119, 91	5.07 ± 0.63	0.40 ± 0.05	14.4 ± 2.4
2 repeated	38, 40, 11	4.51 ± 0.65	0.38 ± 0.08	13.5 ± 3.4
3	41, 67	2.94 ± 0.58	0.74 ± 0.08	4.5 ± 1.0
3 repeated	13, 53, 24	2.77 ± 0.86	0.79 ± 0.16	4.0 ± 1.5

4.4 Discussion

Eyelid pressure was calculated using three models of contact between the eyelid and sensor: whole cell, imprint width and Marx's line. The mean eyelid pressure calculated using these three models for a group of young healthy subjects was 3.8 ± 0.7 mmHg (whole cell), 8.0 ± 3.4 mmHg (imprint width) and 55 ± 26 mmHg (Marx's line).

Some comparison can be made to previous eyelid pressure measurements, although this is limited by different techniques and measurement conditions. Miller (1967) used a manometer system to measure the pressure of a number of subjective blink conditions: light, gentle, deliberate and hard squeeze. The most comparable to static eyelid pressure was the light blink condition. The mean result for 10 subjects aged 17 to 35 years was 2.8 ± 2.2 mmHg of eyelid pressure. Lydon and Tait (1988) appeared to have an improved technique, however on the 9 subjects aged 20 to 35 years reported only that eyelid pressure was "small". Shikura *et al.* (1993) found that the average eyelid pressure during normal lid closure was 1.7 mmHg with a range from -0.50 to 6.7 mmHg (Shikura *et al.* 1993). These pressures are lower than the mean measured by all three models in this study. This is most likely due to the manometer systems used as it is doubtful that they measured localized pressure of the eyelid margin as the measurement were not made directly between the cornea and eyelid margin.

The influence of eyelid pressure measured indirectly is also useful. Measuring the intraorbital pressure in the retrobulbar space, Moller (1954) recorded for one subject that gentle eyelid closure altered pressure by 0.7 mmHg. The change in intraocular pressure by inserting a needle into the anterior chamber of an eye that was to be enucleated was 6 mmHg when the eyelids were closed (Coleman and Trokel 1969). While these two investigations measure the eyelid pressure transferred through ocular tissues and do not directly measure the pressure between the eyelids and the cornea, the measurements correspond to a similar range, as the "whole cell" and "imprint width" eyelid pressures.

There was a large range of eyelid pressure measurements between individuals, though from the repeatability of the measurements it is plausible that eyelid

pressure may vary by this amount. Previous investigations have also reported a large range between individuals with 2.8 ± 2.2 mmHg (Miller 1967) and a mean of 1.7 mmHg and a range from -0.50 to 6.7 mmHg (Shikura *et al.* 1993).

Quantitative measurement of the contact area between the eyelid and the cornea is extremely difficult as it cannot be directly visualized. Examination of several indirect measures gives some indication of the contact width. Marx's line is an anatomical feature present in nearly all individuals, with a mean width around 0.1 mm for the upper eyelid (Hughes *et al.* 2003; Shaw *et al.* 2009). It should be noted that this measurement is made with the eyelid everted which may alter the normal anatomical shape and width of this region compared to its normal shape when in contact with the ocular surface. However the width of Marx's line is an indication of the narrowest possible contact width (0.1 mm). In Chapter 2, the corneal imprint due to the eyelids was measured after steady fixation task. The mean width of the peak-to-peak depressions caused by the upper eyelid were 1.3 mm and 1.4 mm for the two steady fixation conditions at 20° and 40° downward gaze respectively. It can be assumed that to create the peak-valley-peak profile tissue would be distributed away from the depression, with the region of contact being smaller than the resultant peak-to-peak width. These two measurements create limits for the width of contact from 0.1 to 1.4 mm, from Marx's line width and peak-to-peak width respectively.

The contact imprint widths measured in this current study with the Pressurex-micro pressure sensitive paper provide the best estimate of the contact width between the upper eyelid and ocular surface. First it confirms that there is a band of pressure due to the eyelid margin. The mean width for the 11 subjects was 0.6 ± 0.2 mm, with a range from 0.33 to 0.84 mm. These values fall within the limits established by other measurements. Although there is some thickness of the contact lens and pressure sensitive paper between the eyelid and cornea (approximately 0.7 mm) during the measurement (which may slightly alter the relationship between the surfaces), the imprint directly relates to the eyelid pressure measurement which was taken at the same thickness. Pilot investigations found that the eyelid had to be in contact with the paper for a minimum of 10 seconds to record an imprint. By analysing the video, it was determined that there was some movement of the eyelid during the

measurement, on average about 0.17 mm. However it is not known how long the eyelid has to say in a fixed position to cause an imprint. It can be concluded that true area of contact between the eyelid margin and the surface of the paper may be slightly smaller than the measured group mean value of 0.60 mm, but probably not larger.

Further confirmation of the validity of these measurements is the calculation of eyelid pressure from eyelid tension. While tension does not necessarily directly relate to pressure, the calculation gives some insight into whether the eyelid pressure measurements seem reasonable. The eyelid tension measured by (Ehrmann *et al.* 2001) required to lift a stationary eyelid (calculated by (Jones *et al.* 2008)), is about 30 mN. This force acting over a width of 0.6 mm (mean contact imprint width) and an eyelid length of 30 mm equates to 12.5 mmHg of eyelid pressure, which is comparable to the mean “imprint width” eyelid pressure of this study. Therefore the eyelid force measured by Ehrmann *et al.* (2001) using an eyelid tensiometer is comparable to the eyelid force calculated from the eyelid pressure measurements in this study using piezoresistive pressure sensors.

Some improvements could be made to improve the reliability of the instrumentation. Custom designed pressure sensors would significantly improve the system. A sensor slightly smaller than the flat area on the contact lens would eliminate the need to cut and reseal the sensor, a procedure which often caused sensors to malfunction due to tear or alcohol swab fluid leaking into the sensor. A more sensitive sensor which was closer to eyelid pressure values would also be valuable. Higher resolution of the pressure cells within a sensor would also enable the spatial distribution of eyelid pressure to be more easily measured.

Further investigation of different subjects and factors could be studied using the eyelid pressure measurement system. This study measured only the upper eyelid pressure of young healthy subjects with no eyelid or anterior eye abnormalities and the eyelid pressure measurements were collected when the upper eyelid was in contact with the same region of the contact lens for every subject. Measurements could be made for particular angles of downward gaze to support the eyelid pressure inferences made from corneal topography changes in

Chapter 2. This would require the non-measurement eye to be kept open so that fixation could be maintained on targets at the specified angles. Eyelid-induced corneal changes also occur due to the lower eyelid. Several alterations to the sensor-contact lens combination and measurement apparatus would be required to measure lower eyelid pressure. These include either changing the angle of the support beam onto the contact lens so that the camera's view of the lower eyelid would not be blocked or altering the position of the videocamera.

It is possible that eyelid pressure may vary for different groups of subjects. An older age cohort (70+ years) could be considered as a decrease in upper eyelid tension with age has been reported (Vihlen and Wilson 1983) which may translate to a decrease in eyelid pressure on the cornea. Also there are anatomical variations in the eyelid between ethnic groups. While no difference has been found in eyelid tension between Asian and Caucasian subjects (Ehrmann *et al.* 2001), the measurement of eyelid pressure may elicit a difference. Eyelid pressure may also vary depending on corneal topography (particularly astigmatism), and with the presence of eyelid abnormalities such as chalazia, hemangiomas or ectropion.

It should be noted that measurements in this study were for a static eyelid and eyelid pressure could change during blinking. A previous study examining a number of blinking conditions found that eyelid pressure increased by a factor of eighteen times between light blinks and hard squeezes of the eyelids (Miller 1967). Further experimentation could confirm the dynamic nature of eyelid pressure during blinking. Particularly interesting would be investigation of pressure between opening and closing phases of blinking as mathematical modelling has suggested that for tears to flow from under the eyelid, tension during opening needs to be 1/10 of the eyelid tension during closing (Jones *et al.* 2008). Investigation of the dynamic nature of eyelid pressure requires dynamic calibration taking into account the loading and unloading response of the pressure sensor.

In summary, using the Pressurex-micro imprint width as the best estimate of the contact between the eyelid and the pressure sensor, the mean eyelid pressure of a group of young healthy subjects was 8.0 ± 3.4 mmHg. The Pressurex-micro

imprints confirm previous suggestions that a band of the eyelid margin is the primary contact with the ocular surface, with a mean width of 0.6 ± 0.2 mm. Although it is difficult to directly compare these results with previous eyelid pressure measurement attempts, the results of this study are slightly higher than previous manometer measurements but show good agreement with Ehrmann *et al.* (2001).

Chapter 5: Conclusions

5.1 Summary and main findings

5.1.1 Influence of the eyelids on the cornea

In the experiment described in Chapter 2, we found that significant corneal changes can occur after short periods (15 minutes) of near work. Previous investigations have also reported wave-like corneal distortions, but after tasks of one hour duration (Buehren *et al.* 2003; Collins *et al.* 2006). Similar to these previous studies, against-the-rule astigmatism was the predominant corneal change.

Considering that a corneal refractive change of 0.125 D could alter subjective refraction by 0.25 D, the influence of the eyelids was both optically and clinically significant after the 40° downward gaze tasks for the spherical and astigmatic components. For the 40° conditions, the mean corneal sphero-cylindrical change was around 0.25 D, with a maximum recorded change of +0.87 / -0.75 x 90. These magnitudes indicate that even short duration prior near tasks are potentially important when highly accurate corneal and refractive assessment is required.

There was some association between the corneal refractive change and eyelid morphometry. For the 40° tasks when the lower eyelid was in contact with the central 6 mm of the cornea, the J45 astigmatic change was correlated with the tilt of the lower eyelid. The significant influence of the lower eyelid on the cornea has been previously highlighted with an association between lower eyelid tilt and the axis of natural astigmatism (Read *et al.* 2007).

While the anatomical mechanism behind eyelid-induced corneal changes is unknown, various attributes of the changes can give some insight. The time course of eyelid-induced changes is very similar to the changes observed due to orthokeratology contact lenses. In both cases, corneal changes can occur very quickly (in a matter of minutes) (Sridharan and Swarbrick 2003; Shaw *et al.*

2008), increase with longer application of the pressure (Buehren *et al.* 2003; Soni *et al.* 2003; Shaw *et al.* 2009), there is initially fast recovery on removal of the pressure (Polse *et al.* 1983; Collins *et al.* 2005) and the corneal changes are fully reversible (Collins *et al.* 2005; Kobayashi *et al.* 2008). There has been substantial research into the corneal changes due to orthokeratology lenses with the most likely mechanism thought to involve epithelial compression and deformation (Choo *et al.* 2008). It seems likely that eyelid pressure may also predominantly affect the corneal epithelium.

Detailed analysis of the profile of the wave-like change (magnitude and width) for the 4 task conditions in the Chapter 2 experiment enabled several inferences to be made regarding eyelid pressure. The 25% increase in the depth of corneal change for the 40° downward gaze conditions compared to the 20° downward gaze conditions suggests that the upper eyelid exerts more pressure on the ocular surface when resting closer to the corneal centre (that is the "higher" apex of the cornea). In contrast, although the lower eyelid was further from the corneal centre compared to the upper eyelid for the 40° conditions, the depth of the corneal change was greater implying that for this downward gaze angle, the lower eyelid exerts more pressure than the upper eyelid despite its position on the cornea. There was a 3% (20° downward gaze) and 25% (40° downward gaze) increase in the depth of the corneal changes between reading and steady fixation tasks. This suggests that increased eye movements may increase the kinetic friction or pressure between the upper eyelid and ocular surface and influence the magnitude of the corneal change. It is also possible that variations in concentration or squinting during reading could alter the eyelid pressure on the cornea. The ability to directly measure the pressure between the eyelids and the ocular surface would allow a better understanding of the complex interaction between eyelid pressure and the ocular surface.

5.1.2 Development of an eyelid pressure measurement technique

Piezoresistive pressure sensors were chosen as a means to measure eyelid pressure since they are relatively thin, had good sensitivity at low pressure levels and have been widely used in other biomedical engineering applications. To

stabilise the sensor on the eye, they were attached to a custom contact lens with a support beam adhered to its centre. The sensor could then be mounted on a continuously flat surface from the support beam onto a filed flat area on the contact lens surface.

A hydrostatic calibration system was constructed so that the sensor could be calibrated after it had been attached to the contact lens. This system allowed low pressures (below 5 mmHg) to be applied to the sensor. It was demonstrated that "conditioning" is a vital step to increase the consistency of the sensor's response. For measurements of 7.8 mmHg, the model #4201 sensors should be conditioned with four applications of 25.9 mmHg for 1-minute each with 30 seconds break between loads. This should be completed no more than 60 minutes prior to every eyelid pressure measurement.

An understanding of the properties of piezoresistive sensors was attained through several investigations, allowing protocols for eyelid pressure measurement to be developed. Hysteresis of the sensor response was examined, and while it is significant for dynamic measurements it has little influence on static eyelid pressure measurements. The influence of temperature also appears to be minimal. Calibrating the sensor at room temperature (23°C) but measuring at ocular surface temperature (36°C) influenced the raw score values by an average of only 2.5%. Although it is unlikely that the sensor would heat to the ocular surface temperature as it is coated in Mylar polyester, a thermally resistive material. However "drift" (increase in sensor output over time with a static load), needs to be taken into account. The first 10 seconds of the signal after loading should be disregarded due to noisy output. Then the time and length of the recording should be matched between calibration and measurement, to minimise the influence of drift.

Lastly an *in vivo* measurement apparatus was constructed to safely and accurately place the sensor underneath the eyelid margin. Using this system it was determined that the contact lens needed to be placed on the eye with an even post-lens tear film and that for most consistent measurements the non-measurement eye should be occluded. Eyelid position on the sensor was found to be critical and so it was tracked using digital video recordings throughout

eyelid pressure recordings. Using these techniques, it was demonstrated that it is possible to measure eyelid pressure with the piezoresistive pressure sensors.

5.1.3 Contact between the eyelids and cornea

Previous work suggests that a band of the eyelid margin is likely to be the primary contact region between the upper eyelid and ocular surface (Kessing 1967; Korb *et al.* 2002; Doughty *et al.* 2004). The association between the upper eyelid Marx's line and the depth of the corneal changes in the Chapter 2 results suggests that this region of the eyelid is involved in contacting the ocular surface. The width of upper and lower eyelid Marx's line was measured for 18 young, healthy subjects, with mean widths of 0.11 ± 0.05 mm and 0.13 ± 0.10 mm respectively. This finding is similar to previous reports for the upper eyelid (Hughes *et al.* 2003), while it appears to be the first published width of the lower eyelid Marx's line (Shaw *et al.* 2009). The width of the upper eyelid Marx's line was also measured in the eyelid pressure measurement experiment (Chapter 4). A mean width of 0.09 ± 0.02 mm is comparable to the mean result from Chapter 2. The smaller standard deviation is likely to be due to the improved analysis procedure, using a polynomial fit rather than an average of five width samples.

New evidence for the region of the eyelid margin applying pressure to the ocular surface was obtained using Pressurex-micro carbon imprints in Chapter 4. The mean width for 11 subjects was 0.6 ± 0.2 mm with a range from 0.33 to 0.84 mm. Without being able to visualise the contact between the ocular surface and the eyelids, the Pressurex-micro imprints provide the best estimate of the contact width. These estimates are wider than the anatomical feature, Marx's line. Additional staining surrounding Marx's line has been observed with increased friction, for example in dry eye or silicone hydrogel contact lens wear (Korb *et al.* 2002; Korb *et al.* 2005; Varikooty *et al.* 2008). So it is likely that Marx's line is part of a wider region that serves as the primary contact between the eyelids and ocular surface. Jones *et al.* (2008) have suggested that the angle of the eyelid margin is likely to change during the down and up phase of blinking. So the region of contact between the upper eyelid and ocular surface may vary between static eyelid position and during blinking.

5.1.4 Upper eyelid pressure against the eye

Three models of eyelid pressure were proposed based on three possible contact regions between the eyelids and cornea. The “whole cell” model assumes that the contact is greater than a 1.14 mm width and the “Marx’s line” model assumes that this anatomical feature is solely responsible for pressure contact. However the Pressurex-micro imprint results provide the most direct method of estimating the width of contact between the eyelid and ocular surface. Thus the imprint model results of 8.0 ± 3.4 mmHg is the best estimate of mean static upper eyelid pressure on the ocular surface for young adult subjects (Figure 5-1).

There is agreement between the eyelid force measured using an eyelid tensiometer (as calculated by Jones *et al.* (2008) from the data of Ehrmann *et al.* (2001)) and the force calculated from eyelid pressure measurements of this study (Table 5-1). The previous eyelid pressure studies used entirely different instrumentation which did not measure the localised pressure of the eyelid margin. However taking this into consideration the results of 2.8 ± 2.2 mmHg (Miller 1967) and an eyelid pressure range of -0.50 to 6.7 mmHg (Shikura *et al.* 1993) show some agreement with our measurements. It also seems sensible that eyelid pressure should be less than intraocular pressure and considerably less than about 90 mmHg peak pressure required to flatten the cornea during non-contact tonometry (Kaneko *et al.* 2005).

Table 5-1: Upper eyelid force measured using an eyelid tensiometer (Ehrmann *et al.* (2001) as calculated by Jones *et al.* (2008)) and using the piezoresistive pressure sensor in this study. Eyelid pressure of 8 mmHg = 1.067 mN/mm². Contact area = 0.6 mm width x 30 mm eyelid length = 18 mm². Force = Pressure x Area = 1.067 mN/mm² x 18 mm² = 19.3 mN.

	Measurement	***Instrument***	***Upper eyelid force (mN)***
Ehrmann *et al.* (2001)	Eyelid tension	Eyelid tensiometer	~30
Shaw thesis (2009)	Eyelid pressure	Piezoresistive pressure sensor	19.3

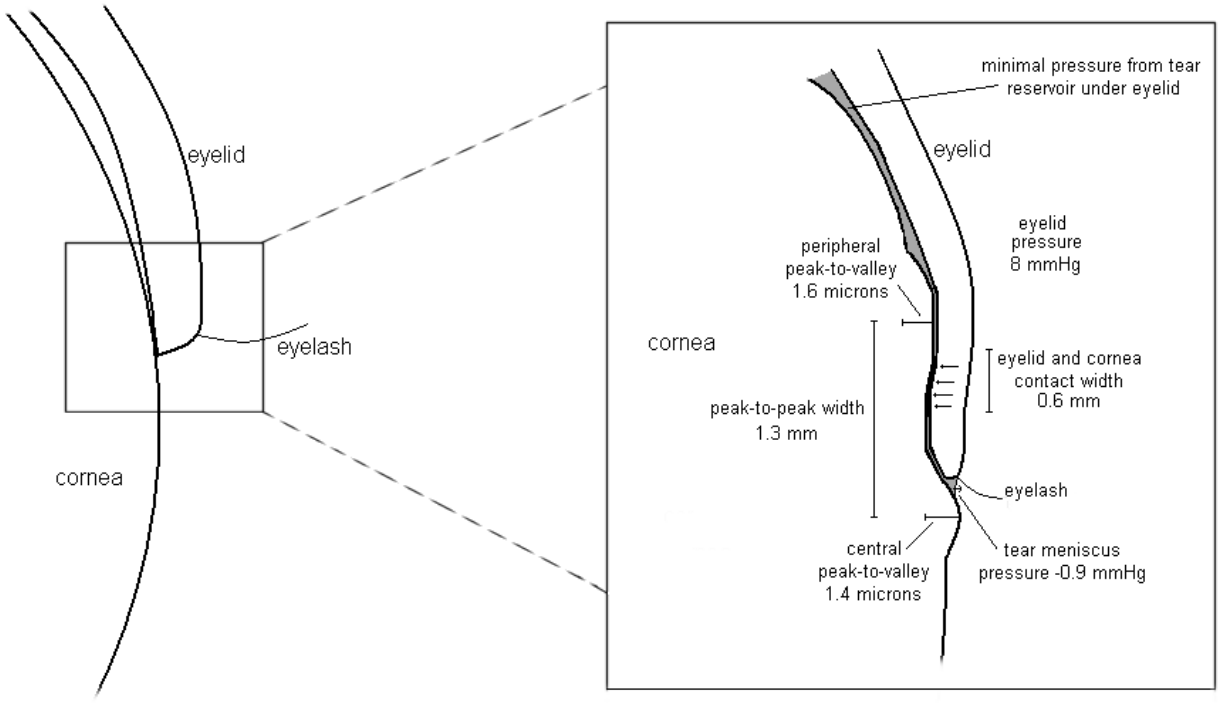

Figure 5-1: Schematic of the interaction between eyelid pressure and the cornea incorporating the results from this thesis: mean corneal changes for the upper eyelid 20° steady fixation condition, Pressurex-micro imprint width (0.6 mm), mean eyelid pressure of 8 mmHg, tear meniscus outward pressure -0.9 mmHg (Jones *et al.* 2008) and minimal pressure of the tear reservoir based on the limited pressure measured once the contact band of the eyelid had moved over the pressure cell.

5.2 Future research directions

The previous studies examining eyelid pressure have used limited numbers of subjects (Miller 1967; Lydon and Tait 1988; Shikura *et al.* 1993), presumably due to the difficult measurement techniques that were used. The development of an eyelid pressure measurement system that is relatively easy for both subject and examiner, leads to many potential applications of this system.

The combination of eyelid pressure measurements with other optometric measures would further knowledge in a number of areas. Obviously there are other factors besides eyelid pressure involved in the eyelid-induced corneal changes described in Chapter 2, particularly corneal biomechanics. Combining corneal topography, eyelid pressure and measures of corneal biomechanics (for example corneal hysteresis from the Ocular Response Analyser), may elicit the relative role of eyelid pressure in the corneal changes.

This work measured only the upper eyelid pressure for young, healthy subjects. Adaption of some elements of the instrumentation would allow eyelid pressure to be measured in other conditions. In particular measurement of eyelid pressure in different angles of downward gaze and for the lower eyelid would allow confirmation of eyelid pressure inferred from the corneal topography changes in Chapter 2. Also the eyelid pressure of different groups of subjects could be considered, for example in the presence of eyelid pathology such as chalazia or hemangiomas and for other age groups and ethnicities. A decrease in upper eyelid tension with age (Vihlen and Wilson 1983) may translate to a decrease in eyelid pressure on the cornea. While no difference has been found in eyelid tension between Asian and Caucasian subjects (Ehrmann *et al.* 2001), the measurement of eyelid pressure may elicit a difference.

During contact lens wear the eyelids have a critical role in influencing the movement, centration, and rotation of lenses on the eye (Waldron 1984). This is particularly important for toric contact lens design when lens stability is vital for clear vision. The eyelids have also been implicated in the adherence of contact lenses (Swarbrick and Holden 1996), the flexure of rigid lenses (Herman 1983) and the formation of superior arcuate epithelial lesions during contact lens wear

(Young and Mirejovsky 1993). It is also likely that eyelid pressure plays a role in the corneal changes due to orthokeratology lenses.

The occurrence of staining along the eyelid margin (lid-wiper epitheliopathy) for symptomatic dry eye patients has shown the potential effects of friction between the eyelids and ocular surface (Korb *et al.* 2002; Korb *et al.* 2005). Recently the severity of the staining has been found to be correlated with symptoms (Korb *et al.* 2002; Korb *et al.* 2005; Berry *et al.* 2008; Pult *et al.* 2008) and lid-wiper epitheliopathy may have a predictive role in better understanding dry eye. The lid-wiper is crucial in the distribution of the tear film and so eyelid pressure may be influential in the presence and severity of lid-wiper epitheliopathy.

5.3 Conclusion

The eyelids are a physical barrier for the eye and are instrumental in replenishing the tear film over the cornea to maintain a smooth optical surface. In this role the eyelids have close contact with the ocular surface, sweeping over it several hundred times every hour. We have shown that the pressure exerted by the eyelids can influence the regularity of the corneal surface and the eye's optics. We also developed novel methods to quantify the contact region and pressure distribution between the cornea and eyelids. The findings of this thesis are important for our understanding of the eyelids role in tear film distribution and the interaction between the eyelids and contact lenses on eye.

References

Adams, A. J. (1987). "Axial length elongation, not corneal curvature, as a basis of adult onset myopia." American Journal of Optometry and Physiological Optics **64**(2): 150-152.

Ahearne, M., Yang, Y., Then, K. Y. *et al.* (2007). "An indentation technique to characterize the mechanical and viscoelastic properties of human and porcine corneas." Annals of Biomedical Engineering **35**(9): 1608-1616.

Albietz, J. M., Lenton, L. M. and McLennan, S. G. (2005). "Dry eye after LASIK: comparison of outcomes for Asian and Caucasian eyes." Clinical & Experimental Optometry: Journal Of The Australian Optometrical Association **88**(2): 89-96.

Alharbi, A. and Swarbrick, H. A. (2003). "The effects of overnight orthokeratology lens wear on corneal thickness." Investigative Ophthalmology and Visual Science **44**(6): 2518-2523.

Anderson, R. L. and Baumgartner, S. A. (1980). "Amblyopia in ptosis." Archives of Ophthalmology **98**(6): 1068-1069.

Andreassen, T. T., Simonsen, A. H. and Oxlund, H. (1980). "Biomechanical properties of keratoconus and normal corneas." Experimental Eye Research **31**(4): 435-441.

Artal, P., Guirao, A., Berrio, E. *et al.* (2001). "Compensation of corneal aberrations by the internal optics in the human eye." Journal of Vision **1**(1): 1-8.

Atchison, D. A. and Smith, G. (2000). Optics of the Human Eye. Oxford, Butterworth-Heinemann.

Augsburger, A. and Polasky, M. (1976). "Effects of non-contact tonometry on refraction." American Journal of Optometry and Physiological Optics **53**(12): 761-763.

Avni-Zauberman, N., Rosen, N. and Ben Simon, G. J. (2008). "Induced corneal astigmatism by palpebral spring for the treatment of lagophthalmos." Cornea **27**(7): 840-842.

Bagheri, A., Farahi, A. and Guyton, D. L. (2003). "Astigmatism induced by simultaneous recession of both horizontal rectus muscles." Journal of AAPOS **7**(1): 42-46.

Bawazeer, A. M., Hodge, W. G. and Lorimer, B. (2000). "Atopy and keratoconus: a multivariate analysis." The British Journal of Ophthalmology **84**(8): 834-836.

Beckingsale, P. S., Sullivan, T. J., Wong, V. A. *et al.* (2003). "Blepharophimosis: a recommendation for early surgery in patients with severe ptosis." Clinical and Experimental Ophthalmology **31**(2): 138-142.

Belin, M. W. and Ratliff, C. D. (1996). "Evaluating data acquisition and smoothing functions of currently available videokeratoscopes." Journal of Cataract and Refractive Surgery **22**(4): 421-426.

Bergmanson, J. P. G., Horne, J., Doughty, M. J. *et al.* (2005). "Assessment of the number of lamellae in the central region of the normal human corneal stroma at the resolution of the transmission electron microscope." Eye and Contact Lens **31**(6): 281-287.

Berry, M., Pult, H., Purslow, C. *et al.* (2008). "Mucins and ocular signs in symptomatic and asymptomatic contact lens wear." Optometry and Vision Science **85**(10): 930-938.

Bogan, S., Simon, J. W., Krohel, G. B. *et al.* (1987). "Astigmatism associated with adnexal masses in infancy." Archives Of Ophthalmology **105**(10): 1368-1370.

Bogan, S. J., Waring, G. O., 3rd, Ibrahim, O. *et al.* (1990). "Classification of normal corneal topography based on computer-assisted videokeratography." Archives of Ophthalmology **108**(7): 945-949.

Boote, C., Dennis, S., Huang, Y. *et al.* (2005). "Lamellar orientation in human cornea in relation to mechanical properties." Journal of Structural Biology **149**(1): 1-6.

Bowman, K. J. and Carney, L. G. (1978). "The effect of non-contact tonometry on corneal topography." Journal of the American Optometric Association. **49**(12): 1389-1390.

Bowman, K. J., Smith, G. and Carney, L. G. (1978). "Corneal topography and monocular diplopia following near work." American Journal of Optometry and Physiological Optics **55**(12): 818-823.

Brimacombe, J. M., Anglin, C., Hodgson, A. J. *et al.* (2005). Validation of calibration techniques for Tekscan pressure sensors. ISB XXth Congress, ASB 29th Annual Meeting, Cleveland, OH.

Bron, A. J., Tripathi, R. C. and Tripathi, B. J. (1997). Wolff's Anatomy of the Eye and Orbit. New York, Oxford University Press Inc.

Brown, M. S., Siegel, I. M. and Lisman, R. D. (1999). "Prospective analysis of changes in corneal topography after upper eyelid surgery." Ophthalmic Plastic and Reconstructive Surgery **15**(6): 378-383.

Bucci, F. A., Jr, Evans, R. E., Moody, K. J. *et al.* (1997). "The annular tinted contact lens syndrome: corneal topographic analysis of ring-shaped irregular astigmatism caused by annular tinted contact lenses." The CLAO Journal **23**(3): 161-167.

Budak, K., Khater, T. T., Friedman, N. J. *et al.* (1999). "Evaluation of relationships among refractive and topographic parameters." Journal of Cataract and Refractive Surgery **25**(6): 814-820.

Buehren, T., Collins, M. J. and Carney, L. (2003). "Corneal aberrations and reading." Optometry and Vision Science **80**(2): 159-166.

Buehren, T., Collins, M. J. and Carney, L. G. (2005). "Near work induced wavefront aberrations in myopia." Vision research. **45**(10): 1297-1312.

Buehren, T., Collins, M. J., Iskander, D. R. *et al.* (2001). "The stability of corneal topography in the post-blink interval." Cornea **20**(8): 826-833.

Buehren, T., Collins, M. J., Loughridge, J. *et al.* (2003). "Corneal topography and accommodation." Cornea **22**(4): 311-316.

Buehren, T., Lee, B. J., Collins, M. J. *et al.* (2002). "Ocular microfluctuations and videokeratoscopy." Cornea **21**(4): 346-351.

Buis, A. W. P. and Convery, P. (1997). "Calibration problems encountered while monitoring stump/socket interface pressures with force sensing resistors: techniques adopted to minimise inaccuracies." Prosthetics and Orthotics International **21**: 179-182.

Buzard, K. A. (1992). "Biomechanics of the cornea--who needs it?" Refractive & Corneal Surgery **8**(2): 125-126.

Cadera, W., Orton, R. B. and Hakim, O. (1992). "Changes in astigmatism after surgery for congenital ptosis." Journal of Pediatric Ophthalmology and Strabismus **29**(2): 85-88.

Cairns, G., McGhee, C. N. J., Collins, M. J. *et al.* (2002). "Accuracy of Orbscan II slit-scanning elevation topography." Journal of Cataract and Refractive Surgery **28**(12): 2181-2187.

Campbell, C. (1998). "Corneal aberrations, monocular diplopia, and ghost images: analysis using corneal topographical data." Optometry and Vision Science **75**(3): 197-207.

Carney, L. G. and Bailey, I. L. (1972). "Hydrophilic contact lenses - their effect on the cornea." The Australian Journal of Optometry: 162-163.

Carney, L. G. and Clark, B. A. (1972). "Experimental deformation of the in vivo cornea." American Journal of Optometry and Archives of American Academy of Optometry **49**(1): 28-34.

Carney, L. G., Liubinas, J. and Bowman, K. J. (1981). "The role of corneal distortion in the occurrence of monocular diplopia." Acta Ophthalmologica **59**(2): 271-274.

Carney, L. G., Mainstone, J. C. and Henderson, B. A. (1997). "Corneal topography and myopia. A cross-sectional study." Investigative Ophthalmology and Visual Science **38**(2): 311-320.

Cartwright, M. J., Kurumety, U. R., Nelson, C. C. *et al.* (1994). "Measurements of upper eyelid and eyebrow dimensions in healthy white individuals." American Journal of Ophthalmology **117**(2): 231-234.

Carvalho, L. A. (2005). "Preliminary results of neural networks and zernike polynomials for classification of videokeratography maps." Optometry and Vision Science **82**(2): 151-158.

Chalita, M. R., Xu, M. and Krueger, R. R. (2003). "Correlation of aberrations with visual symptoms using wavefront analysis in eyes after laser in situ keratomileusis." Journal of Refractive Surgery **19**(6): S682-686.

Chang, S. W., Tsai, I. L., Hu, F. R. *et al.* (2001). "The cornea in young myopic adults." The British Journal of Ophthalmology **85**(8): 916-920.

Cheah, P., Norhani, M., Bariah, M. *et al.* (2008). "Histomorphometric profile of the corneal response to short-term reverse-geometry orthokeratology lens wear in primate corneas: a pilot study." Cornea **27**(4): 461-470.

Cheung, S. W., Cho, P. and Douthwaite, W. (2000). "Corneal shape of Hong Kong-Chinese." Ophthalmic and Physiological Optics **20**(2): 119-125.

Cho, P., Lam, A. K. C., Mountford, J. *et al.* (2002). "The performance of four different corneal topographers on normal human corneas and its impact on orthokeratology lens fitting." Optometry and Vision Science **79**(3): 175-183.

Cho, P., Sheng, C., Chan, C. *et al.* (2000). "Baseline blink rates and the effect of visual task difficulty and position of gaze." Current Eye Research **20**(1): 64-70.

Choo, J., Caroline, P., Harlin, D. *et al.* (2004). "Morphological change in cat epithelium following overnight lens wear with the Paragon CRT lens for corneal reshaping." Investigative Ophthalmology and Visual Science (Suppl). **45**(E-abstract): 1552.

Choo, J. D., Caroline, P. J., Harlin, D. *et al.* (2008). "Morphological changes in cat epithelium following continuous wear of orthokeratology lenses: a pilot study." Contact Lens and Anterior Eye **31**(1): 29-37.

Clark, B. (1973). "Variations in corneal topography." The Australian Journal of Optometry: 400-410.

Coleman, D. J. and Trokel, S. (1969). "Direct-recorded intraocular pressure variations in a human subject." Archives of Ophthalmology **82**(5): 637-640.

Collins, M. J. and Bruce, A. S. (1993). "Soft contact lenses and corneal topography." International Contact Lens Clinics **20**(Sept/Oct): 187-190.

Collins, M. J., Buehren, T., Bece, A. *et al.* (2006). "Corneal optics after reading, microscopy and computer work." Acta Ophthalmologica **84**(2): 216-224.

Collins, M. J., Buehren, T., Trevor, T. *et al.* (2006). "Factors influencing lid pressure on the cornea." Eye and Contact Lens **32**(4): 168-173.

Collins, M. J., Kloevekorn-Norgall, K., Buehren, T. *et al.* (2005). "Regression of lid-induced corneal topography changes after reading." Optometry and Vision Science **82**(9): 843-849.

Collins, M. J., Smythe, W., Seawright, J. *et al.* (1992). "The synkinesis between antero-posterior eye position and lid fissure width." Clinical and Experimental Optometry **75**(2): 38-41.

Corzine, J. C. and Klein, S. A. (1997). "Factors determining rigid contact lens flexure." Optometry and Vision Science **74**(8): 639-645.

Cosar, C. B., Rapuano, C. J., Cohen, E. J. *et al.* (2001). "Chalazion as a cause of decreased vision after LASIK." Cornea **20**(8): 890-892.

Courville, C. B., Smolek, M. K. and Klyce, S. D. (2004). "Contribution of the ocular surface to visual optics." Experimental Eye Research **78**(3): 417-425.

Cronje, S. and Harris, W. F. (1997). "Short-term keratometric variation in the human eye." Optometry and Vision Science **74**(6): 420-424.

da Cunha, R. P. and Moreira, J. B. (1996). "Ocular findings in Down's syndrome." American Journal of Ophthalmology **122**(2): 236-244.

Davson, H. (1972). The Protective Mechanisms. Edinburgh, Churchill Livingstone.

Daxer, A. and Fratzl, P. (1997). "Collagen fibril orientation in the human corneal stroma and its implication in keratoconus." Investigative Ophthalmology and Visual Science **38**(1): 121-129.

Daxer, A., Misof, K., Grabner, B. *et al.* (1998). "Collagen fibrils in the human corneal stroma: structure and aging." Investigative Ophthalmology and Visual Science **39**(3): 644-648.

Denis, D., Bardot, J., Volot, F. *et al.* (1995). "Effects of strabismus surgery on refraction in children." Ophthalmologica. International Journal Of Ophthalmology. **209**(3): 136-140.

Detorakis, E. T., Ioannakis, K. and Kozobolis, V. P. (2005). "Corneal topography in involutional ectropion of the lower eyelid: preoperative and postoperative evaluation." Cornea **24**(4): 431-434.

Dingeldein, S. A. and Klyce, S. D. (1989). "The topography of normal corneas." Archives of Ophthalmology **107**(4): 512-518.

Doane, M. G. (1980). "Interaction of eyelids and tears in corneal wetting and the dynamics of the normal human eyeblink." American Journal of Ophthalmology **89**(4): 507-516.

Doughty, M. J. (2001). "Consideration of three types of spontaneous eyeblink activity in normal humans: during reading and video display terminal use, in primary gaze, and while in conversation." Optometry and Vision Science **78**(10): 712-725.

Doughty, M. J., Naase, T., Donald, C. *et al.* (2004). "Visualisation of "Marx's line" along the marginal eyelid conjunctiva of human subjects with lissamine green dye." Ophthalmic and Physiological Optics **24**(1): 1-7.

Doughty, M. J. and Panju, Z. (1995). "Exploring the hidden surface of the underside of the eyelid." Contact Lens Spectrum: 19-30.

Douthwaite, W. A. (2003). "The asphericity, curvature and tilt of the human cornea measured using a videokeratoscope." Ophthalmic and Physiological Optics **23**(2): 141-150.

Douthwaite, W. A., Hough, T., Edwards, K. *et al.* (1999). "The EyeSys videokeratoscopic assessment of apical radius and p-value in the normal human cornea." Ophthalmic and Physiological Optics **19**(6): 467-474.

Douthwaite, W. A. and Pardhan, S. (1998). "Surface tilt measured with the EyeSys videokeratoscope: influence on corneal asymmetry." Investigative Ophthalmology and Visual Science **39**(9): 1727-1735.

Doxanas, M. T. and Anderson, R. L. (1984). "Oriental eyelids. An anatomic study." Archives of Ophthalmology **102**(8): 1232-1235.

Doyle, S. J., Bullock, J., Gray, C. *et al.* (1998). "Emmetropisation, axial length, and corneal topography in teenagers with Down's syndrome." The British Journal of Ophthalmology **82**(7): 793-796.

du Toit, R., Vega, J. A., Fonn, D. *et al.* (2003). "Diurnal variation of corneal sensitivity and thickness." Cornea **22**(3): 205-209.

Duan, X. and Sheardown, H. (2006). "Dendrimer crosslinked collagen as a corneal tissue engineering scaffold: mechanical properties and corneal epithelial cell interactions." Biomaterials **27**(26): 4608-4617.

Dubbelman, M., Sicam, V. A. D. P. and Van der Heijde, G. L. (2006). "The shape of the anterior and posterior surface of the aging human cornea." Vision Research **46**(6-7): 993-1001.

Edmund, C. (1988). "Corneal elasticity and ocular rigidity in normal and keratoconic eyes." Acta Ophthalmologica **66**(2): 134-140.

Eghbali, F., Yeung, K. K. and Maloney, R. K. (1995). "Topographic determination of corneal asphericity and its lack of effect on the refractive outcome of radial keratotomy." American Journal of Ophthalmology **119**(3): 275-280.

Ehrmann, K., Francis, I. and Stapleton, F. (2001). "A novel instrument to quantify the tension of upper and lower eyelids." Contact Lens and Anterior Eye **24**: 65-72.

Elsheikh, A., Alhasso, D. and Rama, P. (2008). "Assessment of the epithelium's contribution to corneal biomechanics." Experimental Eye Research **86**(2): 445-451.

Elsheikh, A., Wang, D., Brown, M. *et al.* (2007). "Assessment of corneal biomechanical properties and their variation with age." Current Eye Research **32**(1): 11-19.

Erdélyi, B., Csákány, B. and Németh, J. (2005). "Spontaneous alterations of the corneal topographic pattern." Journal of Cataract and Refractive Surgery **31**(5): 973-978.

Evinger, C., Manning, K. A. and Sibony, P. A. (1991). "Eyelid movements. Mechanisms and normal data." Investigative Ophthalmology and Visual Science **32**(2): 387-400.

Evinger, C., Shaw, M. D., Peck, C. K. *et al.* (1984). "Blinking and associated eye movements in humans, guinea pigs, and rabbits." Journal of Neurophysiology **52**(2): 323-339.

Fairmaid, J. (1959). "The constancy of corneal curvature; an examination of corneal response to changes in accommodation and convergence." The British Journal of Physiological Optics **16**(1): 2-23.

Feng, Y., Varikooty, J. and Simpson, T. L. (2001). "Diurnal variation of corneal and corneal epithelial thickness measured using optical coherence tomography." Cornea. **20**(5): 480-483.

Ferguson-Pell, M., Hagisawa, S. and Bain, D. (2000). "Evaluation of a sensor for low interface pressure applications." Medical Engineering and Physics **22**(9): 657-663.

Fledelius, H. C. and Stubgaard, M. (1986). "Changes in refraction and corneal curvature during growth and adult life. A cross-sectional study." Acta Ophthalmologica **64**(5): 487-491.

Ford, J. G., Davis, R. M., Reed, J. W. *et al.* (1997). "Bilateral monocular diplopia associated with lid position during near work." Cornea **16**(5): 525-530.

Francis, B. A., Hsieh, A., Lai, M.-Y. *et al.* (2007). "Effects of corneal thickness, corneal curvature, and intraocular pressure level on Goldmann applanation tonometry and dynamic contour tonometry." Ophthalmology **114**(1): 20-26.

Francis, I. C., Stapleton, F., Ehrmann, K. *et al.* (2006). "Lower eyelid tensometry in younger and older normal subjects." Eye **20**(2): 166-172.

Franklin, R. J., Morelande, M. R., Iskander, D. R. *et al.* (2006). "Combining central and peripheral videokeratoscope maps to investigate total corneal topography." Eye and Contact Lens **32**(1): 27-32.

Friling, R., Weinberger, D., Kremer, I. *et al.* (2004). "Keratometry measurements in preterm and full term newborn infants." The British Journal of Ophthalmology **88**(1): 8-10.

Garcia, M. L., Huang, D., Crowe, S. *et al.* (2003). "Relationship between the axis and degree of high astigmatism and obliquity of palpebral fissure." Journal of AAPOS **7**(1): 14-22.

Goldhahn, A., Schrom, T., Berghaus, A. *et al.* (1999). "Corneal astigmatism as a special complication after lid-loading in patients with lagophthalmos." Ophthalmologe **96**(8): 494-497.

Golnik, K. C. and Eggenberger, E. (2001). "Symptomatic corneal topographic change induced by reading in downgaze." Journal of Neuro-ophthalmology **21**(3): 199-204.

González-Meijome, J. M., González-Pérez, J., Cerviño, A. *et al.* (2003). "Changes in corneal structure with continuous wear of high-Dk soft contact lenses: a pilot study." Optometry and Vision Science **80**(6): 440-446.

Goss, D. A. and Criswell, M. H. (1992). "Bilateral monocular polyopia following television viewing." Clinical Eye Vision Care **4**(1): 28-32.

Goss, D. A. and Erickson, P. (1987). "Meridional corneal components of myopia progression in young adults and children." American Journal of Optometry and Physiological Optics **64**(7): 475-481.

Goss, D. A. and Jackson, T. W. (1995). "Clinical findings before the onset of myopia in youth. I. Ocular optical components." Optometry and Vision Science **72**(12): 870-878.

Goss, D. A., Van Veen, H. G., Rainey, B. B. *et al.* (1997). "Ocular components measured by keratometry, phakometry, and ultrasonography in emmetropic and myopic optometry students." Optometry and Vision Science **74**(7): 489-495.

Goto, T., Klyce, S. D., Zheng, X. *et al.* (2001). "Gender- and age-related differences in corneal topography." Cornea **20**(3): 270-276.

Greenberg, M. H. and Hill, R. M. (1973). "The physiology of contact lens imprints." American Journal of Optometry and Archives of American Academy of Optometry **50**(9): 699-702.

Grey, C. and Yap, M. (1986). "Influence of lid position on astigmatism." American Journal of Optometry and Physiological Optics **63**(12): 966-969.

Grosvenor, T. and Goss, D. A. (1998). "Role of the cornea in emmetropia and myopia." Optometry and Vision Science **75**(2): 132-145.

Grosvenor, T. and Scott, R. (1993). "Three-year changes in refraction and its components in youth-onset and early adult-onset myopia." Optometry and Vision Science **70**(8): 677-683.

Grosvenor, T. and Scott, R. (1994). "Role of the axial length/corneal radius ratio in determining the refractive state of the eye." Optometry and Vision Science **71**(9): 573-579.

Gudmundsdottir, E., Jonasson, F., Jonsson, V. *et al.* (2000). "'With the rule' astigmatism is not the rule in the elderly. Reykjavik Eye Study: a population based study of refraction and visual acuity in citizens of Reykjavik 50 years and older." Acta Ophthalmologica **78**(6): 642-646.

Guillon, M., Lydon, D. P. and Wilson, C. (1986). "Corneal topography: a clinical model." Ophthalmic and Physiological Optics **6**(1): 47-56.

Guirao, A. and Artal, P. (2000). "Corneal wave aberration from videokeratography: accuracy and limitations of the procedure." Journal of the Optical Society of America **17**(6): 955-965.

Guirao, A., Redondo, M. and Artal, P. (2000). "Optical aberrations of the human cornea as a function of age." Journal of the Optical Society of America **17**(10): 1697-1702.

Hachisuka, K., Takahashi, M., Ogata, H. *et al.* (1998). "Properties of the flexible pressure sensor under laboratory conditions simulating the internal environment of the total surface bearing socket." Prosthetics and Orthotics International **22**(3): 186-192.

Han, W., Kwan, W., Wang, J. *et al.* (2007). "Influence of eyelid position on wavefront aberrations." Ophthalmic and Physiological Optics **27**(1): 66-75.

Handa, T., Mukuno, K., Niida, T. *et al.* (2002). "Diurnal variation of human corneal curvature in young adults." Journal of Refractive Surgery **18**(1): 58-62.

Haque, S., Fonn, D., Simpson, T. *et al.* (2004). "Corneal and epithelial thickness changes after 4 weeks of overnight corneal refractive therapy lens wear, measured with optical coherence tomography." Eye and Contact Lens **30**(4): 189.

Harper, C. L., Boulton, M. E., Bennett, D. *et al.* (1996). "Diurnal variations in human corneal thickness." The British Journal of Ophthalmology **80**(12): 1068-1072.

Harris, M. G. and Chu, C. S. (1972). "The effect of contact lens thickness and corneal toricity on flexure and residual astigmatism." American Journal of Optometry and Archives of American Academy of Optometry **49**(4): 304-307.

Harris, M. G., Sarver, M. D. and Polse, K. A. (1975). "Corneal curvature and refractive error changes associated with wearing hydrogel contact lenses." American Journal of Optometry and Physiological Optics **52**(5): 313-319.

Harris, W. F. (2000). "Astigmatism." Ophthalmic and Physiological Optics **20**(1): 11-30.

Hartstein, J. (1965). "Corneal warping due to wearing of corneal contact lenses. A report of 12 cases." American Journal of Ophthalmology **60**(6): 1103-1104.

Hashemi, H., Firoozabadi, M. R., Mehravaran, S. *et al.* (2008). "Corneal stability after discontinued soft contact lens wear." Contact Lens and Anterior Eye **31**(3): 122-125.

Hashemi, H. and Mehravaran, S. (2007). "Corneal changes after laser refractive surgery for myopia: comparison of Orbscan II and Pentacam findings." Journal of Cataract and Refractive Surgery **33**(5): 841-847.

Haugen, O. H., Høvding, G. and Eide, G. E. (2001). "Biometric measurements of the eyes in teenagers and young adults with Down syndrome." Acta Ophthalmologica **79**(6): 616-625.

He, J. C., Gwiazda, J., Thorn, F. *et al.* (2003). "Change in corneal shape and corneal wave-front aberrations with accommodation." Journal of Vision **3**(7): 456-463.

Herman, J. P. (1983). "Flexure of rigid contact lenses on toric corneas as a function of base curve fitting relationship." Journal of the American Optometric Association. **54**(3): 209-213.

Hersh, P. S., Steinert, R. F. and Brint, S. F. (2000). "Photorefractive keratectomy versus laser in situ keratomileusis: comparison of optical side effects. Summit PRK-LASIK Study Group." Ophthalmology **107**(5): 925-933.

Hill, S. E., Han, H. and Thorn, F. (2005). "Visual posture and focus during recreational and study reading." Investigative Ophthalmology and Visual Science (Suppl) **46**(E-Abstract): 5598.

Hjortdal, J. O. (1995). "Extensibility of the normo-hydrated human cornea." Acta Ophthalmologica **73**(1): 12-17.

Hjortdal, J. O. (1996). "Regional elastic performance of the human cornea." Journal of Biomechanics. **29**(7): 931-942.

Hjortdal, J. O., Erdmann, L. and Bek, T. (1995). "Fourier analysis of video-keratographic data. A tool for separation of spherical, regular astigmatic and irregular astigmatic corneal power components." Ophthalmic and Physiological Optics **15**(3): 171-185.

Holck, D. E., Dutton, J. J. and Wehrly, S. R. (1998). "Changes in astigmatism after ptosis surgery measured by corneal topography." Ophthalmic Plastic and Reconstructive Surgery. **14**(3): 151-158.

Holden, B. A., Mertz, G. W. and McNally, J. J. (1983). "Corneal swelling response to contact lenses worn under extended wear conditions." Investigative Ophthalmology and Visual Science **24**(2): 218-226.

Holden, B. A. and Sweeney, D. F. (1985). "The oxygen tension and temperature of the superior palpebral conjunctiva." Acta Ophthalmologica **63**(1): 100-103.

Holden, B. A., Sweeney, D. F. and Collin, H. B. (1989). "The effects of RGP and silicone elastomer lens binding on corneal structure." Investigative Ophthalmology and Visual Science (Suppl) **30**: 481.

Holden, B. A., Sweeney, D. F., Vannas, A. *et al.* (1985). "Effects of long-term extended contact lens wear on the human cornea." Investigative Ophthalmology and Visual Science **26**(11): 1489-1501.

Holladay, J. T. (1997). "Corneal topography using the Holladay Diagnostic Summary." Journal of Cataract and Refractive Surgery **23**(2): 209-221.

Horner, D. G., Armitage, K. S. and Wormsley, B. S. (1992). "Corneal molding recovery after contact lens wear." Optometry and Vision Science **69**: 156.

Horner, D. G., Soni, P. S., Vyas, N. *et al.* (2000). "Longitudinal changes in corneal asphericity in myopia." Optometry and Vision Science **77**(4): 198-203.

Hubbe, R. E. and Foulks, G. N. (1994). "The effect of poor fixation on computer-assisted topographic corneal analysis. Pseudokeratoconus." Ophthalmology **101**(10): 1745-1748.

Hughes, C., Hamilton, L. and Doughty, M. J. (2003). "A quantitative assessment of the location and width of Marx's line along the marginal zone of the human eyelid." Optometry and Vision Science **80**(8): 564-572.

Hung, G., Hsu, F. and Stark, L. (1977). "Dynamics of the human eyeblink." American Journal of Optometry and Physiological Optics **54**(10): 678-690.

Hykin, P. G. and Bron, A. J. (1992). "Age-related morphological changes in lid margin and meibomian gland anatomy." Cornea **11**(4): 334-342.

Hyman, L., Gwiazda, J., Hussein, M. *et al.* (2005). "Relationship of age, sex, and ethnicity with myopia progression and axial elongation in the correction of myopia evaluation trial." Archives Of Ophthalmology **123**(7): 977-987.

Iskander, D. R., Collins, M. J. and Davis, B. (2001). "Optimal modeling of corneal surfaces with Zernike polynomials." IEEE Transactions on Bio-Medical Engineering **48**(1): 87-95.

Iskander, D. R., Collins, M. J. and Davis, B. (2005). "Evaluating tear film stability in the human eye with high-speed videokeratoscopy." IEEE Transactions on Bio-Medical Engineering **52**(11): 1939-1949.

Iskander, D. R., Collins, M. J., Mioschek, S. *et al.* (2004). "Automatic pupillometry from digital images." IEEE Transactions on Bio-medical Engineering. **51**(9): 1619-1627.

Jafri, B., Lichter, H. and Stulting, R. D. (2004). "Asymmetric keratoconus attributed to eye rubbing." Cornea **23**(6): 560-564.

Jayakumar, J. and Swarbrick, H. A. (2005). "The effect of age on short-term orthokeratology." Optometry and Vision Science **82**(6): 505-511.

Jayasuriya, A. C., Ghosh, S., Scheinbeim, J. I. *et al.* (2003). "A study of piezoelectric and mechanical anisotropies of the human cornea." Biosensors and Bioelectronics **18**(4): 381-387.

Jayasuriya, A. C., Scheinbeim, J. I., Lubkin, V. *et al.* (2003). "Piezoelectric and mechanical properties in bovine cornea." Journal of Biomedical Materials Research **66A**(2): 260-265.

Jeong, S., Lemke, B. N., Dortzbach, R. K. *et al.* (1999). "The Asian upper eyelid: an anatomical study with comparison to the Caucasian eyelid." Archives of Ophthalmology **117**(7): 907-912.

Jones, M. B., Fulford, G. R., Please, C. P. *et al.* (2008). "Elastohydrodynamics of the eyelid wiper." Bulletin of Mathematical Biology **70**(2): 323-343.

Kaneko, M., Tokuda, K. and Kawahara, T. (2005). "Dynamic sensing of human eye." In Proceedings of the 2005 IEEE International Conference on Robotics and Automation: 2871-2876.

Kanpolat, A., Simayek, T. and Alp, N. M. (1997). "The evaluation of normal corneal topography in emmetropic eyes with computer-assisted videokeratography." The CLAO Journal **23**(3): 168-171.

Kasprzak, H. and Jankowska-Kuchta, E. (1996). "A new analytical approximation of corneal topography." Journal of Modern Optics **43**(6): 1135-1148.

Kasprzak, H. T. and Iskander, D. R. (2007). "Spectral characteristics of longitudinal corneal apex velocities and their relation to the cardiopulmonary system." Eye **21**(9): 1212-1219.

Kasprzak, H. T. and Iskander, R. D. (2006). "Approximating ocular surfaces by generalised conic curves." Ophthalmic and Physiological Optics **26**(6): 602-609.

Keller, P. R., Collins, M. J., Carney, L. G. *et al.* (1996). "The relation between corneal and total astigmatism." Optometry and Vision Science **73**(2): 86-91.

Kessing, S. V. (1967). "A new division of the conjunctiva on the basis of x-ray examination." Acta Ophthalmologica **45**(5): 680-683.

Kiely, P. M., Carney, L. G. and Smith, G. (1982). "Diurnal variations of corneal topography and thickness." American Journal of Optometry and Physiological Optics **59**(12): 976-982.

Kiely, P. M., Carney, L. G. and Smith, G. (1983). "Menstrual cycle variations of corneal topography and thickness." American Journal of Optometry and Physiological Optics **60**(10): 822-829.

Kiely, P. M., Smith, G. and Carney, L. G. (1982). "The mean shape of the human cornea." Optica Acta **29**(8): 1027-1040.

King-Smith, P. E. (2008). "A link between tear instability and hyperosmolarity in dry eye." Investigative Ophthalmology and Visual Science **49**(E-abstract): 1540.

King-Smith, P. E., Fink, B. A., Hill, R. M. *et al.* (2004). "The thickness of the tear film." Current Eye Research **29**(4-5): 357-368.

Kirwan, C. and O'Keefe, M. (2008). "Corneal hysteresis using the Reichert ocular response analyser: findings pre- and post-LASIK and LASEK." Acta Ophthalmologica **86**(2): 215-218.

Knoll, H. A. (1961). "Corneal contours in the general population as revealed by the photokeratoscope." American Journal of Optometry and Archives of American Academy of Optometry **38**: 389-397.

Knoll, H. A. (1975). "Letter: bilateral monocular diplopia after near work." American Journal of Optometry and Physiological Optics **52**(2): 139-140.

Knoll, H. A. (1976). "The stability of the shape of the human cornea." American Journal of Optometry and Physiological Optics **53**(7): 359-361.

Kobayashi, Y., Yanai, R., Chikamoto, N. *et al.* (2008). "Reversibility of effects of orthokeratology on visual acuity, refractive error, corneal topography, and contrast sensitivity." Eye and Contact Lens **34**(4): 224-228.

Koh, S., Maeda, N., Kuroda, T. *et al.* (2002). "Effect of tear film break-up on higher-order aberrations measured with wavefront sensor." American Journal of Ophthalmology **134**(1): 115-117.

Kommerell, G. (1993). "Monocular diplopia caused by pressure of the upper eyelid on the cornea. Diagnosis based on the "Venetian blind phenomenon" in streak retinoscopy." Klinische Monatsblatter fur Augenheilkunde **203**(6): 384-389.

Korb, D. R., Greiner, J. V., Herman, J. P. *et al.* (2002). "Lid-wiper epitheliopathy and dry-eye symptoms in contact lens wearers." The CLAO Journal **28**(4): 211-216.

Korb, D. R., Herman, J. P., Greiner, J. V. *et al.* (2005). "Lid wiper epitheliopathy and dry eye symptoms." Eye and Contact Lens **31**(1): 2-8.

Kotecha, A., Elsheikh, A., Roberts, C. R. *et al.* (2006). "Corneal thickness- and age-related biomechanical properties of the cornea measured with the ocular response analyzer." Investigative Ophthalmology and Visual Science **47**(12): 5337-5347.

Kuwabara, T., Perkins, D. G. and Cogan, D. G. (1976). "Sliding of the epithelium in experimental corneal wounds." Investigative Ophthalmology **15**(1): 4-14.

Kwitko, S., Sawusch, M. R., McDonnell, P. J. *et al.* (1991). "Effect of extraocular muscle surgery on corneal topography." Archives of Ophthalmology **109**(6): 873-878.

Laiquzzaman, M., Bhojwani, R., Cunliffe, I. *et al.* (2006). "Diurnal variation of ocular hysteresis in normal subjects: relevance in clinical context." Clinical and Experimental Ophthalmology **34**(2): 114-118.

Lam, A. K., Chan, C. C., Lee, M. H. *et al.* (1999). "The aging effect on corneal curvature and the validity of Javal's rule in Hong Kong Chinese." Current Eye Research **18**(2): 83-90.

Lam, A. K. C. and Loran, D. (1991). "Designing contact lenses for oriental eyes." Journal of British Contact Lens Association **14**: 109-114.

Lam, B. L., Lam, S. and Walls, R. C. (1995). "Prevalence of palpebral fissure asymmetry in white persons." American Journal of Ophthalmology **120**(4): 518-522.

Lemp, M. and Mathers, W. (1991). "Renewal of the corneal epithelium." The CLAO Journal **17**(4): 258-266.

Leung, G. Y., Peponis, V., Varnell, E. D. *et al.* (2005). "Preliminary in vitro evaluation of 2-octyl cyanoacrylate (Dermabond) to seal corneal incisions." Cornea **24**(8): 998-999.

Levin, M. H. and Verkman, A. S. (2006). "Aquaporin-3-dependent cell migration and proliferation during corneal re-epithelialization." Investigative Ophthalmology and Visual Science **47**(10): 4365-4372.

Li, L. and Tighe, B. (2007). "Nonlinear analysis of static axisymmetric deformation of the human cornea." Computational Materials Science **38**(4): 318-324.

Lieberman, D. M. and Grierson, J. W. (2000). "The lids influence on corneal shape." Cornea **19**(3): 336-342.

Liu, J. and Roberts, C. J. (2005). "Influence of corneal biomechanical properties on intraocular pressure measurement: quantitative analysis." Journal of Cataract and Refractive Surgery **31**(1): 146-155.

Liu, Z., Huang, A. J. and Pflugfelder, S. C. (1999). "Evaluation of corneal thickness and topography in normal eyes using the Orbscan corneal topography system." The British Journal of Ophthalmology **83**(7): 774-778.

Liu, Z. and Pflugfelder, S. C. (2000). "The effects of long-term contact lens wear on corneal thickness, curvature, and surface regularity." Ophthalmology **107**(1): 105-111.

Löpping, B. and Weale, R. A. (1965). "Changes in corneal curvature following ocular convergence." Vision Research **5**(3): 207-215.

Lu, F., Simpson, T., Sorbara, L. *et al.* (2008). "Malleability of the ocular surface in response to mechanical stress induced by orthokeratology contact lenses." Cornea **27**(2): 133-141.

Luo, Z., Berglund, L. and An, K. (1998). "Validation of F-Scan pressure sensor system: a technical note." Journal of Rehabilitation Research and Development **35**(2): 186-191.

Lydon, D. and Tait, A. (1988). "Lid pressure: its measurement and probable effects on the shape and form of the cornea-rigid contact lens system." Journal of the British Contact Lens Association **11**(1): 11-22.

Lyu, J. and Joo, C.-K. (2006). "Expression of Wnt and MMP in epithelial cells during corneal wound healing." Cornea **25**(10 Suppl): S24-8.

Mainstone, J. C., Carney, L. G., Anderson, C. R. *et al.* (1998). "Corneal shape in hyperopia." Clinical and Experimental Optometry **81**(3): 131-137.

Malbouisson, J. M., Baccega, A. and Cruz, A. A. (2000). "The geometrical basis of the eyelid contour." Ophthalmic Plastic and Reconstructive Surgery **16**(6): 427-431.

Maloney, R. K., Bogan, S. J. and Waring, G. O., 3rd (1993). "Determination of corneal image-forming properties from corneal topography." American Journal of Ophthalmology **115**(1): 31-41.

Mandell, R. B. (1966). "Bilateral monocular diplopia following near work." American Journal of Optometry and Archives of American Academy of Optometry **43**(8): 500-504.

Mandell, R. B. (1996). "A guide to videokeratography." International Contact Lens Clinics **23**(Nov/Dec): 205-228.

Mandell, R. B., Chiang, C. S. and Klein, S. A. (1995). "Location of the major corneal reference points." Optometry and Vision Science **72**(11): 776-784.

Mandell, R. B. and St Helen, R. (1971). "Mathematical model of the corneal contour." British Journal of Physiological Optics **26**: 183-197.

Mandell, R. B. and St Helen, R. S. (1968). "Stability of the corneal contour." American Journal of Optometry and Archives of American Academy of Optometry **45**(12): 797-806.

Mansour, A. M. and Haddad, R. S. (2002). "Corneal topography after ocular rubbing." Cornea **21**(8): 756-758.

Martinez-Afanador, A. M. and Ortiz-Nieva, G. (2008). "Hysteresis and corneal resistance factor evaluation in patients with different stages of keratoconus." Investigative Ophthalmology and Visual Science (Suppl) **49**(E-Abstract): 4349.

Marx, E. (1924). "Uber anatomie, physiologie und pathologie des augenlidrandes un der tranenpunkte." Grafes Archive of Ophthalmology **114**: 465-482.

Mattioli, R. and Tripoli, N. K. (1997). "Corneal geometry reconstruction with the Keratron videokeratographer." Optometry and Vision Science **74**(11): 881-894.

Maurer, J., Ronsky, J., Loitz-Ramage, B. *et al.* (2003). "Prosthetic socket interface pressures: customized calibration technique for the Tekscan F-socket system." Summer Bioengineering Conference: (June 25-29) 1073-1074.

Mavrikakis, I., Beckingsale, P., Edward, L. *et al.* (2006). "Changes in corneal topography with upper eyelid gold weight implants." Ophthalmic Plastic and Reconstructive Surgery **22**(5): 331-334.

McMonnies, C. W. (2007). "Incomplete blinking: exposure keratopathy, lid wiper epitheliopathy, dry eye, refractive surgery, and dry contact lenses." Contact Lens and Anterior Eye **30**(1): 37-51.

Medeiros, F. A. and Weinreb, R. N. (2006). "Evaluation of the influence of corneal biomechanical properties on intraocular pressure measurements using the ocular response analyzer." Journal of Glaucoma **15**(5): 364-370.

Mengher, L. S., Pandher, K. S. and Bron, A. J. (1986). "Non-invasive tear film break-up time: sensitivity and specificity." Acta Ophthalmologica **64**(4): 441-444.

Merriam, W. W., Ellis, F. D. and Helveston, E. M. (1980). "Congenital blepharoptosis, anisometropia, and amblyopia." American Journal of Ophthalmology **89**(3): 401-407.

Mertz, G. W. (1980). "Overnight swelling of the living human cornea." Journal Of The American Optometric Association **51**(3): 211-214.

Miller, D. (1967). "Pressure of the lid on the eye." Archives of Ophthalmology **78**(3): 328-330.

Miller, K. L., Polse, K. A. and Radke, C. J. (2002). "Black-line formation and the "perched" human tear film." Current Eye Research **25**(3): 155-162.

Moller, P. M. (1954). "Tissue pressure in the orbit." Acta Ophthalmologica **32**(5): 597-604.

Montés-Micó, R. (2000). "Astigmatism in infancy and childhood." Journal of Pediatric Ophthalmology and Strabismus **37**(6): 349-353.

Montés-Micó, R., Alió, J. L., Muñoz, G. *et al.* (2004). "Temporal changes in optical quality of air-tear film interface at anterior cornea after blink." Investigative Ophthalmology and Visual Science **45**(6): 1752-1757.

Morgan, P. B., Soh, M. P., Efron, N. *et al.* (1993). "Potential applications of ocular thermography." Optometry and Vision Science **70**(7): 568-576.

Moses, R. A. (1987). The Eyelids. Adler's Physiology of the Eye. R. A. Moses and W. Hart Jnr. St Louis, Mosby.

Moses, R. A. and Grodzki, W. J. (1971). "Theory and calibration of the Schiotz tonometer. III. Friction between tonometer footplate and cornea." Investigative Ophthalmology **10**(8): 589-591.

Mountford, J. (1998). "Retention and regression of orthokeratology with time." International Contact Lens Clinics **25**(March/April): 59-64.

Mountford, J. (2004). A Model of Forces Acting in Orthokeratology. Orthokeratology: Principles and Practice. J. Mountford, D. Ruston and T. Dave. London, Butterworth-Heinemann**:** 269-301.

Mountford, J. and Pesudovs, K. (2002). "An analysis of the astigmatic changes induced by accelerated orthokeratology." Clinical and Experimental Optometry **85**(5): 284-293.

Nagyova, B. and Tiffany, J. M. (1999). "Components responsible for the surface tension of human tears." Current Eye Research **19**(1): 4-11.

Nardi, M., Rizzo, S., Pellegrini, G. *et al.* (1997). "Effects of strabismus surgery on corneal topography." Journal of Pediatric Ophthalmology and Strabismus **34**(4): 244-246.

Nash, I. S., Greene, P. R. and Foster, C. S. (1982). "Comparison of mechanical properties of keratoconus and normal corneas." Experimental Eye Research **35**(5): 413-424.

Nathan, J., Kiely, P. M., Crewther, S. G. *et al.* (1986). "Astigmatism occurring in association with pediatric eye disease." American Journal of Optometry and Physiological Optics **63**(7): 497-504.

Németh, J., Erdélyi, B. and Csákány, B. (2001). "Corneal topography changes after a 15 second pause in blinking." Journal of Cataract and Refractive Surgery **27**(4): 589-592.

Németh, J., Erdélyi, B., Csákány, B. *et al.* (2002). "High-speed videotopographic measurement of tear film build-up time." Investigative Ophthalmology and Visual Science **43**(6): 1783-1790.

Nemoto, Y., Morikawa, K. and Kaneko, H. (2008). "A case of blepharoptosis associated with long-term use of soft contact lenses." Nippon Ganka Gakkai Zasshi **112**(10): 876-881.

Newton, R. H. and Meek, K. M. (1998). "Circumcorneal annulus of collagen fibrils in the human limbus." Investigative Ophthalmology and Visual Science **39**(7): 1125-1134.

Newton, R. H. and Meek, K. M. (1998). "The integration of the corneal and limbal fibrils in the human eye." Biophysical Journal **75**(5): 2508-2512.

Nichols, J. J., Marsich, M. M., Nguyen, M. *et al.* (2000). "Overnight orthokeratology." Optometry and Vision Science **77**(5): 252-259.

Nicolopoulos, C. S., Anderson, E. G., Solomonidis, S. E. *et al.* (2000). "Evaluation of the gait analysis FSCAN pressure system: clinical tool or toy?" The Foot **10**(3): 124-130.

Nisted, M. and Hofstetter, H. W. (1974). "Effect of chalazion on astigmatism." American Journal of Optometry and Physiological Optics **51**(8): 579-582.

Norn, M. (1985). "Meibomian orifices and Marx's line. Studied by triple vital staining." Acta Ophthalmologica **63**(6): 698-700.

Norn, M. S. (1980). "Vital staining of external eye of rabbit." Acta Ophthalmologica **58**(3): 454-458.

Nyquist, G. W. (1968). "Stress-induced birefringence of the cornea." American Journal of Ophthalmology **65**(3): 398-404.

O'Donnell, C. (2005). "Agreement and repeatability of central thickness measurement in normal corneas using ultrasound pachymetry and the OCULUS Pentacam." Cornea **24**(8): 920-924.

Oh, J. Y., Jung, K. A., Kim, M. K. *et al.* (2006). "Effect of mechanical strain on human limbal epithelial cells in vitro." Current Eye Research **31**(12): 1015-1020.

Orndahl, M. J. and Fagerholm, P. P. (1998). "Phototherapeutic keratectomy for map-dot-fingerprint corneal dystrophy." Cornea **17**(6): 595-599.

Orssengo, G. J. and Pye, D. C. (1999). "Determination of the true intraocular pressure and modulus of elasticity of the human cornea in vivo." Bulletin of Mathematical Biology **61**(3): 551-572.

Oshika, T., Klyce, S. D., Applegate, R. A. *et al.* (1999). "Changes in corneal wavefront aberrations with aging." Investigative Ophthalmology and Visual Science **40**(7): 1351-1355.

Oshika, T., Klyce, S. D., Applegate, R. A. *et al.* (1999). "Comparison of corneal wavefront aberrations after photorefractive keratectomy and laser in situ keratomileusis." American Journal of Ophthalmology **127**(1): 1-7.

Otto, J., Brown, T. and Callaghan, J. (1999). "Static and dynamic response of a multiplexed-array piezoresistive contact sensor." Experimental Mechanics **39**(4): 317-323.

Owens, H., Garner, L. F., Craig, J. P. *et al.* (2004). "Posterior corneal changes with orthokeratology." Optometry and Vision Science **81**(6): 421-426.

Owens, H. and Phillips, J. (2001). "Spreading of the tears after a blink: velocity and stabilization time in healthy eyes." Cornea **20**(5): 484-487.

Papas, E. B., Petznick, A., Stapleton, F. *et al.* (2006). "Involvement of Matrix Metalloproteinase-9 and tissue inhibitor of Matrix Metalloproteinase-1 (TIMP-1) during orthokeratology." Investigative Ophthalmology and Visual Science **47**(E-Abstract): 117.

Parsons, J. (1904). The Pathology of the Eye. London, Hodder and Stoughton.

Pärssinen, T. O. (1993). "Corneal refraction and topography in school myopia." The CLAO Journal **19**(1): 69-72.

Patel, S., Bevan, R. and Farrell, J. C. (1988). "Diurnal variation in precorneal tear film stability." American Journal of Optometry and Physiological Optics **65**(3): 151-154.

Patel, S. and Farrell, J. C. (1989). "Age-related changes in precorneal tear film stability." Optometry and Vision Science **66**(3): 175-178.

Pepose, J. S., Feigenbaum, S. K., Qazi, M. A. *et al.* (2007). "Changes in corneal biomechanics and intraocular pressure following LASIK using static, dynamic and noncontact tonometry." American Journal of Ophthalmology **143**: 39-47.

Pierścionek, B., Popiołek-Masajada, A. and Kasprzak, H. (2001). "Corneal shape change during accommodation." Eye **15**(6): 766-769.

Plager, D. A. and Snyder, S. K. (1997). "Resolution of astigmatism after surgical resection of capillary hemangiomas in infants." Ophthalmology **104**(7): 1102-1106.

Polliack, A. A., Craig, D. D., Sieh, R. C. *et al.* (2002). "Laboratory and clinical tests of a prototype pressure sensor for clinical assessment of prosthetic socket fit." Prosthetics and Orthotics International **26**(1): 23-34.

Polliack, A. A., Sieh, R. C., Craig, D. D. *et al.* (2000). "Scientific validation of two commercial pressure sensor systems for prosthetic socket fit." Prosthetics and Orthotics International **24**(1): 63-73.

Polse, K. A., Brand, R. J., Vastine, D. W. *et al.* (1983). "Corneal change accompanying orthokeratology. Plastic or elastic? Results of a randomized controlled clinical trial." Archives of Ophthalmology **101**(12): 1873-1878.

Pult, H., Purslow, C., Berry, M. *et al.* (2008). "Clinical tests for successful contact lens wear: relationship and predictive potential." Optometry and Vision Science **85**(10): E924-9.

Punjabi, O. S., Kniestedt, C., Stamper, R. L. *et al.* (2006). "Dynamic contour tonometry: principle and use." Clinical and Experimental Ophthalmology **34**(9): 837-840.

Purslow, C. and Wolffsohn, J. (2007). "The relation between physical properties of the anterior eye and ocular surface temperature." Optometry and Vision Science **84**(3): 197-201.

Purslow, C., Wolffsohn, J. S. and Santodomingo-Rubido, J. (2005). "The effect of contact lens wear on dynamic ocular surface temperature." Contact Lens and Anterior Eye **28**(1): 29-36.

Rabinowitz, Y. S. (1993). "Corneal topography." Current Opinion In Ophthalmology **4**(4): 68-74.

Rabinowitz, Y. S. and Klyce, S. E. (1993). A Color Atlas of Corneal Topography: Interpreting Videokeratography. New York, Tokyo, Igaku-Shoin Medical Publishers Inc.

Rabinowitz, Y. S., Yang, H., Brickman, Y. *et al.* (1996). "Videokeratography database of normal human corneas." The British Journal of Ophthalmology **80**(7): 610-616.

Randolph, A. L., Nelson, M., Akkapeddi, S. *et al.* (2000). "Reliability of measurements of pressures applied on the foot during walking by a computerized insole sensor system." Archives of Physical Medicine and Rehabilitation **81**(5): 573-578.

Rasheed, K., Rabinowitz, Y. S., Remba, D. *et al.* (1998). "Interobserver and intraobserver reliability of a classification scheme for corneal topographic patterns." The British Journal of Ophthalmology **82**(12): 1401-1406.

Read, S. A., Buehren, T. and Collins, M. J. (2007). "Influence of accommodation on the anterior and posterior cornea." Journal of Cataract and Refractive Surgery **33**(11): 1877-1885.

Read, S. A., Collins, M. J. and Carney, L. G. (2005). "The diurnal variation of corneal topography and aberrations." Cornea **24**(6): 678-687.

Read, S. A., Collins, M. J. and Carney, L. G. (2007). "The influence of eyelid morphology on normal corneal shape." Investigative Ophthalmology and Visual Science **48**(1): 112-119.

Read, S. A., Collins, M. J., Carney, L. G. *et al.* (2006). "The topography of the central and peripheral cornea." Investigative Ophthalmology and Visual Science **47**(4): 1404-1415.

Read, S. A., Collins, M. J., Carney, L. G. *et al.* (2006). "The morphology of the palpebral fissure in different directions of vertical gaze." Optometry and Vision Science **83**(10): 715-722.

Read, S. A., Collins, M. J. and Iskander, D. R. (2008). "Diurnal variation of axial length, intraocular pressure, and anterior eye biometrics." Investigative Ophthalmology and Visual Science **49**(7): 2911-2918.

Ren, H. and Wilson, G. (1997). "The effect of a shear force on the cell shedding rate of the corneal epithelium." Acta Ophthalmologica **75**(4): 383-387.

Reynolds, D. R. and Poynter, H. L., 3rd (1970). "Diurnal variation in central corneal curvature." American Journal of Optometry and Archives of American Academy of Optometry **47**(11): 892-899.

Riley, A. F., Grupcheva, C. N., Malik, T. Y. *et al.* (2001). "The Auckland Cataract Study: demographic, corneal topographic and ocular biometric parameters." Clinical and Experimental Ophthalmology **29**(6): 381-386.

Robb, R. M. (1977). "Refractive errors associated with hemangiomas of the eyelids and orbit in infancy." American Journal of Ophthalmology **83**(1): 52-58.

Roberts, C. (1998). "A practical guide to the interpretation of corneal topography." Contact Lens Spectrum **13**(3): 25-33.

Salmon, T. O. and Horner, D. G. (1995). "Comparison of elevation, curvature, and power descriptors for corneal topographic mapping." Optometry and Vision Science **72**(11): 800-808.

Schanzer, M. C., Mehta, R. S., Arnold, T. P. *et al.* (1989). "Irregular astigmatism induced by annular tinted contact lenses." The CLAO Journal **15**(3): 207-211.

Schwiegerling, J. and Greivenkamp, J. E. (1996). "Keratoconus detection based on videokeratoscopic height data." Optometry and Vision Science **73**(12): 721-728.

Schwiegerling, J., Greivenkamp, J. E. and Miller, J. M. (1995). "Representation of videokeratoscopic height data with Zernike polynomials." Journal of the Optical Society of America **12**(10): 2105-2113.

Seo, H. and Lee, C. (2002). "Head-free reading of horizontally and vertically arranged texts." Vision Research **42**(10): 1325-1337.

Shah, S., Laiquzzaman, M., Cunliffe, I. *et al.* (2006). "The use of the Reichert ocular response analyser to establish the relationship between ocular hysteresis, corneal resistance factor and central corneal thickness in normal eyes." Contact Lens and Anterior Eye **29**(5): 257-262.

Shaw, A. J., Collins, M. J., Davis, B. A. *et al.* (2008). "Corneal refractive changes due to short-term eyelid pressure in downward gaze." Journal of Cataract and Refractive Surgery **34**(9): 1546-1553.

Shaw, A. J., Collins, M. J., Davis, B. A. *et al.* (2009). "Eyelid pressure: inferences from corneal topographic changes." Cornea **28**(2): 181-188.

Sheedy, J. E., Gowrisankaran, S. and Hayes, J. R. (2005). "Blink rate decreases with eyelid squint." Optometry and Vision Science **82**(10): 905-911.

Sheridan, M. and Douthwaite, W. A. (1989). "Corneal asphericity and refractive error." Ophthalmic and Physiological Optics **9**(3): 235-238.

Shikura, H., Yamaguchi, T. and Nakajima, S. (1993). "A new system for measuring the pressure between the eyelids and the cornea." Investigative Ophthalmology and Visual Science (Suppl) **34**: 1250.

Shin, T. J., Vito, R. P., Johnson, L. W. *et al.* (1997). "The distribution of strain in the human cornea." Journal of Biomechanics **30**(5): 497-503.

Shore, J. W. (1985). "Changes in lower eyelid resting position, movement, and tone with age." American Journal of Ophthalmology **99**(4): 415-423.

Sjontoft, E. and Edmund, C. (1987). "In vivo determination of Young's modulus for the human cornea." Bulletin of Mathematical Biology **49**(2): 217-232.

Small, R. G. and Meyer, D. R. (2004). "Eyelid metrics." Ophthalmic Plastic And Reconstructive Surgery **20**(4): 266-267.

Smolek, M. K. and Klyce, S. D. (2005). "Goodness-of-prediction of Zernike polynomial fitting to corneal surfaces." Journal of Cataract and Refractive Surgery **31**(12): 2350-2355.

Soni, P. S., Nguyen, T. T. and Bonanno, J. A. (2003). "Overnight orthokeratology: visual and corneal changes." Eye and Contact Lens **29**(3): 137-145.

Soni, P. S., Nguyen, T. T. and Bonanno, J. A. (2004). "Overnight orthokeratology: refractive and corneal recovery after discontinuation of reverse-geometry lenses." Eye and Contact Lens **30**(4): 254.

Sridharan, R. and Swarbrick, H. (2003). "Corneal response to short-term orthokeratology lens wear." Optometry and Vision Science **80**(3): 200-206.

Stamenovic, D. (2005). "Microtubules may harden or soften cells, depending of the extent of cell distension." Journal Of Biomechanics **38**(8): 1728-1732.

Stampfer, K. A. and Tredici, T. J. (1975). "Monocular diplopia in flying personnel." American Journal of Ophthalmology **80**(4): 759-763.

Stone, R. A., Quinn, G. E., Francis, E. L. *et al.* (2004). "Diurnal axial length fluctuations in human eyes." Investigative Ophthalmology and Visual Science **45**(1): 63-70.

Strang, N. C., Schmid, K. L. and Carney, L. G. (1998). "Hyperopia is predominantly axial in nature." Current Eye Research **17**(4): 380-383.

Swarbrick, H. A. and Holden, B. A. (1996). "Ocular characteristics associated with rigid gas-permeable lens adherence." Optometry and Vision Science **73**(7): 473-481.

Swarbrick, H. A., Wong, G. and O'Leary, D. J. (1998). "Corneal response to orthokeratology." Optometry and Vision Science **75**(11): 791-799.

Takei, K. (2002). "Is abnormal focal steepening of the cornea related to persistent monocular diplopia?" Journal of Refractive Surgery **18**(3): 253-262.

Takei, K., Sano, Y., Achiron, L. R. *et al.* (2001). "Monocular diplopia related to asymmetric corneal topography after laser in situ keratomileusis." Journal of Refractive Surgery **17**(6): 652-657.

Tan, J. C. H., Kalapesi, F. B. and Coroneo, M. T. (2006). "Mechanosensitivity and the eye: cells coping with the pressure." The British Journal of Ophthalmology **90**(3): 383-388.

Tang, W., Collins, M. J., Carney, L. *et al.* (2000). "The accuracy and precision performance of four videokeratoscopes in measuring test surfaces." Optometry and Vision Science **77**(9): 483-491.

Thibos, L. N., Applegate, R. A., Schwiegerling, J. T. *et al.* (2002). "Standards for reporting the optical aberrations of eyes." Journal of Refractive Surgery **18**(5): S652-60.

Thibos, L. N., Hong, X., Bradley, A. *et al.* (2004). "Accuracy and precision of objective refraction from wavefront aberrations." Journal of Vision **4**(4): 329-351.

Thoft, R. A. and Friend, J. (1983). "The X, Y, Z hypothesis of corneal epithelial maintenance." Investigative Ophthalmology and Visual Science **24**(10): 1442-1443.

Tierney, W. S., Enos, M. M., Lim, J. E. *et al.* (2008). "Diurnal variation of corneal epithelial permeability of non-contact-lens wearers." Investigative Ophthalmology and Visual Science (Suppl) **49**(E-abstract): 2554.

Tripoli, N. K., Cohen, K. L., Holmgren, D. E. *et al.* (1995). "Assessment of radial aspheres by the arc-step algorithm as implemented by the Keratron keratoscope." American Journal of Ophthalmology **120**: 658-664.

Tsukiyama, J., Miyamoto, Y., Higaki, S. *et al.* (2008). "Changes in the anterior and posterior radii of the corneal curvature and anterior chamber depth by orthokeratology." Eye and Contact Lens **34**(1): 17-20.

Ugurbas, S. H. and Zilelioglu, G. (1999). "Corneal topography in patients with congenital ptosis." Eye **13**(4): 550-554.

van den Bosch, W. A., Leenders, I. and Mulder, P. (1999). "Topographic anatomy of the eyelids, and the effects of sex and age." The British Journal of Ophthalmology **83**(3): 347-352.

van den Bosch, W. A. and Lemij, H. G. (1992). "Blepharoptosis induced by prolonged hard contact lens wear." Ophthalmology **99**(12): 1759-1765.

Varikooty, J., Srinivasan, S. and Jones, L. (2008). "Atypical manifestation of upper lid margin staining in silicone hydrogel lens wearers with symptoms of dry eye." Contact Lens and Anterior Eye **31**: 44-46.

Vasudevan, B., Ciuffreda, K. J. and Wang, B. (2007). "Nearwork-induced changes in topography, aberrations, and thickness of the human cornea after interrupted reading." Cornea **26**(8): 917-923.

Vihlen, F. S. and Wilson, G. (1983). "The relation between eyelid tension, corneal toricity, and age." Investigative Ophthalmology and Visual Science **24**(10): 1367-1373.

Voetz, S. C., Collins, M. J. and Lingelbach, B. (2004). "Recovery of corneal topography and vision following opaque-tinted contact lens wear." Eye and Contact Lens **30**(2): 111-117.

Waldron, H. E. (1984). "Influence of the lids on contact lens location and orientation." American Journal of Optometry and Physiological Optics **61**(2): 129-132.

Walland, M. J., Stevens, J. D. and Steele, A. D. (1994). "The effect of recurrent pterygium on corneal topography." Cornea **13**(5): 463-464.

Wang, F. M., Millman, A. L., Sidoti, P. A. *et al.* (1990). "Ocular findings in Treacher Collins syndrome." American Journal of Ophthalmology **110**(3): 280-286.

Wang, J., Fonn, D., Simpson, T. L. *et al.* (2003). "Precorneal and pre and postlens tear film thickness measured indirectly with optical coherence tomography." Investigative Ophthalmology and Visual Science **44**(6): 2524-2528.

Wang, J., Fonn, D., Simpson, T. L. *et al.* (2003). "Topographical thickness of the epithelium and total cornea after overnight wear of reverse-geometry rigid contact lenses for myopia reduction." Investigative Ophthalmology and Visual Science **44**(11): 4742-4746.

Wang, L., Dai, E., Koch, D. D. *et al.* (2003). "Optical aberrations of the human anterior cornea." Journal of Cataract and Refractive Surgery **29**(8): 1514-1521.

Wang, X., McCulley, J. P., Bowman, R. W. *et al.* (2002). "Time to resolution of contact lens-induced corneal warpage prior to refractive surgery." The CLAO Journal **28**(4): 169-171.

Wildsoet, C. F., Oswald, P. J. and Clark, S. (2000). "Albinism: its implications for refractive development." Investigative Ophthalmology and Visual Science **41**(1): 1-7.

Wilson, D. C., Niosi, C. A., Zhu, Q. A. *et al.* (2006). "Accuracy and repeatability of a new method for measuring facet loads in the lumbar spine." Journal of Biomechanics **39**(2): 348-353.

Wilson, D. R., Apreleva, M. V., Eichler, M. J. *et al.* (2003). "Accuracy and repeatability of a pressure measurement system in the patellofemoral joint." Journal of Biomechanics **36**(12): 1909-1915.

Wilson, G., Bell, C. and Chotai, S. (1982). "The effect of lifting the lids on corneal astigmatism." American Journal of Optometry and Physiological Optics **59**(8): 670-674.

Wilson, S. E. and Klyce, S. D. (1991). "Quantitative descriptors of corneal topography. A clinical study." Archives of Ophthalmology **109**(3): 349-353.

Wilson, S. E., Klyce, S. D. and Husseini, Z. M. (1993). "Standardized color-coded maps for corneal topography." Ophthalmology **100**(11): 1723-1727.

Wilson, S. E., Lin, D. T., Klyce, S. D. *et al.* (1990). "Topographic changes in contact lens-induced corneal warpage." Ophthalmology **97**(6): 734-744.

Woodburn, J. and Helliwell, P. (1996). "Observations on the F-Scan in-shoe pressure measuring system." Clinical Biomechanics **11**(5): 301-304.

Xu, S., Cai, C., Wang, J. *et al.* (2008). "Changes in corneal biomechanical properties after long-term soft contact lens wear." Investigative Ophthalmology and Visual Science (Suppl) **49**(E-Abstract): 661.

Yan, X.-m., Liu, S. and Li, H.-l. (2008). "Preliminary observation the correlation between lid-wiper epitheliopathy and dry eye." Chinese Journal of Ophthalmology **44**(5): 436-441.

Yasuda, A. and Yamaguchi, T. (2005). "Steepening of corneal curvature with contraction of the ciliary muscle." Journal of Cataract and Refractive Surgery **31**(6): 1177-1181.

Yasuda, A., Yamaguchi, T. and Ohkoshi, K. (2003). "Changes in corneal curvature in accommodation." Journal of Cataract and Refractive Surgery **29**(7): 1297-1301.

Yeniad, B., Seidu Adam, Y., Bilgin, L. K. *et al.* (2004). "Effect of 30-day continuous wear of silicone hydrogel contact lenses on corneal thickness." Eye and Contact Lens **30**(1): 6-9.

Yeniad, B., Yigit, B., Issever, H. *et al.* (2003). "Effects of contact lenses on corneal thickness and corneal curvature during usage." Eye and Contact Lens **29**(4): 223-229.

Yokoi, N., Bron, A., Tiffany, J. *et al.* (1999). "Reflective meniscometry: a non-invasive method to measure tear meniscus curvature." The British Journal of Ophthalmology **83**(1): 92-97.

Young, G. and Mirejovsky, D. (1993). "A hypothesis for the aetiology of soft contact lens-induced superior arcuate keratopathy." International Contact Lens Clinic **20**(9): 177-177.

Zhu, M., Collins, M. J. and Iskander, D. R. (2007). "Dynamics of ocular surface topography." Eye **21**(5): 624-632.

Appendices

Appendix 1: Ethics – Eye Dynamics

EYE DYNAMICS

Information Sheet

The Research Team

The research team are students and staff of the Centre for Eye Research and School of Mathematics in the Faculties of Health and Science at the Queensland University of Technology.

Program Leader: Dr Michael Collins Ph W 3864 5702 H 3289 3940

The Project

The project we are undertaking is designed to provide us with information regarding the dynamic changes that naturally occur on the surface of the eye (in the tears and cornea) and in the internal structures of the eye. This study aims to investigate the mathematical characteristics of these fluctuations.

You will be required to undergo an initial screening examination of your eyes to determine your suitability for this study. In this study the shape of the front surface of the eye (tears and cornea) will be measured using a videokeratoscope and the internal optics of your eye will be measured with a wavefront sensor. You will be asked to look into a clinical instrument, the videokeratoscope or wavefront sensor, while your optics are measured. The videokeratoscope and wavefront sensors are normal clinical instruments and pose no risk to the health of your eyes. We may also photograph the eye with a digital camera or high speed camera.

We have contacted you as a potential participant in the study after reviewing your clinical record in the Optometry Clinic at QUT.

Expected Benefits

Your involvement in this project will not directly benefit you. We are interested in modelling the natural fluctuations which occur in the optics of the human eye. Data collected from this study is expected to improve understanding of this area and aid further research.

Risks

There are no greater risks in this study than those associated with your routine eye examinations.

Confidentiality

The research data we gather from the experiments will not personally identify you by name, or in any way that allows you to be identified. Any publication of data arising from this research will use a code system which does not identify you personally. The data will be stored securely in the Centre for Eye Research.

Voluntary Participation

We have identified you as a potential subject for this study after reviewing your clinical record at the QUT Optometry Clinic. Your participation in this study is entirely voluntary and you can withdraw from the study at any stage without comment or penalty. Your decision not to participate or to withdraw from the study will in no way influence your relationship with QUT (such as your student grades, employment or clinical care).

Questions and further information

If you wish to discuss any aspect of this study or have any further enquiries feel free to contact Dr Michael Collins (listed above).

Concerns or complaints

You may also contact the Secretary of the University Human Research Ethics Committee on 3864 2902 if you wish to raise any concerns about the conduct of this research.

Feedback

We will be happy to discuss your individual results during or after the experiment. We will provide you with a written copy of any reports or publications arising from this research if you so request.

EYE DYNAMICS

RESEARCH CONSENT FORM

Name of Chief Investigator: Dr Michael Collins Ph W 3864 5702 H 3289 3940

By signing below, you are indicating that:

The tests and procedures involved in this study have been explained to me,

I have read the information sheet,

I have been given the opportunity to ask questions regarding this project and the tests involved,

I understand that if I have additional questions I can contact any member of the research team,

I have been informed that I am free to withdraw from the study at any time, without comment or penalty;

The project is for the purpose of research and not for treatment of my eyes;

I can contact the Secretary of the University Human Research Ethics Committee on 3864 2902 if I wish to raise any concerns about the conduct of this research.

I consent to participate in this project.

Participant's name:.....

Signature: ..... Date .....

Appendix 2: Extended corneal topography maps

Introduction

The objective of this study was to examine the eyelid-induced corneal changes over a larger corneal area then had previously been studied. Most videokeratoscopes including the Medmont E300 Corneal Topographer (Medmont Pty. Ltd., Victoria, Australia), use a Placido faceplate where the image of the illuminated rings is reflected from the cornea and captured by the video camera. Angular constraints due to the nose, cheekbone and eyebrow and shadows from eyelashes, limit the map size to between 7 and 9 mm. A technique was developed which combines a standard central topography map with peripheral topography maps in order to view the topography of nearly the entire cornea (Franklin *et al.* 2006) (Figure 1). This process of "map pasting" has been used to investigate the central and peripheral topography of a group of 100 young subjects with normal refractive errors (Read *et al.* 2006).

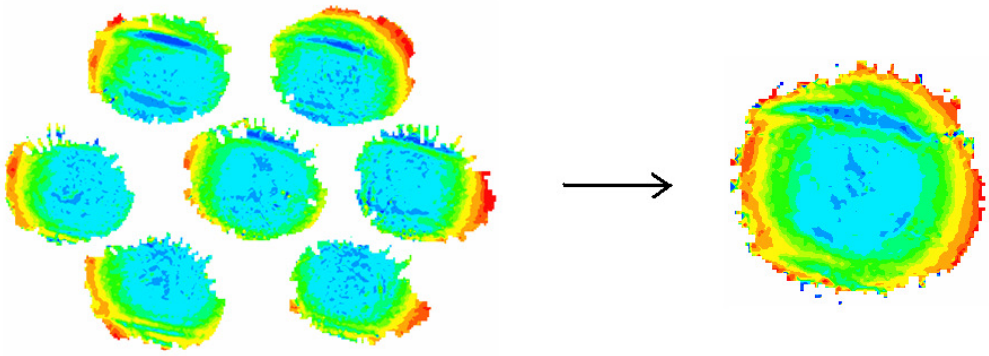

Figure 1: A standard central map and six peripheral maps combined to form a limbus to limbus topography map

Eyelid-induced corneal changes have been previously studied using central topography maps (Buehren *et al.* 2001; Buehren *et al.* 2003; Collins *et al.* 2005; Collins *et al.* 2006; Collins *et al.* 2006). The application of this "map pasting" technique to eyelid-induced corneal changes enabled the complete extent of these changes to be examined.

Methods

Protocol

Five subjects from the eighteen subjects who participated in the experiment in Chapter 2 underwent an extended measurement protocol for each of the four task conditions:

1. Reading at 20° downward gaze;
2. Steady fixation at 20° downward gaze;
3. Reading at 40° downward gaze; and
4. Steady fixation at 40° downward gaze.

Preliminary screening and eyelid morphometry were completed according to the main task protocol (Chapter 2). However for the topography measurement, multiple maps were captured to be combined to form the larger topography map. The peripheral maps were captured by using a fixation chart positioned 1.5 m from the right eye and viewed through a mirror system. This chart had 6 peripheral fixation targets to capture maps in 0º, 60º, 120º, 180º, 240º, and 300º directions. Prior to the measurements, the centre of the fixation chart viewed with the right eye was aligned with the central videokeratoscope Placido ring viewed with the left eye. The central Placido ring was used as the fixation point for the capture of the central topography maps and the fixation targets on the chart were used for the capture of the peripheral maps.

For the baseline condition, a total of 24 maps (six central and three each of the six peripheral fixation maps) were acquired prior to the visual task. However the 24 maps post-task maps could not be captured consecutively as it is known that eyelid-induced corneal distortions dissipate quite rapidly (Collins *et al.* 2005). So after the 15-minute visual task, half the topography maps were captured and then an additional near task session was added to the protocol to maintain the corneal changes before the remaining topography maps were captured.

The duration of the additional visual task was determined following a pilot study on three subjects. The central tangential peak-to-valley amplitudes were

calculated from the 90° meridian as a measure of the corneal change. It was found that an additional 10 minutes of the task was required to approximately return the corneal peak-to-valley to the amplitude measured immediately after the initial 15-minute task. So the measurement sequence was: visual task (15 minutes), acquisition of three maps each for the central target and three peripheral fixation targets, the additional visual task (10 minutes) and then capture of another three central maps and three maps each for the final three peripheral targets. This protocol was conducted for 3 subjects with 2 trials for subject 3 and the time progression of tangential peak-to-valley amplitudes for the three subjects is shown in Figure 2.

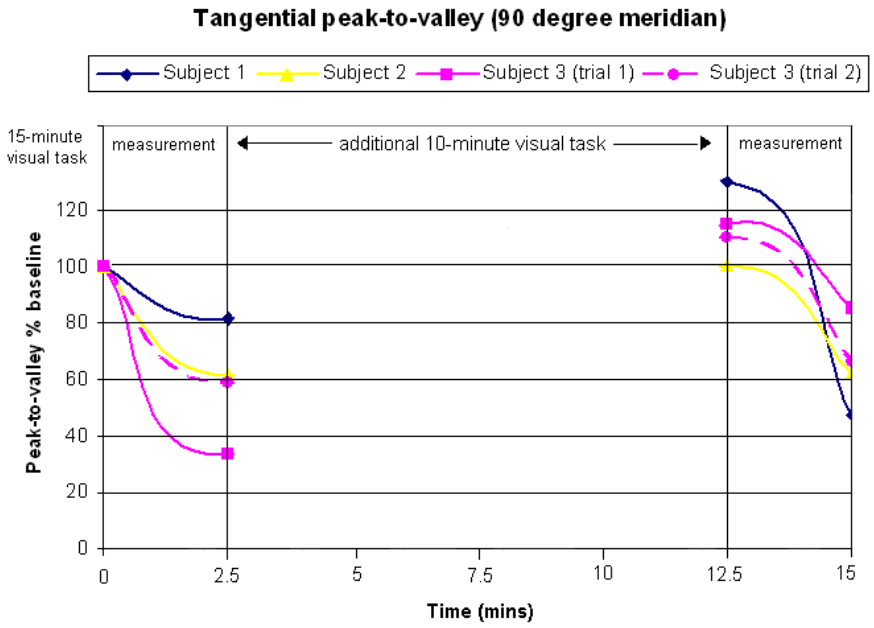

Figure 2: Tangential power peak-to-valley (90° semi-meridian) percentage compared to baseline (after 15 mins reading, time = 0) then after 2.5 mins break, 10 mins additional reading and a final 2.5 mins break. On average the peak-to-valley amplitude decreased to 59% after 2.5 minutes break, increased to 110% after the additional 10-minute task and decreased to 67% after the final 2.5 minute break.

Analysis

The central and peripheral maps were combined according to the method of Franklin *et al.* (2006) using custom software written in MATLAB (The Mathworks, Inc., Natick, MA). This process involved finding the vertex normal within the central map and matching it to the same point located within the peripheral maps. Every peripheral map was paired with each central map and the sum of squared error calculated. A 6 mm diameter of the central map, with the lowest total sum of squared error for the combination of peripheral maps, was chosen to be pasted with the peripheral maps.

As tangential maps describe localised changes in curvature, they are easily influenced by eye position fluctuations. Some smoothing was applied with a Savitzky-Golay filter fitting a 2nd order polynomial to 7 surrounding points. This smoothed the noise in the data, while the high frequency eyelid-induced corneal distortions were retained (Figure 3).

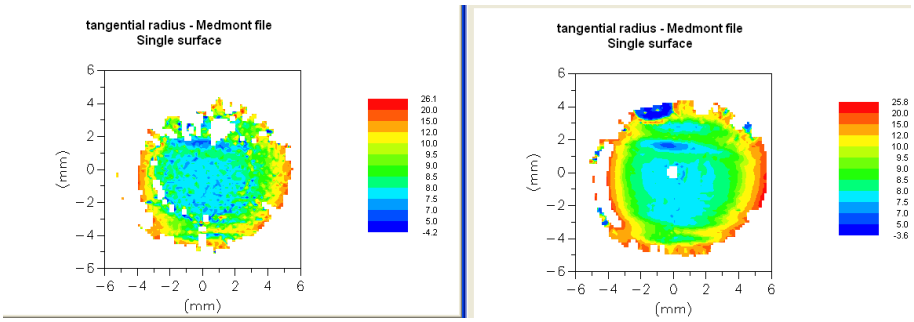

Figure 3: A) Unfiltered tangential combined topography map B) Combined map after Savitzky-Golay filter applied.

Results

The pasted topography maps were not used for quantitative statistical analysis as eyelid-induced corneal changes are time-dependent and the maps were not captured simultaneously. However, the combined post-task topography maps were useful for visual qualitative analysis of eyelid-induced corneal changes (Figure 4).

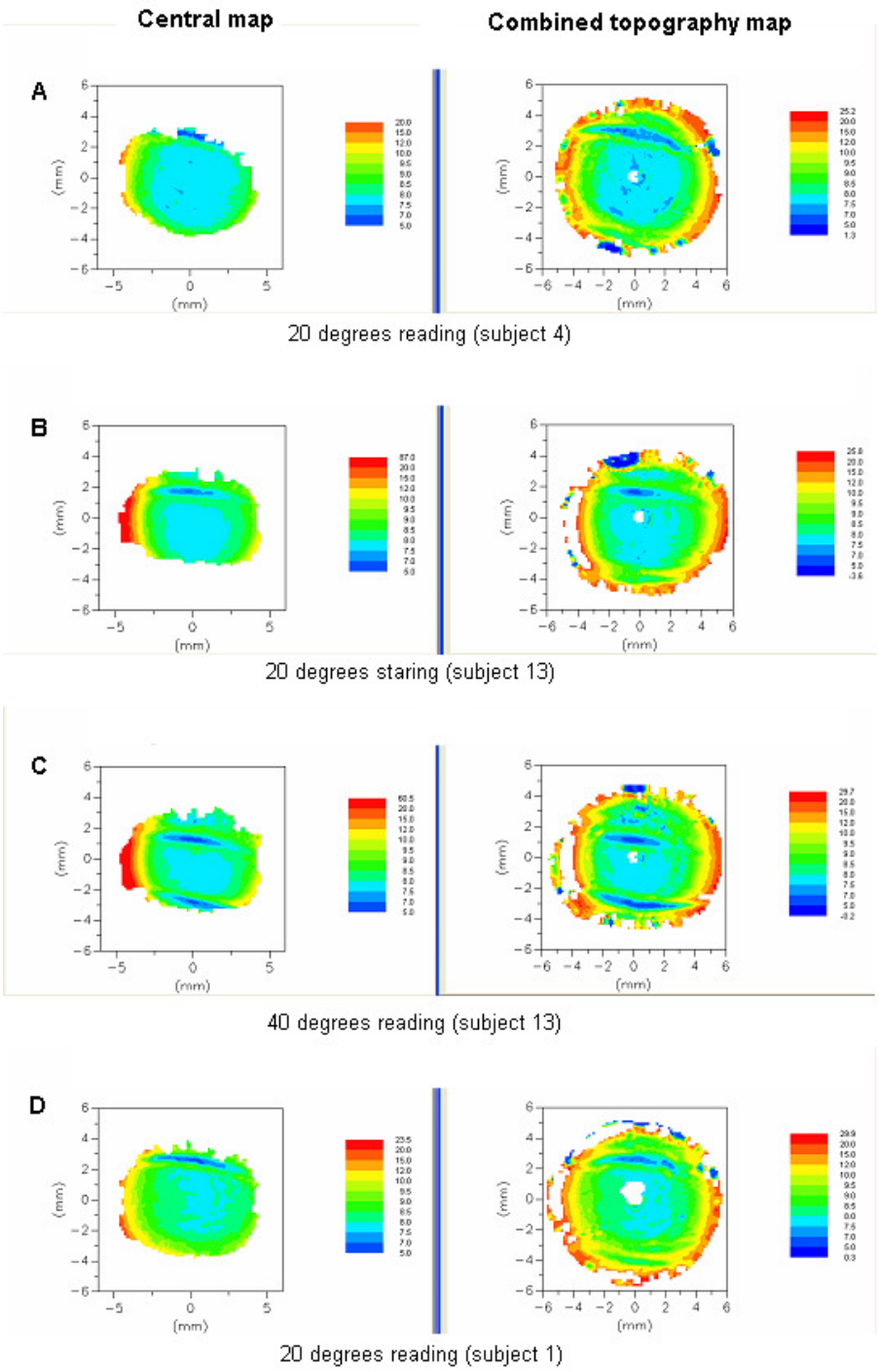

Figure 4: Post-task tangential standard central topography map (left) and the combined pasted tangential map (right) for A) 20° reading (subject 4), B) 20° steady fixation (subject 13), C) 40° reading (subject 13) and D) 20° reading (subject 1).

Discussion

The major limiting factor of standard central topography maps in the analysis of eyelid-induced changes is the peripheral limits of the captured map. Often in downward gaze, the lower eyelid was in contact with the peripheral cornea so the induced change was not captured in the standard central map, but could be observed in the combined map (Figure 4 A, B, D). This primarily occurred for the 20° downward gaze tasks where the lower eyelid was positioned outside the central 7 mm of the cornea. So the combined topography maps assisted in the confirmation of a lower eyelid-induced change when there was no change visible in the standard central topography map.

Due to the shadows from the upper lid eyelashes, upper eyelid-induced changes were often on the edge of the captured topography map. Sometimes this may make it difficult to determine whether the change is due to the eyelid (horizontal band) or if it is an artefact at the edge of the map. The combined topography maps enabled confirmation of upper eyelid-induced corneal changes that were at the edge of the standard central maps (Figure 4 A).

The peripheral limits of the central topography maps also prevented visualisation of the vertical and horizontal extents of the corneal change. From the assessment of the combined topography maps it was noted that both the upper and lower eyelid-induced corneal changes usually extend horizontally to the edge of the cornea (Figure 4 A, B, C and D). Additionally while the valley and central peak are usually visible in the standard central map, the peripheral peak could also be visualised in the combined map.

Due to the transient nature of eyelid-induced corneal changes, pasted combined topography maps were not suitable for quantitative analysis. However it was valuable to capture and visualise these changes in the peripheral cornea. It is now known that eyelid-induced changes do not only occur in the central cornea but are often present in the peripheral cornea and usually extend horizontally near to the limbus.

Appendix 3: Specifications of Tekscan sensor model #4201

MAP AND SENSOR MODEL NUMBER: 4201
SENSOR NAME: WRIST

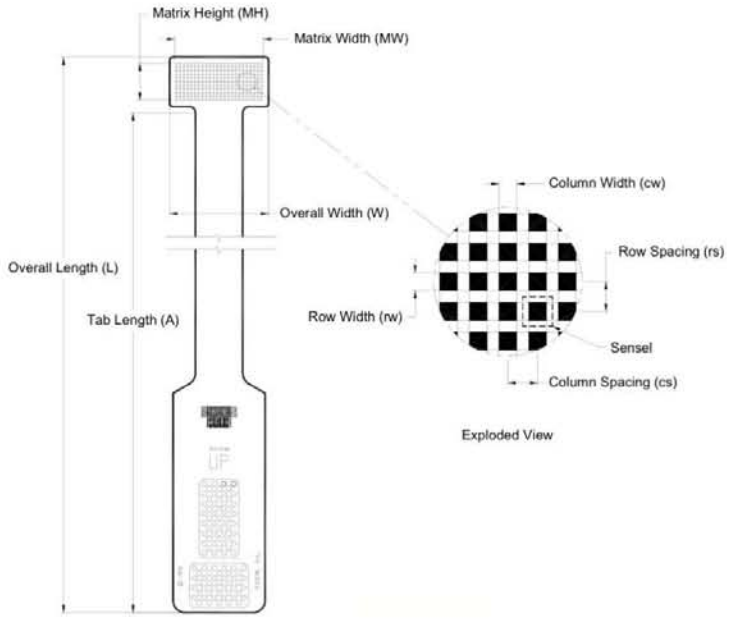

	General Dimensions			Sensing Region Dimensions								Summary	
Model Number	Overall Length	Overall Width	Tab Length	Matrix Width	Matrix Height	Columns			Rows			No. of Sensels	Sensel Density
	L	*W*	*A*	*MW*	*MH*	*CW*	*CS*	*Qty.*	*RW*	*RS*	*Qty.*		
US	(in)	(in)	(in)	(in)	(in)	(in)	(in)		(in)	(in)			(sensel per sq-in)
4201	17	2	15.84	1.875	0.9	0.045	0.075	24	0.045	0.075	11	264	178
Metric	(mm)	(mm)	(mm)	(mm)	(mm)	(mm)	(mm)		(mm)	(mm)			(sensel per sq-cm)
4201	432	51	402	48	23	1.14	1.91	24	1.14	1.91	11	264	27.6

Application Examples: Human joint studies in wrists and elbows. Low pressure ergonomic studies of pressure garmets. Comfort studies with stockings and face masks.

Special Features: Can be trimmed from any edge to fit application. Sensor needs to be resealed after it is trimmed.
- Internal vents.

Tekscan, Inc., 307 West First Street, South Boston, MA 02127 Phone:617-464-4500 Fax 617-464-4266 Website: www.tekscan.com

Appendix 4: Toxicity test for 5 minute araldite

NAmSA® World Leader in Testing Services for the Medical Device Industry

9 Morgan
Irvine, CA 92718
TEL.: (714) 951-3110
FAX: (714) 951-3280

LAB NO. 94C 10209 00
P.O. NO. Q20821

QUT
2 GEORGE STREET
GPO BOX 2434
BRISBANE, Q4001 AUSTRALIA
ATTN: MICHAEL SYDENHAM

ID NO. Not Supplied

CYTOTOXICITY - AGAROSE OVERLAY, SOLID

Test Article: Araldite 1

Test Article Description: Lens; 1 unit

Procedure: A monolayer of L-929 mouse fibroblast cells was grown to confluency and overlaid with Minimum Essential Medium supplemented with serum, antibiotics, neutral red, and 2% agarose. The test article, a 0.5 cm x 0.5 cm piece of Latex #015 as a positive control, and a 1.0 cm length piece of USP negative control were placed on the solidified overlay surface. Following incubation for 24 hours, the culture was macroscopically examined for evidence of cell decolorization to determine the zone of cell lysis. Any decolorized zone present was examined microscopically to confirm cell lysis.

Score	Observations
N (Nontoxic)	Normal cell morphology in proximity to test sample.
T (Toxic)	Cellular death and degeneration associated with the area beneath the test sample and possibly extended beyond the perimeter of the test sample. Where a zone of lysis was observed, the distance from the edge of the sample to the edge of the zone was measured and reported in millimeters (mm).

Results:

Test/Control Articles	Score	Zone of Lysis (mm)
Test Article	N	0
USP Negative Control	N	0
NAmSA Positive Control: Latex #015	T	4

Conclusion: The above test article was nontoxic for L-929 mouse fibroblast cells under the above described test parameters.

Date Prepared: 5-10-94 Date Terminated: 5-11-94

1NE Completed 5-12-94 Approved For: Laiani D. Venegas, B.S.

MG030-110

Appendix 5: Ethics – Eyelid pressure

PARTICIPANT INFORMATION for QUT RESEARCH PROJECT

Eyelid Pressure

Research Team Contacts	
Prof. Michael Collins 3138 5702 m.collins@qut.edu.au	Alyra Shaw 3138 5715 aj.shaw@qut.edu.au

Description

This project is being undertaken as part of the PhD research for Alyra Shaw.

The purpose of this project is to measure the pressure exerted by the eyelids on the front surface of the eye (cornea). The research team requests your assistance because we have developed a new technique of mounting a pressure sensor onto a contact lens. When the contact lens is placed on the eye we can then directly measure the eyelid pressure against the contact lens surface.

Participation

You will be required to undergo an initial screening examination of your eyes to determine your suitability for this study. This includes ensuring that the front surface of the eye (cornea) is healthy and has a normal shape. The instruments used for the screening are those used routinely for eye examinations and pose no risk to the health of your eyes.

The pressure of the eyelids will be measured using a contact lens with a pressure sensor attached to its front surface. You will be positioned in a head rest and asked to remain quite still while the measurements are being taken. Anesthetic eye drops that are routinely used in eye examinations will be used so there is not any discomfort when you wear the contact lens. Video will be taken to track the position of the sensor and any eye movements that may occur.

Your participation in this project is voluntary. If you do agree to participate, you can withdraw from participation at any time during the project without comment or penalty. Your decision to participate will in no way impact upon your current or future relationship with QUT (for example your grades, employment or clinical care).

The project will be conducted in the Contact Lens and Visual Optics Laboratory at QUT, Kelvin Grove. It is estimated that the experiment will require an hour and a half of your time.

Expected benefits

Your involvement in this project will not directly benefit you. However the data collected from this project is expected to increase the understanding of the influence of the eyelids on the front surface of the eye. This information may be used to help design better contact lenses and in understanding corneal changes due to eyelid pressure.

Risks

A number of tests may be used to examine the health and dimensional characteristics of your eyes. To test vision we may use a range of tests, including letter charts, and you simply are required to tell us what you can see. These tests post no significant risk to you. Instruments used to measure the dimensional characteristics of the eyes, including videokeratoscopes, shine a light into your eyes and photograph the reflected image. This poses no significant risk to you and should not cause any discomfort as the instrument does not touch your eye.

There are minor risks associated with wearing contact lenses at any time. Contact lenses often cause initial mild discomfort when first inserted. Occasionally the lens can irritate your eyes if it is not inserted or removed correctly or if the solutions used to clean the lenses have not been properly rinsed from the lens surface. If the contact lenses cause you discomfort we will immediately remove them from your eyes and check the health of your eyes.

When using anesthetic drops it is possible to scratch the eye without being able to feel it. You will be advised not to rub your eyes for 45 minutes after the instillation of these drops. At the conclusion of testing the front surface of your eye will be assessed for any abrasions to the surface. An optometrist will then give you advice about the health of your eyes and offer any ongoing eyecare that you may need (at no cost).

Confidentiality

The research data collected will not personally identify you by name, or in any way allow you to be identified. Any publication of data from this study will use a code system which does not identify you personally. The data will be stored securely in the School of Optometry.

Consent to Participate

After reading the information about this project we would like to ask you to sign a written consent form (enclosed) to confirm your agreement to participate.

Questions / further information about the project

Please contact the researcher team members named above to have any questions answered or if you require further information about the project.

Concerns / complaints regarding the conduct of the project

QUT is committed to researcher integrity and the ethical conduct of research projects. However, if you do have any concerns or complaints about the ethical conduct of the project you may contact the QUT Research Ethics Officer on 3138 2340 or ethicscontact@qut.edu.au. The Research Ethics Officer is not connected with the research project and can facilitate a resolution to your concern in an impartial manner.

Feedback

We will be happy to discuss your individual results during or after the experiment. We will provide you with a written copy of any reports or publications arising from this research if you so request.

CONSENT FORM for QUT RESEARCH PROJECT

Eyelid Pressure

Statement of consent

By signing below, you are indicating that you:

have had the tests and procedures involved in this study explained to you

have read and understood the information document regarding this project

have had the opportunity to ask any questions and have these answered to your satisfaction

understand that if you have any additional questions you can contact the research team

understand that you are free to withdraw at any time, without comment or penalty

understand that the project is for the purpose for research and not for the clinical care of your eyes

understand that you can contact the Research Ethics Officer on 3138 2340 or ethicscontact@qut.edu.au if you have concerns about the ethical conduct of the project

agree to participate in the project

Name _____

Signature _____

Date _____ / _____ / _____

Appendix 6: Spectral frequency analysis of eyelid pressure measurements

In Chapter 4, mean eyelid pressure of a static eyelid was measured using a piezoresistive sensor. Variation around the mean was thought to be physiological in origin as it appeared to be sinusoidal and was greater in the measurement signals than in the calibration signals. Frequency analysis was conducted on calibration and eyelid pressure measurement signals to investigate any underlying frequencies. No obvious peaks were present in the power spectrum of the calibration data compared with the eyelid pressure measurement which had peaks at 0.43 and 0.92 Hz (Figure 1). These values are likely to correspond with respiration and pulse respectively. These fluctuations are likely to be evident due to the ocular blood supply, which may transfer to the eyelid pressure measurements via the eye globe, eyelid or both. Simultaneous measurements of longitudinal corneal apex movements, pulse and respiration have reported associations between the corneal apex movements and the cardiopulmonary system measures (Kasprzak and Iskander 2007).

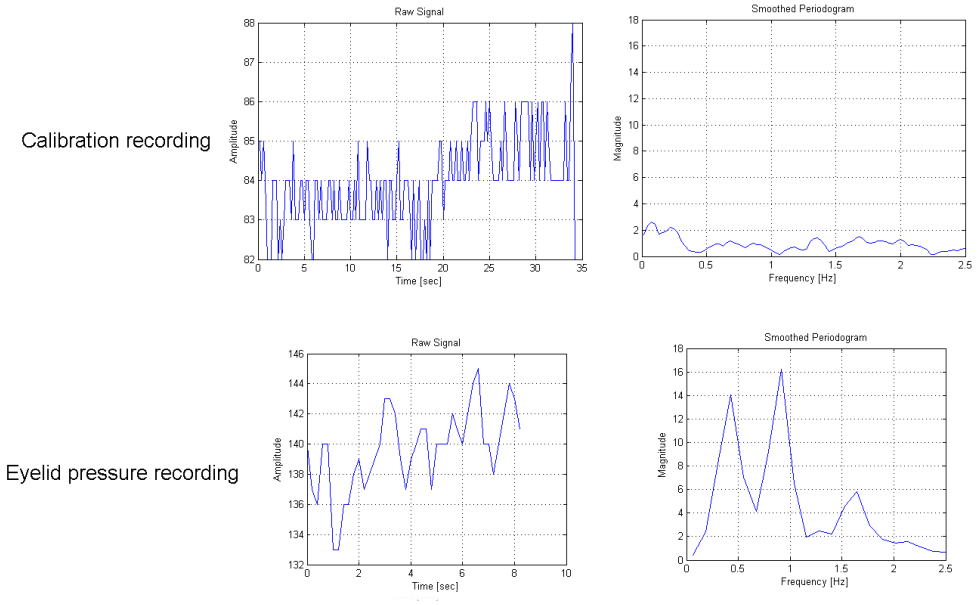

Figure 1: Spectral frequency analysis with raw signal and smoothed periodogram for A) calibration measurement and B) eyelid pressure measurement with peaks at frequencies of 0.42 and 0.92 Hz.

Appendix 7: Abstracts arising from the thesis

Eyelid pressure: inferences from corneal topography changes

Shaw, A. J., Collins, M.J., Davis, B.A., Carney, L.G. (2008). "Eyelid Pressure: inferences from corneal topography changes." Investigative Ophthalmology Visual Science 49 (E-abstract): 1026.

Presented at the Association for Research in Vision and Ophthalmology Annual Conference, Fort Lauderdale, Florida, April 2008.

Development of a method to measure upper eyelid pressure on the cornea

Shaw, A. J., Collins, M.J., Davis, B.A., Carney, L.G. (2009). "Development of a method to measure upper eyelid pressure on the cornea." Clinical and Experimental Optometry 92(1): 60-61.

Presented at the 12th Biennial Scientific Meeting in Optometry, University of Auckland, September 2008.

The measurement of eyelid margin pressure on the ocular surface

Shaw, A. J., Collins M.J., Davis, B.A., Carney, L.G. (2009)

To be presented at the Association for Research in Vision and Ophthalmology Annual Conference, Fort Lauderdale, Florida, May 2009.

Invest Ophthalmol Vis Sci 2008;49: E-Abstract 1026.

1026—D882

Eyelid Pressure: Inferences From Corneal Topography Changes

A. J. Shaw, M. J. Collins, B. Davis and L. G. Carney

Contact Lens and Visual Optics Laboratory, Queensland University of Technology, Brisbane, Australia

Commercial Relationships: A.J. Shaw, None; M.J. Collins, None; B. Davis, None; L.G. Carney, None.

Support: None.

Abstract

Purpose: The cornea is the principal optical element of the eye so the regularity of its surface topography is critical for visual optics. However the cornea is known to be susceptible to forces exerted by the eyelids. These corneal changes are bands of 'wave-like' change that are parallel to the position of the eyelid margin. There is little known about eyelid pressure on the cornea which is dependent on eyelid force and the contact area. By analysing the depth and width of corneal topography changes after various downward gaze tasks, inferences could be drawn about upper and lower eyelid pressure.

Methods: Corneal topography changes due to eyelid pressure were measured using the Medmont E300 Corneal Topographer (Medmont Pty. Ltd. Victoria, Australia), for eighteen subjects aged between 18 and 29 years. Four conditions were considered, consisting of two downward gaze angles (20° and 40°) and two visual tasks (reading and staring). The amplitude and width of the 'wave-like' changes were analysed for each of the four conditions and for both upper and lower eyelids. Anterior eye digital photography was used to determine the position of the eyelids in downward gaze and the width of Marx's line.

Results: For each condition the average peak-to-valley amplitudes of corneal change were between 1.4 and 2.4 μm. For the upper eyelid, the downward gaze angle magnitude had a significant impact on the peak-to-valley amplitude ($p<0.001$), with corneal changes after the 40° tasks being 25% greater than after the 20° tasks. The topographical changes showed a characteristic 'wave-like' pattern, with an outer peak, a valley and an inner peak (closer to corneal centre). The upper eyelid produced a larger outer peak compared to the inner peak ($p<0.001$). The corneal changes after the 40° downward gaze tasks were greater for the lower eyelid than for the upper eyelid ($p<0.01$). The amplitude of corneal change produced by the upper eyelid was associated with the width of Marx's line ($R^2=0.32$, $p<0.05$).

Conclusions: Analysis of the eyelid-induced corneal topography changes gives insight into the eyelid pressure in different situations. The upper eyelid seems to exert greater pressure on the cornea in larger downward gaze angles. The asymmetrical surface shape (outer versus

inner peaks) suggests that the upper eyelid is angled when in contact with the cornea. In 40° downward gaze, it can be inferred that the lower eyelid exerts greater pressure on the cornea than the upper eyelid. There was some evidence that Marx's line is the site of frictional contact between the eyelids and the cornea.

Key Words: cornea: basic science • topography • eyelid

12th Scientific Meeting in Optometry
Clinical and Experimental Optometry 92.1 January 2009 Journal compilation © 2009 Optometrists Association Australia

Development of a method to measure upper eyelid pressure on the cornea

Alyra J Shaw, Michael J Collins, Brett A Davis, Leo G Carney

Contact Lens and Visual Optics Laboratory, Queensland University of Technology, Brisbane, Australia

Purpose: The cornea is known to be susceptible to forces exerted by eyelids. There have been previous attempts to quantify eyelid pressure but the reliability of the results is unclear. The purpose of this study was to develop a technique using piezoresistive pressure sensors to measure upper eyelid pressure on the cornea.

Methods: The technique was based on the use of thin (0.18 mm) tactile piezoresistive pressure sensors, which generate a signal related to the applied pressure. A range of factors that influence the response of this pressure sensor were investigated along with the optimal method of placing the sensor in the eye.

Results: Curvature of the pressure sensor was found to impart force, so the sensor needed to remain flat during measurements. A large rigid contact lens was designed to have a flat region to which the sensor was attached. To stabilise the contact lens during measurement, an apparatus was designed to hold and position the sensor and contact lens combination on the eye. A calibration system was designed to apply even pressure to the sensor when attached to the contact lens, so the raw digital output could be converted to actual pressure units.

Conclusions: Several novel procedures were developed to use tactile sensors to measure eyelid pressure. The quantification of eyelid pressure has a number of applications including eyelid reconstructive surgery and the design of soft and rigid contact lenses.

ARVO 2009 Annual Meeting
REDUCING DISPARITIES
in Eye Disease and Treatment
MAY 3 - 7, 2009 • FORT LAUDERDALE, FL

Program#/Poster#:	5623/D932
Abstract Title:	The Measurement of Eyelid Margin Pressure on the Ocular Surface
Presentation Start/End Time:	Thursday, May 07, 2009, 8:30 AM -10:15 AM
Location:	Hall B/C
Reviewing Code:	155 contact lens - CO
Author Block:	*A.J. Shaw, M.J. Collins, B.A. Davis, L.G. Carney.* Contact Lens & Visual Optics Laboratory, Queensland University of Technology, Kelvin Grove, Australia.
Keywords:	478 contact lens, 526 eyelid

Abstract Body: Purpose: To estimate the pressure of the eyelid against the ocular surface we developed a novel method using a thin (0.18 mm) tactile piezoresistive pressure sensor (Tekscan Inc., Boston, MA, USA) mounted on a rigid contact lens.
Methods: Curvature of the sensor causes an offset and altered sensitivity, so a contact lens was designed with a flat region where the sensor could be adhered. We examined the response of the sensor in different conditions including the influence of conditioning (prestressing), drift (continued increasing response with a static load) and temperature variations. Techniques were developed to calibrate the sensor output into real pressure units (mmHg) and to hold and optimally place the sensor-contact lens combination under the eyelid margin.
Results: Calibration gave a linear relationship between raw sensor output and actual pressure units, for loads between 1 and 10 mmHg. Conditioning the sensor prior to use regulated the measurement response. Sensor output stabilised about 10 seconds after loading. While the output drifted slightly over several hours, the drift was not significant over the measurement time required for eyelid pressure (<30 seconds). The error associated with calibrating at room temperature but measuring at ocular surface temperature led to a very small overestimation of pressure. Eyelid pressure readings could be seen when the upper eyelid was placed on the sensor and then removed three times during a recording. Also when the eyelid was pulled from the outer canthus (similar to the lid-pull technique

for removing a contact lens) the readings from the sensor significantly increased.
Conclusions: A number of novel procedures were developed to use a tactile sensor to measure eyelid pressure. These included designing a custom contact lens with a flat area to which the sensor could be attached, a hydrostatic calibration system and an *in vivo* measurement apparatus to hold and position the sensor-contact lens combination on the eye.

Commercial Relationships: A.J. Shaw, None; M.J. Collins, None; B.A. Davis, None; L.G. Carney, None.

Support: None

Appendix 8: Publications arising from the thesis

Corneal refractive changes due to short-term eyelid pressure in downward gaze

Shaw, A. J., Collins, M.J., Davis, B.A., Carney, L.G. (2008). "Corneal refractive changes due to short-term eyelid pressure in downward gaze." Journal of Cataract and Refractive Surgery 34(9): 1546-1553.

Eyelid pressure: inferences from corneal topographic changes

Shaw, A. J., Collins, M.J., Davis, B.A., Carney, L.G. (2009). "Eyelid pressure: inferences from corneal topographic changes." Cornea 28(2): 181-188.

A technique to measure eyelid pressure using piezoresistive sensors

Shaw, A. J., Davis, B.A., Collins, M.J., Carney, L.G. (2009). “A technique to measure eyelid pressure using piezoresistive sensors.” IEEE Transactions on Biomedical Engineering 56(10): 2512-2517.

Eyelid pressure and contact with the ocular surface

Shaw, A. J., Collins, M.J., Davis, B.A., Carney, L.G. (2009). “Eyelid pressure and contact with the ocular surface." Investigative Ophthalmology and Visual Science (in press).